ALMA MATER STUDIORUM - UNIVERSITY OF BOLOGNA

ENGINEERING FACULTY
Doctoral School on Energy, Nuclear
and Environmental Control Engineering

REACTOR PHYSICS AND NUCLEAR TECHNOLOGY

Doctoral Cycle XXV
Settore Concorsuale di Afferenza: 09/C3
Settore scientifico-disciplinare: ING-IND/18

Power Transient Analysis of Experimental Devices for Jules Horowitz Material Testing Reactor (JHR)

Presented by:
PATRIZIO CONSOLE CAMPRINI

Doctoral School Director:
Prof. ANTONIO BARLETTA

Supervisor:
Prof. Ing. MARCO SUMINI

Co-supervisors:
CARLO ARTIOLI (ENEA)
CHRISTIAN GONNIER (CEA)
BERNARD POUCHIN (CEA)
PATRICIA SIRETA (CEA)
SERGE BOURDON (CEA)

Doctoral Defense Year 2013

Abstract

The objective of this thesis is the power transient analysis concerning experimental devices placed within the reflector of Jules Horowitz Reactor (JHR). Since JHR material testing facility is designed to achieve 100 MW core thermal power, a large reflector hosts fissile material samples that are irradiated up to total relevant power of 3 MW. MADISON devices are expected to attain 130 kW, conversely ADELINE nominal power is of some 60 kW. In addition, MOLFI test samples are envisaged to reach a few hundreds kW (for LEU and HEU configurations). Safety issues concern shutdown transients and need particular verifications about thermal power decreasing of these fissile samples with respect to core kinetics, as far as single device reactivity determination is concerned. Calculation model is conceived and applied in order to properly account for different nuclear heating processes and relative time-dependent features of device transients. An innovative methodology is carried out since flux shape modification during control rod insertions is investigated regarding the impact on device power through core-reflector coupling coefficients. In fact, previous methods considering only nominal core-reflector parameters are then improved. Moreover, delayed emissions effect is evaluated about spatial impact on devices of a diffuse in-core delayed neutron source. Delayed gammas transport related to fission products concentration is taken into account through evolution calculations of different fuel compositions in equilibrium cycle. Provided accurate device reactivity control, power transients are then computed for every sample according to envisaged shutdown procedures. Results obtained in this study are aimed at design feedback and reactor management optimization by JHR project team. Moreover, Safety Report is intended to utilize present analysis for improved device characterization.

Contents

List of Figures

List of Tables

Introduction

The objective of the present thesis is the evaluation of thermal power transients regarding experimental devices placed within the reflector of Jules Horowitz Material Testing Reactor (JHR). French Atomic Energy Commission (CEA) has recently launched the construction of this 100 MW irradiation facility which is intended to achieve the most important experimental capability in the European framework for the next decades. The JHR core has been designed in order to exploit a twofold neutron spectrum. In fact, in-core fast neutron flux is utilized for structural materials such as cladding alloys and in-vessel components. Conversely, a large beryllium reflector allows an important reactor area in which thermal neutron flux is used for fuel properties and operational experiments.

Research aim and technological motivations

Irradiation test performances aimed at material behavior investigations require particular temperature control concerning material property dependence on thermal environment. For this reason, nominal and time-dependent powers have to be properly evaluated by design. Hence, safety analyses need precise data to characterize possible abnormal scenarios.
Moreover, devices carrying fuel samples imply additional safety concerns to be accounted for, since elevated nominal JHR power induces devices irradiation which is high compared to present technological state-of-the-art performances of research reactors. Thermal and physical properties of considered fissile materials - namely ceramic dioxide pellets and Al alloys - impact temperature dynamics and show critical capability of withstanding particular power transients.
For what concerns safety systems about reflector devices operational control, only core control rods regulation and insertion are envisaged to effectively reduce neutron flux and fission reactions occurring in the devices.
Then, every sample has been modeled as a multiplicative material irradiated by a strong external neutron source provided by JHR core. Core-induced nuclear power deposition has been computed. By contrast, reactivity evaluation of every device has been considered to determine at which extent self-produced contribution influences sample power and its time-dependent behavior.

In the present study, particular reflector devices are considered since they have been conceived to host fuel samples and fissile targets. They are listed hereafter:

- MADISON device hosts up to 4 UO_2 pins 1% U235 enriched to simulate high burnup fuel nominal operating conditions or slow transients for power reactors
- ADELINE device is designed for a single UO_2 fuel pin 1% U235 enriched in order to reproduce abnormal operating conditions leading to clad failure
- MOLFI device is planned to utilize UAl targets (U235 enriched) to perform irradiation aimed at radioisotope production for medical purposes

Therefore, proper evaluations of device power transients during shutdowns are obtained starting from complete analysis of every nuclear energy deposition phenomenon related to core:

- irradiation and fission power due to prompt neutrons coming from core
- irradiation and fission power due to delayed-induced neutrons coming from core
- power deposition related to prompt gamma radiation coming from core
- power deposition caused by delayed gamma radiation coming from core, related to fission products decay

However, sample self-contributions are worth to be accounted for in order to consider even possible time behavior departures with respect to core power shutdown kinetics. These effects are listed as follows:

- power deposition due to device self-generated prompt neutrons
- power deposition due to device self-generated delayed neutrons
- power release regarding prompt gamma radiation generated inside the sample
- delayed gamma production concerning sample fission products inventory has been neglected as only short irradiation periods are taken into account

Once all nuclear irradiation and contributions considered, exhaustive device power deposition modeling has been provided.

Core irradiation source model and analysis

Preparation of core source modeling regarded following approach and methodology:

- thermal hydraulic and neutronic core model conception and implementation
- power transients description for Normal Shutdown and Safety Shutdown by means of DULCINEE point kinetics code

Kinetic transients provided behavior of core neutron and gamma source. Reflector devices irradiation model for power deposition has been based on these time-dependent features.

Effects on device of neutron and gamma core radiation

Once core irradiation source for experimental devices has been obtained, following procedure has been carried out about core effects; simulations have been performed through Monte Carlo TRIPOLI 4.8 code:

- lumped prompt and delayed neutrons irradiation from core has been computed through device-core coupling coefficients linking device power to core fission reactions
- prompt gamma irradiation effects on device power has been evaluated through simulations aimed at obtaining device-core gamma coupling coefficients
- core delayed gamma source has been computed with PEPIN2 evolution code and irradiation simulations have been aimed at energy deposition regarding device samples

Device self-contributions induced by samples

Regarding self-contributions related to fissile material multiplication within the device, twofold nuclear energy deposition has been accounted for:

- estimation of prompt neutrons and prompt gamma self-produced contributions has been achieved
- impact on time-dependent effects induced by delayed neutrons has been evaluated solving point kinetics equations for subcritical devices, through semi-analytical methods

Therefore, particular device-core coupling coefficients about power depositions have been calculated for different control rod insertions - namely nominal configuration, Pilot Rod insertions, Safety Rod insertions for Normal and Safety Shutdown procedures.
In fact, current methodology improvement - compared to previous analyses - regards impact evaluation of flux shape distortion caused by control rod insertion and modification of medium absorption properties. Such an innovative device-core coupling coefficient determination allowed better sample power transients description.
In addition, core burnup composition impact has been considered for four fuel configuration during equilibrium cycle: Beginning of Cycle, Xenon Saturation Point, Middle of Cycle and End of Cycle. Finally, prompt and delayed contributions regarding time-dependent power generation in devices have been evaluated. Neutron and gamma nuclear power deposition phenomena have been accounted for in order to provide detailed results to JHR project team, aiming at design feedback improvement and reactor experimental capability optimization.

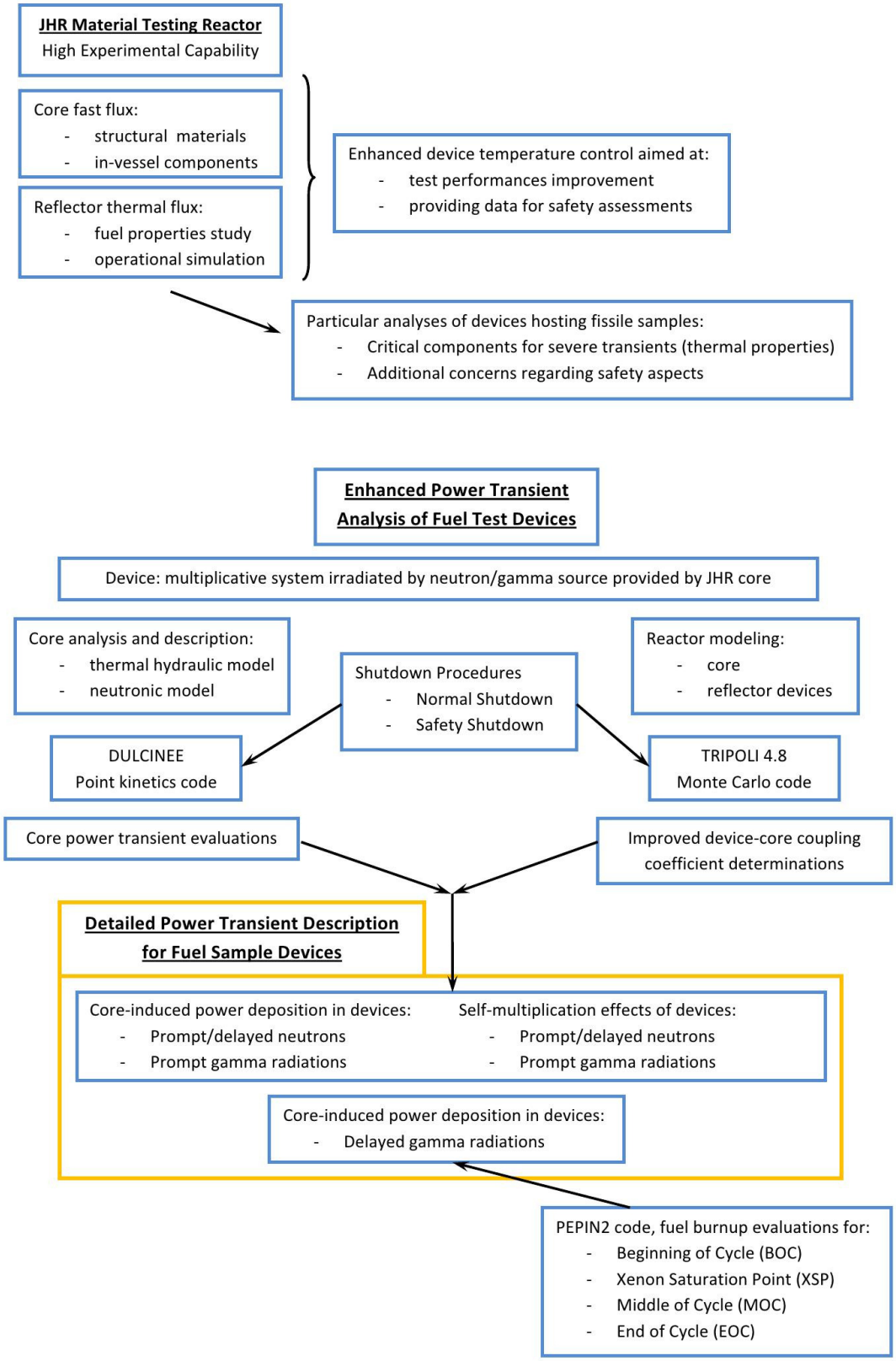

Figure 1: Research aim and methodology flow chart

Chapter 1

The Jules Horowitz Reactor

1.1 Material Testing Reactors

European policy regarding energy supply and resources availability, as well as infrastructures, is expected to gather different domestic power plant fleets searching more and more for shared scenarios. Growing demand for electrical power and greenhouse gases reduction strategies make nuclear energy a significant source in the European mix, since economical competitiveness and very low environmental impact are achieved.
At present time, several nuclear power plants are connected to the grid supplying around 30% of European electrical needs. Research and development supporting this significant network take advantage of Material Testing Reactors (MTR) which provide experimental data to industries, utilities and regulators. In fact, these facilities are very important to study properties of materials that have to withstand critical thermal hydraulics and radiation conditions during operation.
Fuel technology in present and future nuclear power plants is continuously upgraded to achieve better performances and to optimize the fuel cycle, still keeping the best level of safety. By contrast, thermal and mechanical properties of structural materials for cladding and vessel are main design constraints and nuclear technology enhancement is strictly related to their characteristics. For this reason, ageing effects and mechanical deformation are expected to be reproduced as far as operational irradiation periods are concerned.
Considering the number of nuclear power plants all over the Europe, it is worth to highlight how this broad energy network requests a constant improvement of performances and safety features for present Gen II but also for future Gen III water-cooled plants technology. In addition, Gen IV reactors are very important keystones aiming at achieving nuclear energy development and sustainability objectives both regarding resources and waste management.
The French Atomic Energy Commission (CEA) has then launched the construction of a new MTR - the Jules Horowitz Reactor (JHR) - at Cadarache research centre in the framework of an international collaboration (Iracane et al., 2008).
JHR is intended to become the most important MTR in Europe for the next century. It

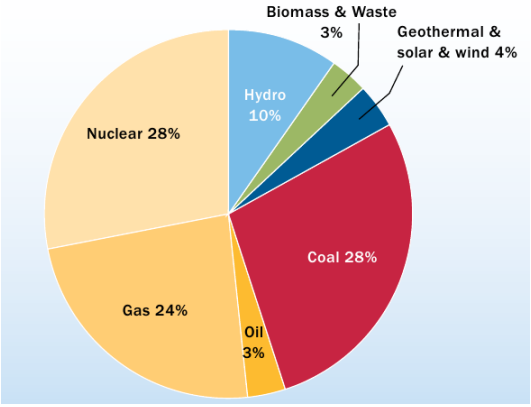

Figure 1.1: IEA Electricity Information about 2010 for EU 27

has been conceived in order to investigate structural material and fuel properties linking industrial and research needs of all partners (Bignan et al., 2012).

- Sustainability of power supply is also related to energy market and then life extension of power plants is a key point in network management, aiming at reducing capital costs and enhancing competitiveness. Gen II nuclear plant lifespan needs several material tests in order to keep the best safety level respecting components qualification procedure. So JHR is equipped with experimental loops able to simulate present PWR, BWR, CANDU and VVER technologies using both a core fast flux and a proper in-reflector thermal neutron spectrum. Gen III reactors deployment phase requires experimental R&D to support and validate material certification for plant life management, safety demonstration, flexibility and economical improvement. Experimental irradiations of structure materials are necessary to understand their behaviours and will contribute to operation optimization which is a significant economical stake leading to capital appreciation, paying-off production facility, less investment required for energy production.
- Moreover, JHR allows fuel performances optimization through particular sample irradiation. Studies are expected to be carried out in order to increase burnup and to enhance resource exploitation. In addition, data concerning fuel properties during normal and abnormal operations are provided depending on utilities and industries technological needs. Fuel evolution for Gen II and III is and will stay an important issue requiring developments, qualification tests and experiments to ensure economical competitiveness. JHR has been conceived for innovative fuel sample selection and testing in representative conditions about operative neutron flux.
- Safety topics are investigated by means of accident simulations and component tests. LOCA (loss of coolant accident) scenarios are then reproduced, as well as power transients and ramps, in order to study fuel materials behaviour. Experimental tests exploring the full range of fuel behaviour determine stability limits and safety margins, as a major input for the fuel reliability analysis.

- High neutron fluxes and elevated temperature loops have been designed in order to reproduce challenging conditions for Gen IV reactors research and development. A quite fast in-core neutron spectrum is also capable to simulate SFR, GFR or LFR neutronic features. Preparing for next innovative Gen IV reactors, many experimental data are needed concerning radiation interaction with advanced materials - namely graphite, nickel alloys and ceramics. High in-core dpa rates allow important experiments aimed at improvement of cladding and in-vessel component materials such as austenitic stainless steel or ferritic steel (mainly utilized in sodium and lead-cooled technologies). In addition, optimized devices have been prepared to study minor actinides partitioning and transmutation issues.
- Increasing in nuclear medicine diffusion and reliability makes radioisotope production and stock very important and strategic activities in the research reactor domain. JHR is going to be capable to supply from around 35% of European needs in Molybdenum-99 to about 50% in case of particular market demand or critical procurement.
- Nuclear research always needs facilities for education and training of young scientists and engineers. Then JHR international project is also aimed at expertise transfer and enhancement to support future European technology.

European Material Testing Reactors (MTR) have provided technological and research support for 40 years (Iracane, 2010). They give the opportunity to perform relevant experiments in reliable conditions to obtain important nuclear data or to improve knowledge and understanding about phenomena involved in the irradiation process. History of research reactors was mainly driven within national policies. The implementation and access to international research infrastructures is becoming a major new trend. Moreover this perspective is an effective way to manage rationalization and optimization of the research reactors network meeting both requirements of safety, scientific and economic efficiency as well as training and competences management (Chauvin, 2009).

Countries	Reactor	First criticality	Power (MWth)
Czech Re.	LVR15	1957	10
Norway	Halden	1960	19
Sweden	R2	1960	50
Netherland	HFR	1961	45
Belgium	BR2	1963	60
France	OSIRIS	1966	70

Figure 1.2: Research reactors in Europe

The international context in which JHR will be developed is important as well. In fact research and industry frameworks are getting over national policies and domestic tools

have no more the required level of economic and technical efficiency. Meanwhile, countries with nuclear energy need an access to high performance irradiation experimental capabilities to support technical skill and guarantee the competitiveness and safety of nuclear energy. Moreover, many research items related to safety or public policy (e.g. waste management, internal components reliability, vessel performances) require international cooperation to share costs and benefits of resulting public acceptance. Then JHR will be the starting point of a European network for nuclear research and technical development, scientists and engineers training as well as knowledge and know-how sharing. Therefore this project is driven and funded by the international JHR Consortium gathering vendors, utilities, technical stakeholders and research bodies. Some important partners are listed below:

- CEA as reactor owner and manager
- EDF French utility for power generation
- European Commission and Joint Research Centre for Europe
- SCK/CEN Mol Research Centre for Belgium
- NRJ/UJV Research Body for Czech Republic
- VTT Technical Research Centre of Finland
- AREVA as industrial partner, designer and constructor
- CIEMAT Spanish Research Centre for safety authority and utilities
- VATTENFALL which is Swedish power utility
- DAE Department for Atomic Energy, India
- IAEC Israel Atomic Energy Commission
- JAEA Japanese Atomic Energy Agency (via bilateral agreement with CEA)

1.2 Reactor Layout

The JHR operation procedures require several facilities and apparatus in order to manage the entire experimental capacity and to host all the opertive staff. Civil compound structure is composed by several zones (JHR Status Report 2006-2007).

- the Reactor Building (RB) and the Nuclear Auxiliaries Building (NAB) forming the nuclear island
- the buildings conceived to host reactor exploitation infrastructures
- the buildings that will host JHR staff and offices, cold assembly workshop and pre-irradiation material storage
- two emergency buildings aimed at hosting diesel generators and atmospheric heat exchangers

JHR Reactor Building is planned to host the reactor core. Its internal layout points out two different zones. All the reactor components are settled in the so called reactor area.

In the remaining part - namely the experimental area - there is room to set up experimental laboratories. One of these laboratories is devoted to high quality on-line examinations in order to analyse even short-lived fission products. Reactor area and experimental area interface was optimised to guarantee operators radiation protection but also high standard acquisition.

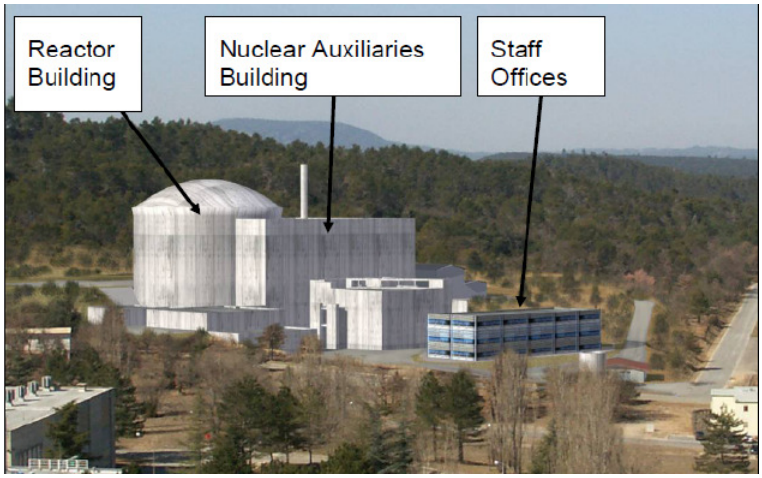

Figure 1.3: Virtual picture of JHR facility (Courtesy by CEA)

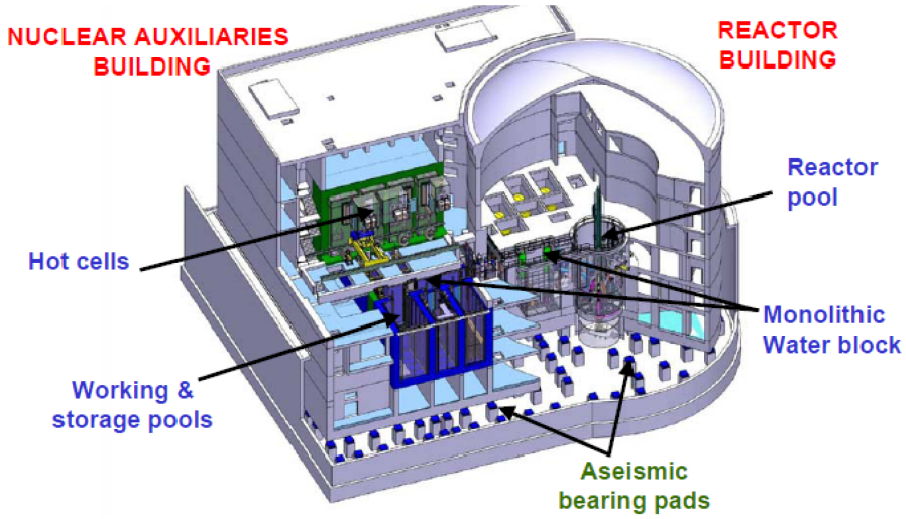

Figure 1.4: Layout of JHR nuclear island (Courtesy by CEA)

Fuel and device underwater transfer are possible through the water channel from reactor core to storage pools in Nuclear Auxiliaries Building. In the Reactor Building the very first part of the channel is the deactivation pool for temporary storage of components just before and after irradiations.
Three cooling loops are then placed in this zone. The primary loop has to assure a proper core cooling both for fuel elements and in-core devices. Regarding the reflector positions,

a secondary loop utilizes reactor pool water to cool down all the devices since different needs have to be faced, particularly in the radionuclide producing rigs. Finally a safety third cooling loop is present to assure core decay heat removal until natural convection is set up. Between Reactor Building and Nuclear Auxiliaries Building a particular watertight and airtight separation lock was designed in order to increase the safety standards.
JHR Nuclear Auxiliaries Building is composed by laboratories and examination facilities strictly concerning high irradiation environment. Through water channel, fuel or material samples can be hosted in three storage pools: depleted fuel elements, material test devices and the mechanical components for maintenance and inspections, respectively.
Then two underwater channels allow to reach the hot cells. Here non destructive examinations (NDE) are performed. Two beta-gamma cells are devoted to material and fuel samples post-irradiation exams. They are equipped with NDE benches. These cells allow also reactor waste management and removal. It is also available a beta-gamma cell for radionuclide transit and dry removal from spent fuel. In addition an alpha-beta-gamma cell is present in order to reach high contamination risks handling.

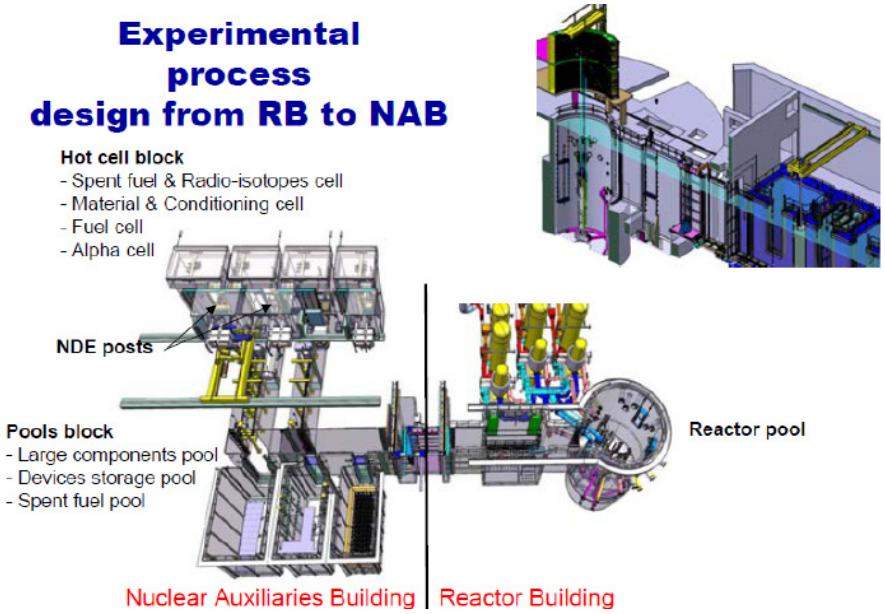

Figure 1.5: Internal water channels layout and hot cells (Courtesy by CEA)

For what concerns cask management, JHR is designed to be able to allow either dry mode loading/unloading procedures or wet mode through dedicated hot cells.
In Nuclear Auxiliaries Building several laboratories provide instrumentation and facilities for analysis and experimentation assistance:

- **Fission Product Analysis Laboratory**: here devices allow to receive on-line measurements about short-lived fission products decay both providing gas flows in controlled test atmospheres and in liquide environments. In fact, coolant radiation analyses are performed by means of mass and gamma spectrometry, gas chro-

matography and plasma torches.

- **Chemistry Laboratory**: investigation of different chemical compounds are needed to support simulation and characterization of nominal and abnormal operative conditions
- **Radiation Protection Laboratory**: all necessary controls regarding installation probes and staff exposition are performed here as well as a first estimation of radioactivity in internal effluents and general reactor wastes
- **Dosimetry Laboratory**: reactor core and all facility parts are equipped with dose integrators which need to be periodically set and restored. Radiological zoning activities and monitoring are also carried out in this part of the facility

Pre-irradiation controls will be possible through proper cold workshops, and inter-irradiation controls will be carried out through NDE benches, in fact often an on-line check and test parameter correction are necessary to optimize capability, time and costs. Non-nuclear Buildings will host personnel and support staff. Even cold workshops for test device handling before irradiation are set in non-nuclear facility part.
Control rooms are conceived to enhance scientists and operators interface. In fact a pilot control room and an experiment control room are devoted to, respectively, piloting staff and researcher personnel for test monitoring. Thus interconnections between the two control rooms for most relevant parameters transfer are considered in design phase. Operating systems and procedures as well as different experimental configurations have been considered in order to assure the best performances with respect to safety needs, capability and flexibility.

1.3 Reactor Features

JHR core has been conceived in order to achieve high experimental performances and to better exploit a twofold neutron spectrum. Innovative core design lead to a conception in which fast and thermal components are split in core and reflector regions. In fact, its design has been aimed at:

- high experimental capability in terms of test positions and cycle management
- flexibility and availability for a large number of reactor parameters
- high fast and thermal neutron fluxes in order to simulate broad material and fuel test conditions.

For what concerns flexibility and high capability, several experimental positions are available in different parts of the reactor. They are mainly divided into:

- in-core test positions
- in-reflector test positions

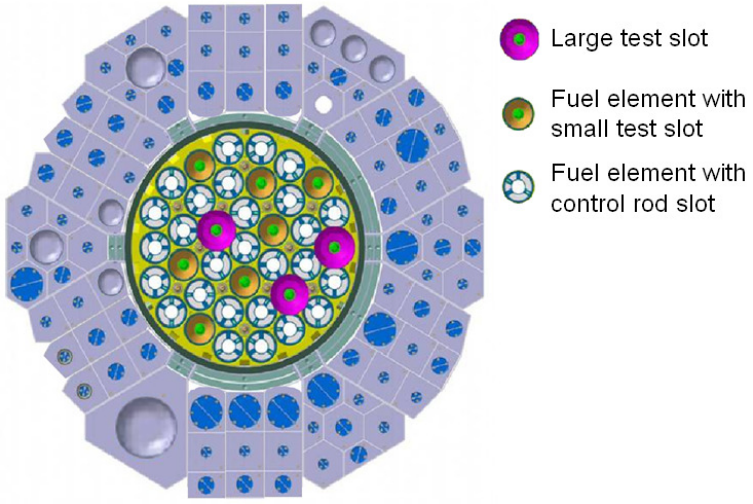

Figure 1.6: JHR core and reflector (Courtesy by CEA)

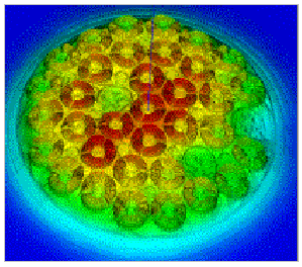

Figure 1.7: Core fast flux (HORUS3D)

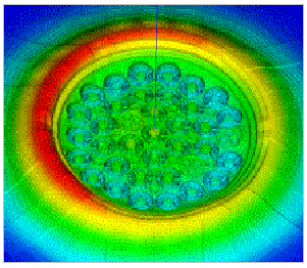

Figure 1.8: Reflector thermal flux (HORUS3D)

In-core experimental positions take advantage of a high fast flux since this is an important part of the JHR core neutron spectrum.
In-reflector experimental positions are located within the reflector area, outside the core. It is possible to enhance capability since device loading and regulation do not need either reactor operation or shut down. Here several moving frameworks allow performance adjustment and flexibility in a number of test positions. In addition fixed in-reflector locations remain within the reflector structure for all the experimental cycle.

1.3.1 Core Description

The core rack is a 90 cm height, 71 cm diameter cylinder made of aluminium in which 37 drilled holes can host both 34 fuel elements and 3 sample holders within the so called large test positions. By contrast, small test locations are placed in the centre of 7 cylindrical plate fuel elements in order to reach the fast flux as close as possible to the fuel. These 10 experimental slots are available at the same time in order to maximize fast neutron utilization for structural irradiation and high dpa rates. Relevant performances are

achievable in both cases: high fast neutron flux (E $>$ 0,9 MeV) up to 5 10^{14} n/cm^2/s is available in small locations, large locations can deliver flux (E $>$ 0,9 MeV) up to 4 10^{14} n/cm^2/s (Doderlein et al., 2008). Both values are referred to perturbed flux - namely evaluated within experimental test device.

This objective of keeping a fast neutron flux within the core has been reached thanks

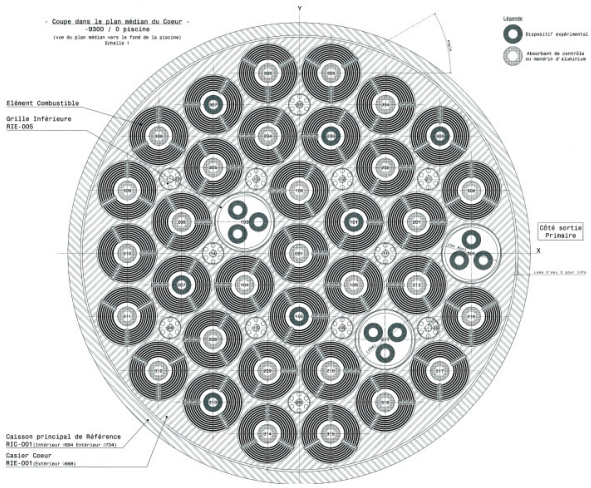

Figure 1.9: Core radial cross-section (Courtesy by CEA)

to a very low coolant volume fraction. Fuel, water and structure materials compositions were optimized taking into account neutron physics objectives, thermal hydraulic requirements, and mechanical aspects. For example, distance between plates takes into account also possible aluminium swelling under irradiation, manufacturing fabrication uncertainties are considered as well.

Two different nominal conditions are envisaged to optimize experimental availability and operative costs: the first one is about 100 MW thermal power as described before and the second foresees some 70 MW. Even a possible twofold core charging is accepted: 37 or 34 fuel elements depending on test needs from international partners.

Reactor operations have been foreseen with at least 10 fuel cycles of about 25 days. Design has been set for low 20% enrichment UMo fuel. The latter is still under qualification phase. The use of U_3Si_2 equivalent to UMo will require 27% U235 enriched fuel. Anyway the reactor is expected to start with low 20% enrichement U_3Si_2 fuel and to operate at 70 MW nominal power. The ultimate fuel is expected to be a metallic UMo 19,75% enriched alloy. Among issues for using 20% enriched fuel, initial core excess reactivity related to 27% enrichment configuration has been retained. This choice will nevertheless lead to 5 additional fix control rods utilization, within the core rack. The need for keeping representative neutron flux induces 70 MW power level. The cladding material is an aluminium alloy and every fuel element is composed by 8 cylindrical and concentric plates kept together by 3 stiffeners (JHR Status Report 2008). This particular geometry has been considered since:

- cylindrical plates present good mechanical resistance even withstanding significant

coolant velocity
- fuel element does not significantly change initial shape as far as neutron radiation swelling is concerned
- fabrication experience of AREVA-TA takes advantage of a reliable good practice, it is also the geometry of BR2 in Belgium.

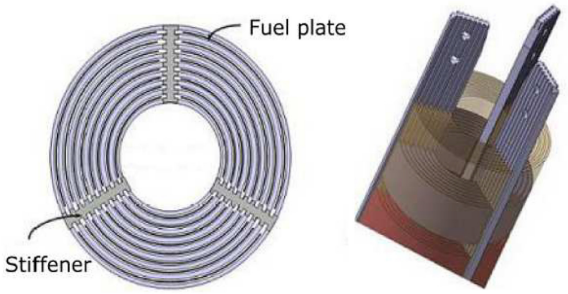

Figure 1.10: JHR fuel element (Courtesy by CEA)

Remaining 27 fuel elements not hosting sample holders are utilized for control rods insertion. In the inner part, two cylindrical shell hafnium rods are envisaged to pilot the reactor both to provide poisoning or depletion compensation and to assure safety shutdowns. A group of 19 Compensation Rods (CR) is designed to one by one withdrawal throughout the cycle to provide extra reactivity and assure system criticality. Moreover, a 4 Pilot Rods (PR) bank is kept as close as possible to the core mid-plane in order to take advantage of the highest differential worth. Remaining 4 Safety Rods (SR) are clustered in a bank as well and completely extracted from the core during normal operations.

1.3.2 Reflector Description

Outside the core, a beryllium reflector allows to get a thermal neutron flux suitable for several tests concerning fuel properties. Beryllium has been chosen for the following reasons:

- heavy water has not been considered since it needs resistant tanks, and reflector reconfiguration procedures for JHR have to be optimized
- since operational temperature in JHR core is significantly low, graphite used as neutron reflecting material would not rearrange atom dislocations due to Wigner effect inducing dangerous accumulation of energy in material lattice
- considering core geometry, neutron retention induced by light water would not be optimal for criticality balance and thermal neutron flux gradient. In addition, the latter is steeper in water configuration than with beryllium, and it would be even less accurate for power control in experimental devices.

Here neutrons coming from the centre of the reactor undergo many collisions and slow down up to representative energies to simulate LWR spectra. In-reflector experiments are

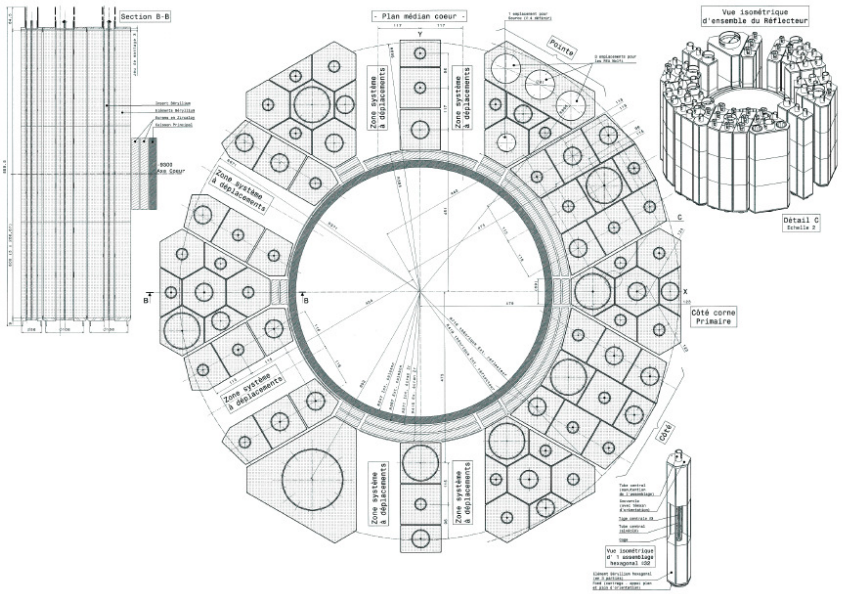

Figure 1.11: Reflector plans and radial cross-section (Courtesy by AREVA-TA)

focused on fuel behaviour tests and in these cases it is possible to reach 500 W/cm linear heat rate in high burnup equivalent fuel samples, moreover even a fast flux of about 8 10^{13} n/cm^2/s is available for PWR pins. Slow ageing processes are also reproduced for vessel and structural materials.
Zircaloy shield is placed around half a core to reduce gamma heating in some reflector regions. This shielding is removed in regions where highest value of neutron flux is required.

1.4 Material Irradiation for Technology Research

JHR investigations are focused on structural materials as far as different characterizations of thermal and mechanical properties are concerned. Material behaviour under irradiation is planned to be studied in connection with several environment conditions such as high temperature, chemical interactions and tensile stresses. As mentioned, a large number of nuclear reactor technologies and generations is envisaged to be properly represented, taking advantage of a significantly hard in-core neutron spectrum. About 10 experimental positions are available there, for cladding and in-vessel component alloys such as stainless steels. Inconel alloys, titanium, zirconium and nickel alloy, aluminium and control rod materials are envisaged.

1.4.1 Structural Materials for Nuclear Reactors

The objectives of material irradiation experiments are usually aimed to mechanical behavior investigations under temperature and irradiation accurate control. Strain tests are performed as well as bowing and swelling effects analyses. Additional needs will deal with the interaction between materials and chemical environment. In fact corrosion or irradiation assisted stress corrosion cracking (IASCC) are main topics. These requirements lead to more sophisticated test devices allowing a representative and well controlled chemical environment.
In order to provide examples of material irradiation experiments, the next paragraphs are focused on specific requests dedicated to properties change concerning cladding materials, core internals and pressure vessel structures.
Cladding material properties are focused on irradiation growth and strain or creep tests as well as bowing and swelling effects. Particular devices can host zircaloy samples and set axial strain in order to perform on-line measurements. Cladding resistance to biaxial loading is usually simulated through gas pressurisation which leads to fixed ratios between axial and circumferential stress in different material cylindrical samples. Nevertheless these ratios must be modified in order to add other effects such as fuel pellet growth phenomena. Therefore, particular devices are designed in which biaxial strains are superimposed to gas pressure effect in order to be able to investigate differential contributions. Material irradiation growth is evaluated by means of samples in which free blades undergo simple irradiation effects and loaded blades exhibit superimposed strains. Provided the same irradiation conditions, it is then possible to separate the effects.
Mainly concerning internal components, stress relieving after irradiation periods requests suitable tests for strain components and tightening screws performances. For this purpose, simple structural blades at which a previous load is imposed are planned to be utilised - blended blades are going to be frequently implemented. Superposition phenomena are possibly investigated within gamma and neutron radiation fields.
LWR material irradiation tests dealing only with temperature, stress and doses, require optimized loops regarding thermal hydraulics. In order to reach proper flat temperature profiles within the samples, liquid metal NaK is utilized as device coolant.
For what concerns tests about chemical environment impact, the specimen will be installed in a pressurized water loop. For instance, impact of Zr ageing is considered since chemical reaction kinetics is strongly influenced by neutron irradiation which induces lattice damages, corrosion and oxidation. Radiolysis due to strong ionizing radiation field - such as in nuclear reactors core - is important to be simulated and analyzed as well.
Specimen with particular cracks can be irradiated and then analyzed even by means of on-line tests during irradiation cycles, crack resistance tests can be also produced after irradiation and then investigated.
Experiments are also planned to define ionizing environment to study radiation induced diffusion. Several parametric tests are then conceived with respect to mainly temperature

and neutron flux spectrum.
Latter investigations turned out to be very complicated tasks because zirconium alloys properties have proved to be influenced by matrix composition and grain sizes. Secondary precipitate phases evolution under irradiation is a key point in determining mechanical properties and corrosion behaviour.
Nuclear reactor technology experience shows that matrix features vary after several irradiation cycles and neutron flux induced phenomena are planned to be investigated among JHR material tests. Microstructure of zirconium alloys, for instance Zr-4 and M5 in which significant amounts of additive are dispersed, can be irradiated and then analyzed by means of X diffraction or gamma radiography.
Previously explained experimental capabilities are interesting for vessel and internal components materials - nevertheless stainless steel cladding for Gen IV reactors are studied as well. Swelling due to fast ($E > 1$ MeV) and epithermal ($E > 100$ keV) neutron spectra are very important as well as toughness variation. Therefore it is planned to design devices in which spectrum parametrical tests will be available and the flux ratio between the two energy groups will be set by the operators.
Material irradiations are envisaged to be performed in core for internals and reactor core structures. Conversely, pressure vessel steels which are concerned by much lower ageing rates (of the order of 0,1 dpa/year and even less) are planned to be tested taking advantage of the remaining fast neutron flux available in the reflector. Irradiation combined with thermal effects - such as creep and ageing - are supposed to be studied for different temperatures and operating conditions.
There is a need to assess the behaviour under irradiation of a wide range of structural materials such as graphite (VHTR and MSR), austenitic and ferritic steels (VHTR, SFR, GFR, and LFR), Ni based alloys (SCWR), ceramics (GFR). These innovative structural materials are often common to fission and fusion applications. Experimental irradiations have to be carried out in order to study microstructural and dimensional evolution, but also the behaviour under stress.
Cladding and internals materials are then analyzed ranging from operative to accidental scenario configurations. JHR experimental data will be a relevant reference for selection, qualification, optimization, processing, lifetime assessment, licensing and abnormal operation tests both for safety regulators and industries.

1.4.2 Nuclear Fuel Development

Among JHR objectives, nuclear fuel technology research is aimed at developing new materials and at enhancing the existing ones. Fuel properties are typically studied taking advantage of thermal representative neutron spectra for LWR. In fact within JHR beryllium reflector, both fixed and moving experimental locations allow different kinds of fuel tests. Foremost, it is worth to notice that thermal hydraulic separation of device loops with respect to the core one assures safe and flexible experimental management. So it is possible to reproduce a lot of operational conditions namely PWR, BWR, and VVER tun-

ing pressure and temperature parameters of the single cooling loop. HTR environments are created by means of gas circuits properly connected to chemical facilities. In addition, heavy water cooling may allow CANDU operational simulations for HWR reactor technology. JHR is so capable to support Gen II and Gen III nuclear power plants as far as fuel optimization, property improvement and resources exploitation are concerned.
Fixed and moving positions inside the reflector are utilized to reproduce LWR conditions, CANDU heavy water cooled and fast reactor chemical environments. Some 20 fixed slots are available with external maximum dimension of about 100 mm. One particular position may host up to 200 mm large test devices.
JHR reflector may host up to 6 moving structures in order to perform transient tests such as power cycling and neutron flux stress. These performances are particularly useful to simulate reactor load follow operations. Moreover, power ramping reproduces fuel behaviour during unexpected control rod withdrawal. For this last purpose, it is possible to reach linear powers up to 600 W/cm even with a very low content of fissile materials in order to simulate very high burnup fuels. Achievable power ramp levels range from nominal 200 W/cm/min up to 700 W/cm/min just changing sample distance from the core and then flux intensity within the fuel. It is possible to achieve a maximum velocity of some 50 mm/s using a test slot of about 350 mm depth (Dousson et al., 2012).

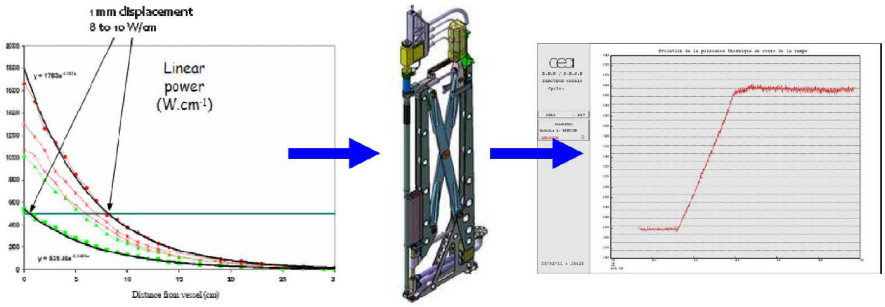

Figure 1.12: Simulation of power transients and ramps (Courtesy by CEA)

It is worth to highlight that irradiation in research reactor is a necessary stage for fuel study and development. Foremost a large amount of small samples are irradiated in order to perform microstructure analysis with respect to specific system parameters (fission rate, temperature, and lattice).
Then a first selection is done and just the samples which seem to be able to cope with the targets are considered. General behaviour and macroscopic laws are investigated thanks to different on-line measurements and multi-effect experiments. Long time irradiations are realized in order to reach comprehensive results.
The third step is very close to industrial characterization and the fuel is tested in contexts close to service conditions. Different burnup histories and reactivity variations, as well as different linear heat rate simulations will be available in JHR (Parrat et al., 2009).
Concerning mechanical and performance tests, several incidental and accidental conditions need to be verified and JHR is capable to guarantee normal and abnormal condi-

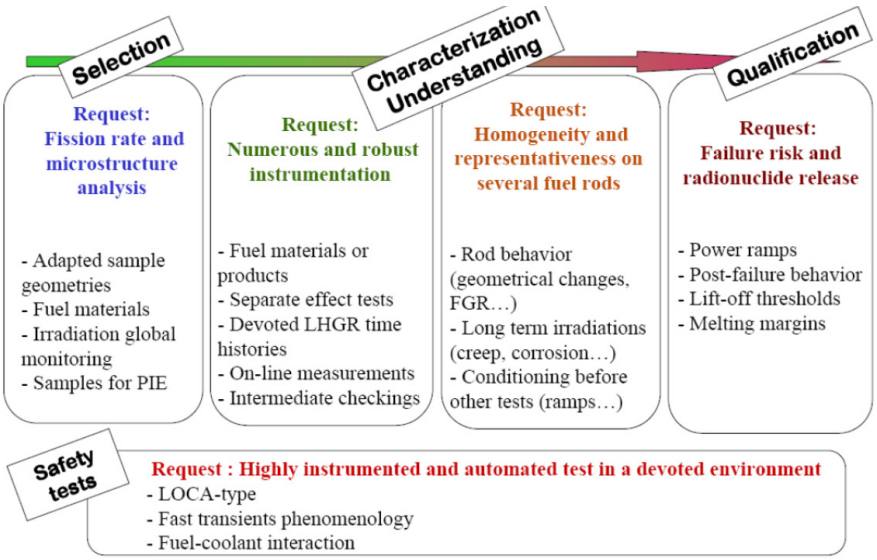

Figure 1.13: Different phases in fuel research

tions test channels. For instance, LOCA and rod failure experiments are conceived to be realized in dedicated locations.
Regarding existing fuel optimization, mainly uranium and uranium-plutonium oxides and MOX fuel will be studied even up to high enrichment ($> 5\%$). New microstructure and geometry are under discussion for JHR tests.
Burnable poisons such as gadolinium and erbium are interesting for safety criteria and microstructure features.
Challenging performances are expected from over cladding breach operations and steep power ramps. Burnup improvement is also a key point since sustainability and economical issues about fuel are getting more and more crucial.
It is worth to underline that reduction of fission gas release is a major target in fuel performances enhancement since one of the most important upper limitations to burnup concerns fission products gas accumulation in high burnup fuel rods. Several fission gas products are planned to be analyzed thanks to on-line laboratories close to reactor pool in Reactor Building.
Innovative development of a new generation of fuels, which resists to high temperatures and fast neutron flux in different environments, is necessary for the development of future Gen IV reactors. These new fuels need to be characterized and qualified in research reactors as well.

1.5 Experimental Capacity

JHR experimental capability ranges from material structural irradiations to fuel performances analysis. Then several apparatus have been developed in order to cope with

these objectives (Colin et al., 2012).
The present study is focused on fuel-loaded reflector test devices since significant power is released in fissile samples, anyway JHR is designed to carry out many experiments. Some devices dedicated to material testing are listed hereafter:

- CALIPSO and MICA devices are expected to be located in the core to exploit fast neutron spectra for cladding and core internal structures. Liquid metal NaK coolant loops are conceived and particular thermal hydraulic conditions are studied in order to change temperature conditions taking advantage of a flat profile thanks to metal conductivity features. They are planned to utilize both forced (CALIPSO) and natural (MICA) convection
- Various sample holders are designed for precise objectives - such as creep and swelling analyses. In order to meet requirements for strain tests with multi-axial mechanical loadings imposed to structural materials samples, a sophisticated sample carrier MELODIE has been designed for elevated temperature environments creep experiments. Manufacturing phase is ongoing and a prototype is planned to be tested in OSIRIS reactor.
- An adaptation of MICA with helium environment instead of NaK allowed to perform strain test (CEDRIC experiment in OSIRIS) for ceramic materials, SiC/SiC compounds was tested
- vessel component material qualifications are carried out in OCCITANE experimental device. Here pressure vessel representative dpa rates are reached in a temperature-controlled representative framework (in the reflector)

Other test devices are dedicated to fuel behaviour study. MADISON is conceived for fuel testing under nominal conditions and ADELINE is aimed at fuel testing under incidental situations. The latter will be described in next sections. Moreover, LORELEI device is dedicated to safety simulations concerning LOCA scenarios. Fissions product inventory is reproduced thanks to proper irradiation periods and then loss of coolant is induced controlling thermal hydraulic parameters. Steam is injected and cladding balloning and burst are analysed. Radiological and mechanical effects of multi-phase interactions are simulated within this apparatus.

1.5.1 MADISON Test Device

MADISON device (Multi-rod Adaptable Device for Irradiations of experimental fuel Samples Operating in Normal conditions) is designed to perform fuel tests concerning PWR, BWR and VVER reactor technologies. It can embark 4 fuel pins (even 8 pins capacity is conceived) and reproduce normal operating conditions not aiming at clad failure. In order to exploit a proper thermal neutron flux it is placed inside the JHR reflector. Nominal reactor operation conditions are achieved also through an independent loop in which representative thermal hydraulic and chemical conditions are set up (PWR conditions achieved through pressure of some 160 bar and temperature of about 320°C). Different

slow power transients are induced thanks to a moving structure whose distance from JHR core is controlled to modify neutron flux within the fuel samples. MADISON is expected to study either slow power slopes or long period irradiations (up to 3 years). Fuel material properties (microstructure, fission gas release, mechanical features) are investigated with respect to burn-up and linear heat generation rates. Clad corrosion are also interesting topics for long irradiation tests. (Roux et al., 2010).

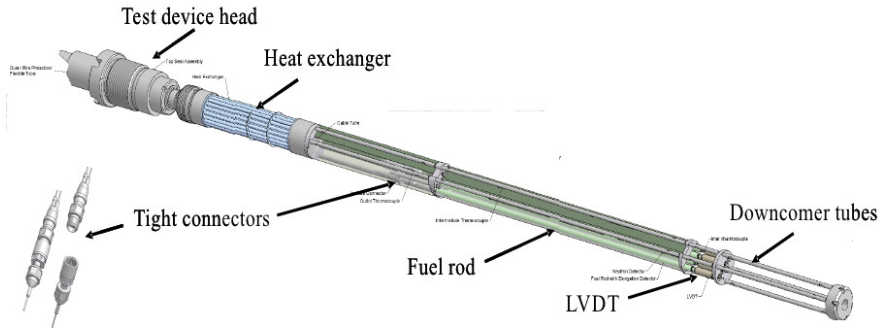

Figure 1.14: MADISON test device layout (Courtesy by CEA)

Very homogeneous neutron irradiations as well as high precision measurements are significant features of this device. Nominal linear power can reach about 400 W/cm even for high burn-up fuels allowing ageing process faster than what occurs in nuclear power plants.
MADISON is going to perform different kind of experiments:

- selection tests to irradiate and compare innovative samples
- characterization tests to irradiate few samples and to obtain physical information or to improve our knowledge about phenomena involved in the irradiation process
- qualification and validation tests for reactor operative conditions

This device is capable to utilize several JHR facility apparatus and examination tools. MADISON design takes advantage of important collaborations between French CEA and IFE Halden expertise which started from domestic know-how to reproduce in JHR an innovative and challenging loop. Design and feasibility phases are completed; realization and manufacturing stages are ongoing.

1.5.2 ADELINE Test Device

ADELINE experimental device is conceived in order to perform single LWR fuel pin tests concerning up to limit and incidental scenarios. It is hosted on a moving structure placed within the reflector area. Rod internal over-pressurization and free gas sweeping, as well as fuel centre melting approach, are investigated since clad failure configuration is allowed in this apparatus. Then precise measurements in clad failure timing and linear heat generation rate related to incidental situations are achieved in this device.

Moreover, normal conditions after clad failure are envisaged since the loop is designed to operate with contaminated coolant. Fission gas release during transients is detected by Fission Product Laboratory instrumentation through on-line gamma spectrometry and delayed neutron detection techniques. In addition, permanent purification and radiology controls are performed on the out-of-pile part of the loop. In order to limit the amount of contaminated coolant a jet pump is installed inside the device. The thermal hydraulic and chemical representative environment are achieved for what concerns failure simulations. ADELINE apparatus is placed on reflector moving structure to set thermal flux and then power levels. Typically both PWR, BWR and VVER technologies are studied and either UO_2 12% 235U enriched fuel or MOX 20% Pu/(Pu+U) enriched fuel are utilized.
Moving structure allows power cycling or power ramps. As an example, the foreseen experimental protocol may induce a first irradiation plateau (1 day up to 1 week) at a linear power of some 100 W/cm; then a ramp is induced ranging from 100 W/cm/min up to 700 W/cm/min. Furthermore a high power plateau is kept for about 24 hours at about 620 W/cm. As explained before, the facility design allows withstanding clad failure during this procedure (JHR Status Report 2011).

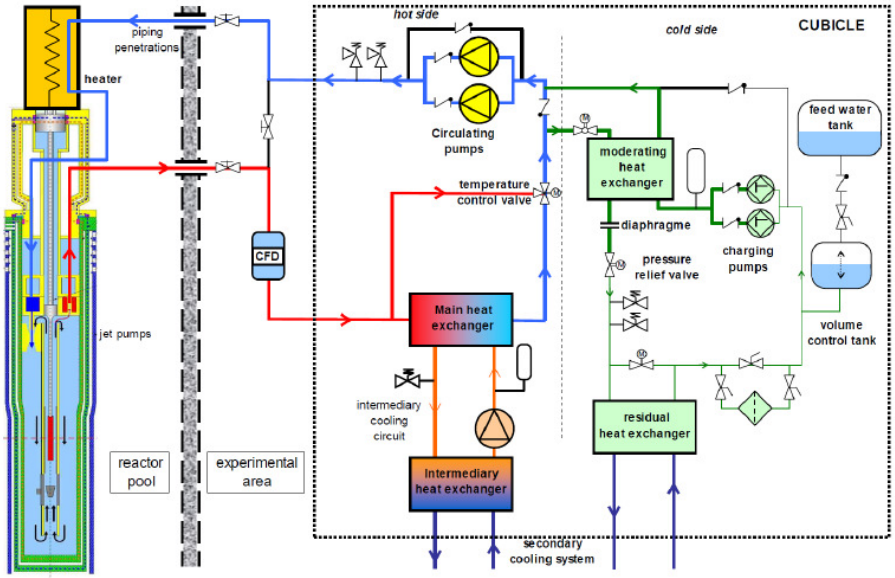

Figure 1.15: ADELINE test device layout (Courtesy by CEA)

1.5.3 MOLFI Test Device

Medical radioisotopes production and procurement is becoming a more and more strategic issue within the framework of worldwide healthcare system. Nuclear physics applications have allowed precise imagining and effective therapies for twenty years. Nuclear medicine diagnostics involves several kinds of radiation and procedures taking advan-

tage of unstable artificial nuclei undergoing decay. In this branch of medicine, the most important radioisotope is Technetium-99m and it is used nowadays in around 20 millions diagnostic procedures (Verbeek, 2010).
Concerning these needs, JHR is expected to be able to supply about 25% of European needs up 50% in case of critical procurement scenarios (Alberman et al., 2010).
MOLFI device is then conceived to host targets with significantly elevated enrichment level up to 93% in U235. A low enriched uranium version is under development in order to replace the previous design. Molybdenum-99, which is present in irradiated targets since it is generated as fission product, is then delivered to pharmaceutical plants and extracted by means of nuclear chemistry techniques. Decay process induces this parent nuclei to transmute into the daughter Technetium-99m that is provided to end users for utilization, within the framework of health care system (Carassou et al., 2010).

Chapter 2

Safety Requirements and Study Presentation

2.1 Control System Features

Nuclear reactors and facilities are complex technological installations which involve many procedures for operation and maintenance as far as all performed activities are concerned.
Safety analysis for nuclear plants regards all the tasks, procedures and design features which are necessary to avoid or to control all events that may induce significant radioactivity release with respect to operators and the public at large. The objective is to reduce all possible dangerous interaction of the nuclear plant with the environment, even in case of damage or unexpected system fail.
Nuclear engineering and design practices have been massively influenced by accidents and plant failures occured since nuclear energy has been exploited for civil purposes. Nowadays, every installation is conceived and operated according to peculiar features and safety procedures are envisaged.
JHR material testing reactor requires particularly versatile operative procedures since it is conceived to carry out many experiments at the same time optimising the test device fleet.
For this reason, control system has to face multiple needs and integrate many components:

- **Reactor control system** which is responsible for reactor operation concerning piloting and safey procedures, machine-user interface and supporting information to operators.
- **Experimental devices control system** that accomplishes all management functions for test devices. In-pile part is devoted to piloting and safety functions as well as test on-line analysis. Out-of-pile part regards probes and detectors concerning loops and connections interacting with different laboratories.

These control systems have been designed to manage accidental and incidental events without interfering each other. Both of them are conceived to be flexible and to support new experimental devices installation.
Reactor control system may integrate even experimental control system in order to process external inputs coming from device failures or unexpected parameter perturbations. Relevant separation is made between piloting and safety instrumentation, both in utilization procedures and material devices. Particular optimisation required optimal reactor-device coupling procedures to reduce operational costs, enhancing testing capacity both for fuel irradiation and radioisotope production.

2.2 Defense-in-Depth Levels

The criterion which permits taking into account safety analysis starting from the very first design phases is the so-called defense-in-depth approach. Instrumentation and control as well as normal plant components are able to withstand failures and incidental or accidental events are foreseen by design.
JHR plant characteristics regard four levels of such a safety defense which rules procedures about design, construction, operation and maintenance.

- **First Level**: it mainly concerns normal operational conditions. The aim is to conceive a system able to withstand their own failures. It is accomplished through design simplifying and, possibly, taking advantage of proven technology. Anomalies are supposed to remain limited withouht triggering unsafe events: the reactor parameters are kept below normal thresholds
- **Second Level**: it implies that the nuclear installation is equipped with several detectors related to significant physical quantities which interact with plant management systems. The latter are capable to adjust operative conditions in order to bring back to normal values the parameter which has just failed. This level is interested by normal and expected transients or predictable incidental sequences. This is a first system self-regulation response
- **Third Level**: it envisages several incidental or even accidental events which are considered by design. Safety control systems are then considered to lead the reactor to safe conditions. These systems are diversified in a redundancy approach. Active technology is utilized but passive or inherently safe devices are preferred.
- **Fourth Level**: some accidental situations characterised by a very low probability to occur are considered. Particular safety devices or complementary procedures are then conceived. Severe scenarios with cladding oxidation and melting are considered, fuel degradation and release or explosions are here concerned. Some accidents have to prove to be managed by the system safety devices or they may be excluded as not realistic to occur, if deterministic evaluation is provided.

The fifth level of the defense-in-depth does not impact plant design since is about external release and thus just evacuation plans and civil procedures are eventually concerned. Protection is devoted to preserve three system barriers wich protect fuel preventing release:

- First Barrier: cladding preventing fuel and fission products release
- Second Barrier: primary cooling loop piping preventing radioactive materials or even contaminated water to escape
- Third Barrier: main reactor building tightness which prevents even volatile nuclides to get released in the environment

Protection objectives of the previous barriers is the criterion to define particular Safety Equipments which are important to maintain reactor in safe conditions.
Safety equipments are characterised and defined as follows:

- Its failure may induce incident or accident events with radiological consequences
- Its operation is necessary to reduce and limit effects of incidental or accidental conditions
- They are key components to detect internal failure or damage wich induce one of previous effects
- Its function may be to control and provide a system response to previous listed accidents or incidents

2.3 Working Situations Classing

All operating conditions the system may face during possible situations are supposed to be referred to as starting point which is an initial event and a series of different sequences bring the system to a final state according to safety objectives. Starting conditions are classed and grouped in a conservative way and for each group particular safety limits are respected. This event classing allows to design and configure control system and devices in order to provide defined safety procedures for initial event groups.
Starting event classing is divided in two main groups: **Working Situations** and **Risk Limitation Situations**.
Working Situations may correspond to incidental or accidental events with significant probability to occur and are related to third level defense-in-depth categories. They are divided as follows:

- Working Situation category 1 (WS1): normal situations are considered here
- Working Situation category 2 (WS2): incidental situations are accounted for
- Working Situation category 3 (WS3): accidental situations with low likelihood to occur
- Working Situation category 4 (WS4): accidental situations defined as hypothetical with very low probability to take place

Event classing in previous categories is made following a deterministic approach and expert evaluations, taking into account frequency related to every initial event.

Frequency > 1/year	Working Situation Category 1 (WS1)
10^{-2}/year $<$ Frequency < 1/year	Working Situation Category 2 (WS2)
10^{-4}/year $<$ Frequency $< 10^{-2}$/year	Working Situation Category 3 (WS3)
10^{-6}/year $<$ Frequency $< 10^{-4}$/year	Working Situation Category 4 (WS4)

Table 2.1: Working Conditions classing frequencies

In addition, concerning the fourth defense-in-depth level, events with very low probability to occur are classed within Risk Limitation Situations:

- Complex Situations (CS): situations concerning previous conditions are here grouped, in this case redundancy failure of a key component is also considered. These events are accounted for in view of severe accidents prevention.
- Controlled Severe Accidents (CSA): very unlikely events are here grouped mainly inducing to fuel melting and fission product release. Explosions and severe installation degradation are analysed too in this class.
- Excluded Severe Accidents (ESA): all event chains and initial causes which are retained not possible to occur and then classified as excluded by design. They are evaluated on deterministic basis and considerations.

Such a classification has brought to a twofold approach in scenario simulations. In fact, components responses and plant parameters involve uncertainties and sometimes conservative data may bring to overestimations which are too elevated for an exhaustive plant analysis. For this reason, the following approach for initial events effect evaluation has bee retained:

- Normal Situations (WS1): normal operations and conventional transients involve just control system actions by design
- Incidental or Accidental Situations (WS2,3,4): for these categories control system design is based on conservative grouped initial events, elevated uncertainties are considered as well as power transients data. One failure about the most important control device is always assumed to hold.
- Risk Limitation Situations (RLS): concerning these events, control component design and simulations regard non conservative but best estimated parameters. Power transients features are evaluated starting from realistic data. No failure is accounted and all components are supposed to properly work.

Demonstration regarding radioactive product release consistency with safety objectives is mandatory requested and performed for every possible operational situation.
Risk analysis criteria account for product of damage and frequency - namely the risk. Provided a situation in which elevated release condition is estimated, technological design feedback are aimed at risk reduction. In fact, a twofold approach is pursued. First, event

Working Situation	Frequency (Initiating event)	Safety Objectives	
		Workers	Public
WS1: Normal	$F > 1/year$	10 mSv/year	Annual dose: 1 mSv
WS2: Incidental	$10^{-2}/year < F < 1/year$	10 mSv/inc.	Dose per incident 0,1 mSv
WS3: Accidental (low probability)	$10^{-4}/year < F < 10^{-2}/year$	30 mSv/acc.	Dose < 10 mSv (over 1 year) Other additional constraints...
WS4: Accidental (hypothetical)	$10^{-6}/year < F < 10^{-4}/year$	100 mSv/acc.	
Severe Accident or Excluded Situations	$F < 10^{-6}/year$		Dose < 10 mSv (over 1 week) Other additional constraints...

Table 2.2: Safety objectives concerning external dose release

frequency may be lowered increasing plant and system redundancy or improving materials and components performances. By contrast, consequences and impacts are possibly reduced acting on safety features and control devices in terms of additional confinement or safety apparatus injections.
Concerning test devices which are the subject of the present thesis, safety analyses are expected to investigate all possible device-core interactions. The latter have to remain acceptable during all possible incidental and accidental scenarios. Either impact on the emergency shutdown system or residual power cooling system have to be excluded by design. Otherwise, design team must provide additional lines of defence in order to reduce event frequeny and/or event consequences.
If the failure of the test device structures could lead to a strong impact on the core (residual power core cooling system or emergency shutdown) or if the public dose is higher than 1 mSv, the test device must be equipped with 2 safety barriers - namely 2 tight structures with high manufacturing quality.
Very important topics concerning test device safety analysis are thermal power transients during Normal Shutdown and Safety Shutdown. It involves the control system devices presented in the next section.
Therefore, the aim of this study deals with this power evolution and will be presented in sections 4 and 5.

2.4 Control System Devices

Reactor piloting and control is accomplished by means of reactivity measurement and management. JHR needs particular flexibility since flux delivering and sustaining is the objective of a material testing reactor hosting samples to be irradiated.
Reactivity management system is composed of following parts:

- moving control rods
  - 4 Pilot Rods
  - 4 Safety Rods

  - 19 Compensation Rods
- fixed control rods
- detectors and measurement chain systems
- all actions and procedures involved in reactor piloting
- ultimate systems for reactivity control

Fixed control rods are not expected to be always implied as standard procedure, although they may be implemented for highly reactive start-up core configurations. Soluble poisons are to be retained only as control strategy for ultimate accident or incident response.

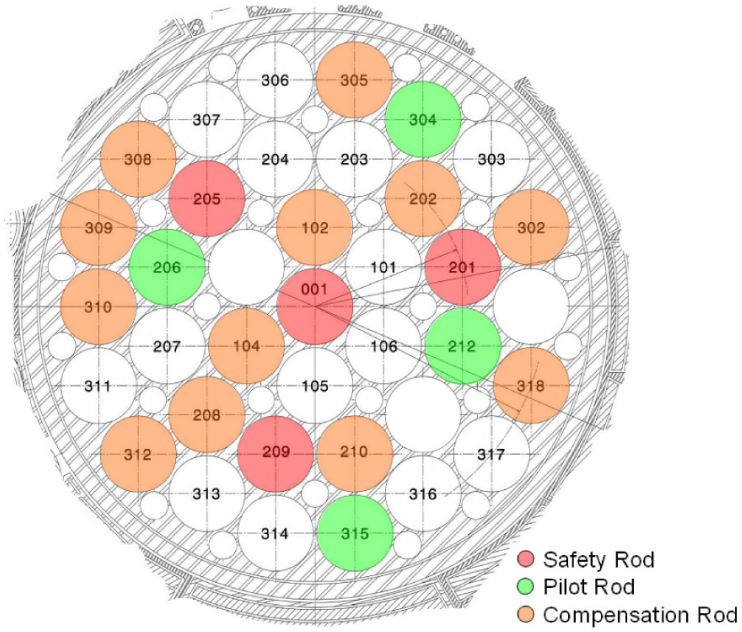

Figure 2.1: Control rod locations in core

2.4.1 Reactor Piloting and Service

First utilization of control rods and devices is for reactor piloting. It is necessary to provide a stable a constant neutron flux to all experimental locations. The objective of the reactor is to provide a pre-set neutron spectrum either thermal or fast with a certain duration.
Core total power needs to be controlled as well and criticality has to be maintained. Factors impacting reactivity of the system are considered. Experimental devices insertion provides anti-reactivity, or reactivity in particular for significantly enriched samples - such as MOLFI devices - and for that “compensation rods” are envisaged to compensate these reactivity effects.
In fact burnup and fission products buildup - in particular some neutron absorbing materials such as xenon and samarium - reach an equilibrium level during the first part of

the cycle and additional reactivity has to be provided by control rod extraction. Cooling water and fuel temperatures modify reactivity and pilot rods positions take into account some margins in the minimum insertion level possible.
These functions are expected to be performed by a cluster of 4 Pilot Rods. They are managed within a particular insertion interval to take advantage of a high differential worth. By design they have to prove to be sufficient for events belonging to WS1 and WS2 condition classes through:

- Power regulation and reduction: response procedure performed for WS1 and normal operation piloting
- Fast power decrease: safety measure to face WS2 events providing significant power reduction without utilization of Safety Shutdown
- Automatic Preventive Shutdown: procedure utilised for planned reactor shutdown without Safety Shutdown, for WS2 events or for incidental conditions in which power decresing is not sufficient to guarantee safety margins

Normal or fast power decrease without important antireactivity insertions are mainly provided in order to keep reactor in operation and enhance experimental capability and load factor. By contrast, Automatic Preventive Shutdown has been envisaged for all those situations in which the reactor is expected to reach very soon criticality again. Such cases may regard failures related to quick manageable maintenance procedures (electronic card substitution, out-of-service standby component start-up or system switching to alternative electrical source). A reduced amount of antireactivity introduced in the reactor allows operator to turn back to nominal conditions before xenon peak.
Since only 4 Pilot Rods are utilized, 4 remaining Safety Rods remain available to provide extra antireactivity as a backup solution. Automatic Preventive Shutdown manages Pilot Rods within a so called "operational interval". The margin at top is required since rods are supposed to remain close to core mid-plane reaching higher differential worth. Conversely, the bottom limit is envisaged in order to compensate for reactivity feedbacks due to reactor cooling down (mainly for Doppler effect and moderator density increase).
In order to bring back system to criticality after this shutdown, Pilot Rods are withdrawn up to piloting insertion and approach to criticality is attained by means of a Compensation Rod.

2.4.2 Reactor Safety Functions

The objective of safety purposes is mainly the reactivity control in every possible operational situation. Prompt criticality has to be avoided in all cases. Since the reactor presents low feedbacks coefficients, severe accident analysis implies only large rectivity injection prevention. Reactivity has to be maintained controlled as well in all reactor states such as: shutdown procedures, start-up procedures, nominal operations, power transients.
Maintenance processes have to be performed in safe way and control devices have to keep reactor subcritical in all fuel and components loading and unloading. Regarding

safety objectives, first barrier has to be mandatory protected as last safety level defense. For this reason event hot channel factor has to be kept above safety constraints. For all safety control rods management, both 4 Pilot Rods and 4 Safey Rods clusters are envisaged. They are inserted during:

- Normal Safety Shutdown
- Fast Safety Shutdown

Both the previous are invoked using Pilot Rods and Safety Rods but initial delay times are different. The shutdown ignition is operated by electrical alimentation cut-off regarding magnets keeping rods withdrawn. Control systems corresponding to these procedures are different for safety purposes. Normal Safety Shutdown is initiated by controlers and computer devices, Fast Safety Shutdown is directly started by neutron flux detectors in order to have a quicker response.
Situations envisaged for such a procedure are considered more relevant than previous ones. They may regard failures of important Safety Equipements or loss of electrical alimentation for instance. Manily such shutdown is foreseen also to follow an Automatic Preventive Shutdown if the first does not prove to insert sufficient antireactivity.
For all previously listed procedures, long term antireactivity involves xenon peak management and neutronic poison in-core concentrations change. Thus, Compensation Rods are supposed to be available for late insertions after a delay of about 2 hours. Core reactivity control is then completely assured respecting safety measures and keeping optimal level of reactor operations.

2.5 Objective of Present Study

JHR test devices are devoted to structural materials and fuel samples irradiation experiments. Basically, safety analysis of these devices is extremely important since irradiation features are very challenging and elevated temperatures are then attained. In addition, experiment conditions are worth to be properly monitored during all test phases in order to prevent failures which may interfere with other devices or normal reactor operations. Moreover, any incidental or accidental situations have to be confined to device and properly controlled.
In addition, irradiation devices presence imposes design team to envisage and take into account systems failure. Scenarios regarding these independent systems - for which heat decay concerns have to be considered - may range from normal transients up to severe conditions such as large breaks affecting cooling system loops.
Hence, even though structural materials sample holders are concerned by abnormal and accidental transients, fuel-loaded test devices have to be particularly analyzed since fissile samples are hosted within these facilities; then JHR design team asked for specific and more detailed calculations.
Power within these critical components is controlled by means of varying core reaction rates and flux level. On the contrary to the core itself, devices reactivity coefficients are

not always negative and in case of core control rod insertion - or a device damage - the main effect driving sample power release is core neutron irradiation and then core kinetics. Then in case of anomaly detection inducing dangerous consequences, core shutdown procedures have to be implemented. Thus, the effectiveness in terms of time device power decreasing is mainly related to instrumentation and control time responses acting on device power reduction.
In addition, some fuel samples are characterized by very critical thermal features which make them not capable to withstand severe transients. In fact, MOLFI devices are charged with UAl alloy targets with low heat capacity and fusion temperatures (about 660°C) operating at elevated linear powers of some 1500 W/cm. By contrast MADISON and ADELINE devices work with lower linear power around 400 W/cm but in this case it is possible to rely on higher ceramic heat capacity and fusion temperatures (around 2600°C).
Therefore, precise evaluations about transients induced in fissile samples by different shutdown procedures are very important to be performed in order to optimize management of these reactivity insertions.
Twofold neutronic aspects impact and determine device power decreasing. First, it is necessary to properly determine neutron population decreasing in terms of core kinetics thought of as neutron source. Moreover, flux shape distortion induced by control rod insertion influences power distribution within the reflector and then inside analyzed samples. Correct power response computing involves prompt and delayed neutronic effects. Gamma irradiation coming from core and delayed gamma produced by fission products decay is worth to be accounted for as well.

Chapter 3

Neutron Kinetics for Reactor Transients

The research topic of the present thesis is particularly aimed at power transients analysis of Jules Horowitz Material Testing Reactor as far as fuel-loaded reflector experimental devices are concerned. Since the reactor power is significantly elevated, the amount of energy deposited within these devices is consequently high and this feature requires to focus the attention even on the devices thought of as independent neutronic systems in order to perform a detailed description.
Neutron kinetics will be briefly revised to explain the model which has been conceived and utilized in the present study and to illustrate characteristics of this research work.

3.1 Elements of Nuclear Reactor Theory

The description of a nuclear reactor involves information about the interactions of neutrons present in the system and all the materials which may undergo different kinds of nuclear reactions. Neutron may be either scattered or absorbed depending on the probability of a certain reaction which is theoretically a function of the incident neutron energy and of its direction. This probability is called cross section since it is thought of as the area which the nucleus offers to the neutron imagined like a projectile flying towards a target.
Scattering reactions lead the incident neutron to change direction and velocity after the interaction and may be referred to as:

- **elastic scattering** when the total amount of kinetic energy of neutron and nucleus do not change after the interaction
- **inelastic scattering** occurs when a part of the incident neutron kinetic energy is transferred to the target nucleus to excite some energy levels and to be released in form of nuclear particle emission or photon generation

Conversely, if an absorption takes place, the neutron induces the target nucleus to increase its internal energy by means of the acquisition of the projectile kinetic energy and

of its bounding energy. This provokes a nuclear excitation and different possible neutron-induced reactions. In fact, the neutron is absorbed in the system and energy increase of the nucleus may cause it to reach energy thresholds for different reactions:

- **radiative capture** occurs when the acquired energy is emitted through photons
- **neutron production** takes place if the energy gained is sufficient to reach the magnitude of some neutron bonding energies which make them able to escape
- **fission reaction** is possible only for some heavy nuclei and it causes them to split in usually two parts if the energy delivered to the target is sufficient to exceed the binding forces and let the electrostatic repulsion to prevail.

This last process generates on average 2,5 neutrons and some 200 MeV of energy that may be deposited and recovered for power generation purposes. This neutron multiplication feature is utilized to induce the system to be self-sustaining and to perform a so-called chain reaction.
In order to utilize and properly control a nuclear reactor it is necessary to define the reaction rates which take place at a given time by whose balance the neutron population within the system is changed.
Provided a certain reaction probability concerning the amount of nuclei of some isotopes, the volumetric reaction rate depends on the quantity of neutrons scattering throughout the reactor.
The following Boltzmann equation states this balance referred to a given volume in phase space. Since the tendency for a reaction to occur regards neutron velocity and direction at a given place, the neutron flux is defined in such a phase space for every time.

$$\frac{1}{v}\frac{\partial\varphi}{\partial t} = -\hat{\mathbf{\Omega}}\cdot\boldsymbol{\nabla}_r\varphi - \Sigma\varphi + \iint \Sigma_s(\mathbf{r}, E'\to E, \hat{\mathbf{\Omega}}'\to\hat{\mathbf{\Omega}}, t)\varphi'\,\mathrm{d}E'\,\mathrm{d}\hat{\mathbf{\Omega}}' + \\ + \frac{\chi_p}{4\pi}\iint(1-\beta)\nu\Sigma_f(\mathbf{r}, E'\hat{\mathbf{\Omega}}', t)\varphi'\,\mathrm{d}E'\,\mathrm{d}\hat{\mathbf{\Omega}}' + \sum_{i=1}^{m}\frac{\chi_{d_i}}{4\pi}\lambda_i c_i + \hat{q} \quad (3.1)$$

In the previous equation, the objective is to determine the neutron flux $\varphi(\mathbf{r}, E, \hat{\mathbf{\Omega}}, t)$ accounting for several contributions due to fissions and losses induced by absorption and leakage. This is performed by means of a sort of a continuity equation related to a volume in phase space.
In operator form it yields:

$$\frac{1}{v}\frac{\partial\varphi}{\partial t} = -\underline{G}\varphi - \underline{\Sigma}\varphi + \underline{\Sigma}_s\varphi + \underline{M}_p\varphi + \sum_{i=1}^{m}\frac{\chi_{d_i}}{4\pi}\lambda_i c_i + \hat{q} \quad (3.2)$$

The different terms which appear in the Boltzmann equation are then listed and commented:

- $\underline{G}\varphi = \hat{\mathbf{\Omega}}\cdot\boldsymbol{\nabla}_r\varphi$: it is a streaming term which accounts for the net amont of neutrons entering a geometrical volume in phase space without modifying either velocity or direction

- $\underline{\Sigma}\varphi = \Sigma\varphi$: it takes into account all the processes which lead to neutron distruction referred to the considered volume. In this term all absorption reactions are accounted as well as scattering which induces a variation in energy and particle direction. In the latter case the neutron does not belong any more to the volume in phase space
- $\underline{\Sigma}_s\varphi = \iint \Sigma_s(\mathbf{x}, E' \to E, \hat{\mathbf{\Omega}}' \to \hat{\mathbf{\Omega}}, t)\varphi' \,\mathrm{d}E' \,\mathrm{d}\hat{\mathbf{\Omega}}'$: conversely it considers the neutrons incoming from other volumes since they change velocity after a scattering event which leads them to fall into the considered phase space region
- $\underline{M}_p\varphi = \frac{\chi_p}{4\pi} \iint (1-\beta)\nu\Sigma_f(\mathbf{r}, E'\hat{\mathbf{\Omega}}', t)\varphi' \,\mathrm{d}E' \,\mathrm{d}\hat{\mathbf{\Omega}}'$: this contribution adds all neutrons generated from fission reactions. They are suddenly emitted and with no delay - namely they are called prompt neutrons - and they represent a fraction corresponding to $(1-\beta)$ of the total produced. The integral, carried out over all the domain in energy and direction, takes into account all neutron generated at a given position for all possible velocities. The prompt energy neutron distribution $\frac{\chi_p}{4\pi}$ then selects only those belonging to the considered phase space volume.
- $\underline{M}_{d_i}\varphi = \iint \beta_i\nu\Sigma_f(\mathbf{r}, E', \hat{\mathbf{\Omega}}', t)\varphi' \,\mathrm{d}E' \,\mathrm{d}\hat{\mathbf{\Omega}}'$: in the same way as before, this term accounts for delayed neutron productions
- $\sum_{i=1}^{m} \frac{\chi_{d_i}}{4\pi}\lambda_i c_i$: a fraction of neutron released in fission reactions is deferred in time since it appears thanks to neutron precursors decay process. Some groups are listed with particular decay behaviours. Neutron produced by activities of these families are emitted depending of distributions $\frac{\chi_{r_i}}{4\pi}$ and the corresponding fraction is added to the considered phase volume
- $\hat{q}$: finally, an independent neutron source may be present within the system. It is considered in this term which may depend on time and on every coordinate of phase space

The neutron precursor balance is then stated thinking that during every fission a fraction equal β_i of produced neutrons are stocked and released with time delays that vary from some microseconds to some seconds.

$$\frac{\partial c_i}{\partial t} = -\lambda_i c_i + \iint \beta_i\nu\Sigma_f(\mathbf{r}, E', \hat{\mathbf{\Omega}}', t)\varphi' \,\mathrm{d}E' \,\mathrm{d}\hat{\mathbf{\Omega}}' \tag{3.3}$$

It is worth to be underlined how the time behaviour is ruled by the decay constants and that these deferred emissions allow reactors to be easily controlled due to this delayed response of the system.
An equivalent operator expression may be formulated as follows:

$$\frac{\partial c_i}{\partial t} = -\lambda_i c_i + \underline{M}_{d_i}\varphi \tag{3.4}$$

Finally, these $m+1$ equations are coupled with proper boundary conditions regarding the system domain. In fact it is always possible for convex geometries that

$$\varphi(\mathbf{r}, E, \hat{\mathbf{\Omega}}, t) = 0$$

In some cases, even the initial concentrations of delayed neutron precursors $c_i(\mathbf{r}, t)$ may be imposed. The solution of Boltzmann equation is possible only in some simple cases. It allows a detailed description of the entire system as far as dynamic behaviour in phase space is concerned. Such an exhaustive description of the system is always referred to as spatial dynamics and it allows the most comprehensive reactor analysis.

3.2 The Neutron Transport Equation

Reactor studies are often aimed at designing self-sustained systems in which a neutron population balance is reached thanks to fission reactions occurring within nuclear fuel. A system is referred to as "critical" if homogeneous and time-independent neutron transport equation coupled with surface boundary conditions has a proper non vanishing solution in the domain. In fact, system between eqs. (3.1) and (3.3) may be turned into a static formulation in order to investigate if geometry of the system and its material composition allow a time-independent angular flux distribution.
If it is the case, previous Boltzmann equation leads to a well defined static neutron flux:

$$\underline{L}\varphi = \underline{M}\varphi \tag{3.5}$$

where

$$\begin{aligned} \underline{L}\varphi = \hat{\mathbf{\Omega}} \cdot \boldsymbol{\nabla}_r \varphi + \Sigma\varphi - \iint \Sigma_s(\mathbf{r}, E' \to E, \hat{\mathbf{\Omega}}' \to \hat{\mathbf{\Omega}}, t)\varphi' \,\mathrm{d}E' \,\mathrm{d}\hat{\mathbf{\Omega}}' \\ \underline{M}\varphi = \frac{\overline{\chi}}{4\pi} \iint \nu\Sigma_f(\mathbf{r}, E'\hat{\mathbf{\Omega}}', t)\varphi' \,\mathrm{d}E' \,\mathrm{d}\hat{\mathbf{\Omega}}' \end{aligned} \tag{3.6}$$

are respectively defined as leakage and multiplication operators.
Basically, it is not obvious that a geometry - namely surface leakage - coupled with a certain material composition may bring to a criticality configuration. The mathematical consequence is that the only flux which satisfies boundary conditions and static equations is vanishing everywhere in the domain.
Conversely, it is meaningful to correct some system parameters in order to restore a sustaining neutron balance. This may be pursued by means of introducing a coefficient to change some neutronic features. This is the reason why an eigenvalue method is operated. The usual approach simulates a modification in the average attitude of the materials in neutron multiplication.
Therefore, the previous eq. (3.5) and related boundary conditions are turned into an eigenvalue problem as follows:

$$k\underline{L}\phi = \underline{M}\phi \tag{3.7}$$

for which the only non vanishing solution consists of a series of eigenfunctions matched with respective eigenvalues, more precisely:

$$k_i\underline{L}\phi_i = \underline{M}\phi_i \tag{3.8}$$

These functions represent all possible neutron fluxes as far as boundary conditions are concerned. Only the first eigenvalue and related eigenfunction have a physical meaning, since only this flux is non-negative over all the domain.
Therefore this states that a modification of the system is needed in order to sustain a constant neutron flux. The eigenvalue is usually thought of as a rate by which the multiplication coefficient ν in transport equation needs to be changed to reach criticality.
This first eigenvalue is defined as the effective one and it is the k_{eff}. It is worth to highlight the amount of information about the reactor which are summarized in this parameter. If it turns out to be greater than unity the multiplication has to be reduced to attain criticality multiplication $\nu_c = \nu/k_{eff}$ and so the system is referred to as "supercritical".
By contrast, if it is less than unity, criticality parameter about multiplication is increased compared to the real one and the system is said to be "subcritical".
The k_{eff} may also be seen, in a sense, like a neutron population generation ratio. New produced neutrons are compared to all the previously generated. This explains better the larger or less than unity meaning.
If k_{eff} were exactly unitary, system modification would not be necessary. The calculated flux would coincide with the static and self-sustaining neutron population.
If it is not the case, the neutron flux - obtained as eigenfunction - is not the static flux within the system since no time-independent solution is possible for such a given geometry and material composition. Therefore, the first eigensolution represents a static flux obtainable in a system which is similar to the real one but a multiplication change is made.
In fact, it is useful to consider the entire eigenfunction set related to all possible neutron transport equation eigenvalues. Completeness of this set in terms of functions space basis has been proved to be not consistent. Fundamental reactor physics dissertations and modelling (Henry, 1975) state that it is common practice to deal with a sort of completeness adding all eigenfunctions related to vanishing eigenvalue.
Such a completeness is then missing unless this second eigenfunctions set is taken into account. Therefore, any continuous function - obeying to flux boundary conditions - is likely to be expanded in eigenfunction series - as neutron flux. Extending such a concept, it is possible to state even series expantion for time-dependent flux provided time-dependent related coefficients, as follows:

$$\varphi(\mathbf{r}, E, \hat{\mathbf{\Omega}}, t) = \sum_{i=1}^{+\infty} c_i(t)\phi_i(\mathbf{r}, E, \hat{\mathbf{\Omega}}) + \sum_{j=1}^{+\infty} c_j^0(t)\phi_j^0(\mathbf{r}, E, \hat{\mathbf{\Omega}}) \tag{3.9}$$

In the previous, first part of the basis regards eq. (3.8) and the second concerns particular case $\underline{M}\phi_j^0 = 0$ at which an infinity of solutions is associated.
Every term ϕ_i or ϕ_j^0 is the associated to a state - eingenstate - of the reactor. As multiplication occurs, system generates neutrons and operates on every component - namely state - of neutron population and it reproduces itself as far as the corresponding eigenvalue is concerned. Then the smallest ones disappear very rapidly and the first component still remains significantly elevated only if the related eigenvalue is in the proximity of unity.

Needless to say, vanishing eigenvalue terms of the basis die away really soon.
For eigenvalues close to unity, the first term in such a series is slowly decreasing or increasing and then the static flux is sufficiently representative and gives the best possible information concerning static neutron induced reactions within the system.
Static studies about nuclear reactor systems are, for this mathematical reason, the fundamental approach in neutronic characterization and design.

3.3 Adjoint Neutron Transport Equation

Considering static neutron transport equation, a particular importance is given to a formulation which is adjoint to the previous analysis. Then objective is to create a tool aimed at neutron flux description and representation even for the time-dependent one. For such a study, first eigenfunction may be not enough precise especially for kinetics evaluation purposes. In addition, perturbation theory and variational calculation methods utilise adjoint flux as well.
The interesting feature is that, in a sense, solutions of adjoint neutron transport equation are orthogonal to solutions of the direct neutronic problem.
In fact, if $\underline{A}$ is a well defined functional operator, η and μ are continuous and well-behaved functions with respect to a certain domain about a set of variables referred to as ξ, then an inner product may be presented as follows:

$$\left(\eta, \underline{A}\mu\right) = \int \eta(\xi)\underline{A}\mu(\xi)\,\mathrm{d}\xi \tag{3.10}$$

where the integral is carried over the entire definition domain of ξ and the operator is then applied to the second term. Only real quantities are considered hereafter and thus conjugate functions are not dealt with.
If an operator $\underline{B}$ is Hermitian or self-adjoint, a particular relation holds:

$$\left(\eta, \underline{B}\mu\right) = \left(\mu, \underline{B}\eta\right) \tag{3.11}$$

In addition, eigenfunctions are orthogonal and related eigenvalues are always real.
Basically, some operators are not self-adjoint, as it is the case for some terms in neutron transport equation. Provided a regular operator $\underline{O}$ and coupled boundary conditions, say C, it is straightforward to define a new set of boundary conditions, C^+ and a properly defined operator $\underline{O}^+$, which is referred to as "adjoint" to $\underline{O}$ which fills the following:

$$\left(\psi, \underline{O}\varphi\right) = \left(\varphi, \underline{O}^+\psi\right) \tag{3.12}$$

for every φ and ψ functions belonging to C and C^+ boundary conditions respectively. A sort of dual space is created by means of operators and boundary conditions. In fact, they link two sets of functions.
Starting from the usual neutron transport equation in the time-independent form, it is possible to introduce the respective adjoint equation such as:

$$k_i\underline{L}\phi_i = \underline{M}\phi_i \qquad \Rightarrow \qquad k_j^\dagger\underline{L}^\dagger\phi_j^\dagger = \underline{M}^\dagger\phi_j^\dagger \tag{3.13}$$

Every adjoint operator is obtained by means of the previous definition (3.12) and a boundary condition of vanishing outcoming adjoint flux is imposed, the physical meaning will be explained later.
A series of eigenfunctions - namely adjoint solutions - is deduced and a corresponding series of eigenvalues is obtained. In order to highlight some important features, it is possible to multiply both sides of direct and adjoint equations by adjoint and direct flux respectively taking the inner product.
Direct equation gives the following statement:

$$k_i\big(\phi_j^\dagger, \underline{L}\phi_i\big) = \big(\phi_j^\dagger, \underline{M}\phi_i\big) \quad \Rightarrow \quad k_i\big(\phi_j^\dagger, \underline{L}\phi_i\big) = \big(\phi_i, \underline{M}^\dagger\phi_j^\dagger\big) \tag{3.14}$$

in which the definition of adjoint operator is applied.
Conversely, adjoint equation yields the following:

$$k_j^\dagger\big(\phi_i, \underline{L}^\dagger\phi_j^\dagger\big) = \big(\phi_i, \underline{M}^\dagger\phi_j^\dagger\big) \quad \Rightarrow \quad k_j^\dagger\big(\phi_j^\dagger, \underline{L}\phi_i\big) = \big(\phi_i, \underline{M}^\dagger\phi_j^\dagger\big) \tag{3.15}$$

Taking left-hand sides of eqs. (3.14) and (3.15) it is easy to find a relation between direct and adjoint eigenvalues and functions:

$$(k_i - k_j^\dagger)\big(\phi_j^\dagger, \underline{L}\phi_i\big) = 0 \quad \Rightarrow \quad \frac{k_i - k_j^\dagger}{k_i}\big(\phi_j^\dagger, \underline{M}\phi_i\big) = 0 \tag{3.16}$$

In the same way it is possible to find the following relations:

$$(k_i - k_j^\dagger)\big(\phi_i, \underline{L}^\dagger\phi_j^\dagger\big) = 0 \quad \Rightarrow \quad \frac{k_i - k_j^\dagger}{k_j^\dagger}\big(\phi_i, \underline{M}^\dagger\phi_j^\dagger\big) = 0 \tag{3.17}$$

Thus, the most significant property about adjoint flux introduction is presented. For a given flux ϕ_i in eigenfunctions spectrum, corresponding $\underline{L}\phi_i$ function is then orthogonal to what is referred to "corresponding adjoint". Then by means of the first part of eq. (3.16) it is possible to match the adjoint eigenfunction $\phi_j^\dagger$ which is parallel to $\underline{L}\phi_i$ yielding a non-vanishing inner product. Following from eq. (3.16) respective eigenvalues must be equal. Therefore, indixes in direct and adjoint eigenfunctions will satisfy this criterion: $k_i = k_j^\dagger$ for $i = j$.
A peculiar relation is then highlighted for which direct and adjoint eigenfunctions are referred to as L-orthogonal or M-orthogonal. Hence:

$$\big(\phi_j^\dagger, \underline{L}\phi_i\big) = a_{ij}\delta_{ij} \quad \Leftrightarrow \quad \big(\phi_j^\dagger, \underline{M}\phi_i\big) = b_{ij}\delta_{ij} \tag{3.18}$$

Provided the same index, direct and adjoint eigenvalues are equal. For different indexes direct and adjoint fluxes are M- or L-orthogonal. Assumption has been made about neglecting the possibility to find more than one non-vanishing projection of a $\underline{L}\phi$ or $\underline{M}\phi$ on the $\phi_j^\dagger$ eigenvalues spectrum. Thus it is also possible to turn out a physical meaning for neutron adjoint flux:

$$\phi_j^\dagger \propto \underline{M}\phi - \underline{L}\phi \tag{3.19}$$

Above, it expresses something which is locally proportional to the difference between new generated neutrons and all the disappeared ones either through leakage or absorption reactions.
Conversely, the reciprocity relation brings to an equivalent statement:

$$\left(\phi_i, \underline{L}^\dagger \phi_j^\dagger\right) = c_{ij}\delta_{ij} \quad \Leftrightarrow \quad \left(\phi_i, \underline{M}^\dagger \phi_j^\dagger\right) = d_{ij}\delta_{ij} \tag{3.20}$$

The significant physical meaning of neutron adjoint flux is referred to as neutron importance. Searching for adjoint operators in Boltzmann equation and applying relation (3.12), it is easy to verify how scattering and streaming terms are not self-adjoint.
For every operator introduced in (3.1), the definition gives:

$$\begin{aligned}
&\left(\eta, \underline{G}\mu\right) = \left(\mu, \underline{G}^\dagger \eta\right) = -\left(\mu, \underline{G}\eta\right) \\
&\left(\eta, \underline{\Sigma}\mu\right) = \left(\mu, \underline{\Sigma}^\dagger \eta\right) = \left(\mu, \underline{\Sigma}\eta\right) \\
&\left(\eta, \underline{\Sigma_s}\mu\right) = \left(\mu, \underline{\Sigma_s}^\dagger \eta\right) \\
&\left(\eta, \underline{M}_p\mu\right) = \left(\mu, \underline{M}_p^\dagger \eta\right) = \left(\mu, \underline{M}_p\eta\right) \\
&\left(\eta, \underline{M}_{d_i}\mu\right) = \left(\mu, \underline{M}_{d_i}^\dagger \eta\right) = \left(\mu, \underline{M}_{d_i}\eta\right)
\end{aligned} \tag{3.21}$$

Fission and absorption operators are related to quite symmetric phenomena, conversely in-scattering reaction is connected to the probability of velocity and direction modification which is not necessarily equivalent for symmetric positions in phase space. Finally, after some manipulations, the streaming operator expression turns out not to be self-adjoint as well.
It is worth to investigate this neutron importance meaning starting from time-independent neutron equation in presence of a previously imposed source, namely:

$$\underline{L}\phi_s = \underline{M}\phi_s + Q \tag{3.22}$$

and the related adjoint equation which may present, in principle, an adjoint source as follows:

$$\underline{L}^\dagger \phi_s^\dagger = \underline{M}^\dagger \phi_s^\dagger + Q^\dagger \tag{3.23}$$

ϕ_s satisfying proper boundary condition C and $\phi_s^\dagger$ associated to relative boundary conditions C^+. These last transport direct and adjoint equations are not eigenvalue problems since a source is present. As far as liner algebra analogy holds for infinte dimension functional spaces, whether only one solution is present in the system - namely constituted by a certain operator and boundary conditions - this can not be vanishing everywhere in the domain since a translation is imposed by the non-homogeneous source term. Then, there is no need to impose operator modification to find out a non-vanishing neutron population for a given reactor. Needless to say, the static solution of neutron transport equation with a source is different from the first eigensolution of the homogeneous system even though operators are the same.

Taking the inner product of both sides of eq. (3.22) with $\phi_s^\dagger$ and of both sides of eq. (3.23) with ϕ_s, it follows that:

$$\begin{aligned}\left(\phi_s^\dagger, \underline{L}\phi_s\right) &= \left(\phi_s^\dagger, \underline{M}\phi_s\right) + \left(\phi_s^\dagger, Q\right)\\ \left(\phi_s, \underline{L}^\dagger\phi_s^\dagger\right) &= \left(\phi_s, \underline{M}^\dagger\phi_s^\dagger\right) + \left(\phi_s, Q^\dagger\right)\end{aligned} \tag{3.24}$$

Subtracting previous equations, it is possible to eliminate all operator contributions. In fact self-adjoint operators, such as fission and absorption, are equivalent. In-scattering contribution compensates the outgoing ones when an integration over all the phase space domain is carried out. The same for the adjoint expression. Through some manipulations, both terms in streaming direct and adjoint cancel each other. Then the result is as shown hereafter:

$$\left(\phi_s^\dagger, Q\right) = \left(\phi_s, Q^\dagger\right) \tag{3.25}$$

Now the adjoint source may be thought of as a macroscopic cross section of a proper neutron detector placed somewhere within the nuclear system. So $Q^\dagger = \Sigma_d(\mathbf{r}, E, \hat{\mathbf{\Omega}})$. This yields:

$$\left(\phi_s^\dagger, Q\right) = \left(\Sigma_d(\mathbf{r}, E, \hat{\mathbf{\Omega}}), \phi_s\right) \tag{3.26}$$

On the left-hand side it is easy to find out the global detector response, if one neutron of a given energy and direction, E and $\hat{\mathbf{\Omega}}$ is placed in a certain position $\mathbf{r}$ it may be seen as a pointwise source defined as $Q = \delta(\mathbf{r} - \mathbf{r}_0)\delta(E - E_0)\delta(\hat{\mathbf{\Omega}} - \hat{\mathbf{\Omega}}_0)$. The meaning of neutron importance is then very clear:

$$\phi_s^\dagger(\mathbf{r}_0, E_0, \hat{\mathbf{\Omega}}_0) = \left(\Sigma_d(\mathbf{r}, E, \hat{\mathbf{\Omega}}), \phi_s\right) \tag{3.27}$$

since it is the total response of a detector placed in the system, after a static neutron population due to a single neutron insertion is established (Bell and Glasstone, 1970). It varies depending upon the effect of such a neutron insertion and then it changes as far as phase space location of that neutron is concerned. Adjoint flux is then a particular property of a point in phase space $\mathbf{r}$, E, $\hat{\mathbf{\Omega}}$ and that detector response may be seen also as asymptotic increase in neutron population ΔN due to single neutron insertion. Neutron population increase from N_0 to $N_0 + \Delta N$ depends upon phase space position of injected particle. Thermal neutron within the fuel or fast moving away neutron placed in reflector will give rise to different asymptotic levels, this is worth to evaluate through neutron importance (Henry, 1975).
Even if adjoint flux can give several information about detectors and sources in the reactor, for mathematical applications related to kinetics analyses purposes, it is common practice taking advantage of L- and M- relationships shown just before.

3.4 Neutron Kinetics Models

Spatial dynamics leads to detailed system analyses but in a number of situations the objective of the study is related to physical quantities regarding the entire reactor. Therefore,

the aim of the kinetics evaluation concerns a global approach and then a lumped parameters description is required. Some details about derivation of neutron kinetics equation are given here in order to better explain the model proposed and utilised in the present thesis.
Looking for a lumped model, the general time-dependent neutron transport equation showed in paragraph 3.1 is not expected to concern phase space description anymore but only time-dependent global equation is requested (Trombetti, 1975). Thus, an integration is carried over the whole domain. Both sides of eq. (3.1) are multiplied for a weight function ψ which has to be a priori only sufficiently smooth and continuous in the domain, it yields:

$$\begin{cases} \left(\psi, \frac{1}{v}\frac{\partial \varphi}{\partial t}\right) = -\left(\psi, \underline{L}\varphi\right) + \left(\psi, \underline{M}_p\varphi\right) + \sum_{i=1}^{m}\left(\psi, \frac{\chi_{d_i}}{4\pi}\lambda_i c_i\right) + \left(\psi, \hat{q}\right) \\ \left(\psi, \frac{\partial c_i}{\partial t}\right) = -\left(\psi, \lambda_i c_i\right) + \left(\psi, \underline{M}_{d_i}\varphi\right) \end{cases} \tag{3.28}$$

In the previous, the leakage operator $\underline{L}$ includes all the absorption and net streaming losses of particles in the volume of phase space and then $\underline{L} = \underline{G}+\underline{\Sigma}-\underline{\Sigma}_s$. Now, the neutron flux is factorized splitting it in two components, namely $\varphi(\mathbf{r}, E, \hat{\mathbf{\Omega}}, t) = A(t)\Phi(\mathbf{r}, E, \hat{\mathbf{\Omega}}, t)$: an amplitude $A(t)$ and a shape $\Phi(\mathbf{r}, E, \hat{\mathbf{\Omega}}, t)$ are defined. The weight function may be chosen imposing a proper normalization condition as follows:

$$\left(\psi, \frac{1}{v}\Phi\right) = 1 \quad \Rightarrow \quad \left(\psi, \frac{1}{v}\varphi\right) = A(t) \tag{3.29}$$

It is worth to emphasize that this expression for neutron flux is always exact for every shape and amplitude provided their coherence and properties requested hereabove. The left-hand side of first of eqs. (3.28) yields an amplitude derivative and it suggests to transpose the expression in a kind of amplitude transport equation.
Such an amplitude $A(t)$ may be also considered as an averaged neutron population. Right side of previous inner product is exactly the amount of neutrons for every volume in phase space. Weighted average process is therefore carried out using ψ weight function. Following this principle, reduced kinetics equations deal with every physical quantity of interest which is proportional to such an averaged neutron population, provided both sides multiplication for a suitable coefficient (for instance total power).
In fact, it is possible to turn eq. (3.28) into the following form:

$$\begin{cases} \frac{dA(t)}{dt} = \alpha_0(t)A(t) + \sum_{i=1}^{m}\lambda_i C_i(t) + S(t) \\ \frac{dC_i(t)}{dt} = -\lambda_i C_i(t) + \alpha_i(t)A(t) \end{cases} \tag{3.30}$$

in which coefficients are defined as follows:

$$\alpha_0(t) = \frac{\left(\psi, \underline{M}_p\Phi - \underline{L}\Phi\right)}{\left(\psi, \Phi/v\right)}, \quad \alpha_i(t) = \frac{\left(\psi, \underline{M}_{d_i}\Phi\right)}{\left(\psi, \Phi/v\right)} \tag{3.31}$$

and, multiplying both sides of second eq. (3.28) for delayed neutrons energy distribution, it is possible to make the following position:

$$C_i(t) = \left(\psi, \frac{\chi_{d_i}}{4\pi} c_i\right), \quad S(t) = \left(\psi, \hat{q}\right) \tag{3.32}$$

The latter coefficients α still contain neutron flux which is the quantity to be determined and then some hypothesis are needed to obtain parameters easy to be evaluated before solving the equations. Anyway it is important to notice that they depend upon flux shape Φ and not on flux amplitude $A(t)$ since it is always possible to simplify the latter being α ratios of linear expressions of neutron flux φ.
Two approaches are normally envisaged:

- **Point kinetics**: $\varphi = A(t)\phi(\mathbf{r}, E, \hat{\mathbf{\Omega}})$. The shape coincides with the first eigensolution of neutron transport equation (3.8). Operators are evaluated at time zero. The weight function is the neutron importance which corresponds to this flux at time zero as well.
- **Quasistatic kinetics**: $\varphi = A(t)\phi(\mathbf{r}, E, \hat{\mathbf{\Omega}}, t)$. The shape may change with time as far as operators vary. Weight function is an adjoint flux calculated through coherently time-dependent adjoint operators.

Anyway, lumped parameters are expressed as follows:

$$\rho(t) = \frac{\left(\psi, \underline{M}\Phi - \underline{L}\Phi\right)}{\left(\psi, \underline{M}\Phi\right)} = \frac{k_{eff}(t) - 1}{k_{eff}(t)} \tag{3.33a}$$

$$\beta_{eff}(t) = \frac{\left(\psi, \underline{M}_d\Phi\right)}{\left(\psi, \underline{M}\Phi\right)} \tag{3.33b}$$

$$\beta_i(t) = \frac{\left(\psi, \underline{M}_{d_i}\Phi\right)}{\left(\psi, \underline{M}\Phi\right)} \tag{3.33c}$$

$$\ell(t) = \frac{\left(\psi, \Phi/v\right)}{\left(\psi, \underline{M}\Phi\right)} \tag{3.33d}$$

Coherently with previous expressions:

$$\alpha_0(t) = \frac{\rho(t) - \beta_{eff}(t)}{\ell(t)}, \quad \alpha_i(t) = \frac{\beta_i(t)}{\ell(t)} \tag{3.34}$$

Moreover, they are usually referred to as:

- **Reactivity** $\rho(t)$: it accounts, at a first order, for the relative change in multiplication factor - namely the first eigenvalue - of the system.
- **Total Delayed Fraction** $\beta_{eff}(t)$: it is the fraction of the total amount of neutrons which are emitted with a certain delay with respect to the prompt ones which are generated during fission reaction. If weighting function would be unity it were the exact average β of fissile nuclei.

- **Delayed Neutron Fraction i** $\beta_i(t)$: it concerns the amount of delayed neutrons which appears depending on the decay constant of neutron precursor group i.
- **Neutron Generation Time** $\ell(t)$: it shows the average amount of time that neutron population needs to completely self-regenerate. During this interval, say n_0/k_{eff} neutrons are either lost or absorbed producing on average n_0 new neutrons.

3.4.1 Point Kinetics

The pointwise approximation exhibits time-dependent effects only through amplitude variations. It is assumed that all perturbations inducing time behaviour of the reactor are homogenized within the system in order to be coherent with a time-independent Φ function.
Since neutron shape has been supposed constant, theoretically lumped coefficients do not change in time being the operators constant. Following this approximation, only reactivity variation is accounted for by means of k_{eff} modifications considering only operator variations $\delta\underline{L}$ and $\delta\underline{M}$ and neglecting corresponding $\delta\phi$ defined as perturbation concerning an initial equilibrium state such that $\phi = \phi_0 + \delta\phi$. In fact, reactivity is the only parameter in which even slight modifications in operators result to be significant. A given perturbation is more effective in operator differences. Then, kinetics parameters result to be:

$$\rho(t) = \frac{\left(\phi_0^\dagger, \delta\underline{M}\phi_0 - \delta\underline{L}\phi_0\right)}{\left(\phi_0^\dagger, \underline{M}\phi_0\right)} \tag{3.35a}$$

$$\beta_{eff} = \frac{\left(\phi_0^\dagger, \underline{M}_d\phi_0\right)}{\left(\phi_0^\dagger, \underline{M}\phi_0\right)} \tag{3.35b}$$

$$\beta_i = \frac{\left(\phi_0^\dagger, \underline{M}_{d_i}\phi_0\right)}{\left(\phi_0^\dagger, \underline{M}\phi_0\right)} \tag{3.35c}$$

$$\ell = \frac{\left(\phi_0^\dagger, \phi_0/v\right)}{\left(\phi_0^\dagger, \underline{M}\phi_0\right)} \tag{3.35d}$$

Finally, it is worth to emphasize the physical meaning of a such a constant shape assumption. It is obtained solving static transport equation and then features of the reactor are assumed to be constant - namely the operators. Point model may correspond to calculation needs if just averaged quantities related to the reactor as a whole are investigated and short transients are treated. The mathematical tools by which such an average process is performed is the weight function. This is the reason why it has been taken as neutron importance.

3.4.2 Quasistatic Kinetics

Dealing with kinetics of neutronic systems, calculation needs may concern effects about flux shape for computation times which are relevant compared to neutron precursor decay constants. In addition, evolution or burnup analyses may turn out to be necessary

and for these topics simple point approach has proved to be not enough precise. The reason is not due to spatial dynamics description but just because, during relatively long simulation periods, neutron flux and importance may be caused to vary in order to provide different importances to reactor core regions.
Therefore, flux and weight functions are not supposed to remain constant and are updated during calculation. These two latter features of the system reflect operators modifications which may be caused by control rod insertion, fuel depletion, geometry variation and so on.
Direct and adjoint operators are so updated as far as system evolution is concerned and direct and adjoint fluxes are computed and utilized. This gives rise to a time dependence of kinetics lumped parameters:

$$\rho(t) = \frac{\left(\phi^\dagger(t), \underline{M}(t)\phi(t) - \underline{L}(t)\phi(t)\right)}{\left(\phi^\dagger(t), \underline{M}(t)\phi(t)\right)} = \frac{k_{eff}(t) - 1}{k_{eff}(t)} \tag{3.36a}$$

$$\beta_{eff}(t) = \frac{\left(\phi^\dagger(t), \underline{M}_d(t)\phi(t)\right)}{\left(\phi^\dagger(t), \underline{M}(t)\phi(t)\right)} \tag{3.36b}$$

$$\beta_i(t) = \frac{\left(\phi^\dagger(t), \underline{M}_{d_i}(t)\phi(t)\right)}{\left(\phi^\dagger(t), \underline{M}(t)\phi(t)\right)} \tag{3.36c}$$

$$\ell(t) = \frac{\left(\phi^\dagger(t), \phi(t)/v\right)}{\left(\phi^\dagger(t), \underline{M}(t)\phi(t)\right)} \tag{3.36d}$$

Where point approach consists of an effective separation of variables, quasistatic description gives a twofold time relation. Functions $\phi(t)$ and $\phi^\dagger(t)$ even though depending on time, are solutions to static direct and adjoint problems. They always come from static calculations and possible to be evaluated independently with respect to main problem.
A key aspect following this model is the feature to be quasistatic. The assumption made consider the evolution of real φ neutron flux as a merge in time of a first eigenfunction series corresponding to timely operator variations. This assumes that several equilibrium conditions are joined neglecting transients and disequilibrium phenomena which may sometimes be the score of a detailed analysis.
In both previous point and quasistatic models, shape and weight functions may change in time dependence but they still remain direct and adjoint flux. Beyond the rationale of using the only flux expression possible to obtain and the adjoint function seen as importance, some mathematical properties makes this choice meaningful.
In kinetics coefficients, neutron flux is required for every time. Taking advantage of space completeness about all possible eigenfunctions ϕ_i, ϕ_i^0 or $\phi_i^\dagger$ associated to an eigenvalues problem, a function may be expressed as in eq. (3.9) or, in a more general form:

$$\varphi(\mathbf{r}, E, \hat{\mathbf{\Omega}}, t) = \sum_{i=1}^{+\infty} c_i(t)\phi_i(\mathbf{r}, E, \hat{\mathbf{\Omega}}, t) + \sum_{j=1}^{+\infty} c_j^0(t)\phi_j^0(\mathbf{r}, E, \hat{\mathbf{\Omega}}, t) \tag{3.37}$$

then it is possible to take advantage of relations (3.18) to eliminate all the remaining terms in series except for the first one in kinetic parameters defined in eqs. (3.35) and (3.36).

As explained before, such an expasion is possible referring coefficients through L- and M-orthogonality relations multiplying both sides of previous series yielding:

$$\left(\phi_m^\dagger(t), \underline{M}(t)\varphi(t)\right) = \sum_{i=1}^{+\infty} c_i(t)\left(\phi_m^\dagger(t), \underline{M}(t)\phi_i(t)\right) + \sum_{j=1}^{+\infty} c_j^0(t)\left(\phi_m^\dagger(t), \underline{M}(t)\phi_j^0(t)\right) \quad (3.38)$$

Multiplication operator is just tool for orthogonality property use, then:

$$c_m(t) = \frac{\left(\phi_m^\dagger(t), \underline{M}(t)\varphi(t)\right)}{\left(\phi_m^\dagger(t), \underline{M}(t)\phi_m(t)\right)} \quad (3.39)$$

Procedure to obtain coefficients c_j^0 regards less obvious orthogonality relations which have to be supposed on a physical ground.
Finally, thinking about a time-dependent complete basis, flux is timely represented and error cancellation is effective as far as coherent adjoint flux is chosen and used.

3.5 Kinetic Model for Reactor Device Transients

In the framework of the present thesis, the main objective of neutron kinetic analysis is the evaluation of power released within the devices placed in the reflector. Since they contain fissile material, they are expected to present a behaviour which is influenced also by fission reactions and local neutron generation which occurs inside.
A particular model is then utilized for every device in order to separate it from the reactor core and to analyze it as an independent coupled system (Abramov, 2001). A sample being irradiated by neutron coming from reactor core may be thought of as a subcritical system whose neutron population is strongly influenced by an intense external source. This peculiar approach is mainly aimed at defining the time-dependent behaviour of device power with respect to core evolution. The usual pointwise description showed before is able just to provide reactor lumped quantities and system split is then required. The first objective of this analysis is the definition of a model which could describe and take into account all power contributions and relative time features. In fact, it is always possible to assume a flux split between prompt and delayed neutrons (Lee and Kulik, 2005). Moreover, it is worth to distinguish both neutrons coming from core and neutrons self-produced within the device. Finally, the total flux yields as follows:

$$\phi(\mathbf{r}, E, \hat{\mathbf{\Omega}}, t) = \phi_p(\mathbf{r}, E, \hat{\mathbf{\Omega}}, t) + \sum_{j=1}^{m} \phi_{d_j}(\mathbf{r}, E, \hat{\mathbf{\Omega}}, t) + \varphi_p(\mathbf{r}, E, \hat{\mathbf{\Omega}}, t) + \sum_{j=1}^{m} \varphi_{d_j}(\mathbf{r}, E, \hat{\mathbf{\Omega}}, t) \quad (3.40)$$

In which ϕ_p and ϕ_{d_i} are core prompt and delayed neutrons respectively. By contrast φ_p and φ_{d_i} represent prompt and delayed neutrons generated by presence of fissile material in the device. Delayed neutron precursor contributions may be simplified in order to make expressions compact and turn out the four following terms:

$$\phi(\mathbf{r}, E, \hat{\mathbf{\Omega}}, t) = \phi_p(\mathbf{r}, E, \hat{\mathbf{\Omega}}, t) + \phi_d(\mathbf{r}, E, \hat{\mathbf{\Omega}}, t) + \varphi_p(\mathbf{r}, E, \hat{\mathbf{\Omega}}, t) + \varphi_d(\mathbf{r}, E, \hat{\mathbf{\Omega}}, t) \quad (3.41)$$

Concerning device geometrical domain, it is possible to split usual Boltzmann equation description in different components aiming at highlighting core-induced effects and device self-produced power. Balance equation for prompt neutrons coming from core and diffusing in the device do not consider generation term since new produced particles by means of fission reactions are not referred to as core neutrons anymore. The same is for delayed neutrons going out from the core and reaching the device as well. Both species have just scattering and, generally speaking, leakage terms:

$$\begin{aligned} \frac{1}{v}\frac{\partial \phi_p}{\partial t} &= -\underline{L}\phi_p \\ \frac{1}{v}\frac{\partial \phi_d}{\partial t} &= -\underline{L}\phi_d \end{aligned} \tag{3.42}$$

In order to link device behavior to core transient which is the external neutron source, it is possible to distinguish incoming and outcoming contributions inside leakage term. In fact, there is a $\underline{G}^{(in)}\phi_p$ corresponding to total incoming particles. A term $\underline{G}^{(out)}\phi_p$ should correspond to normal absorption and leakage from device domain neglecting self-produced neutrons reflection in sample coolant volume. This operator split is local in phase space for the moment, but once equations integrated over all domain, it is the total amount of neutron coming from core - namely a kind of source term. Thus eqs. (3.42) may be rewritten as:

$$\begin{aligned} \frac{1}{v}\frac{\partial \phi_p}{\partial t} &= -\underline{G}^{(out)}\phi_p - \underline{\Sigma}\phi_p + \underline{G}^{(in)}\phi_p \\ \frac{1}{v}\frac{\partial \phi_d}{\partial t} &= -\underline{G}^{(out)}\phi_d - \underline{\Sigma}\phi_d + \underline{G}^{(in)}\phi_d \end{aligned} \tag{3.43}$$

The interest of the analysis is to obtain integral quantities regarding associated powers and a sort of integration similar to that previously explained in reactor kinetics is required. Normally, concerning subcritical systems, point kinetics still holds (Eriksson et al., 2005) and error cancellation techniques related to adjoint flux utilization is still valid but with some modifications.
In order to carry out the integration all over the volume it is necessary to find a proper weight function. As far as device model is concerned, it is worth to underline that the external surface source does not allow usual eigenvalue problem model - namely boundary conditions are not homogeneous.
It is possible to show that for neutron source systems, the flux factorization split is different with respect to what previously reported.
Neutron flux is $\varphi(\mathbf{r}, E, \hat{\mathbf{\Omega}}, t) = A(t)\Phi(\mathbf{r}, E, \hat{\mathbf{\Omega}}, t)$ where:

- flux shape Φ is obtained through static non-homogeneous transport equation which includes the actual source, possibly evaluated at different time configurations
- weight function ψ is conversely the neutron importance for homogeneous system

Integrating eqs. (3.43) in phase space domain considering related weighting functions - prompt and delayed - from homogeneous adjoint problem, it yields amplitude $A(t)$

lumped transport relations as in previous eqs. (3.30). Finally, once the amplitude equations are expressed, it is possible to relate them to power generated within the device, for prompt and delayed neutrons:

$$\begin{aligned} P_p(t) &= \int E_d \Sigma_f A_p(t) \Phi_p(\mathbf{r}, E, \hat{\mathbf{\Omega}}) \, \mathrm{d}\mathbf{r} \, \mathrm{d}E \, \mathrm{d}\hat{\mathbf{\Omega}} \\ P_d(t) &= \int E_d \Sigma_f A_d(t) \Phi_d(\mathbf{r}, E, \hat{\mathbf{\Omega}}) \, \mathrm{d}\mathbf{r} \, \mathrm{d}E \, \mathrm{d}\hat{\mathbf{\Omega}} \end{aligned} \tag{3.44}$$

The latter eqs. (3.43) state that neutrons come from core to the device and they may diffuse out or get absorption on site. Source terms may be expressed linking their values to core quantities through coupling coefficients $C_p(t)$ and $C_d(t)$ which may in principle depend on time. As it is possible to find out analysing previous equations (3.43), neutron lifetime $\ell_0(t)$ expresses ratio between total amount of either prompt or delayed neutrons in the system with respect to total leakage rate.
Therefore, the core contribution in device power generation is found. It considers just external neutrons supposing no multiplication but only energy deposition in the samples.

$$\begin{cases} \dfrac{dP_p}{dt} = -\dfrac{1}{\ell_0(t)} P_p + C_p(t) P_{core} \\ \dfrac{dP_d}{dt} = -\dfrac{1}{\ell_0(t)} P_d + C_d(t) P_{core} \end{cases} \tag{3.45}$$

in which $C_p(t)$ and $C_d(t)$ coefficients express coupling in terms of power flux from core to device (having measure of $[t^{-1}]$). In addition, a model for neutrons generated in the device is possible to be conceived and relative contribution to total power is expected to be evaluted. As usual, prompt and delayed distinction is operated as follows:

$$\begin{aligned} \frac{1}{v}\frac{\partial \varphi_p}{\partial t} &= -\underline{L}\varphi_p + \underline{M}_p\phi_p + \underline{M}_p\phi_d + \underline{M}_p\varphi_p + \underline{M}_p\varphi_d \\ \frac{1}{v}\frac{\partial \varphi_d}{\partial t} &= -\underline{L}\varphi_d + \lambda c \\ \frac{\partial c}{\partial t} &= -\lambda c + \underline{M}_d\phi_p + \underline{M}_d\phi_d + \underline{M}_d\varphi_p + \underline{M}_d\varphi_d \end{aligned} \tag{3.46}$$

Now generation terms appear for both neutron families since fissions taking place within the device may be induced by external neutrons coming from core or from self-generated internal ones indicated with φ_p and φ_d. In the first case it is a kind of source with respect to device neutron population. It is then possible to integrate as before in order to reach amplitude transport equations.
Considering delayed formulation, it is straightforward to notice how generation term is only due to precursors families decay. A fraction of absorbed neutrons is expected to give rise to prompt fissions and then source term depending on delayed neutrons appears in first equation.
First equation concerns prompt neutrons. It points out self-contribution of the prompt ones and then all the generation terms caused by other neutron species. Normally, this kind of model is used for subcritical system modelling in external source presence. In

this case for sake of completeness all contributions have been introduced . The source is present in the same way being function of another neutron flux as previously explained. Kinetics equations regarding neutron species are turned into power expressions as already done herebefore:

$$\begin{cases} \dfrac{dp_p}{dt} = \dfrac{\rho(t)-\beta(t)}{\ell(t)}p_p + \left(\dfrac{1-\beta(t)}{\ell(t)}p_d + \dfrac{1-\beta(t)}{\ell(t)}P_p + \dfrac{1-\beta(t)}{\ell(t)}P_d\right) \\ \dfrac{dp_d}{dt} = -\dfrac{1}{\ell_0(t)}p_d + \lambda C^* \end{cases} \tag{3.47}$$

Where power evolution in the system is stated through relation (3.44), both for core neutrons and for self-produced ones. Thus, neutron precursors concentration is coherently transposed to associated power as follows:

$$C^*(t) = \int E_d \Sigma_f C(t) \Phi_d(\mathbf{r}, E, \hat{\mathbf{\Omega}})\, \mathrm{d}\mathbf{r}\, \mathrm{d}E\, \mathrm{d}\hat{\mathbf{\Omega}} \tag{3.48}$$

Summarizing all terms previously commented, the total device power is due to all following contributions:

$$\begin{cases} \dfrac{dP_p}{dt} = -\dfrac{1}{\ell_0(t)}P_p + C_p(t)P_{core} \\ \dfrac{dP_d}{dt} = -\dfrac{1}{\ell_0(t)}P_d + C_d(t)P_{core} \\ \dfrac{dp_p}{dt} = \dfrac{\rho(t)-\beta(t)}{\ell(t)}p_p + \left(\dfrac{1-\beta(t)}{\ell(t)}p_d + \dfrac{1-\beta(t)}{\ell(t)}P_p + \dfrac{1-\beta(t)}{\ell(t)}P_d\right) \\ \dfrac{dp_d}{dt} = -\dfrac{1}{\ell_0(t)}p_d + \lambda C^* \end{cases} \tag{3.49}$$

Finally, total power generated and released within the experimental sample is, generally speaking, the sum of all terms as follows:

$$P_{tot}(t) = P_p(t) + P_d(t) + p_p(t) + p_d(t) \tag{3.50}$$

This model that has been obtained in present section allows to distinguish all different contributions to device power. It has been conceived in order to be able to show at which extent some fractions may be relevant with respect to others, at a first stage and theoretically speaking. In fact, this split permits an improved and precise time-dependent description of power transients as far as every single term evolution is concerned.
Coupling coefficients and energy depositions are computed about neutron effects and prompt gamma radiation. Delayed gamma due to fission products decay component has to be added as described in chapter 6.
First, prompt and delayed core neutron contributions are supposed to behave as core transient does, according to particular shutdown procedure. Moreover, prompt self-produced device power follows that latter time dependence. In addition, self-delayed neutron generation may introduce dynamic distortions which have to be accounted for in order to provide detailed power evolutions (Camprini et al., 2012a).
The objective of the present thesis regarding power transient description enhancements is then achieved by means of this approach.

Chapter 4

Computational Tools Description

4.1 Simulation Objectives and Approach

The main subject of the present thesis is the power transient analysis concerning the experimental devices placed within the JHR reflector. Some technical needs in applied engineering involve different codes and matching in order to achieve the selected results even by means of tools cross-utilization.
Innovative features of the present study is mainly a dynamic and spatial evaluation which is very important to properly account for reflector devices and core interactions during transients. For this reason a twofold analysis has been carried out and related computational tools are considered hereafter:

- **core** transient evaluations through a lumped approach for some shutdowns have been performed through the DULCINEE kinetics code
- **reflector** coupling with core accounting for spatial effects, as far as complex core geometry is concerned, required Monte Carlo computation by means of TRIPOLI 4.8 transport code utilization

Therefore, point kinetics and global evaluations concerned core thought of as a neutron source delivering significant neutron fluxes to experimental devices placed all around. This distinction allows to split reactor in parts which reflect what is the effective score to be calculated. Core transients were described by kinetics evaluations and core-reflector coupling was properly defined only keeping a very detailed description about reflector geometry and radiation transport description.

4.2 DULCINEE Code

Power transient evaluations have been performed by means of the DULCINEE kinetics code. It has been developed by CEA (French Atomic Energy Commission) and IRSN (French Radioprotection and Nuclear Safety Institute) and it was mainly used and validated during safety tests at CABRI reactor in Cadarache (Ritter et al., 2010). In addition,

it has been tested for planar fuel plates at CEA Grenoble research center.
It was conceived to analyse different operational conditions:

- normal and accidental reactivity insertions
- fast power evolutions
- loss of flow conditions
- changes in coolant inlet temperature

This code is composed by different modules in order to solve classical point kinetics equations providing all thermal feedbacks relations coming from temperature field effects on neutron multiplication feature of the system.
In fact, a twofold analysis is allowed with this tool:

- provided reactivity insertion scenarios or thermal boundary condition modifications, power evolution may be investigated
- power transient can be imposed and then related reactivity excursion may be calculated through inverse solution of kinetics equations

In both cases, external reactivity is taken into account but thermal feedbacks are calculated and considered as well.
This tool may deal with either cylindrical pin fuel elements or planar fuel plates. Typically fuel elements are divided in two regions in order to account for double power generation coefficients and to simulate the hottest channel of the core. The coolant may be modelled in double-phase flow, which is not the case for JHR since pressure conditions in core allow water to remain always liquid.
The plant region which is simulated is exactly the active part and so coherent thermal hydraulic boundary conditions are considered. Concentrated pressure drop may be imposed and distributed friction effects are evaluated by the code itself.
Reactivity feedbacks regard solid and liquid temperature fields and for that Fourier's equations and hydrodynamic relations are solved respectively. Physical properties of the solid material - namely cladding and fuel - are given as functions of temperature by the user. Properties of water are calculated and tabulated by the code (Fache and Khadhraoui, 2009).

4.2.1 Thermal Hydraulic Module

Evaluations of temperature field within the coolant are performed solving mass, linear momentum and energy balance equations for a single fluid. The velocity field is supposed to be mono-dimensional in the channel and the fluid homogeneous. Cooling direction can be imposed by the user. As mentioned before, conservation equations are solved in every node of the domain accounting for local boiling through void fraction

parameter.

$$\begin{aligned}
&\frac{\partial \rho_{th}}{\partial t} + \frac{\partial(\rho_{th} v)}{\partial z} = 0 \\
&\frac{\partial(\rho_{th} v)}{\partial t} + \frac{\partial(\rho_{th} v^2)}{\partial z} = -\rho_{th} g cos\theta - \frac{\partial p}{\partial z} - F \\
&\rho \frac{\partial h}{\partial t} + \rho_{th} v \frac{\partial h}{\partial z} = G
\end{aligned} \tag{4.1}$$

Here the velocity term is oriented in z-direction, F is the friction force and G accounts for the heat generation term per unit volume in the coolant. According to heating phenomena in nuclear reactors, the most important contribution is due to fissions and then to heat flux through the wall. A balance relative to this flux ϕ_h at the external perimeter gives the Q volumetric power generation term respect to a coolant flow cross section: $\mathcal{S}Q = \phi_h p_w$. The fluid density is considered as a function of enthalpy and pressure. $\rho_{th} = \rho_{th}(h, p)$.
Node distances are set by the user and time step is computed starting from the latter and the average velocity in the channel. In fact $\Delta T_{channel} = \Delta z / \overline{v}$ and Δz comes from the amount of z nodes chosen.
The term G contains both the heat flux at the wall in terms of energy transmission and the percentage C_γ of gamma radiation deposited directly outside the fuel into the coolant. Then: $G = Q(1 + C_\gamma)$
Void fraction α is used to find density at every node through the ones of liquid and vapour. Finite differences method puts the previous system of eqs. (4.1) into the form which follows hereafter. Indexes P and m define, respectively, the time evaluation and the node location for every calculation step.

$$\begin{aligned}
&\frac{\rho_m^P - \rho_m^{P-1}}{\Delta T_{channel}} + \frac{q_m^P - q_{m-1}^P}{\Delta z} = 0 \\
&\frac{q_m^P - q_m^{P-1}}{\Delta T_{channel}} + 2\big(sq\big)_m^P \frac{q_m^P - q_{m-1}^P}{\Delta z} + \big(q^2\big)_m^P \frac{s_m^P - s_{m-1}^P}{\Delta z} + \frac{P_m^P - P_{m-1}^P}{\Delta z} = F \\
&\frac{h_m^P - h_m^{P-1}}{\Delta T_{channel}} + \big(q/\rho\big)_{m-1}^{P-1} \frac{h_m^{P-1} - h_{m-1}^{P-1}}{\Delta z} = \frac{G}{\rho_{m-1}^{P-1}} \\
&\rho_m^P = \rho_l\big(h_m^P\big)\big(1-\alpha\big)_m^P + \rho_v\big(P_m^P\big)\alpha_m^P
\end{aligned} \tag{4.2}$$

Where P means the total pressure which considers the static one and the gravity force, q is the mass rate per unit surface and s is the average specific volume defined with the following expression that holds for relatively low pressures:

$$s = \frac{(1 - X_r)^2}{\rho_l(1-\alpha)} + \frac{X_r^2}{\rho_v \alpha} \tag{4.3}$$

while X_r is the steam quality of the coolant. Boundary and initial conditions solve a stationary problem. Initial density is computed for a single phase fluid since liquid features

are set by the user.

$$\begin{aligned} &q_0^P = q_0 \quad h_0^P = h_0 \\ &P_0^P = P_0 \quad q_m^1 = q_0 \\ &\frac{P_m^1 - P_{m-1}^1}{\Delta z} - \left(q^2/\rho^2\right)_m^1 \frac{\rho_m^1 - \rho_{m-1}^1}{\Delta z} = F \\ &\frac{h_m^1 - h_{m-1}^1}{\Delta z} = \frac{G}{q_0} \end{aligned} \tag{4.4}$$

Static solution scheme starts from the first node in which enthalpy is known and goes on in this way:

$$h_m^P = \left(1 - \left(q/\rho\right)_{m-1}^{P-1} \frac{\Delta T_{channel}}{\Delta z}\right) h_m^{P-1} + \left(q/\rho\right)_{m-1}^{P-1} \frac{\Delta T_{channel}}{\Delta z} h_{m-1}^{P-1} + \frac{\Delta T_{channel} G}{\rho_{m-1}^{P-1}} \tag{4.5}$$

Then it is possible to obtain density for liquid phase since it is a function of the enthalpy and quantities related to the previous node.

$$\left(\rho_m^P\right)^{liq} = \rho_l\left(h_m^P\right)\left(1-\alpha\right)_{m-1}^P + \rho_v\left(P_{m-1}^P\right)\alpha_{m-1}^P \tag{4.6}$$

Now a guess density value can be used in mass and momentum conservation equation in order to reach the convergence. From mass equation it is possible to know the mass rate $q_m^P(\rho_m^P)^{(i-1)}$ and, in the same way, the momentum equation gives total pressure $P_m^P(\rho_m^P)^{(i-1)}$. Both are depending upon guess hypothesis and this trick can be repeated until the chosen convergence is reached.

$$\left|(\rho_m^P)^{(i)} - (\rho_m^P)^{(i-1)}\right| < \varepsilon \tag{4.7}$$

Proper convergence values can be fixed by the user both for density and for pressure iterations. At this point the internal loop is completed. For every node distribution the external time loop is solved as well.
This output permits to the present module to define enthalpy for every node of the fluid. This is the starting point and external boundary condition for solid equation solution. At the same way it allows also to obtain coolant dilatation and void.

4.2.2 Solid Conduction Module

In order to define the temperature field in solid media such as fuel and cladding, the code solves the Fourier's equations neglecting axial conduction and taking advantages from angular symmetry of the domain. In fact, it yields:

$$\frac{\partial(c_{th}T)}{\partial t} = \frac{1}{r}\frac{\partial}{\partial r}\left(\lambda_{th} r \frac{\partial T}{\partial r}\right) + Q \tag{4.8}$$

for cylindrical geometry and

$$\frac{\partial(c_{th}T)}{\partial t} = \frac{\partial}{\partial r}\left(\lambda_{th} r \frac{\partial T}{\partial r}\right) + Q \tag{4.9}$$

for the plate fuel elements. In both cases c_{th} is the heat capacity and λ_{th} is the thermal conductivity of the material.
Initial conditions can be computed as stationary case or inserted by the user. Anyway it is possible to state that $T(r,0) = T_0(r)$. Boundary conditions accounts for heat exchange between external surface of the cladding and coolant bulk temperature. $\overline{T}$ is exactly the previous module output in terms of enthalpy.

$$\lambda_{th}\frac{\partial T}{\partial r} = h_c\big(T_w - \overline{T}\big) \tag{4.10}$$

The heat convection coefficient is computed through Margoulis number and proper correlations. It is also allowed to describe different materials and their thermal resistance in terms of contact between solids. Then it is allowed to impose a thermal conductivity since the heat flux is related to temperature difference in this way.

$$\phi_h R_{th} = T_2 - T_1 \tag{4.11}$$

If a mechanical play has to be taken into account, models are available to update geometrical dimensions with respect to temperature and then to express the related thermal resistance.
Moreover finite volumes method is used with respect to either cylindrical or linear shells. For every node a shell volume placed on it is considered, it is split in two portions and an energy balance is carried on through Fourier's equation. There is then a right (plus) part and a left (minus) part.

$$\int_{\Delta V}\frac{1}{r^\alpha}\frac{\partial}{\partial r}\big(\lambda r^\alpha\frac{\partial T}{\partial r}\big)r^\alpha\,\mathrm{d}V + \int_{\Delta V} Q r^\alpha\,\mathrm{d}V = \int_{\Delta V}\frac{\partial}{\partial t}(cT)r^\alpha\,\mathrm{d}V \tag{4.12}$$

Which gives the expression given below for a specific node i at a distance r_i from the centre either of the plate or the pin, the interval amplitude is set by the user through h_i parameter which means the half distance between two nodes. These hold for both cylindrical $\alpha = 1$ and plate geometry $\alpha = 0$.

$$\Big[\lambda r^\alpha\frac{\partial T}{\partial r}\Big]_{r_i-h_{i-1}}^{r_i+h_i} + \int_{r_i-h_{i-1}}^{r_i+h_i} Q r^\alpha\,\mathrm{d}r = \int_{r_i-h_{i-1}}^{r_i+h_i}\frac{\partial}{\partial t}(cT)r^\alpha\,\mathrm{d}r \tag{4.13}$$

It is worth to say that for this type of equation in mono-dimensional domain the final expression of the system is like the following:

$$\begin{aligned}&(VM-UM)T_{i-1}^t + (3VM+3VP+UM+UP)T_i^t + (VP-UP)T_{i+1}^t = \\ &(VM+UM)T_{i-1}^{t-\Delta t} + (3VM+3VP-UM-UP)T_i^{t-\Delta t} + (VP+UP)T_{i+1}^{t-\Delta t} + \\ &+ Q_{r_i+\frac{1}{2}h_i}\left[\frac{(r_i+h_i)^{\alpha+1}-r_i^{\alpha+1}}{\alpha+1}\right] + Q_{r_i-\frac{1}{2}h_{i-1}}\left[\frac{r_i^{\alpha+1}-(r_i-h_{i-1})^{\alpha+1}}{\alpha+1}\right]\end{aligned} \tag{4.14}$$

in which the right hand side might be thought as a source term depending only on previous time step data. Where:

$$\begin{aligned} VP &= c_{r_i+\frac{1}{2}h_i}\left[\frac{(r_i+h_i)^{\alpha+1}-r_i^{\alpha+1}}{\alpha+1}\right]\frac{1}{4\Delta T_{conduction}} \\ VM &= c_{r_i-\frac{1}{2}h_{i-1}}\left[\frac{r_i^{\alpha+1}-(r_i-h_{i-1})^{\alpha+1}}{\alpha+1}\right]\frac{1}{4\Delta T_{conduction}} \end{aligned} \tag{4.15}$$

are terms which take into account the time-dependent amount of thermal energy in volumes placed in right (VP) and left (VM) position with respect to the considered node. Obviously the very first VM and the last VP are always equal to zero. Conversely:

$$\begin{aligned} UP &= \frac{\lambda_{r_i+h_i}(r_i+h_i)^{\alpha}}{4h_i} \\ UM &= \frac{\lambda_{r_i-h_{i-1}}(r_i-h_{i-1})^{\alpha}}{4h_{i-1}} \end{aligned} \tag{4.16}$$

account for thermal conduction terms. They are in the same way referred to the left and the right side of the volume.
This form of the equation is easy to consider different media and interfaces. In fact it is possible for the user to set particular values of these coefficients if a material interface is present. In the case of plate fuel elements the highest possible thermal conductivity is inserted in order to account for the perfect contact between cladding and fuel meat. Power generation term is computed starting from axial and radial profiles, respectively $g(z)$ and $h(r)$. Volumes V_r and average neutron flux $\overline{\phi}_r$ are inserted for every region, as well as height H_r, number of fuel elements NB_r and pellet surface S_r. Then it is possible to compute the proper generation term as showed through a general integral below. Needless to say the generation term is just the function to be integrated by means of the profiles which are properly normalized by the code, weighting function is also the ratio between the power of different regions to the total one.

$$P_{core} = \iint_V P_{core} g(z)h(r)\frac{\overline{\phi}_r V_r}{\sum_r \overline{\phi}_r V_r}\frac{dzdS}{H_r NB_r S_r} \tag{4.17}$$

Finally it is easy to recognise that the equation form for temperature T at a given time step is the following:

$$\begin{aligned} &a_i T_{i-1} + b_i T_i + c_i T_{i+1} = S_i \\ &T_1 = 0 \\ &T_{N+2} = \overline{T} \qquad i \in \left[2, N+1\right] \end{aligned} \tag{4.18}$$

Here N is the total amount of nodes in the fuel and in the cladding volumes. The first temperature is obviously equal to zero in order to obtain a general method for every point and the last one is exactly the coolant bulk temperature, in fact through setting the thermal conductivity value to adjust it for convection process it is possible to use that one

as a boundary condition. The matrix associated to this system is tri-diagonal and then a simplified Gauss method is useful to solve it.

$$\begin{aligned} T_i &= \alpha_i T_{i+1} + \beta_i \\ T_{N+1} = \beta_{N+1} \qquad & i \in \left[2, N+1\right] \end{aligned} \tag{4.19}$$

with the following variables:

$$\begin{aligned} \alpha_i = \frac{-c_i}{b_i + a_i\alpha_{i-1}} \quad \beta_i = \frac{-S_i + a_i\beta_{i-1}}{b_i + a_i\beta_{i-1}} \quad & i \in \left[2, N\right] \\ \alpha_1 = \frac{c_1}{b_1} \quad \beta_1 = \frac{-S_1}{b_1} & \end{aligned} \tag{4.20}$$

Finally the determination of the temperature fields in the solid media is achieved in every axial node and for radial user-imposed meshes.

4.2.3 Neutron Kinetics Module

Kinetics calculations are mainly oriented to power evolutions and then this is the main module in which all thermal interactions are accounted for. DULCINEE was developed for safety studies in experimental reactors and then very short power changes were planned to be analysed. In addition, small experimental reactors allow point wise modelling since neutronic parameters are coherent with these assumptions.
In fact the whole neutron population number is expressed as proportional to usual flux amplitude $A(t)$ whose behavior is stated in eq (3.30). Then it is supposed to behave like a point and only integral evaluations are performed neglecting space dependence. As usual, six neutron precursor groups are taken into account through their C_i concentrations.

$$\begin{cases} \dfrac{dA(t)}{dt} = \dfrac{\rho(t) - \beta_{eff}}{\Lambda} A(t) + \displaystyle\sum_{i=1}^{6} \lambda_i C_i(t) \\ \dfrac{dC_i(t)}{dt} = -\lambda_i C_i(t) + \dfrac{\beta_i}{\Lambda} A(t) \end{cases} \tag{4.21}$$

As showed in the previous chapter, neutron population - then flux amplitude - may be thought of as proportional to the total thermal power. Thus it is possible to write:

$$\begin{cases} \dfrac{dP_{core}(t)}{dt} = \dfrac{\rho(t) - \beta_{eff}}{\Lambda} P_{core}(t) + \displaystyle\sum_{i=1}^{6} \lambda_i C_i^*(t) \\ \dfrac{dC_i^*(t)}{dt} = -\lambda_i C_i^* + \dfrac{\beta_i}{\Lambda} P_{core}(t) \end{cases} \tag{4.22}$$

Where transposition from flux amplitude to related power is obtained as previously stated in eqs. (3.44) and (3.48). Neutronic parameters of the system yield β_{eff}, the different β_i values and the prompt neutron lifetime Λ. Reactivity $\rho(t)$ is a function of time and it accounts for all the different feedbacks taking place during the simulation.
Mainly it is possible to distinguish three contributions to total reactivity:

$$\rho(t) = \rho_0 + \rho_{ext}(t) + \rho_{fb}(t) \tag{4.23}$$

The first term is associated to an initial reactivity if the reactor is not critical at the beginning of the simulation. The external reactivity is then considered in the second term to describe control rod insertion or piloting procedures. The last term is responsible for feedbacks with respect to thermal effects. Reactivity coefficient profiles are set by the user concerning:

- $C_v(z)$ void effect axial profile
- $C_D(z)$ Doppler effect axial profile
- $C_T(z)$ coolant temperature effect axial profile

Several thermal phenomena are responsible for reactivity feedbacks:

- **Structure dilatation**: it causes reactivity variation by means of changing in moderation ratio in terms of coolant volume fraction
- **Coolant dilatation**: it modifies neutron moderation through particle density and scattering events which induce the neutron to slow down differently
- **Void fraction**: a change in phase causes the previous effect to be more important since density drops by up to 3 orders of magnitude
- **Doppler effect**: materials presenting important resonance reactions - namely the fuel for fission and absorption reactions - are interested by change in cross section value for temperature variations. Increase in relative speed induces self-shielding to reduce and resonances to broaden

Once the total reactivity change is calculated, power evolution can be obtained in solving point wise kinetic system. That is possible to be put in the following form:

$$\frac{dF}{dt} = Z(t)F, \qquad F(0) = F_0 \tag{4.24}$$

Then it is solved by the code utilising a Runge-Kutta fourth order method after a proper temporal domain split.

$$\frac{dF}{dt} = Z(t_i)F, \quad F(t_i) = F_i, \quad t \in \left[t_i, t_{i+1}\right] \tag{4.25}$$

The DULCINEE code starts in solving coolant temperature field. Then these data are used as boundary conditions in order to determine temperature distribution within the conduction domain. Once these iterations are completed for every radial node, the axial position is modified until the domain is swept at all.
As far as reactivity feedbacks are concerned the thermal results are used to determine the behaviour of neutron population in the system since at this step it is possible to know integral information as explained above.
The last iteration is devoted to power calculation through the solution of point wise kinetics model. A new thermal power value is obtained which is going to present the same radial and axial profile according to point wise kinetics hypothesis. Then calculation procedure is repeated until time loop is completed and the end of the simulation is reached.

4.3 TRIPOLI Monte Carlo Code

Several codes are referred to as using Monte Carlo techniques since they take advantage of a statistical approach to solve the previously explained neutron transport equations. Even if the latter are integro-differential equations, some manipulations may allow to treat scores of interest in a neutronic problem as integral quantities.
Monte Carlo is used to complement or even replace experimental measurements. These features make it the reference approach for criticality safety, radiation shielding, dosimetry calculation, detector modelling and validation of deterministic codes.
Statistical simulations are the key feature and often this induces relevent computational efforts which are less and less crucial provided the increasing computer performances.
Different Monte Carlo tools are quite spread in the framework of European and international research in nuclear science. For instance MCNP (Monte Carlo N-Particle) is the reference code for United States, related industries and regulators, developed at Los Alamos National Laboratory (LANL) (Brown et al., 2003); and SERPENT has been recently developed as a Finnish project powered by domestic utility VTT (Leppanen, 2012).
TRIPOLI is the reference domestic transport code for CEA and French industrial framework as well as research and regulator scopes (Petit et al., 2011).
Monte Carlo is a well established method to solve particle transport problems, thus only a brief introduction is provided hereafter. Even though statistical approach to calculation started in XVIII century, first industrial applications saw the light during Manhattan project concerning nuclear technology.
Some features make Monte Carlo suitable for physical analysis:

- score is associated to a relative uncertainty which may properly match statistical errors
- method remains precise even for high dimension problems and complex geometry
- slow convergence and calculation effort now take advantage of improved computer performances

The most important property is the possibility to handle nuclear data as continuous functions avoiding the need for phase space discretisation as in deterministic codes; multigroup split and condensing is not necessary anymore. In fact, every particle is simulated on its own since neutron are supposed not to interact each other. It is followed starting from generation to absorption or until it escapes from the domain and it counts as a “history” in statistic evaluation. All distributions regarding physical interactions or events for neutrons are sampled and related probabilities are evaluated thanks to a random number generator. The life of the particle is then a succession of event in a Markov’s chain so all previous do not influence the probability of the next interaction. Once the random variable is extracted, the inversion is made and the particular event chosen, this is what particle will undergo and it is treated with exact physical laws and no approximations are needed. The score determination is obtained through the collection of several histories and results.

4.3.1 Monte Carlo and Statistics

Provided a group of random variables with a given average $\overline{\mu}$ and a certain variance σ^2 expressing the average distance of an element from the value of $\overline{\mu}$, it is possible to consider a specific new variable which is the sum of n of the previous ones. "Great Numbers Law" states that the average of that sum tends to the previous average $\overline{\mu}$ as the quantity n increases. A strong formulation may yield:

$$\lim_{n \to +\infty} \frac{S_n}{n} = \overline{\mu} \tag{4.26}$$

Basically, the principle is collecting a huge number of simulations (histories) which are treated in order to obtain global reliable data of the simulation. Accuracy mainly regards statistical average quantities compared with experimental or analytical results which deal with average behaviour of the complex system.
In addition, if a great number of samples of that sum is considered, Central Limit Theorem states that the result is represented by a normal (Gauss) distribution which is characterized by the same average of every sample $\overline{\mu}$ and a variance which may be reduced enlarging the sample number.
An important parameter in defining performances of a Monte Carlo calculation depends on tightness of variance and computation time. The first is mainly influenced by complexity of the system and the second rely on computational power. Factors called Figure of Merit (FOM) are introduced to express a combination of these two features, such that:

$$FOM = \frac{1}{\sigma^2 T_{calc}} \tag{4.27}$$

in which σ^2 is variance and T_{calc} is calculation time. The requested variable usually is a mathematical combination of neutron flux $\varphi(\xi)$ and a function of phase space $f(\xi)$ (which is the tally) in such a way:

$$\text{Score} = \int_V f(\xi)\varphi(\xi)\,\mathrm{d}\xi \tag{4.28}$$

The sampling procedure starts from physical laws and it computes a statistical evaluation of the previous integral.

4.3.2 Statistical Particle Transport

Numerical evaluation of integrals is straightforward thanks to Monte Carlo method and for this reason it is necessary to turn transport equation into an equivalent integral form (Litaize and Roesslinger, 2008). The quantity of interest is not neutron flux anymore but incoming and outcoming collision density with respect to a phase space volume.

- Incoming collision density accounts for the amount of neutrons arriving in a point x of the domain undergoing collision in that place just before being scattered all around:

$$\zeta(\xi) = \Sigma_t(\xi)\varphi(\xi) \tag{4.29}$$

- Outcoming collision density is the amount of neutrons coming from a point in phase space to another given after probability of a certain path is verified:

$$\kappa(\mathbf{r}, \mathbf{v}) = \iint \zeta(\mathbf{r}, \mathbf{v}')\mathcal{C}(\mathbf{v}' \to \mathbf{v}; \mathbf{r})\, \mathrm{d}\mathbf{v}' + \hat{q}(\mathbf{r}, \mathbf{v}) \tag{4.30}$$

Finally, the global transport equation is turned out into a form in which the local collision density is the superposition of several integrated paths and histories. The formulation is a II order Fredholm's equation and yields:

$$\kappa(\mathbf{r}, \mathbf{v}) = \iint \kappa(\mathbf{r}', \mathbf{v}')\mathcal{L}(\mathbf{r}', \mathbf{v}' \to \mathbf{r}, \mathbf{v}) d\mathbf{r}' d\mathbf{v}' + \hat{q}(\mathbf{r}, \mathbf{v}) \tag{4.31}$$

Total collision operator $\mathcal{L}$ sums over all the previous particle interactions which are analysed one by one:

- nuclear reactions induce attenuation through absorption and scattering, considering distance in $\mathbf{r}$ direction
- scattering reactions modify particle velocity, considering distance in $\mathbf{v}$ direction

All required scores are then functions of $\zeta(\xi)$ taking the integral and managing all the histories in a statistic way. The choice regards the volume of interest and the physical quantity - tally - which has to be evaluated.
Scores are computed taking advantage of estimators depending upond the volume dimension:

- volumetric estimator: it evaluates integrated fluxes or reaction rates associated to a particular function of phase space parameters if an event has undergone within the selected volume (collision estimator based on outcoming collisions κ and track-lenght estimator uses incoming ζ)
- surface estimator: it computes the amount of particle passing through a given surface, eventually using a weight function.
- punctual estimator: it yields just pointwise reactions being intended as a Dirac delta in a given point.

A large number of physical quantities of interest are easy to obtain thanks to this method. Typically neutron or photon flux is requested, volume or surface reaction rates, energy deposition utilising particular cross sections which account for particle interaction in energy exchange. This high fidelity performance in simulation and flexibility for complex geometry description make Monte Carlo the best tool for detailed domain description and physical modelization (Roesslinger, 2005).

Chapter 5

Core Transients Simulations

The first part of the present thesis work has concerned the simulations of the JHR core power transients regarding two different shutdown procedures: Normal Shutdown and Safety Shudown.
The aim is to verify the effectiveness of the reactivity insertions in power and temperature decreasing. Reactivity insertion evaluation required the implementation of a thermal hydraulic model of the core which is representative as far as simulation objectives are concerned. In this thesis, DULCINEE code has been chosen for peculiar capacity to achieve fast thermal hydraulic analyses. Nuclear reactor shutdowns normally spend few seconds to complete and for that, proper models for fluid properties variations need to be implemented.
Thus, neutronic parameters and feedback coefficients account multiplication response of the system facing a reactivity transient. Finally, the antireactivity insertion laws are provided to consider proper shutdown features.

5.1 Thermal Hydraulic Model

Thermal hydraulic description is required to account for temperature field determination mainly in fuel and cladding. It is necessary for safety reasons concerning capability of material to withstand severe thermal conditions but also to take into account reactivity thermal feedbacks on multiplication (Camprini et al., 2011).
Foremost, core geometry is divided in different portions in order to highlight the important media for kinetics analysis and at which extent. First, cylindrical JHR core rack is completely made of aluminum. The second part is composed by fuel elements as a whole or experimental in-core devices placed whithin the core structure holes (JHR Status Report 2009).
Thus, properly described geometry requires to deal with DULCINEE code in-built functions and features. It can handle pin-shaped or planar plate domains.
System core components are classified as follows for transients simulations:

- **fuel element**: fuel and cladding plates are completely modelled for power and

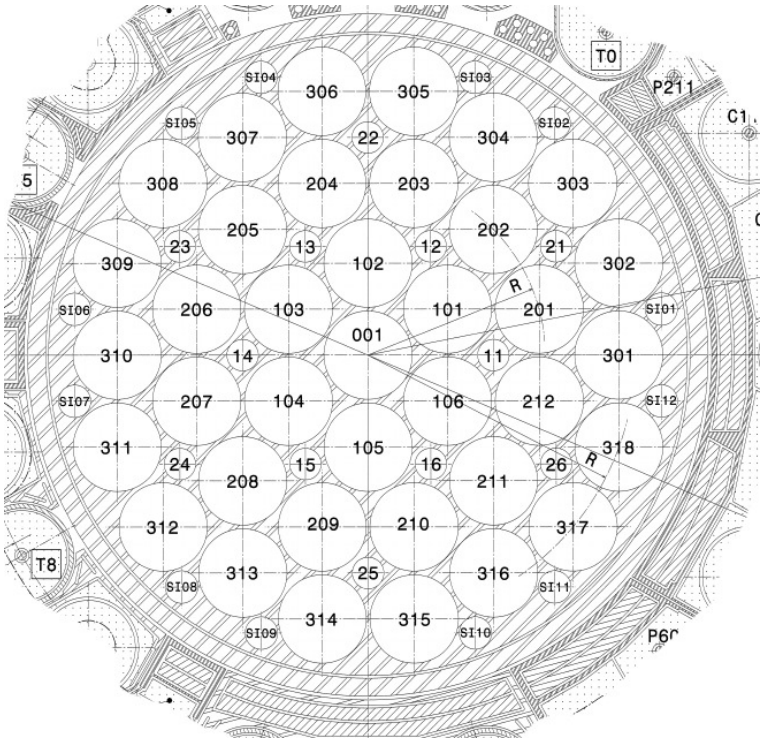

Figure 5.1: JHR core cross-section (Courtesy by AREVA-TA)

feedbacks evaluations

- **core rack**: at thermal equilibrium with average coolant temperature, it does not significantly contribute to thermal inertia
- **experimental devices**: no fissile material samples are introduced in core and they are not supposed to influence reactivity transients

In addition, DULCINEE code allows only two-region cores modelling and modular geometry is mandatory implemented concerning code in-built functions. The objective is to perform time-dependent simulations and then the aim in similar geometry conceiving is to preserve the overall dynamic behaviour of the system. This part regards temperature field of different media and then dynamic evolution of this physical quantity is expected to be maintained. Theoretically, fuel and cladding temperature equations are referred to as source-free and source term Fourier's equation, respectively. Provided separation of variables, as it is possible for this kind of equations (Hancock, 2006), it is straightforward to see how the average temperature obeys to the same time behaviour of local temperature in every point of the domain (Barletta, 2006).
Therefore, it has been possible to define an equivalent fuel plate which maintains representative lumped parameters - namely physical quantities which rule temporal evolution of average temperature as stated in eqs. (5.1).
In this way, pointwise temperature field transients are similarly reproduced keeping problem characteristics reliable for time-dependent simulations. The particular JHR plate

has been replaced with a planar and similar model. It is worth to underline how JHR

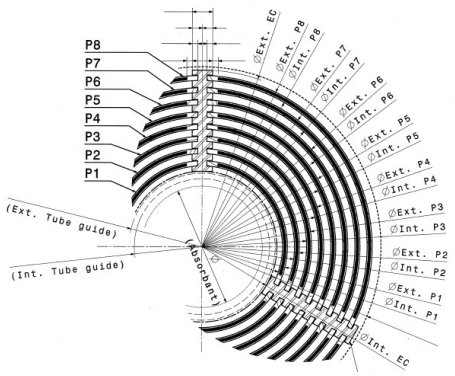

Figure 5.2: JHR fuel element cross-section (Courtesy by AREVA-TA)

plates are thermally uncoupled since stiffeners presence introduces a kind of thermal resistance and so it is possible to consider all fuel plates singularly. Inner channel is designed to be completely full of coolant but either small experimental devices or control rods are normally introduced. The water channel related to every fuel plate is then supposed to present the same thickness.
An equivalent geometry is then introduced for DULCINEE code which is a planar series of equivalent plates. Fuel, cladding and coolant average temperatures are ruled by the following lumped equations which highlight key parameters (Gaheen, 2012) to conceive a similarity thermal hydraulic model:

$$m_f c_f \frac{dT_f}{dt} = \dot{Q}_p - \alpha A_f \big(T_f - T_c\big) \tag{5.1a}$$

$$m_c c_c \frac{dT_c}{dt} = \alpha A_f \big(T_f - T_c\big) - h A_c \big(T_c - T_w\big) \tag{5.1b}$$

$$m_w c_w \frac{dT_w}{dt} = h A_c \big(T_c - T_w\big) - \dot{m}_w c_w \big(T_{w_{out}} - T_{w_{in}}\big) \tag{5.1c}$$

Equation (5.1a) states a balance between the power generated within the single plate and the amount of energy released through the surface toward the cladding. In the same way, equation (5.1b) makes a balance between power received from the fuel and that delivered throughtout the wall to the coolant. Finally, equation (5.1c) accounts for the lumped coolant volume and the enthalpy balance applied to fluid mass rate (Bortot et al., 2010).
Quantities of interest are then:

- m_f, m_c, m_w: fuel, cladding and coolant mass in the plate
- c_f, c_c, c_w: fuel, cladding and coolant specific heat capacity
- α, h: fuel-cladding global transfer coefficient and coolant convection coefficient
- A_f, A_c: external fuel and cladding surfaces
- $\dot{Q}_p$: power produced within the single plate

- $\dot{m}_w$, $T_{w_{in}}$: thermal hydraulic boundary conditions for inlet coolant mass rate and temperature

In order to preserve physical previously listed quantities, volumes and surfaces have to be conserved in the average equivalent plate. Computations have been carried out for what concerns a fuel element sector - namely a third part of the fuel element.

5.1.1 Elementary Cell Geometry

Representative thermal hydraulic conditions impose geometrical similarity regarding the following parameters in what has been retained as an elementary cell matching code requests for simulation:

- V_f: fuel volume
- V_c: cladding volume
- V_w: coolant volume
- A_f: fuel exchange surface
- A_c: cladding exchange surface

DULCINEE models deal with modular repetition of an elementary cell in a plate geometry as showed in figure 5.3. Fuel and cladding cross-sections have been computed on average with respect to a fuel element sector. Fuel and cladding exchange surface proved to be equivalent since fuel meat thickness is quite negligible compared to azimuthal lenght. Geometrical features presented in table 5.1 lead to define the similarity equivalent plate whose parameters are listed in table 5.2. For what concerns thermal hydraulic boundary conditions, no local pressure drops in core crossing are considered here; just inlet and outlet concentrated pressure drops are retained.

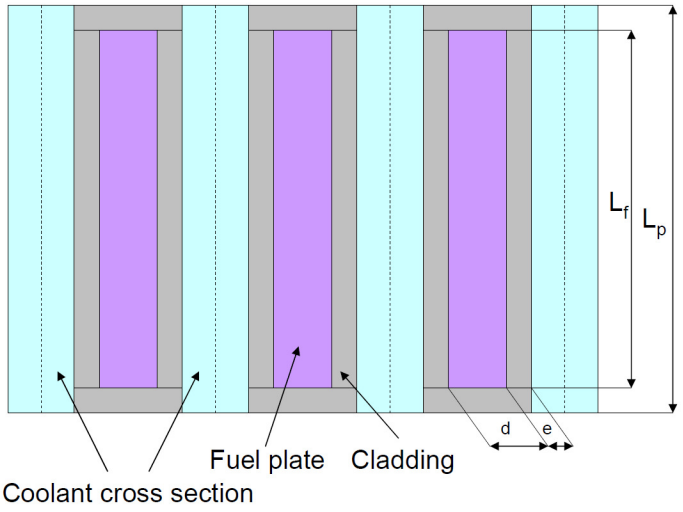

Figure 5.3: DULCINEE model fuel element cross-section

Fuel Cross-sections for Sector		
Fuel plate 1	[mm^2]	23,79
Fuel plate 2	[mm^2]	28,03
Fuel plate 3	[mm^2]	32,28
Fuel plate 4	[mm^2]	36,52
Fuel plate 5	[mm^2]	40,76
Fuel plate 6	[mm^2]	45,00
Fuel plate 7	[mm^2]	49,24
Fuel plate 8	[mm^2]	53,48
Total fuel	[mm^2]	309,13

Plate Surfaces for Sector		
Surface plate 1	[cm^2]	46,81
Surface plate 2	[cm^2]	55,15
Surface plate 3	[cm^2]	63,50
Surface plate 4	[cm^2]	71,84
Surface plate 5	[cm^2]	80,18
Surface plate 6	[cm^2]	88,53
Surface plate 7	[cm^2]	96,87
Surface plate 8	[cm^2]	105,22

Clad Coolant Cross-sections for Sector		
Inner clad plate 1	[mm^2]	14,43
Outer clad plate 1	[mm^2]	15,21
Inner clad plate 2	[mm^2]	17,07
Outer clad plate 2	[mm^2]	17,86
Inner clad plate 3	[mm^2]	19,71
Outer clad plate 3	[mm^2]	20,50
Inner clad plate 4	[mm^2]	22,35
Outer clad plate 4	[mm^2]	23,14
Inner clad plate 5	[mm^2]	24,99
Outer clad plate 5	[mm^2]	25,78
Inner clad plate 6	[mm^2]	27,64
Outer clad plate 6	[mm^2]	28,42
Inner clad plate 7	[mm^2]	30,28
Outer clad plate 7	[mm^2]	31,07
Inner clad plate 8	[mm^2]	32,92
Outer clad plate 8	[mm^2]	33,71
Total clad	[mm^2]	385,15
Sector stiffener	[mm^2]	184,46
Total clad+stiffener	[mm^2]	569,61
Coolant	[mm^2]	1216,68

Table 5.1: Media cross-section computations for equivalent plate

5.1.2 Material Physical Properties

Thermal inertias and heat capacities influence time behaviour of temperature field as explained before and for this reason proper physical properties have been chosen for fuel and cladding media. DULCINEE allows them to be selected by the user as function of temperature.
Provided data concerned following materials according to CEA internal database (Marelle et al., 2005):

- thermal expansion coefficient
- heat capacity
- thermal conductivity

JHR fuel meat is composed by a uranium silicide U_3Si_2 27% enriched in U235 metallic alloy. Fissile compound is accomodated within an aluminum matrix. Cladding alloy is an innovative Al-Fe-Ni compound. Thermal characteristics of 5754-O aluminum alloys are taken into account as showed.

5.1.3 Core Power Distribution

Fission generation within the fuel plate presents an axial distribution which is influenced by neutron flux shape. Conversely, since JHR fuel plate thickness results to be very narrow, fission profile has not been supposed to change radially.

Simulation Average Plate Parameters			
V_f	Fuel volume	[cm^3]	23,18
V_c	Cladding volume	[cm^3]	28,88
V_s	Stiffener volume	[cm^3]	13,83
V_w	Coolant volume	[cm^3]	91,25
H	Plate total height	[cm]	60,00
L_f	Fuel lenght	[mm]	63,35
d	Fuel thickness	[mm]	0,61
e	Cladding thickness	[mm]	0,38
$L_p - L_f$	Stiffner	[mm]	8,42
A_f	Coolant cross-section	[mm^2]	152,09
Wet perimeter		[cm]	16,4
Hydraulic diameter		[mm]	3,71

Table 5.2: Media surfaces computations for equivalent plate

Fuel Meat U_3Si_2-Al	
Fuel Composition	45,3% U_3Si_2 51% Aluminum (1050A) 3,7% Porosity
Density [kg/m^3]	6904
Thermal Conductivity [W/mK]	λ = 83 for fresh fuel λ = 42 for 3 cycles irradiated fuel
Specific Heat Capacity [J/kg/K]	c_v = 0,0833 T + 338
Thermal Dilatation Coefficient [10^{-6} K]	α = 5,85 10^{-3} T + 20,16

Table 5.3: Fuel meat physical properties (Marelle et al., 2005)

Cladding Aluminum Alloy	
Cladding Composition	0,40% Si 0,40% Fe 0,10% Cu 0,50% Mn 3,60% Mg 0,30% Cr 0,20% Zn 0,15% Ti Al remaining percentage
Density [kg/m^3]	2670 (20°)
Thermal Conductivity [W/m/K]	λ = 1,62 10^2 - 3,77 10^2 T^{-1} + 5,83 10^{-2} T (50$\leq T \leq$400°C)
Specific Heat Capacity [J/kg/K]	c_v = 945 (20$\leq T \leq$ 450°C) c_v = 9,23 10^2 - 3,41 10^2 T^{-1} + 2,88 10^{-1} T (100$\leq T \leq$ 450°C)
Thermal Dilatation Coefficient [10^{-6} K]	α = 23,8 (T=100°C) α = 24,7 (T=200°C) α = 25,7 (T=300°C)

Table 5.4: Cladding physical properties (Marelle et al., 2005)

Provided an initial homogeneous material composition, fission reaction macroscopic cross section is quite constant. Fuel irradiation during cycle induces depletion as far as reaction rate is concerned. Thus, high flux zones are caused to burn more fissile and then to

Coolant Thermal Parameters	
Reynolds number (turbulent)	76800
Coolant mass rate [kg/s]	1803
Average inlet coolant velocity [m/s]	14,5
Inlet pressure [bar]	9,3
Outlet pressure [bar]	6,3
Average core pressure drop [bar]	3,0
Convection coefficient relation	$h = M_s c_p \rho v$
Margoulis relation	0,27 $\mathrm{Re}^{0,2}$ $\mathrm{Pr}^{0,66}$

Table 5.5: Coolant physical properties

locally reduce fission rates.
Concerning axial flux shape, a significant departure from bare reactor profile is expected since light water in top and bottom parts of the core provides sufficient moderation due to important volume fractions. This induces thermal flux to rise enhancing fission reaction rates and then local power generation (Edon, 2008).
Fuel temperature is a main safety constraint and its lower limit is influenced by coolant bulk temperature and local thermal resistance, for a given power transferred to the fluid. In topper part of the core water reaches higher temperatures and then it is necessary to locally reduce reaction rates avoiding axial neutron reflection of water there.
Boron plates are then charged at the top of the fuel element taking advantage of neutron absorption properties of isotope B^{10}. During the cycle, boron nuclides depletion impacts this effect and flux shape rises.
Monte Carlo calculation produced normalized power profiles as shown in pictures 5.4 (Courtesy by Bernard Pouchin). and 5.5. The depletion effects cause a reduction in central maximum values at EoC fuel composition. In the same way, top flux minimum is described to rise according to top plates boron consumption with respect to BoC core configuration.
As previously explained, DULCINEE code allows a twofold region core modelization, it is then possible to take into account the hottest channel and the average one.
First "hot channel" region concerns only the hottest fuel plate with a Hot Channel Factor of about 2,21 (Edon, 2008). Fuel axial profile is not supposed to change there. By contrast, second "average" region regards a representative plate within the core and it is applied to remaining 815 plates. Axial power shape is modified according to previously described depletion effects.

5.2 Neutronic Model

Since reactor transients description is the objective of this part of the present thesis, it is worth to represent the neutronic behaviour of the system during equilibrium cycle. For some reasons that will be explained later, the effects of reactor shutdowns taken into account in this study may change with respect to average fuel burnup. In addition, a

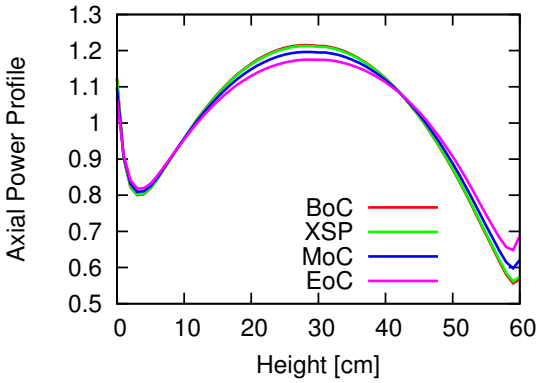

Figure 5.4: Average plate power profile (Pouchin, 2011)

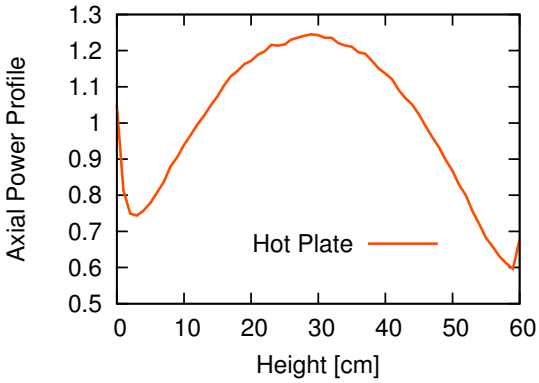

Figure 5.5: Hot plate power profile (Pouchin, 2011)

given control rod utilization may induce different reactivity insertions and then evolution of these features are reported hereafter in order to properly simulate shutdown transients for some relevant core configurations and compositions.

5.2.1 Kinetics Parameters

Neutronic parameters of the system regard multiplication features and its attitude to face reactivity variations and insertions. They depend on fuel composition and mainly on fissile materials presence. For this purpose, the 25 days fuel equilibrium cycle has been considered and four different isotope inventories have been taken into account. During neutron irradiation processes, fissile materials may either undergo fission or neutron capture. By contrast if fission occurs, several fission products are created. Some of them exhibit a significant neutron absorption cross-section mainly at thermal energies. Basically, xenon and samarium are quite important from this point of view. Particular ^{135}Xe effects impact reactivity of the system since it is created directly in fission and through the decay chain of two different fission products - namely ^{135}Te and ^{135}I. It presents a high thermal capture cross section of about 2.6 10^6 b (Lamarsh and Baratta, 2001). As every radioactive material, its concentration is a trade-off between fission generation related to neutron flux and decay process. After an initial buildup, it is possible to find a steady equilibrium concentration of this isotope. At this moment particular concentration is considered after about 2 days operation - independently of power since it is referred to volumetric quantity.
By means of deterministic code APOLLO2, long irradiation has been simulated and composition libraries are created.

- BoC: Beginning of Cycle (0 days)
- XSP: Xenon Saturation Point (2 days)
- MoC: Middle of Cycle (12 days)
- EoC: End of Cycle (25 days)

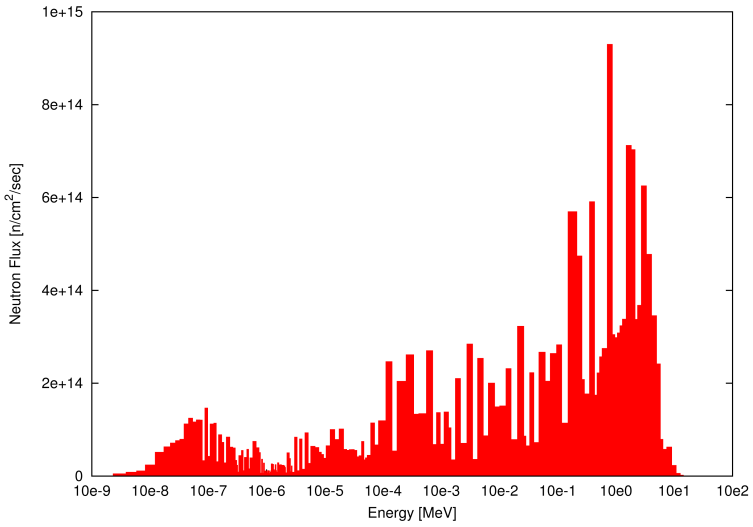

Figure 5.6: JHR core averaged neutron spectrum

Concerning kinetics parameters, irradiation provides effects in terms of fissile material buildup related to transmutation of some fertile nuclides into fissile ones. Normally in U-fuelled reactors, this process regards U238 absorption phenomena which may induce Pu239 production via transmutation and β decay. Such a breeding process is function of irradiation time and U238 concentration for a given flux level - namely power density.

β_{eff} **for Fuel Compositions**				
	BoC	XSP	MoC	EoC
Burnup [GWD/ton]	44,81	47,02	59,19	74,67
β_{eff} [pcm]	720	718	712	705

Table 5.6: Beta fraction swing during cycle

Reaching criticality is main constraint for reactor operation and balance between neutron production and leakage is mandatory for that. For a given geometry, neutron production is on average proportional to total volume via the volumetric generation rate that is proportional to power density. By contrast, leakage magnitude is related to total external surface for a convex domain. Then, volume to surface ratio states this balance.
JHR has been conceived as material testing reactor which is expected to deliver high fluxes to devices by design. Provided design constraint trade-off, power limitation imposes reduced dimensions in order to attain such elevated neutron irradiations (JHR Status Report 2004).
Finally, small dimensions imposes ratios between surface and volume which imply important leakage - properly compensated by the presence of important volume beryllium reflector. Due to that, elevated enrichement is necessary to reach criticality and enhance neutron production volumic rate for a given particle density imposed by U_3Si_2 fuel material.

Significant fissile material inventory reduces fertile abundance within the core and thus breeding rate (Artioli, 2011). In addition, short operational cycle does not permit enough time to transmute the latter fertile into important amount of fissile, thus final breeding gain is low. System response and neutronic behaviour is based on kinetics parameters explained in chapter 3, they consist of:

- delayed neutron fraction β_{eff}
- delayed neutron fraction associated to precursors group i β_i
- mean generation time Λ
- reactivity ρ

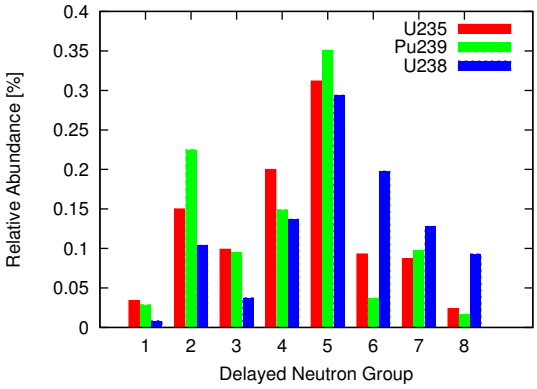

Figure 5.7: Delayed groups (JEFF 3.1)

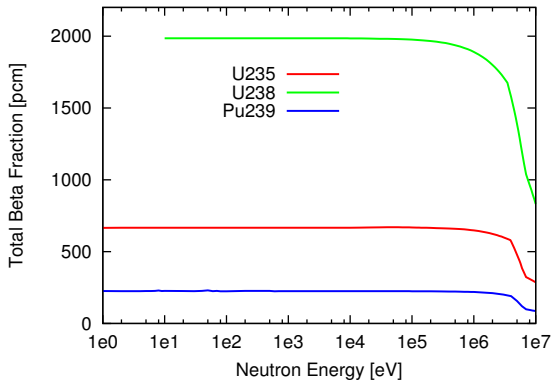

Figure 5.8: Delayed fractions (JEFF 3.1)

As previously mentioned, delayed neutron fraction considered in transient simulations depends on fissile materials hosted in reactor core. Average burnup is then related to β fraction as far as plutonium production is concerned. Low plutonium generation corresponds to a slight reduction in delayed neutron fraction and then in negligible response modification of the system as a whole, as indicated in table 5.6. Therefore, the usual split in 6 different delayed neutron groups is considered constant for a given β - namely all β_i fractions are constant in \$.
Even for mean generation time Λ, burnup calculations shown a non relevant dependence with burnup. This is coherent with information which may be inferred from a low and unchanged amount of fission contributions by U238. At the same time, delayed spectrum and fractions of U235 and Pu239 are coherent provided the small amount in fission contributions by Pu239.

5.2.2 Reactivity Coefficients

Multiplication attitude of the system is influenced by temperature field within fuel and moderator through feedback coefficients which express reactivity insertions related to changes in temperature (Hamieh and Saidinezhad, 2012).
For best-esimate evaluations, feedback coefficients regarding critical control rod insertions have been taken into account concerning:

Fuel Composition at BoC [#/cm^3]			
Composition [MWD/ton]	Fuel Plates	U235	Pu239
0	192	6,37 E-23	0,00
24000	24	7,07 E-22	2,45 E-20
28000	120	3,46 E-23	1,44 E-21
32000	72	2,03 E-23	9,89 E-20
52000	24	6,04 E-22	5,12 E-20
56000	48	1,17 E-23	1,08 E-21
60000	96	2,29 E-23	2,29 E-21
64000	24	5,60 E-22	6,03 E-20
80000	24	5,02 E-22	7,04 E-20
84000	48	9,75 E-22	1,45 E-21
88000	72	1,42 E-23	2,23 E-21
92000	48	9,17 E-23	1,53 E-21
96000	24	4,44 E-22	7,82 E-20
Total	816	2,14	1,38 E-2
U235 99,36%		**Pu239 0,64%**	

Table 5.7: Fissile balance at BoC (Pouchin, 2011)

Fuel Composition at XSP [#/cm^3]			
Composition [MWD/ton]	Plates Plates	U235	Pu239
2500	48	1,57 E-23	1,79 E-19
1500	24	7,91 E-22	3,50 E-18
2000	120	3,94 E-23	2,98 E-19
28000	72	2,07 E-23	8,65 E-20
32000	144	4,06 E-23	1,97 E-21
56000	96	2,35 E-23	2,17 E-21
64000	72	1,68 E-23	1,80 E-21
68000	24	5,45 E-22	6,30 E-20
80000	24	5,02 E-22	7,04 E-20
84000	24	4,87 E-22	7,25 E-20
88000	24	4,73 E-22	7,46 E-20
92000	96	1,83 E-23	3,06 E-21
96000	48	8,89 E-22	1,56 E-21
Total	816	2,12	1,43 E-2
U235 99,33%		**Pu239 0,67%**	

Table 5.9: Fissile balance at XSP (Pouchin, 2011)

Fuel Composition at MoC [#/cm^3]			
Composition [MWD/ton]	Fuel Plates	U235	Pu239
104000	72	1,24 E-23	2,44 E-21
108000	48	8,03 E-22	1,65 E-21
112000	24	3,87 E-22	8,41 E-20
12000	96	3,00 E-23	4,29 E-20
16000	96	2,94 E-23	6,17 E-20
40000	72	1,94 E-23	1,22 E-21
44000	120	3,16 E-23	2,22 E-21
48000	24	6,18 E-22	4,79 E-20
64000	24	5,60 E-22	6,03 E-20
68000	24	5,45 E-22	6,30 E-20
72000	48	1,06 E-23	1,31 E-21
76000	72	1,55 E-23	2,04 E-21
80000	24	5,02 E-22	7,04 E-20
92000	24	4,58 E-22	7,65 E-20
96000	24	4,44 E-22	7,82 E-20
100000	24	4,30 E-22	7,99 E-20
Total	816	1,96	1,75 E-2
U235 99,12%		**Pu239 0,88%**	

Table 5.8: Fissile balance at MoC (Pouchin, 2011)

Fuel Composition at EoC [#/cm^3]			
Composition [MWD/ton]	Fuel Plates	U235	Pu239
108000	24	4,01 E-22	8,28 E-20
112000	120	1,93 E-23	4,20 E-21
124000	48	6,90 E-22	1,74 E-21
128000	24	3,31 E-22	8,80 E-20
24000	24	7,07 E-22	2,45 E-20
28000	96	2,77 E-23	1,15 E-21
32000	72	2,03 E-23	9,89 E-20
52000	24	6,04 E-22	5,12 E-20
56000	48	1,17 E-23	1,08 E-21
60000	120	2,87 E-23	2,87 E-21
64000	24	5,60 E-22	6,03 E-20
80000	24	5,02 E-22	7,04 E-20
84000	48	9,75 E-22	1,45 E-21
88000	24	4,73 E-22	7,46 E-20
92000	72	1,37 E-23	2,29 E-21
96000	24	4,44 E-22	7,82 E-20
Total	816	1,78	2,11 E-2
U235 98,83%		**Pu239 1,17%**	

Table 5.10: Fissile balance at EoC (Pouchin, 2011)

Contribution to Fissions				
	BoC	XSP	MoC	EoC
Fissions in U235 [%]	97,62	97,54	97,09	96,58
Fissions in U238 [%]	0,78	0,78	0,78	0,78
Fissions in Pu239 [%]	1,60	1,68	2,12	2,63
Total [%]	100,00	100,00	100,00	100,00

Table 5.11: Fission reactions split per nucleus

β_i **Delayed Neutron Fractions**						Λ **Neutron Lifetime**
β_1 [\$]	β_2 [\$]	β_3 [\$]	β_4 [\$]	β_5 [\$]	β_6 [\$]	[μ sec]
0,0404	0,1795	0,1743	0,3795	0,0837	0,1427	39

Table 5.12: Beta fractions and Neutron lifetime

λ_i **Delayed Neutron Decay Constants**					
λ_1 [s^{-1}]	λ_2 [s^{-1}]	λ_3 [s^{-1}]	λ_4 [s^{-1}]	λ_5 [s^{-1}]	λ_6 [s^{-1}]
0,01330	0,03250	0,12182	0,31651	0,98880	2,94956

Table 5.13: Delayed precursors decay constants

- Moderator coefficient
- Doppler coefficient
- Void coefficient

Retained void coefficient both for safety and best estimate analyses has been of $4,53\ 10^5$ pcm/m^3 (Sireta, 2011). Moderator and Doppler parameters are considered from parametric analysis.
Considered moderator average temperature is about 40°C, fuel conditions for Doppler evaluations are estimated around 90°C. This is coherent with simulation results.
Control rod configuration impacting feedback coefficients has been provided as corresponding to criticality insertion. In fact, source data (Edon, 2004) regard static calculations coherent with these simulation hypothesis.

Once model prepared, a stationary calculation has been carried out to verify hypothesis concerning temperatures of different media - namely fuel and coolant for feedback coefficients, plots are reported in figures 5.9 and 5.10.
Regarding the hot channel simulations, maximum fuel temperature of about 125,6°C and maximum cladding temperature of some 107,5°C as well as axial profiles allowed model control and validation with respect to technical AREVA Reports. Conversely, average channel temperature profiles reach maximum fuel value of about 77,4°C and 69,2°C for cladding.

Fuel Element Average Burnup				
Fuel Element	BoC [MWD/ton]	XSP [MWD/ton]	MoC [MWD/ton]	EoC [MWD/ton]
001	94833	97316	111348	128157
101	88264	90625	103830	120079
102	91966	93852	106825	123322
104	92862	95117	108582	124668
105	89570	91968	105038	121322
106	89653	92092	105321	121705
201	60569	62855	75277	90916
202	53207	55055	65251	79740
203	59771	62034	74728	90154
204	83809	86054	98694	113549
205	63579	66025	79616	95756
206	83039	85241	97393	112376
207	61333	63627	76288	92043
208	0	2245	14442	29472
209	79256	81504	93489	108556
210	57418	59279	69176	85239
212	31021	33461	46680	63796
302	0	2243	14552	30169
303	0	2307	14642	30061
304	0	2379	15107	30710
305	0	1982	12687	25438
306	29454	31788	44475	59265
307	56644	58867	70976	85128
308	30033	32411	45282	60787
309	0	1966	12625	26880
310	26355	28161	38323	54459
311	59021	61189	72953	87936
312	30051	32399	45272	61050
313	29736	32067	44440	59644
314	29682	32001	44149	59540
315	27284	29493	41029	56281
316	24992	27154	38510	53804
317	0	2199	13851	29671
318	0	1715	11636	27168
Average	44806	47020	59191	74672

Table 5.14: Fuel element burnup during cycle

5.2.3 Shutdown Procedures

Positive or negative reactivity insertion is the most significant variation in kinetics parameters of the reactor. Since in present analysis only shutdown transients are simulated, negative external reactivity will be dealt with - namely antireactivity.
Total magnitude and time evolution vary depending upon particular shutdown proce-

Moderator Coefficient [pcm/°C]				
Configuration		20°	40°	100°
BoC	Rods up	-9,6	-13,9	-23,9
	Critical	-12,1	-17,0	-28,4
	Rods down	-14,0	-19,5	-32,1
XSP	Rods up	-8,9	-13,1	-22,9
	Critical	-10,6	-15,3	-26,2
	Rods down	-12,4	-17,5	-29,4
MoC	Rods up	-9.5	-13,7	-23,4
	Critical	-10,5	-14,9	-25,2
	Rods down	-12,5	-17,5	-29,0
EoC	Rods up	-10,0	-14,2	-23,9
	Critical	-10,1	-14,4	-24,2
	Rods down	-12,3	-17,1	-28,0

Table 5.15: Moderator coefficients

Doppler Coefficient [pcm/°C]				
Configuration		30°	90°	200°
BoC	Rods up	-3,08	-2,78	-2,42
	Critical	-3,02	-2,75	-2,37
	Rods down	-3,03	-2,75	-2,39
XSP	Rods up	-3,07	-2,81	-2,43
	Critical	-3,06	-2,79	-2,41
	Rods down	-3,04	-2,75	-2,39
MoC	Rods up	-3,15	-2,86	-2,48
	Critical	-3,14	-2,85	-2,47
	Rods down	-3,12	-2,82	-2,46
EoC	Rods up	-3,24	-2,94	-2,54
	Critical	-3,22	-2,94	-2,56
	Rods down	-3,20	-2,92	-2,53

Table 5.16: Doppler coefficients

	Moderator Coefficient		Doppler Coefficient	
	Best Estimate	Safety	Best Estimate	Safety
BoC	-17,00	-23,63	-2,75	-3,92
XSP	-15,30	-23,63	-2,79	-3,92
MoC	-14,90	-23,63	-2,85	-3,92
EoC	-14,40	-23,63	-2,94	-3,92

Table 5.17: Feedback coefficients for DULCINEE simulations

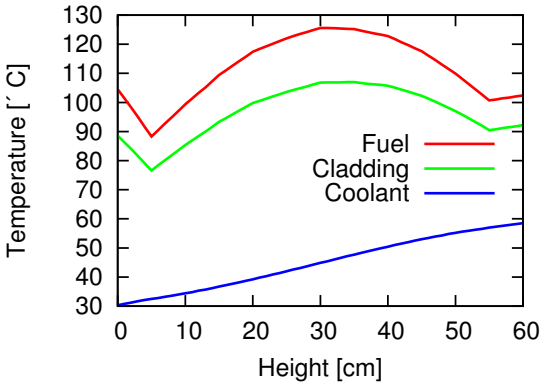

Figure 5.9: Initial hot channel profiles

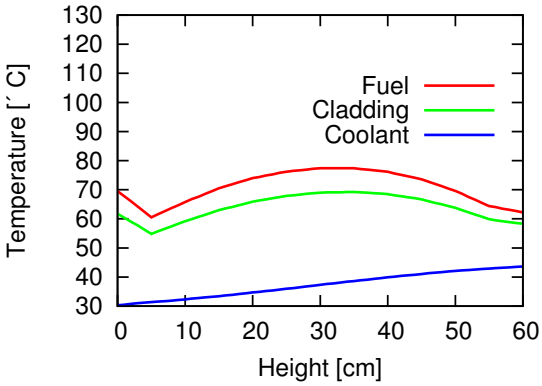

Figure 5.10: Initial average profiles

dure which is considered. For this purpose, Normal Shutdown and Safety Shutdown are considered in the present thesis (Guillot, 2007).
Both are expected to be applied at different instants during equilibrium cycle and then antireactivity insertion impact on burnup has to be evaluated.
Foremost, control rod configuration for nominal - namely critical - operation conditions has been found. As explained before, design constraints regarding control devices man-

agement are:

- Compensation Rods (CR) are either inserted or extracted one by one
- Safety Rods (SR) are always completely extracted
- Pilot Rods (PR) have to remain close to core mid-plane within a proper operation interval

Detailed locations are showed in figure 2.1. Compensation Rod extraction path has been imposed by design team and preserved in order to respect constraints on PR position (Guélénec and Le Roux, 2010).
According to JHR experimental capacity configurations, some devices are loaded as follows:

- Locations 103, 211, 301 are charged with large sample devices
- Locations 101, 105, 203, 207, 211, 303, 307, 311 are charged with sample CALIPSO devices

Concerning Pilot Rods criticality insertion within operational interval, TRIPOLI calculations reported following levels for nominal configurations:

- BoC: 24 cm insertion corresponding to k_{eff}=1,00016 $\pm$ 15 pcm (1 σ)
- XSP: 13 cm insertion corresponding to k_{eff}=0,99989 $\pm$ 15 pcm (1 σ)
- MoC: 15 cm insertion corresponding to k_{eff}=0,99997 $\pm$ 15 pcm (1 σ)
- EoC: 24 cm insertion corresponding to k_{eff}=0,99987 $\pm$ 15 pcm (1 σ)

Control Rods Loading				
Fuel Element	BoC	XSP	MoC	EoC
001	**SR**	**SR**	**SR**	**SR**
102	CR ↓	CR ↓	CR ↑	CR ↑
104	CR ↓	CR ↑	CR ↑	CR ↑
106	CR ↑	CR ↑	CR ↑	CR ↑
201	**SR**	**SR**	**SR**	**SR**
202	CR ↓	CR ↓	CR ↓	CR ↑
204	CR ↑	CR ↑	CR ↑	CR ↑
205	**SR**	**SR**	**SR**	**SR**
206	**PR**	**PR**	**PR**	**PR**
208	CR ↓	CR ↓	CR ↓	CR ↓
209	**SR**	**SR**	**SR**	**SR**
210	CR ↓	CR ↓	CR ↓	CR ↑
212	**PR**	**PR**	**PR**	**PR**

Control Rods Loading				
Fuel Element	BoC	XSP	MoC	EoC
302	CR ↓	CR ↑	CR ↑	CR ↑
304	**PR**	**PR**	**PR**	**PR**
305	CR ↓	CR ↓	CR ↓	CR ↑
306	CR ↑	CR ↑	CR ↑	CR ↑
308	CR ↓	CR ↑	CR ↑	CR ↑
309	CR ↓	CR ↓	CR ↓	CR ↑
310	CR ↓	CR ↓	CR ↑	CR ↑
311	CR ↑	CR ↑	CR ↑	CR ↑
312	CR ↓	CR ↑	CR ↑	CR ↑
314	CR ↑	CR ↑	CR ↑	CR ↑
315	**PR**	**PR**	**PR**	**PR**
316	CR ↑	CR ↑	CR ↑	CR ↑
317	CR ↑	CR ↑	CR ↑	CR ↑
318	CR ↓	CR ↓	CR ↑	CR ↑

Normal Shutdown

This shutdown procedure involves only Pilot Rods clustered in a bank and inserted starting from criticality position. It has turned out to be modified by fuel cycle configuration and burnup since operational insertion is from time to time optimised in order to reach criticality.
TRIPOLI calculations showed rod worth for complete insertions starting from 4 fuel configurations as follows:

- BoC PR configuration: top k_{eff} = 1,00843; bottom k_{eff} = 0,97755 $\rightarrow \Delta\rho$ = 3159 pcm
- XSP PR configuration: top k_{eff} = 1,00100; bottom k_{eff} = 0,97261 $\rightarrow \Delta\rho$ = 2919 pcm
- MoC PR configuration: top k_{eff} = 1,00260; bottom k_{eff} = 0,97387 $\rightarrow \Delta\rho$ = 2949 pcm
- EoC PR configuration: top k_{eff} = 1,00793; bottom k_{eff} = 0,97785 $\rightarrow \Delta\rho$ = 3075 pcm

Operational interval limits offer two different boundaries between every possible antireactivity insertion is comprised. In fact, criticality position of Pilot Rods is between a bottom and a top extreme imposed by operational interval.

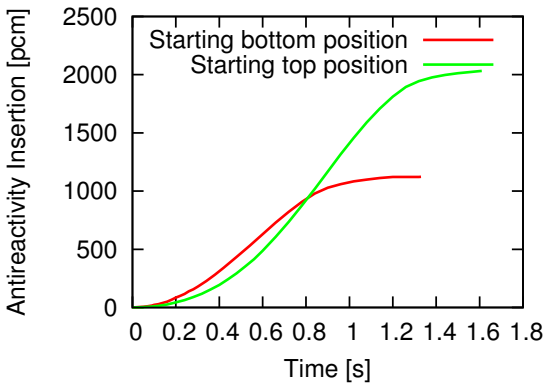

Figure 5.11: Best estimate PR insertions

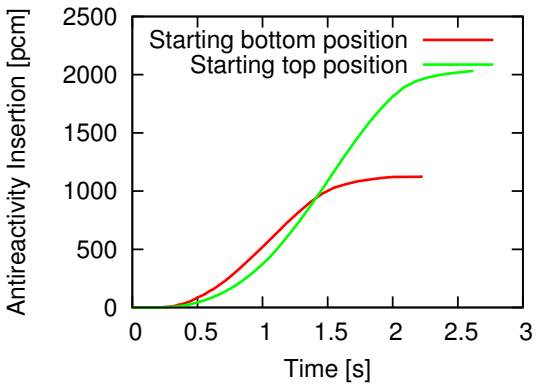

Figure 5.12: Safety PR insertions

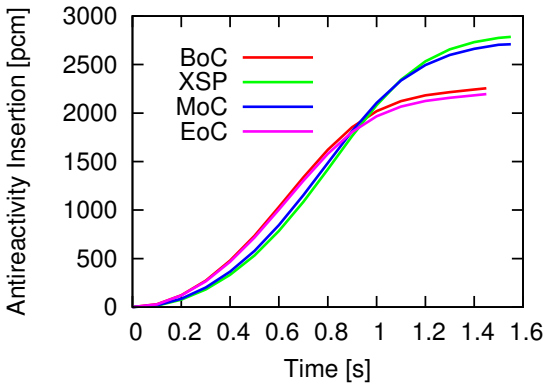

Figure 5.13: Best estimate PR insertions

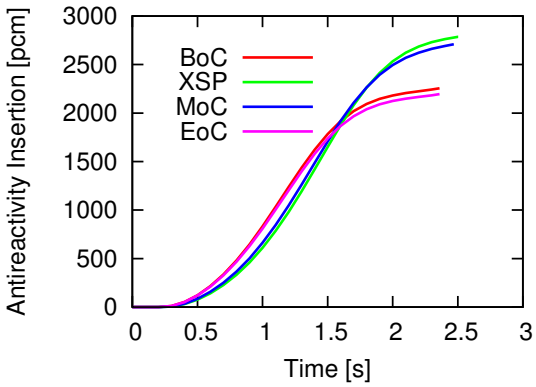

Figure 5.14: Safety PR insertions

Considering previously showed criticality insertions and evaluated control rod worth, Normal Shtdown procedures for different possible equilibrium fuel cycle configurations have been computed:

- BoC Normal Shutdown total worth: 2256 $\pm$ 30 pcm (1 σ) (in 2,36 sec)
- XSP Normal Shutdown total worth: 2785 $\pm$ 30 pcm (1 σ) (in 2,50 sec)
- MoC Normal Shutdown total worth: 2709 $\pm$ 30 pcm (1 σ) (in 2,47 sec)
- EoC Normal Shutdown total worth: 2196 $\pm$ 30 pcm (1 σ) (in 2,36 sec)

Normal Shutdown performances have then turned out to be significantly dependent on fuel cycle instant. Compensation Rods extraction is planned in order to provide reactivity to balance fuel depletion and mainly to compensate fission product poisoning due to xenon at XSP.
In fact, first step in control path envisages xenon peak build-up compensation. Positive reactivity is injected by means of 4 Compensation Rods extraction: 308, 312, 302, 104. Except for 104, they are placed in the periphery of the core and regard quite fresh fuel elements. 308 and 312 assemblies belong to third quarter and 302 may be referred to as fresh fuel since it corresponds to last quarter in charging management. Neutron importance reduction regarding core periphery locations are compensated by thermal neutron contributions from reflector. In fact, even if JHR neutron spectrum is quite hard around some 220 keV, thermal fissions drive reactor operations. Concerning fuel element 104 position, central core importance and first quarter composition are matched since it is necessary to extract a central element in order not to perturb to a great extent flux global shape. In addition, Pilot Rods need to be partially withdrawn since xenon concentration slope in poisoning results to be very effective in this first equilibrium cycle fraction. Therefore, during Normal Shutdown, Pilot Rods insertion causes the highest antireactivity injection coherently with reduced operational insertion to reach criticality.
Xenon equilibrium peak being reached, second step in Compensation Rods extraction at MoC has planned and rods 310, 318 and 102 are withdrawn. Like previous step, 310 and 318 assemblies regard periphery region and are third and fourth quarter respectively. Now mainly fuel depletion is compensated and flux shape is maintained thanks also to a central rod extraction in a relatively depleted assembly, 102. In fact, xenon concentration being already reached, Pilot Rods may be reinserted.
Third step provides extraction of 4 Compensation Rods more. Elements 202, 210, 305, 309 belong to peripherical last quarter fresh fuel for 305 and 309. By contrast, second quarter regards 202 and 210. Such a reactivity insertion is needed to bring Pilot Rods back to initial criticality insertion and enhance differential worth in piloting procedures.
As far as previous control device management scheme, it is worth to take into account burnup core features since they impact control rod insertion performances and, finally, shutdown effectiveness.

Safety Shutdown

Safety Shutdown procedure involves both Pilot and Safety Rods. The two banks of clustered rods are activated and injected at the same time starting from initial positions.
In this case, Safety Rods are evaluated with only one insertion time for best estimate and safety purposes. By contrast, a twofold transient description is performed for Safety Rods. They are designed in order to have the first one which operates on a relevant amount of reactivity as far as neutron importance and location are concerned.
For this reason, transient analyses are operated for:

- 4 Safety Rods cluster
- 3 Safety Rods supposing unavailable the central one (001)

In fact, TRIPOLI calculation highlighted the following results for 4 Safety Rods complete insertions:

- BoC 4 Safety Rods total worth: 4950 $\pm$ 30 pcm (1 σ)
- XSP 4 Safety Rods total worth: 4854 $\pm$ 30 pcm (1 σ)
- MoC 4 Safety Rods total worth: 4785 $\pm$ 30 pcm (1 σ)
- EoC 4 Safety Rods total worth: 4605 $\pm$ 30 pcm (1 σ)

TRIPOLI evaluations concerning only 3 Safety Rods yielded as follows:

- BoC 3 Safety Rods total worth: 4363 $\pm$ 30 pcm (1 σ) (in 1,23 sec)
- XSP 3 Safety Rods total worth: 3523 $\pm$ 30 pcm (1 σ) (in 1,23 sec)
- MoC 3 Safety Rods total worth: 3583 $\pm$ 30 pcm (1 σ) (in 1,23 sec)
- EoC 3 Safety Rods total worth: 4033 $\pm$ 30 pcm (1 σ) (in 1,23 sec)

Conversely, total effect of Safety Shutdown with both Safety and Pilot Rods is about:

- BoC 4 Safety and 4 Pilot Rods total worth: 7206 $\pm$ 30 pcm (1 σ) (in 2,36 sec)
- XSP 4 Safety and 4 Pilot Rods total worth: 7640 $\pm$ 30 pcm (1 σ) (in 2,50 sec)
- MoC 4 Safety and 4 Pilot Rods total worth: 7494 $\pm$ 30 pcm (1 σ) (in 2,47 sec)
- EoC 4 Safety and 4 Pilot Rods total worth: 6802 $\pm$ 30 pcm (1 σ) (in 2,36 sec)

Central location is characterized by the highest neutron importance and thus it is possible to distinguish a gap between different fuel configurations which becomes relevant in 3 rods shutdown as it is depicted in figures 5.15 and 5.16.
Control rods are accelerated in topper part according to gravitational or forced insertion. Conversely, deceleration in core bottom induces a distortion of the s-shape depicted in these latter plots since dashpot breaks affect insertion law. For this reason a slope change in plot is pointed out at about 0,6 sec. Finally the entire Safey Shutdown may be composed through effects superposition since second order contributions have been evaluated of the same magnitude of Monte Carlo statistical uncertainty.
The impact of Safety Rods is underlined by a strong change in reactivity plot slope corresponding to higher differential worth until about 0,6 sec. These latter shutdowns are showed in figures 5.17 and 5.18.

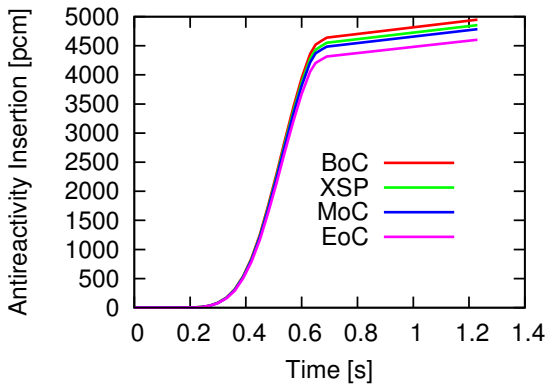

Figure 5.15: 4 Safety Rods insertion

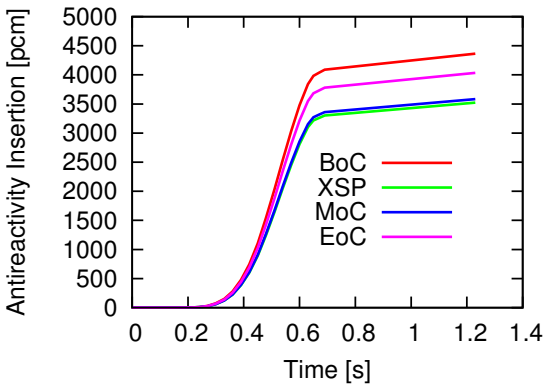

Figure 5.16: 3 Safety Rods insertion

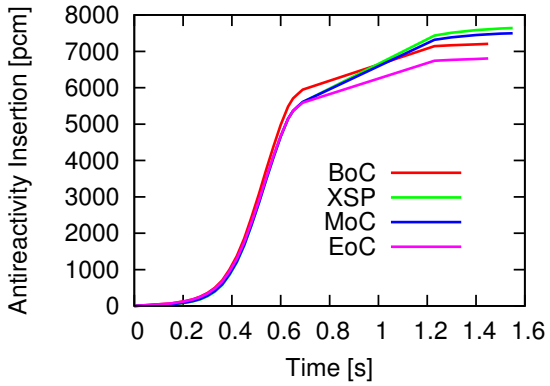

Figure 5.17: Best estimate SR + PR

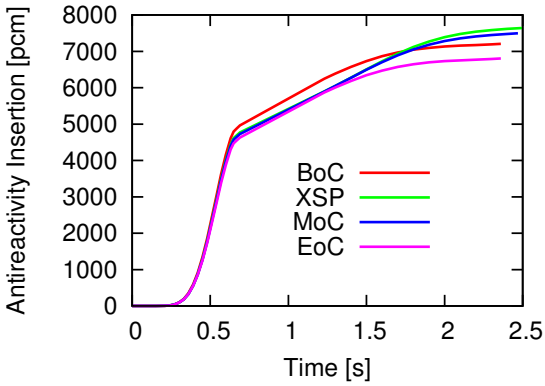

Figure 5.18: Safety SR + PR

5.3 Core Power Deposition Model

Fission reaction energy is deposited through different nuclear interactions of radiation and particles with matter. Basically, nucleus fragmentation is suddenly followed by gamma and neutron emission. Most of recoverable power appears as fission fragments kinetic energy. This kinetic energy released to matter (KERMA) is the main contribution to core heating and the deposition path is very short regarding diffusion range of highly charged particles in a medium.

As explained regarding nuclear reactor theory, some 2,5 neutrons are generated on average per fission and they may be either prompt or delayed. Moreover, their kinetic energy is transmitted to the moderator in order to be slowed down. After such an energy transfer, they may be captured due to nuclei resonances even during slowing down process. Subsequent gamma emission is likely to be recovered by the system itself inducing secondary radiation heating.

Gamma production is related to fission fragments both during fission - so they are referred to as prompt gammas - and via decay process of delayed neutron precursors - namely delayed gammas. Finally, β radiation is coupled to delayed neutron emission

since fission fragments are neutron rich and such a decay and related transmutation induce β in order to respect charge conservation for nuclei. Energy carried by neutrinos which are always released if a β decay occurs is not recoverable since no significant interaction with matter is detectable.
An exemple for U235 fissions is given in table 5.18.

Form	Emitted Energy [MeV]	Recoverable Energy [MeV]
Fission fragments	168	168
Fission product decay		
β rays	8	8
γ rays	7	7
neutrinos	12	–
Prompt γ rays	7	7
Fission neutrons (kinetic energy)	5	5
Capture γ rays	–	3-12
Total	207	198-207

Table 5.18: Emitted and recoverable energies for U235 fission

Therefore, a twofold interaction gives rise to a split in a prompt energy and a delayed energy deposition. All prompt effects related to fission reaction may be modelled as following same dynamic behaviour as neutron flux. Kinetics equations are then useful to describe this fraction of deposited energy as showed in chapter 3, eq. (3.30). If the total amount of recoverable energy is referred to as $P_{fiss}(t)$, it is possible to suppose its generation proportional to neutron flux as follows:

$$\begin{cases} \dfrac{dP_{fiss}(t)}{dt} = \dfrac{\rho - \beta_{eff}}{\Lambda} P_{fiss}(t) + \displaystyle\sum_{i=1}^{6} \lambda_i C_i^* \\ \dfrac{dC_i^*}{dt} = -\lambda_i C_i^* + \dfrac{\beta_i}{\Lambda} P_{fiss}(t) \end{cases} \tag{5.2}$$

The effective deposition $P_{dep}(t)$ is split in two parts, the first is a prompt fraction of the total $P_{fiss}(t)$ which would be potentially released and the second one is delayed as far as fission product decay is concerned:

$$P_{dep}(t) = \Big(1 - \sum_j E_j\Big) P_{fiss}(t) + P_{del}(t) \tag{5.3}$$

The total power $P_{fiss}(t)$ is reduced of a fraction which corresponds to a sum over all possible decay processes which involve heat generation. This amount is deferred in time and then it may be thought of as stocked in some nuclei referred to as decay heat precursors. Main nuclear interactions are due to α, β and γ radiations and corresponding activities are related to average energy in order to provide a model of these multiple interactions.

$$P_{del}(t) = \sum_{j=1}^{k} \overline{E}_j^{\alpha} \lambda_j^{\alpha} C_j^{\alpha} + \sum_{j=1}^{l} \overline{E}_j^{\beta} \lambda_j^{\beta} C_j^{\beta} + \sum_{j=1}^{m} \overline{E}_j^{\gamma} \lambda_j^{\gamma} C_j^{\gamma} \tag{5.4}$$

This analysis has been performed coupling DULCINEE point kinetics code and PEPIN2 isotope evolution code. DULCINEE allowed computing dynamic evolution of such a prompt power and PEPIN2 yielded delayed energy deposition evolution (Tsilanizara et al., 2005) .
Results combination allowed a proper description of core power evolution for all different transients taking into account even long time scale.

5.4 Core Power Transients

As previously explained, core power transients have been calculated for following shutdown procedures:

- Normal Shutdown (NS) (best estimate times) (figure 5.19)
- Normal Shutdown (NS) (safey insertion times) (figure 5.20)
- Safety Shutdown (SS) (4 Safety + 4 Pilot Rods clusters) (figure 5.21)
- Safety Shutdown (SS) (3 Safety Rods only) (figure 5.22)

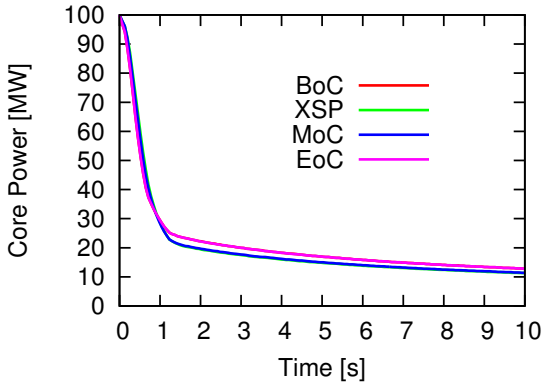

Figure 5.19: Best estimate NS

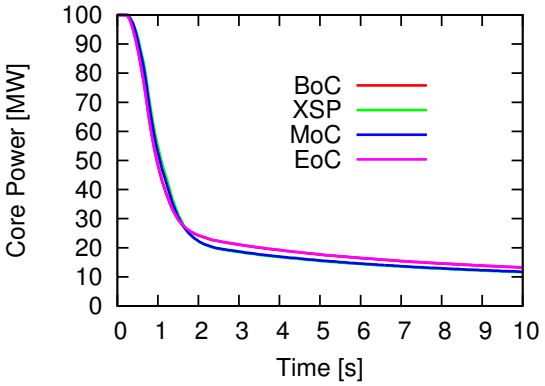

Figure 5.20: Safety NS

Foremost, delayed contribution to decay heat has been evaluated by means of PEPIN2 module of DARWIN package oriented to isotope evolution calculations. Since isotope inventory build-up is related to time orders of magnitude which are long compared to shutdown transients, delayed contribution to decay heat has been computed supposing a stationary cooling regime for fuel assemblies (code settings considered antireactivity insertion for such a cooling scenario of some 4000 pcm) (Tsilanizara et al., 2002).
In addition, only average burnup is indicated in order to take into account lumped quantities for the core as a whole. Power split is obtained through α, β and γ contributions, delayed fissions are accounted for as well.
Calculations correspond to following initial conditions:

- Boc Cooling conditions starting at about 44806 MWD/ton (table 5.19)
- XSP Cooling conditions starting at about 47020 MWD/ton (table 5.20)

- MoC Cooling conditions starting at about 59191 MWD/ton (table 5.21)
- EoC Cooling conditions starting at about 74672 MWD/ton (table 5.22)

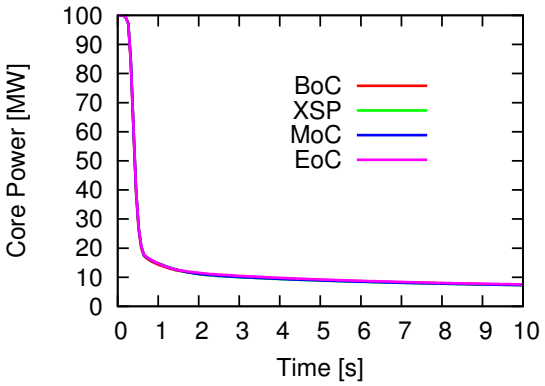

Figure 5.21: 4 SR + 4 PR SS

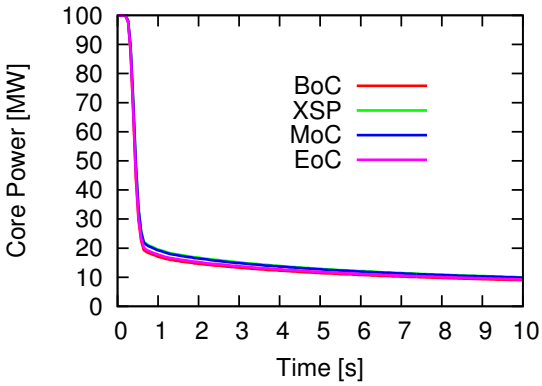

Figure 5.22: 3 Rods SS

Considerations reagarding transient results highlight a global uniform and safe response of the system in case of any kind of shutdown Power decreasing is coherent with safety needs.
As commented before, impact of burnup - namely rods management and cycle portion - is related to inherent core reactivity. Fission product and poisoning concern both 3 Safety Rods and second part of 4 Safety Rods. In first case, a less reactive core in XSP and MoC configuration yields 3 Safety Rods insertion less effective.
Conversely, second phase of 4 SS + 4 PR Safety Shutdown concerns basically just Pilot Rods effects and then initial criticality insertions have to be considered again.
It is worth to point out how a gap of some MW in such a power decreasing is not negligible as far as elevated nominal reactor power is concerned.
Finally, provided the reliability of DULCINEE model and performed thermal analyses, core power evolutions are computed. The aim is then the description of power transients of experimental devices placed in the reflector which are concerned about core transients since their power generation and fission reaction rates are largely caused by core neutron and gamma irradiation and energy deposition.

Cooling Time	Alpha Decay [W]	Beta Decay [W]	Gamma Decay [W]	Total Delayed Power [W]	Delayed Fissions Power [W]
1 sec	1,95E+00	2,95E+06	2,78E+06	5,73E+06	1,34E+07
30 sec	1,47E+00	1,72E+06	1,93E+06	3,65E+06	1,99E+06
1 min	1,47E+00	1,48E+06	1,70E+06	3,18E+06	2,76E+05
2 min	1,47E+00	1,27E+06	1,47E+06	2,74E+06	5,35E+03
4 min	1,47E+00	1,08E+06	1,28E+06	2,36E+06	2,01E+00
5 min	1,47E+00	1,03E+06	1,22E+06	2,25E+06	
10 min	1,47E+00	8,77E+05	1,06E+06	1,94E+06	
30 min	1,47E+00	6,34E+05	8,03E+05	1,44E+06	
1 hour	1,47E+00	4,97E+05	6,37E+05	1,13E+06	
2 hours	1,48E+00	3,93E+05	4,89E+05	8,82E+05	
3 hours	1,48E+00	3,44E+05	4,16E+05	7,60E+05	
4 hours	1,48E+00	3,12E+05	3,72E+05	6,83E+05	
5 hours	1,49E+00	2,88E+05	3,42E+05	6,30E+05	
10 hours	1,50E+00	2,16E+05	2,70E+05	4,86E+05	
12 hours	1,50E+00	1,99E+05	2,54E+05	4,53E+05	
1 day	1,53E+00	1,43E+05	2,00E+05	3,42E+05	
5 days	1,63E+00	6,75E+04	1,06E+05	1,74E+05	
30 days	1,66E+00	2,28E+04	3,02E+04	5,30E+04	
180 days	1,62E+00	4,06E+03	3,80E+03	7,87E+03	

Table 5.19: Decay heat at BoC configuration

Cooling Time	Alpha Decay [W]	Beta Decay [W]	Gamma Decay [W]	Total Delayed Power [W]	Delayed Fissions Power [W]
1 sec	2,22E+00	2,95E+06	2,78E+06	5,73E+06	1,33E+07
30 sec	1,75E+00	1,72E+06	1,93E+06	3,65E+06	1,98E+06
1 min	1,75E+00	1,49E+06	1,70E+06	3,19E+06	2,76E+05
2 min	1,75E+00	1,27E+06	1,48E+06	2,75E+06	5,35E+03
4 min	1,75E+00	1,09E+06	1,28E+06	2,37E+06	2,01E+00
5 min	1,75E+00	1,03E+06	1,23E+06	2,26E+06	
10 min	1,75E+00	8,79E+05	1,07E+06	1,94E+06	
30 min	1,75E+00	6,37E+05	8,06E+05	1,44E+06	
1 hour	1,75E+00	5,00E+05	6,40E+05	1,14E+06	
2 hours	1,75E+00	3,96E+05	4,92E+05	8,88E+05	
3 hours	1,76E+00	3,46E+05	4,19E+05	7,66E+05	
4 hours	1,76E+00	3,14E+05	3,75E+05	6,89E+05	
5 hours	1,76E+00	2,90E+05	3,45E+05	6,35E+05	
10 hours	1,78E+00	2,19E+05	2,73E+05	4,92E+05	
12 hours	1,78E+00	2,01E+05	2,57E+05	4,59E+05	
1 day	1,81E+00	1,45E+05	2,03E+05	3,48E+05	
5 days	1,93E+00	6,96E+04	1,09E+05	1,79E+05	
30 days	1,95E+00	2,40E+04	3,17E+04	5,57E+04	
180 days	1,89E+00	4,38E+03	4,08E+03	8,47E+03	

Table 5.20: Decay heat at XSP configuration

Cooling Time	Alpha Decay [W]	Beta Decay [W]	Gamma Decay [W]	Total Delayed Power [W]	Delayed Fissions Power [W]
1 sec	3,36E+00	2,95E+06	2,78E+06	5,73E+06	1,32E+07
30 sec	2,88E+00	1,73E+06	1,93E+06	3,66E+06	1,97E+06
1 min	2,88E+00	1,49E+06	1,71E+06	3,20E+06	2,75E+05
2 min	2,88E+00	1,28E+06	1,48E+06	2,76E+06	5,34E+03
4 min	2,88E+00	1,09E+06	1,29E+06	2,38E+06	2,02E+00
5 min	2,88E+00	1,04E+06	1,23E+06	2,27E+06	
10 min	2,88E+00	8,85E+05	1,07E+06	1,96E+06	
30 min	2,88E+00	6,43E+05	8,14E+05	1,46E+06	
1 hour	2,89E+00	5,06E+05	6,48E+05	1,15E+06	
2 hours	2,89E+00	4,02E+05	5,00E+05	9,02E+05	
3 hours	2,90E+00	3,53E+05	4,27E+05	7,80E+05	
4 hours	2,90E+00	3,20E+05	3,83E+05	7,03E+05	
5 hours	2,91E+00	2,96E+05	3,54E+05	6,50E+05	
10 hours	2,93E+00	2,25E+05	2,82E+05	5,07E+05	
12 hours	2,94E+00	2,08E+05	2,66E+05	4,74E+05	
1 day	2,99E+00	1,52E+05	2,11E+05	3,63E+05	
5 days	3,14E+00	7,51E+04	1,16E+05	1,91E+05	
30 days	3,14E+00	2,73E+04	3,55E+04	6,28E+04	
180 days	2,93E+00	5,30E+03	4,87E+03	1,02E+04	

Table 5.21: Decay heat at MoC configuration

Cooling Time	Alpha Decay [W]	Beta Decay [W]	Gamma Decay [W]	Total Delayed Power [W]	Delayed Fissions Power [W]
1 sec	5,92E+00	2,95E+06	2,78E+06	5,73E+06	1,31E+07
30 sec	5,44E+00	1,74E+06	1,94E+06	3,67E+06	1,95E+06
1 min	5,44E+00	1,50E+06	1,71E+06	3,21E+06	2,73E+05
2 min	5,44E+00	1,28E+06	1,49E+06	2,77E+06	5,31E+03
4 min	5,44E+00	1,10E+06	1,29E+06	2,39E+06	2,02E+00
5 min	5,44E+00	1,05E+06	1,24E+06	2,29E+06	
10 min	5,44E+00	8,91E+05	1,08E+06	1,97E+06	
30 min	5,45E+00	6,49E+05	8,21E+05	1,47E+06	
1 hour	5,45E+00	5,12E+05	6,55E+05	1,17E+06	
2 hours	5,46E+00	4,08E+05	5,08E+05	9,15E+05	
3 hours	5,47E+00	3,59E+05	4,35E+05	7,94E+05	
4 hours	5,48E+00	3,27E+05	3,91E+05	7,18E+05	
5 hours	5,49E+00	3,03E+05	3,62E+05	6,64E+05	
10 hours	5,53E+00	2,32E+05	2,90E+05	5,22E+05	
12 hours	5,55E+00	2,15E+05	2,74E+05	4,89E+05	
1 day	5,62E+00	1,58E+05	2,19E+05	3,78E+05	
5 days	5,84E+00	8,09E+04	1,23E+05	2,04E+05	
30 days	5,75E+00	3,10E+04	3,97E+04	7,07E+04	
180 days	5,05E+00	6,45E+03	5,80E+03	1,23E+04	

Table 5.22: Decay heat at EoC configuration

Chapter 6

Transients Analysis of Test Devices

The objective of the present thesis is the conception and implementation of a calculation method aimed at properly evaluating power transient of experimental devices placed in reflector locations of JHR material testing reactor.
Studies concerning reactor dynamics and control highlighted how large reflector size impacts time-dependent behaviour of neutron population inducing longer time constants.
In addition, experimental devices are concerned by important neutron fluxes and deposited energies with respect to actual state-of-the-art in research reactor operation, since 100 MW JHR core power is significantly elevated compared to present irradiation facilities in Europe.
Therefore, innovative calculation methods are requested starting from this feature in order to provide more detailed results regarding safety analyses. In fact, presence of some experimental locations within the reflector implies fissile material loading whose power evolution needs detailed description. Improved methodology has to model multiple core-device radiation transport interactions as far as prompt and delayed phenomena are concerned. Prompt neutrons and gammas diffuse from core to samples according to actual reactor kinetics by means of computed energy deposition coupling coefficients. Conversely delayed gammas due to fission products decay process are generated following different laws hence contribution superposition is necessary to properly compute sample heating during shutdown.
Moreover, prompt energy coupling coefficients depend on neutron flux shape which is induced and modified by control rod insertions. Finally, complete analysis required to take into account such a core-coupling modification. Results are intended to optimize normal and safety shutdown procedures utilization and enhance device capability and management.

6.1 Reflector Test Devices

This study concerns some experimental devices placed in JHR reflector. Several irradiations facilities are envisaged to be hosted in beryllium locations but here just fissile material samples are evaluated. In fact they are critical components since prompt and

delayed self-reactions contributions have to be verified to correctly compute power transients. Devices of interest in the present work are:

- MADISON device
- ADELINE device
- MOLFI device

They are designed to be placed within moving structures in order to possibly modify distance from reactor core. This approach is used to control received neutron and gamma flux level. Then the relative thermal power generation in the sample is tuned to simulate different irradiation conditions.
In this study, different reflector locations are taken into account for same device in order to consider impact of flux shape and reactor geometry. Core charge scheme is referred to 4 MOLFI devices, 2 ADELINE devices and 2 MADISON devices as depicted in figure 6.1.

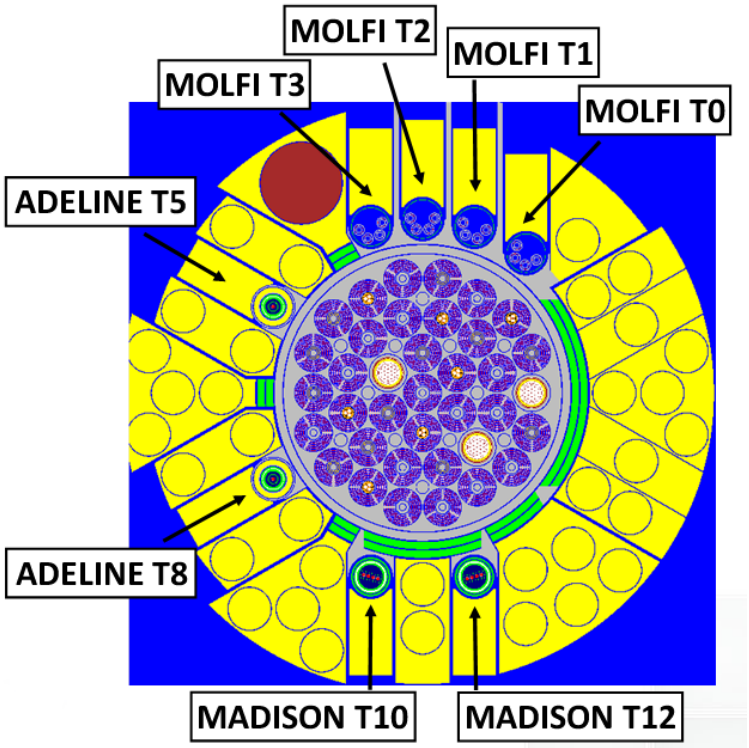

Figure 6.1: TRIPOLI model for JHR core

6.1.1 MADISON Device Model

Two MADISON devices are modeled whithin the framework of the present study, referred to as T10 and T12 depending upon reflector location. The latter are both mounted on moving structures and host 4 fuel PWR-type pins. Simulation configuration regards

UO_2 fuel 1% enriched in U235 pellets of 9,5 mm diameter. TRIPOLI Monte Carlo simulation model cross-section is depicted in figure 6.2. Pin pitch is about 13,5 mm. A rectangular frame box in Zr-alloy is placed all around the pins and a double layer may host Zr shielding in order to reduce gamma heating contribution. The aim is reproducing mid-core flat flux conditions in power reactors.
In addition, this structure is useful also to drive coolant mass rate inside the device having a pressure of about 155 bar and temperature of some 300°C, reproducing PWR thermal hydraulic conditions. Fuel pin cladding is standard PWR Zr-alloy as well. Three Zr-alloy concentric tubes ensure pressurised system. The first is classified as pressurised equipment and has 62 mm inner diameter (5,7 mm thickness). The second is for thermal insulation purposes and the third one is safety backup solution of the first with an inner diameter of some 80 mm. A helium gap (white) ensures proper thermal insulation. Pressurised inner and middle water is operated on forced convection, conversely outer water presents natural convection (Roux, 2012).

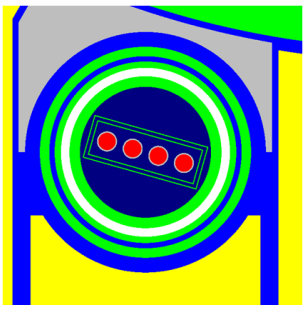

Figure 6.2: TRIPOLI model cross-section for MADISON device

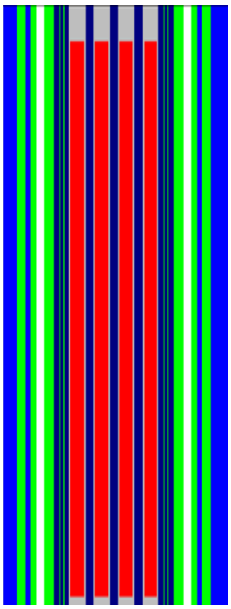

Figure 6.3: TRIPOLI model longitudinal section for MADISON device

6.1.2 ADELINE Device Model

Two ADELINE devices are considered in the model utilised in this thesis. They are referred to as T8 and T5 and placed in left part of reactor reflector. It is worth to say that there is no zirconium shielding between these devices and the core (green shield in fig. 6.1). Conversely an important shielding is present inside the device.
Every ADELINE is depicted as a pin carrier in which a UO_2 1% U235 enriched pin of about 8,2 mm is hosted. A picture of the TRIPOLI model cross-section is reported in

figure 6.4. The cladding is a standard PWR-type 0,65 mm zirconium alloy. The pressurized environment of a power reactor is reproduced with 6,25 mm thick water shielding at about 155 bar and 280°C. 2 mm Zr-alloy tube divides upward inner flowing cooling water from the external one which flows downward. Other two zirconium shields contain a gas gap filled with helium. Outside reactor pool, water cools down the external parts of the device. Beryllium annular shield is placed all around. This preliminary design configuration has been retained for the present simulations.

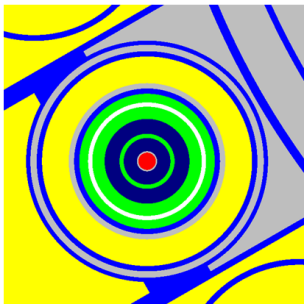

Figure 6.4: TRIPOLI model cross-section for ADELINE device

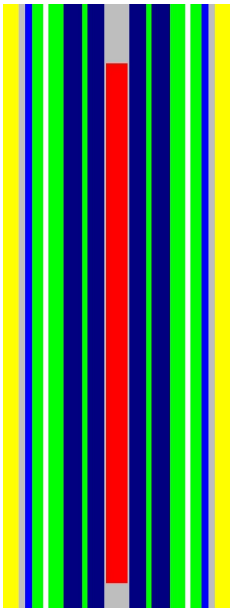

Figure 6.5: TRIPOLI model longitudinal section for ADELINE device

6.1.3 MOLFI Device Model

Four MOLFI devices are considered in present anaysis. They are referred to as T0, T1, T2 and T3 regarding reflector position. They are charged with 12 aluminum uranium alloy targets of HEU UAl 93% enriched in U235. Moreover, LEU uranium targets made of UAl 20% enriched are also taken into account in the present study. This second configuration refers to different geometry and material properties. Main water environement is a cylinder of some 9,6 cm diameter with 0,15 mm thickness Zr-alloy tube around as coolant protection. Targets are divided into 4 groups and are put in cylindrical sample holders inside aluminum tubes. Positions are optimised in order to exploit neutron flux and tubes are 3,5 mm from inner Zr surface and 3 mm each others on a circular path of 3,2 cm radius. Fuel meat of every sample is 14,8 cm height and it reaches 16 cm structural elements included. Inner and outer radii are of about 1,011 cm and 1,062 cm respectively. Aluminum cladding is just 0,38 mm.
Coolant is pool pressure water by means of upward forced circulation between targets

and inside the inner structural tube. Mass rate is mainly split and driven close to the cladding thanks to a proper imposed local pressure drop. Downward back circulation takes place in larger portion of water cylinder, inside Zr tube (Pouchin and Huot-Marchand, 2012). Exaustive description and modeling is performed in the present thesis concerning HEU fuel configuration and geometry. By contrast, LEU analyses are carried out only regarding composition, considered geometry represents a first design solution which is expected to be optimized in next conception steps.

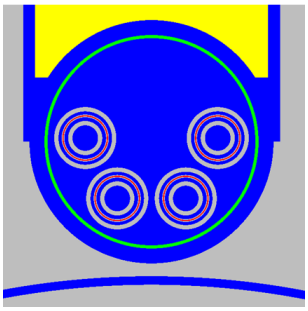

Figure 6.6: TRIPOLI model cross-section for MOLFI device

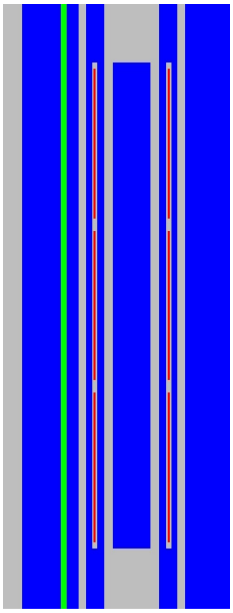

Figure 6.7: TRIPOLI model longitudinal section for MOLFI device

6.2 Device Nominal Conditions

Foremost, initial nominal power for every device has been computed. It is necessary to determine operative conditions and performances. For a given sample enrichment, it is mainly influenced by core flux distribution and neutron generation close to device location, it depends on control rod insertions and on fuel elements burnup. Moving devices have been retained in positions attached to core in order to compute conservative initial powers. In addition, device power has been evaluated with Monte Carlo energy deposition calculations concerning fuel samples, device coolant and structures. The choice about energy deposition with respect to flux evaluation moved from considerations regarding neutron leakage features. Fissions products KERMA, referred to as neutron contribution, still remains within the pellets but gamma and neutron coming out may deposite a significant fraction of this power away from the sample. As far as leakage of this small system is concerned, a great part of those radiation will not be retained. By contrast, a neutron flux ratio between device fuel and core fuel would consider a comparable

leakage rate. It is not the case concerning different volume/surface relations from core to device. Thus energy deposition has easily allowed to concern gamma effects as well. Monte Carlo simulations allowed good statistical results according to $\sigma = 1\%$ calculation uncertainty even for relatively small samples and targets. Summary of these data is given in table 6.1. Neutron and gamma contributions are reported in table 6.2.

	Neutron Deposition [kW]				Gamma Deposition [kW]			
Device	BoC	XSP	MoC	EoC	BoC	XSP	MoC	EoC
MADISON T10	106	108	102	97	20	20	19	18
MADISON T12	108	103	98	96	20	19	18	18
ADELINE T8	38	44	45	41	19	22	22	20
ADELINE T5	34	39	41	44	18	20	21	21
MOLFI (HEU) T0	618	596	586	674	27	25	25	29
MOLFI (HEU) T1	607	565	565	672	28	26	26	31
MOLFI (HEU) T2	609	572	576	666	29	27	27	31
MOLFI (HEU) T3	617	601	610	657	27	26	26	28
MOLFI[1](LEU) T0	347	334	328	378	20	20	19	22
MOLFI[1](LEU) T1	327	308	304	361	21	20	20	23
MOLFI[1](LEU) T2	331	309	311	359	21	20	20	23
MOLFI[1](LEU) T3	337	330	335	359	20	20	20	21

Table 6.1: Device nominal power (neutron + prompt gamma) ($\sigma = 1\%$)

Burnup plan of the core points out 4 regions and is depicted in fig. 6.8. First quarter includes higher burnup fuel elements, fourth quarter refers to fresher assemblies. Compensation Rods extraction procedure during equilibrium cycle is showed in fig. 6.9.
MADISON devices T10 and T12 exhibit almost the same amount of nominal neutron power deposition even if in different locations, see fig. 6.10. Lower burnup in fuel element 210 - namely more significant neutron production - is quite compensated by corresponding Compensation Rod and partial insertion of Pilot Rod in 315 at BoC. Initial power for T12 is slightly higher. Subsequent extraction of mainly Compensation Rods 312, 308 and 104 at XSP causes the flux peaks to shift towards the center and to broaden since less control rods are inserted. Then T10 receives more neutrons since more fission reactions occur in 313 and 314. Such a flux shift reduces also T12 power at XSP even if Pilot Rod 315 is partially extracted.
At MoC this feature does not change and devices continue to present the same relative performances. In fact, T12 shows lower power at MoC since influence of close Compensation Rod 210 remains relevant. Thus, the same lower final power value is reached at last cycle quarter as flux peak moves upward due to 210 and 202 Compensation Rods withdrawal effect even if reduced by Pilot Rod 315 criticality partial insertion (fig. 6.10). Similar performances for both MADISON T10 and T12 in nominal conditions are then

[1]LEU configuration is not optimized, additional studies are under progress to increase the power in the LEU targets and to reach a similar value than the ones of the HEU frame

		BoC [kW]		XSP [kW]		MoC [kW]		EoC [kW]	
Device	Component	Neutron	Gamma	Neutron	Gamma	Neutron	Gamma	Neutron	Gamma
MADISON T12	Fuel	104.2	3.2	99.2	3.0	93.7	2.9	92.5	2.8
	Water	4.2	2.9	4.0	2.8	3.7	2.6	3.7	2.6
	Structure	0.1	13.7	0.1	13.1	0.1	12.4	0.1	12.3
	Total	108.5	19.8	103.3	18.9	97.5	17.9	96.2	17.7
MADISON T10	Fuel	102.1	3.1	104.3	3.2	97.6	3.0	92.6	2.8
	Water	4.2	2.9	4.3	3.0	3.9	2.8	3.7	2.7
	Structure	0.1	13.8	0.1	14.1	0.1	13.2	0.1	12.5
	Total	106.4	19.9	108.6	20.4	101.6	19.0	96.5	18.0
ADELINE T8	Fuel	34.0	1.1	40.0	1.3	40.3	1.3	36.4	1.2
	Water	3.5	2.6	4.2	3.0	4.2	3.0	3.8	2.7
	Structure	0.2	15.5	0.2	17.5	0.2	17.5	0.2	16.2
	Total	37.7	19.2	44.4	21.7	44.8	21.7	40.5	20.1
ADELINE T5	Fuel	30.5	1.0	35.1	1.1	36.7	1.2	39.2	1.2
	Water	3.3	2.5	3.7	2.7	3.9	2.8	4.2	2.9
	Structure	0.2	14.6	0.2	15.9	0.2	16.7	0.2	17.2
	Total	34.0	18.1	39.0	19.8	40.8	20.8	43.6	21.3
MOLFI[1]T0 (LEU)	Fuel	334.1	2.1	321.8	2.0	315.6	2.0	362.9	2.3
	Water	13.6	12.6	12.9	12.0	12.7	11.9	14.6	13.5
	Structure	0.0	5.7	0.0	5.4	0.0	5.4	0.0	6.1
	Total	347.7	20.5	334.7	19.5	328.4	19.3	377.5	21.8
MOLFI[1]T1 (LEU)	Fuel	313.8	2.1	295.6	2.0	292.2	2.0	346.2	2.3
	Water	13.2	13.0	12.4	12.2	12.2	12.2	14.6	14.0
	Structure	0.0	5.8	0.0	5.5	0.0	5.5	0.0	6.3
	Total	327.1	21.0	308.0	19.7	304.4	19.7	360.9	22.6
MOLFI[1]T2 (LEU)	Fuel	317.3	2.2	297.0	2.0	298.6	2.0	344.0	2.3
	Water	13.6	13.3	12.7	12.5	12.7	12.5	14.6	14.1
	Structure	0.0	5.9	0.0	5.6	0.0	5.6	0.1	6.3
	Total	331.0	21.4	309.7	20.2	311.3	20.2	358.6	22.7
MOLFI[1]T3 (LEU)	Fuel	324.5	2.1	316.5	2.1	321.7	2.1	344.8	2.2
	Water	13.3	12.6	12.9	12.2	13.0	12.4	13.8	13.3
	Structure	0.0	5.6	0.0	5.4	0.0	5.5	0.0	5.8
	Total	337.8	20.3	329.5	19.7	334.8	20.0	358.7	21.3
MOLFI T0 (HEU)	Fuel	603.8	1.7	582.2	1.6	572.7	1.6	659.3	1.8
	Water	13.6	12.9	13.0	12.2	12.8	12.1	14.6	13.8
	Structure	0.3	12.2	0.3	11.5	0.3	11.5	0.3	13.0
	Total	617.7	26.8	595.5	25.3	585.7	25.2	674.3	28.6
MOLFI T1 (HEU)	Fuel	593.4	1.8	551.5	1.6	551.7	1.6	657.1	1.9
	Water	13.7	13.6	12.9	12.7	12.9	12.7	15.0	14.7
	Structure	0.3	12.8	0.3	12.0	0.3	11.9	0.3	13.9
	Total	607.4	28.2	564.7	26.3	564.9	26.3	672.5	30.5
MOLFI T2 (HEU)	Fuel	595.0	1.8	558.1	1.7	562.5	1.7	650.0	1.9
	Water	14.1	13.9	13.1	13.0	13.1	13.1	15.4	14.8
	Structure	0.3	13.1	0.3	12.2	0.3	12.3	0.3	13.9
	Total	609.3	28.8	571.5	27.0	575.9	27.1	665.7	30.7
MOLFI T3 (HEU)	Fuel	603.4	1.7	587.8	1.6	596.9	1.7	642.7	1.8
	Water	13.5	13.0	13.1	12.5	13.1	12.7	14.2	13.6
	Structure	0.3	12.2	0.3	11.8	0.3	12.0	0.3	12.8
	Total	617.2	26.9	601.1	25.9	610.4	26.4	657.1	28.2

Table 6.2: Prompt power deposition split in devices (neutron + prompt gamma) (σ=1%)

verified except for XSP.

For what concerns ADELINE devices, the same behaviour is observed for both T5 and T8 pins all cycle long (fig. 6.10). Compensation Rod 309 has a strong impact and induces T5 and T8 to keep a low difference in performances. Fuel element 309 is characterized by a burnup which is lower than 311 of about 2 reactor cycle quarters. This is properly compensated mainly by Compensation Rod in 309. After BoC, both Compensation Rods in 308 and 312 are withdrawn in order to obtain a symmetric pattern and increase flux shape of about the same amount, having the same burnup. This globally causes fissions to increase in respective fuel elements, and T8 and T5 power of the same amount. At MoC, fuel element Compensation Rod 310 extraction affects both, as it is in the middle. Finally, fresher fuel element 309 Compensation Rod is withdrawn at EoC. The effect is

[1]LEU configuration is not optimized, additional studies are under progress to increase the power in the LEU targets and to reach a similar value than the ones of the HEU frame

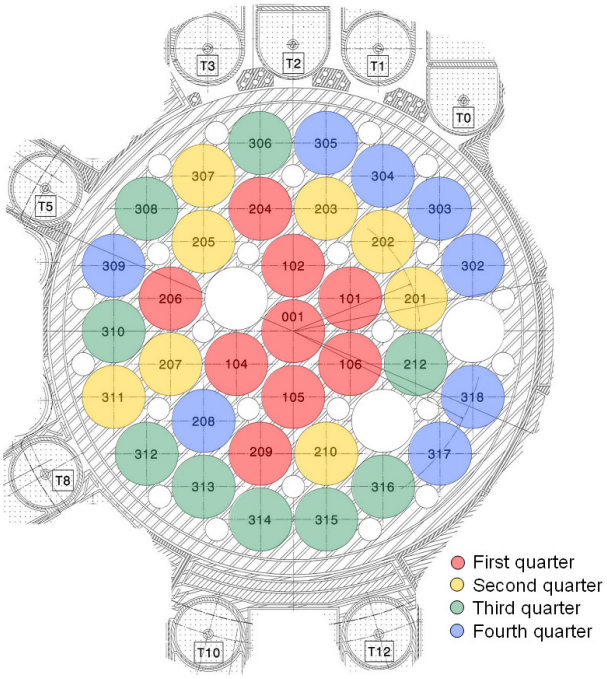

Figure 6.8: Reshuffle pattern for fuel elements

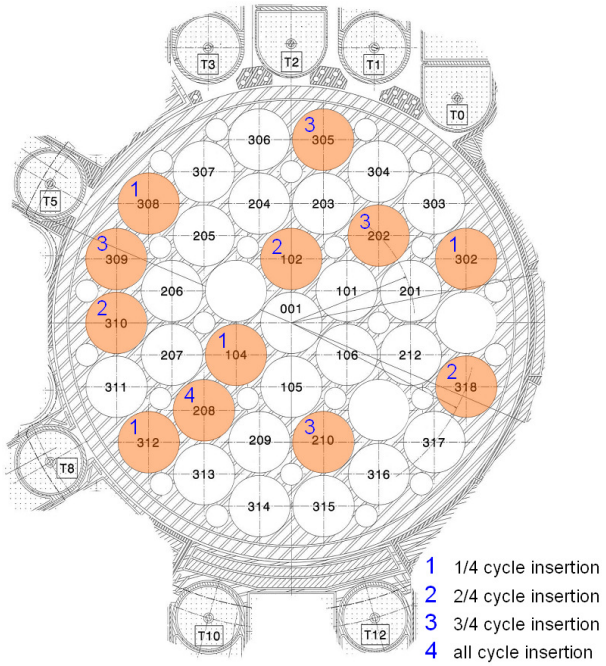

Figure 6.9: Compensation Rods locations and management

so relevant that power relations between the two devices yields an opposite power configuration. This highlights the neutronic impact of 309 Compensation Rod. Equivalent nominal conditions are then achieved for the same kind of device both for ADELINE

and MADISON regardless location. This is also due to the same reflector structure and material composition in corresponding areas. In addition, evaluations have shown how gamma power deposition depends mainly on device geometry, composition and on flux shape.

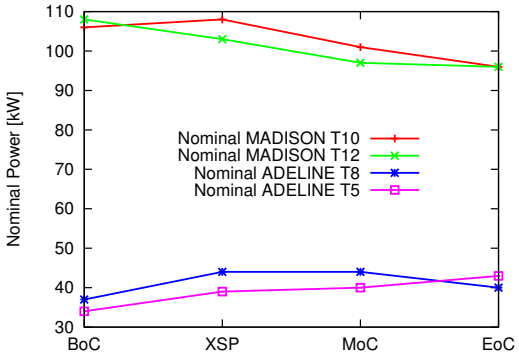

Figure 6.10: Nominal power for MADISON and ADELINE devices

Finally MOLFI devices in nominal conditions exhibit a twofold behaviour. T3 and T0 show higher coupling for neutron power deposition as they are far enough from 305 Compensation Rod. Considering only burnup, T0 should receive effectively produced neutrons from close fresh assemblies. By contrast, the impact of these fuel elements 305, 304, 303, 302 on T0 is then compensated by partial Pilot Rod insertion in 304 and Compensation Rods in 202 and 302. Conversely, T2 and T1 obtain a lower flux because Compensation Rod in 305 and partial inserted Pilot Rod in 304 avoid them to take advantage of close fresh fuel assemblies. This feature remains constant at BoC and XSP configurations since 302 and 308 withdrawal at XSP still induces symmetric effects together with burnup.

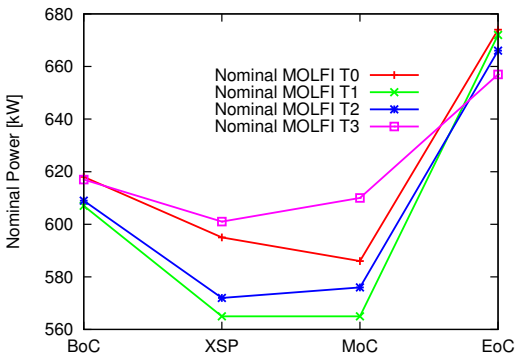

Figure 6.11: Nominal power for MOLFI HEU devices

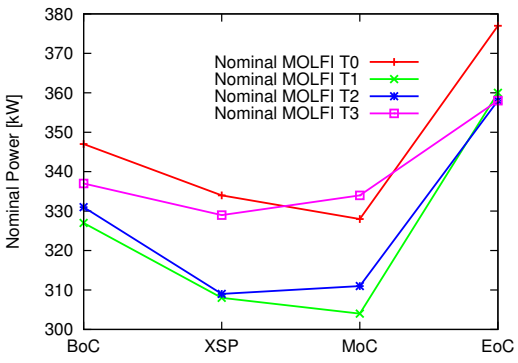

Figure 6.12: Nominal power for MOLFI LEU devices

Power reduction is then due to down flux peak shift. Assembly 102 extraction at MoC provokes a perturbation as 202 and 305 Compensation Rods still remain in core, shield-

ing assemblies 303-305 from center core neutrons. Therefore T2 behaves more like T3 than before and it increases neutron power at MoC. By contrast, T1 and T0 exhibit more similar neutron energy deposition and they do not reach higher power values. Moreover, Compensation Rod 305 and 302 extraction at EoC enables fresher fuel elements 303-305 to locally increase fission reactions and then final values for T0 and T1 highlight more important energy deposition then what occurs in T3 and T2 (fig. 6.11).
LEU MOLFI devices show the same global behaviour. It is worth to notice how HEU to LEU modifications do not concern only enrichment but also geometry configurations. LEU devices are shaped in order to select one neutron direction. Thus, T0 and T3 device plate distributions are more influenced by T0 device flux decrease with respect to T3. Nevertheless, LEU configuration is not fully optimized and should lead to power closer to the HEU reference case. These considerations are related to fission reaction rates plot concerning BoC, XSP, MoC and EoC in evey fuel plate in figures 6.13, 6.14, 6.15 and 6.16.

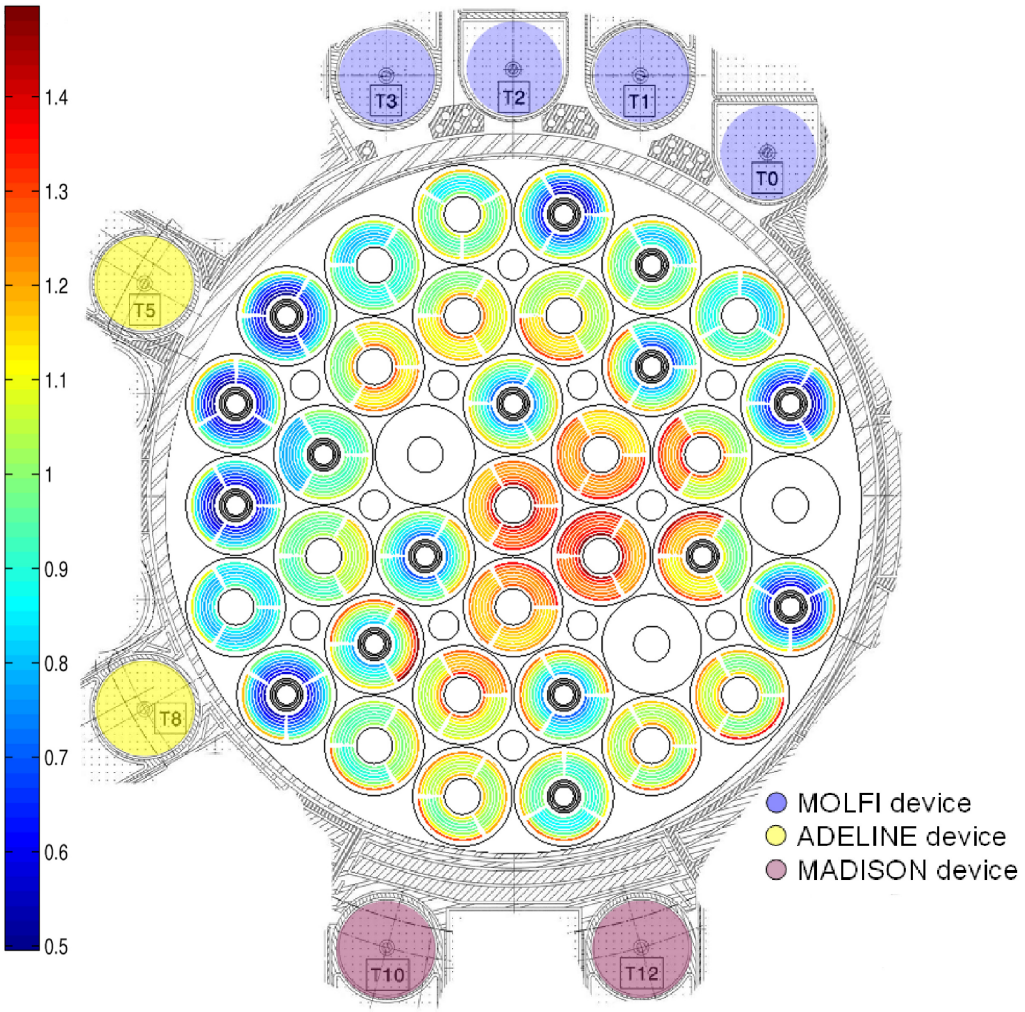

Figure 6.13: Normalized fission reaction rates at BoC (unit average)

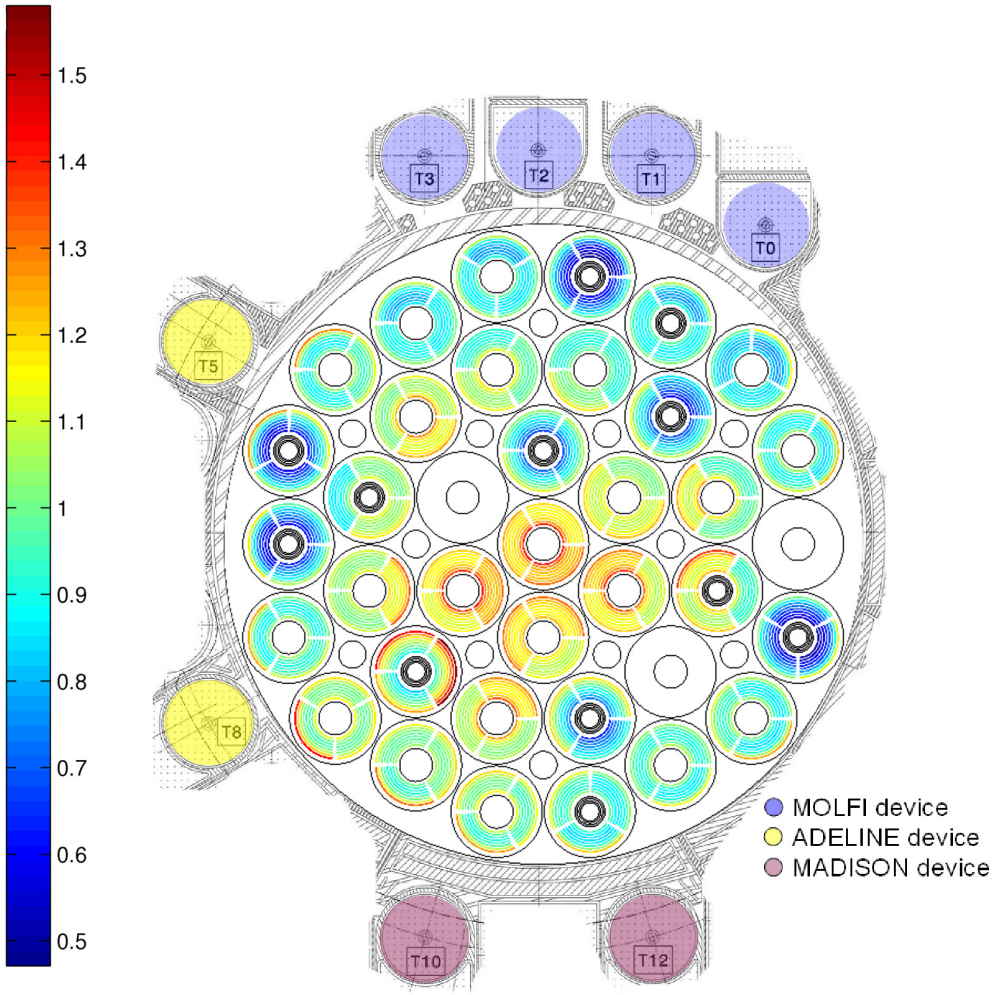

Figure 6.14: Normalized fission reaction rates at XSP (unit average)

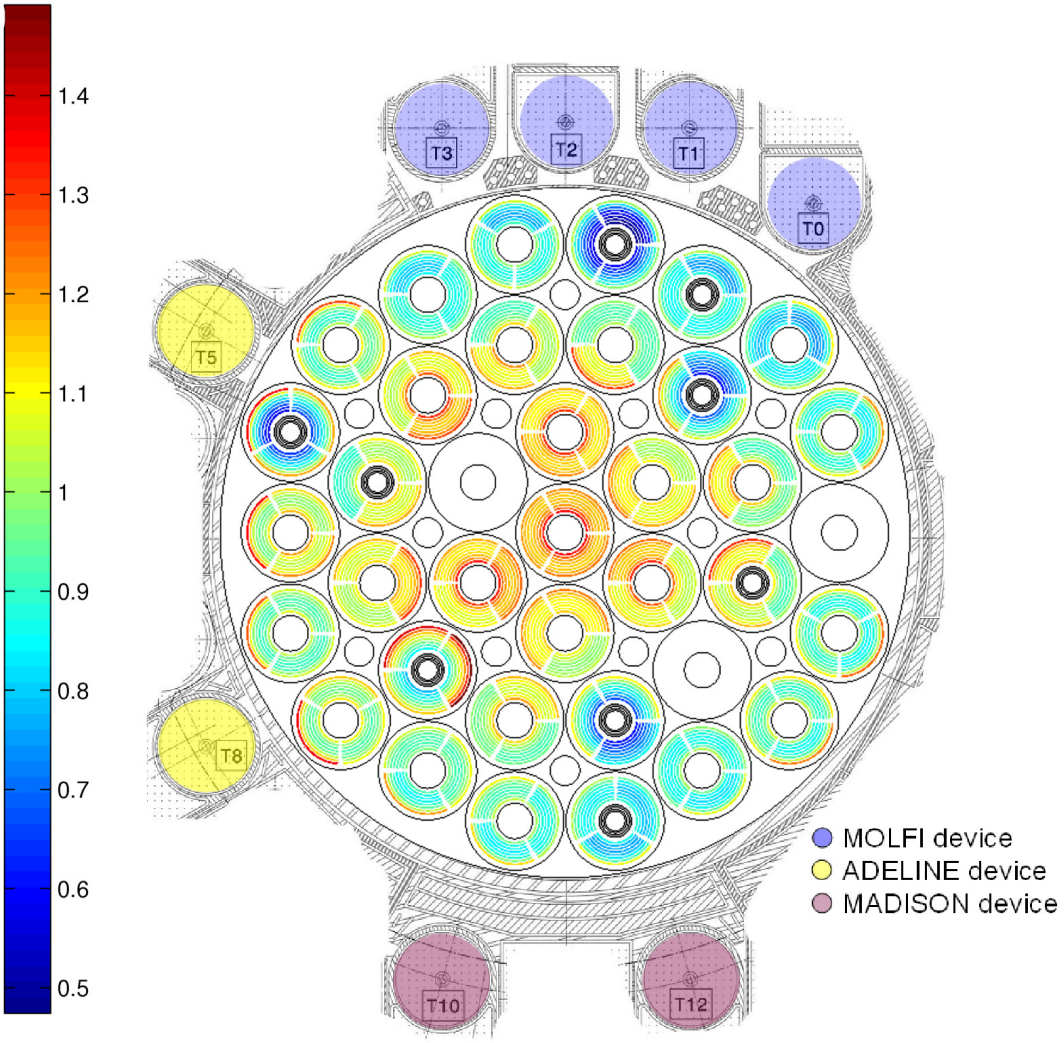

Figure 6.15: Normalized fission reaction rates at MoC (unit average)

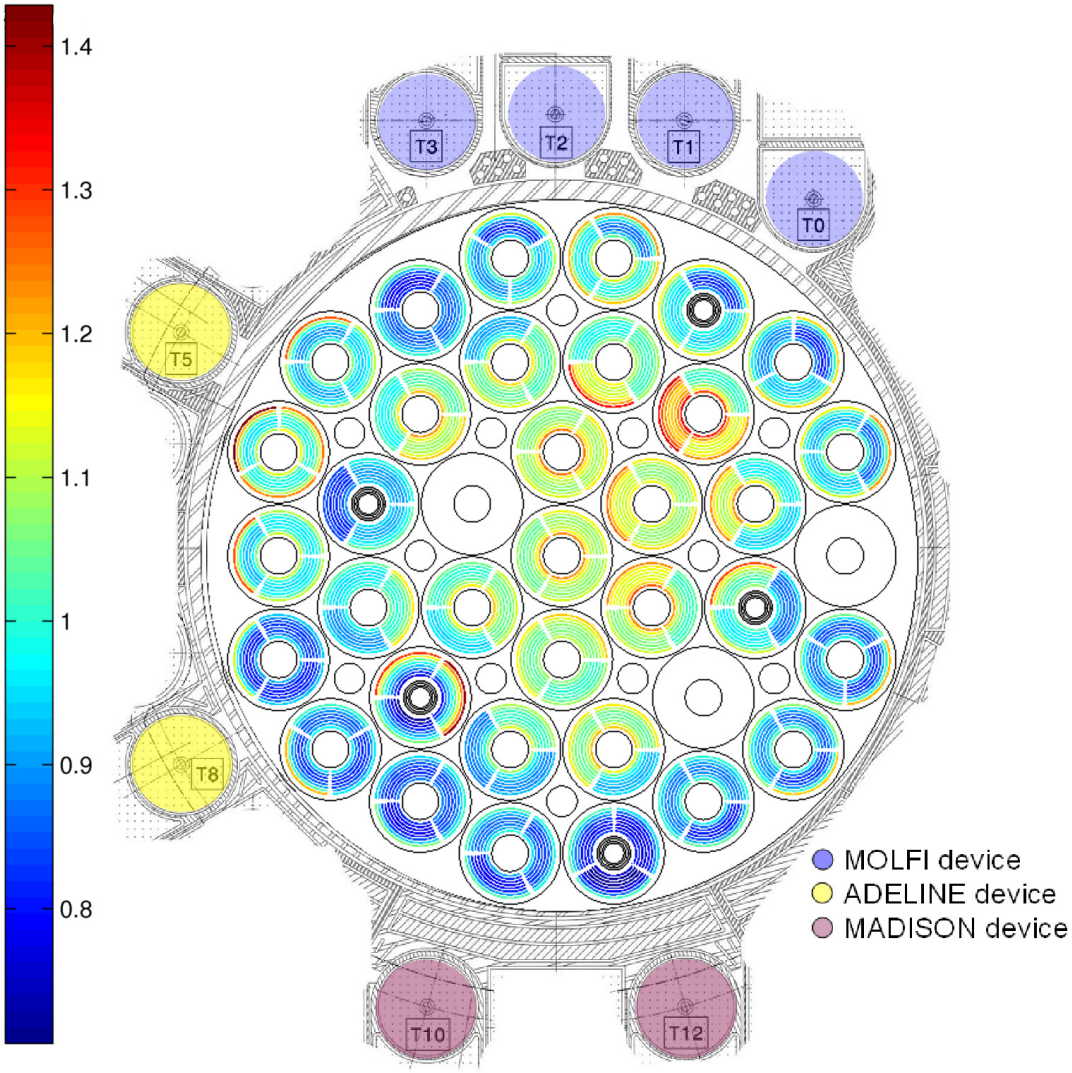

Figure 6.16: Normalized fission reaction rates at EoC (unit average)

6.3 Device Power Transients Model

Following the model presented in chapter 3, power released has been split in different components in order to define power transients in experimental devices:

$$P_{tot}(t) = P_p(t) + P_d(t) + p_p(t) + p_d(t) \tag{6.1}$$

To define a global time dependence of power, it is first necessary to evaluate self-produced neutrons within the device which could constitute a coupled component with respect to the core total behaviour; this departure is stressed mainly by delayed generations. Considering eq. (3.47), it is possible to make device self-contributions vanishing acting on k_{eff}, ρ and β of the single sample. Nuclear libraries JEFF 3.1 nuclide data have been modified in order to virtually switch off neutron generation by means of putting ν term to zero. KERMA fission energy deposition still remains accounted for, but only fission induced by neutrons coming from the core are evaluated. Calculations have then been carried out after nuclear data change. This has been done for nuclei considered in ADELINE and MADISON pins, the same for MOLFI targets. Neutron generations have been deleted for: U234, U235, U236 and U238. No other fissile nuclides are present in the devices since during simulations they are supposed to be irradiated for short periods of time and no burnup effects are analysed. In table 6.3 results of simulations run with or without sample multiplication enabling are presented, regarding BoC configuration. MADISON power deposition is affected locally by up to 3% and ADELINE up to 4% concerning neutron-induced reactions. It may be compared to a calculation uncertainty of about 1,4% for MADISON and 1,3% for ADELINE. More important is the self-contribution for MOLFI (LEU) devices. These values are referred to a composition in which all devices can not multiplicate neutrons. Concerning MOLFI, it is worth to consider also interactions between close samples.

Device	Reference Conditions		Fissile $\nu = 0$ Conditions			
	Neutron [kW]	Gamma [kW]	Neutron [kW]	Gamma [kW]	Neutron [Δ]	Gamma [Δ]
MADISON T12	108.5	19.8	105.0	19.4	3%	2%
MADISON T10	106.4	19.9	103.8	19.6	2%	2%
ADELINE T8	37.7	19.2	37.7	19.4	0%	-1%
ADELINE T5	34.0	18.1	32.6	17.6	4%	3%
MOLFI[1]T0 (LEU)	347.7	20.5	269.8	17.5	22%	14%
MOLFI[1]T1 (LEU)	327.1	21.0	243.5	17.4	26%	17%
MOLFI[1]T2 (LEU)	331.0	21.4	241.1	17.6	27%	18%
MOLFI[1]T3 (LEU)	337.8	20.3	261.4	17.2	23%	15%

Table 6.3: Comparison of coupled device contribution at BoC (σ=1%)

Now an order of magnitude of device self-multiplication is computed and such a deter-

[1]LEU configuration is not optimized, additional studies are under progress to increase the power in the LEU targets and to reach a similar value than the ones of the HEU frame

mination is referred to $p_P(t) + p_D(t)$ contributions. Thus, it is worth to know more about temporal behaviour of these components. In fact, some percentages of nominal power may be related to prompt effects or to delayed ones. In order to evaluate so, devices have been thought of as subcritical systems coupled to reactor core as a strong external source. Point kinetics is a straightforward and robust technique even if quite simple to apply. Kinetics parameters of every device have been computed through TRIPOLI 4.8 code. Evaluation for a particular device has been carried out disabling multiplication features of all core and remaining devices in order to analyse an equivalent system which comprises both moderator and reflector (Kobayashi, 1992). Verifications about method reliability have been performed testing convergency for different amounts of batches and testing uncertainty trend. TRIPOLI computation techniques follow a Monte Carlo batch calculation of neutron importance and it does not allow weighting functions different from homogeneous problem (Brown et al., 2010). According to what has been explained in chapter 3 this is an approximation as far as error cancellation in kinetic parameters determination is concerned. Results of calculations are reported in table 6.4. Needless to say that these samples have very low multiplication attitude since leakage is overall relevant. Multiplication attitude is very low for ADELINE which hosts one single pin. HEU MOLFI present an order of magnitude more in tendency to induce a neutron gain.

Extracted Control Rods

	MADISON		ADELINE		MOLFI (HEU)			
	T10	T12	T5	T8	T0	T1	T2	T3
k_{eff}	0,06388	0,06386	0,02340	0,02351	0,18667	0,17834	0,17767	0,19152
Λ	150 μs	253 μs	207 μs	213 μs	150 μs	137 μs	135 μs	129 μs
β_{eff}	910 pcm	911 pcm	824 pcm	815 pcm	906 pcm	939 pcm	943 pcm	921 pcm

Inserted Control Rods

	MADISON		ADELINE		MOLFI (HEU)			
	T10	T12	T5	T8	T0	T1	T2	T3
k_{eff}	0,06380	0,06378	0,02338	0,02346	0,18645	0,17825	0,17762	0,19169
Λ	150 μs	253 μs	207 μs	213 μs	150 μs	137 μs	135 μs	129 μs
β_{eff}	921 pcm	937 pcm	831 pcm	846 pcm	921 pcm	922 pcm	934 pcm	920 pcm

Table 6.4: Kinetic parameters associated to devices modeled as subcritical systems

Point kinetics calculations have been carried out analytically since thermal feedbacks are largely negligible compared to device k_{eff}. A source term is imposed with a temporal law which is the core evolution one. Kinetics equations are solved imposing a power source and such an initial power for device has been supposed to be the total neutron and gamma deposited energy as previously listed. The hypothesis assumed is that the total amount of power behaves as prompt. The objective is to see if temporal power profile variation appears with respect to the core normalized power. Such a normalization is just to express the source term evolution. Results are depicted in fig. 6.17, 6.18, 6.19, 6.20, 6.21, 6.22, 6.23 and 6.24.
No departure concerning core power shape is observed and calculated. It means that all

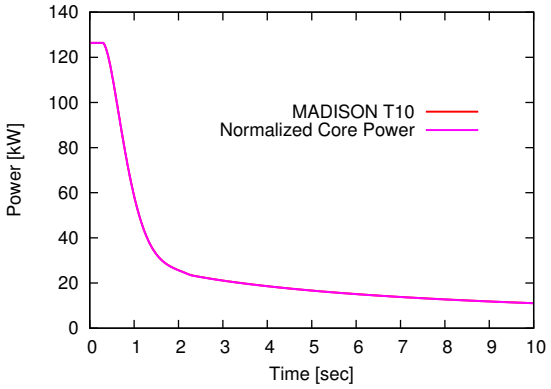

Figure 6.17: MADISON T10 kinetics

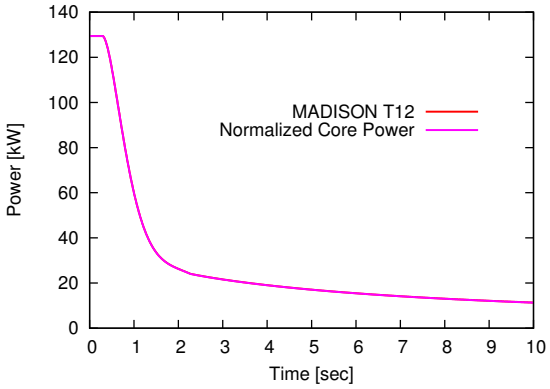

Figure 6.18: MADISON T12 kinetics

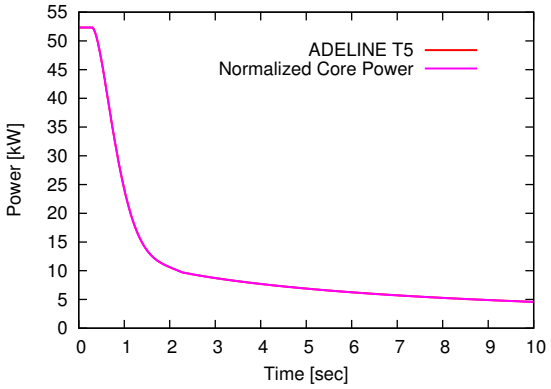

Figure 6.19: ADELINE T5 kinetics

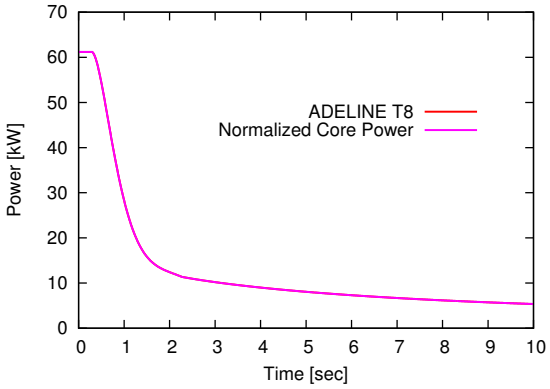

Figure 6.20: ADELINE T8 kinetics

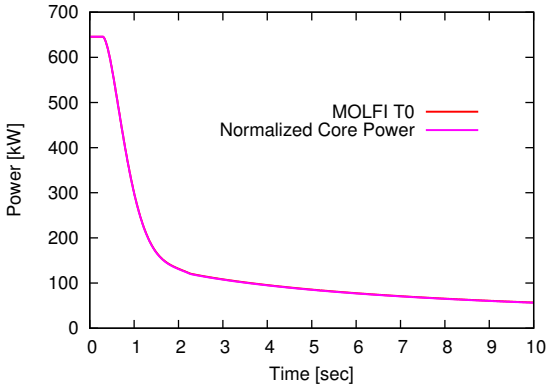

Figure 6.21: MOLFI T0 kinetics

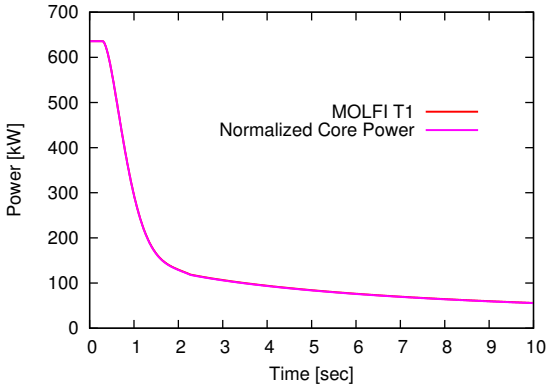

Figure 6.22: MOLFI T1 kinetics

transient is due to prompt deposition (neutrons and gamma) both from core and from the device itself. In addition, the self-generation term which is relevant is only prompt. This induces to assume as negligible $p_d(t) \rightarrow 0$ which is coherent with β order of magnitude. Provided a calculation sensitivity of the order of kW in terms of power deposition, device

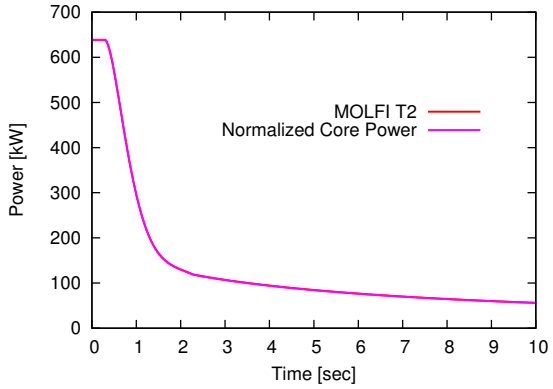

Figure 6.23: MOLFI T2 kinetics

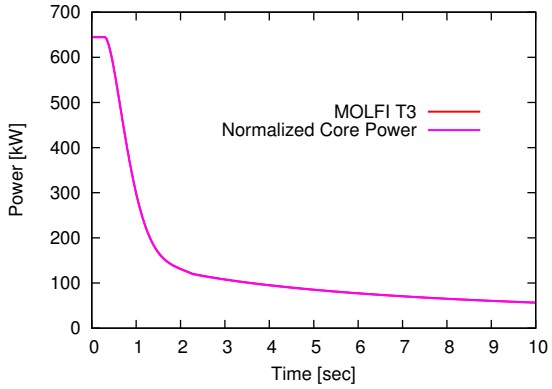

Figure 6.24: MOLFI T3 kinetics

delayed neutrons effects are some 700 pcm - namely 10^{-2} - compared to 1% contributions for ADELINE and MADISON and 10% for MOLFI which means powers of the order of 10^{-4} for MADISON and ADELINE and 10^{-3} for MOLFI. Finally it is possible to state how self-produced delayed neutrons power effect is largely negligible in device transient descriptions.

Turning to model of chapter 3, it is then useful to put together core contribution terms $P_{ex}(t) = P_p(t) + P_d(t)$ and in order to take advantage of global core transient behaviour computed through DULCINEE point kinetics code. Eq. (3.49) yields:

$$\begin{cases} \dfrac{dP_{ex}}{dt} = -\dfrac{1}{\ell_0(t)}P_{ex} + C(t)P_{core} \\ \dfrac{dp_p}{dt} = \dfrac{\rho(t) - \beta(t)}{\ell(t)}p_p + \dfrac{1 - \beta(t)}{\ell(t)}P_{ex} \end{cases} \tag{6.2}$$

The system may be decoupled and solved. External induced power component has the same temporal behaviour of the core power. In fact, provided $P_{core}(t)$ as a sum of exponential functions according to In-hour equation with no thermal feedback just to know more about the time constant of the system as follows:

$$P_{core}(t) = \sum_{i=1}^{7} L_i e^{\alpha_i t} \tag{6.3}$$

It is possible to state that $P_{ex}(t)$ solution is coherent with this form adding one term which is rapidly vanishing according to $e^{-\alpha_0 t}$ law. Table 6.5 provides information for devices in which this term α_0 turns out to be of the order of 10^4, rapidly vanishing compared to core shutdown reactivity insertion which are expressed in table 6.6. Thus it is possible to state:

$$P_{ex}(t) = \sum_{i=1}^{7} M_i e^{\alpha_i t} \tag{6.4}$$

Coherently with this approach, solution for self-contribution power $p_p(t)$ of the device is expected to be a sum of exponential according to eq. (6.2). The homogeneous term is

driven by an exponential $e^{-\beta t}$ coming from coefficient $\frac{\rho-\beta}{\ell}$ and once again this part of the solution is largely negligible compared to core external term (see table 6.5 compared to table 6.6), yielding as usual following expression:

$$p_p(t) = \sum_{i=1}^{7} N_i e^{\alpha_i t} \tag{6.5}$$

Device	$\frac{\rho-\beta}{\ell}$	Device	$\frac{\rho-\beta}{\ell}$
MADISON T10	-97756	MOLFI T0 (HEU)	-29107
MADISON T12	-57977	MOLFI T1 (HEU)	-33697
ADELINE T5	-201658	MOLFI T2 (HEU)	-34354
ADELINE T8	-195038	MOLFI T3 (HEU)	-32794

Table 6.5: Device self-contribution power transient time constants

Rod Insertion	α_1	α_2	α_3	α_4	α_5	α_6	α_7
4 PR (BoC)	-763.23	-2.849	-0.968	-0.286	-0.115	-0.030	-0.0131
3 SR (BoC)	-1303.43	-2.890	-0.977	-0.299	-0.118	-0.031	-0.0132
4 SR (BoC)	-1453.93	-2.896	-0.978	-0.300	-0.118	-0.031	-0.0132
4 PR + 4 SR (BoC)	-2032.37	-2.911	-0.981	-0.305	-0.119	-0.031	-0.0132
4 PR (XSP)	-898.852	-2.864	-0.971	-0.291	-0.116	-0.031	-0.0131
3 SR (XSP)	-1088.06	-2.879	-0.974	-0.295	-0.117	-0.031	-0.0131
4 SR (XSP)	-1429.32	-2.895	-0.978	-0.300	-0.118	-0.031	-0.0132
4 PR + 4 SR (XSP)	-2143.65	-2.913	-0.981	-0.306	-0.119	-0.031	-0.0132
4 PR (MoC)	-879.368	-2.862	-0.971	-0.290	-0.116	-0.031	-0.0131
3 SR (MoC)	-1103.44	-2.880	-0.974	-0.295	-0.117	-0.031	-0.0131
4 SR (MoC)	-1411.62	-2.895	-0.977	-0.300	-0.118	-0.031	-0.0132
4 PR + 4 SR (MoC)	-2106.21	-2.912	-0.981	-0.305	-0.119	-0.031	-0.0132
4 PR (EoC)	-747.854	-2.847	-0.968	-0.285	-0.115	-0.030	-0.0131
3 SR (EoC)	-1218.82	-2.886	-0.976	-0.297	-0.118	-0.031	-0.0132
4 SR (EoC)	-1365.47	-2.893	-0.977	-0.299	-0.118	-0.031	-0.0132
4 PR + 4 SR (EoC)	-1928.78	-2.909	-0.980	-0.304	-0.119	-0.031	-0.0132

Table 6.6: Power shutdown transient time constants

Finally, it is possible to summarize previous results and assumptions stating that all power released within a reflector device containing fissile samples is characterized by transients which behave according to core kinetics. Functional time dependence can be thought of as the same for calculation purposes. Thus, it is worth to express total device power as follows:

$$P_{device}(t) = CP_{core}(t) \tag{6.6}$$

The coupling coefficient C contains all the information regarding power deposition due to neutrons coming from core (Camprini et al., 2012b). In fact, P_{core} refers to only prompt

power according to DULCINEE simulations. It concerns only prompt effects since the delayed ones have been proven to be negligible. Therefore, such a coupling coefficient evaluation is the most significant aspect of the present model and it is the main data to compute in order to correctly determine power trasients within the devices.
In addition, such a C coupling coefficient may be expressed as a function of time $C(t)$ according to table 6.7 in next section. In fact, flux shape modification effects may be summarized inside this term and represented through a kind of time dependence. It is possible to assume validity of quasi-static Monte Carlo calculations during rod drop considering insertion time of some 1-2 sec compared to prompt neutron generation time. Depending upon considered shutdown procedure, linear or polynomial approximation between initial an final flux configuration yields a significant improvement in device power deposition calculations. This enhancement presented in this research work permitted to attain a better power transient description with respect to previous state-of-the-art methodologies retained for present research reactors. Comparisons between cases in which flux change is considered and situations accounting for only nominal device-core coupling are depicted in Appendix B. Further differences in computed energy deposition are outlined in table 6.8.

6.4 Device Transients Calculations

The model utilised in the present analysis and described in the previous sections yielded proportional relation between total power released within an experimental device and lumped total core power. This feature has been inferred in model conceiving in order to take advantage of DULCINEE core transients results according to point kinetics equations. Actually, it is worth to underline how this kind of core-coupling coefficient links prompt power contributions occurring both in core and in the device. It is not an approximation considering both delayed and prompt core neutrons related to prompt effects concerning the device. Following fissions mechanisms and reactor physics describing chain reactions, it is easy to conclude how these two particle species are always mixed and cross-contributions are very important. Thus, it is not possible to divide them without making relevant approximations. In addition, when a fission reaction occurs, it gives rise to prompt nuclear generations both for neutrons and gammas, either it has been induced by a prompt neutron or a delayed one. Therefore, prompt gammas are generated in both cases.
TRIPOLI Monte Carlo code has been utilised for energy deposition calculations and it allows a detailed geometry description of the system. It has been preferred to deterministic time-dependent spatial codes since samples in devices are small compared to reactor dimensions and precise evaluations are requested for this study. Self-shielding phenomena whitin the fuel and spatial scattering for particles in coolant and structures need to be properly represented considering detailed geometry of the system.
Basically, TRIPOLI code does not perform evolution calculations. It carries on only static evaluations which means that time has supposed not to go on and fission products do not

undergo delayed gamma emission. By contrast, delayed neutron production is accounted for since such a detailed balance is necessary to correctly compute system multiplication factor and criticality features.
Thus, neutron and gamma coupled simulations performed by means of TRIPOLI code yield only prompt gamma deposition connected to both prompt and delayed neutrons. It is now necessary to understand the Monte Carlo output data in order to well take advantage of obtained results. When simulations are performed, a normalization coefficient is applied to establish the proportionality between all results and real problem. This is normally reached through real fission reaction number evaluation, starting from nominal power and average fission energy. Thus, prompt and delayed emissions simulated by the code have no temporal importance anymore. They are just all lumped in the same instant in which simulation is supposed to describe the system. In fact, Monte Carlo reports static simulations in the sense that delayed and prompt emissions account for an average representative neutron generation spectrum. It is worth to stress how prompt-to-delayed neutron ratio changes during fast transients and this shift in average spectrum yielding in real simulation is not reproduced in static analysis. However, this approximation turns to be satisfactory.
Finally, total fission reactions are computed and actual deposited energy by neutrons and gammas in devices is evaluated. A far as static calculation is concerned, previous sentence means that all physical quantities computed during a simulation are referred to a particular and static flux shape which regards all the domain. It is again the approach showed in sections 3.4 and 3.5.
Previous methods concerning device transient calculations were related only to nominal configuration. Once core-coupling coefficients determined for operative and standard system - namely flux shape - they were conserved during all transient.
It is a matter of fact that introduction of absorbing materials within the system tends to modify neutron flux shape according to localised depression in neutron population. In addition, control rod insertion during a reactor shutdown procedure rapidly reduces total core power and flux amplitude decreases for a given shape. In fact, homogeneous neutron equations yield a flux which is normalized depending on total system power.
Both effects are present during a shutdown procedure. Control rods insert a significant amount of antireactivity and flux shape undergoes relevant distortion. By contrast, such a shape change is less and less relevant as power decreases since neutron amplitude is reduced.
Power deposition in test devices which is computed by TRIPOLI simulations is affected by this limitation. High 100 MW JHR reactor core power induces significant nominal power even in devices and more detailed description are needed. Provided that coupling coefficients are then referred to a particular flux shape, investigation about shape change impact on this coupling is required according to safety analysis.
In addition, it is worth to underline how a particular control rod dynamic insertion can not be modeled as a succession of several steps in Monte Carlo simulations. Static calculations superpositions is not equivalent to dynamic time-dependent evolution. TRIPOLI

considers equilibrium with delayed neutron precursors for a given power and so transient features are not possible to be inferred.
Nevertheless, TRIPOLI code has been utilized aiming at determining coupling coefficients in terms of power deposition ratio for most important control rod insertion configurations - namely nominal and after-shutdown. In this way, change in device-to-core power ratio has been evaluated. In order to be able to compare results, virtually the same nominal power for the core has been simulated.
Computed coupling coefficients regarding both neutron and prompt gamma contributions are listed in table 6.7.
As previously explained, control rod configurations utilized here are:

- 4 Pilot Rods insertion according to Normal Shutdown
- 3 Safety Rods insertion
- 4 Pilot + 4 Safety Rods insertion according to Safey Shutdown

Foremost, even if nominal powers have proven to exhibit similar evolutions for MADISON, sample location referred to control rods insertion during shutdown yields twofold behaviour in flux shape distortion effects. In fact, it is possible to model these states as equilibrium conditions as far as prompt neutron lifetime is concerned - namely shorter than rod insertion times.
T10 device is characterized by a nominal power which is inferred by a fission peak - namely core neutron source - about fuel element 001, 101, 105 and 106, at BoC. Assemblies 313 and 314 are sufficiently irradiated and can take advantage of this effect to constitute a neutron source close to T10 samples. Consequently, 4 Pilot Rods in Normal Shutdown increase peak-to-average ratios since no more rods are injected with respect to nominal configuration. The flux shape is stressed coherently with nominal outline and fissions increase about elements 208 and 313. For this reason T10 presents more deposited energy of about 3%. Moreover, 3 Safety Rods injection slightly changes flux form. Basically, 209 element rod shields MADISON T10 and fissions in 313 and 314 rise less then before as peak remains about core center since no rods are in this neutronic important region. Finally, Safety Shutdown insertion leads to flatten central core peak as far as high 001 Safety Rod worth is concerned. Thus, fission rate rises far from rods and close to low burnup assemblies. Both 203 and 106 fuel element but also fresher fuel in 208, 313 and 314 attain peaks and close T10 power rises. It is important to underline even a burnup dependence concerning these modifications. In fact, XSP and MoC cores provide higher power deposition increase up to 12% with respect to nominal. Compensation Rod extraction in 312 and 104 induces fission peak to broaden, in addition 312 itself fissions close to fresh fuel in 208 provide more irradiation for T10. Therefore, power deposition increase is more relevant and, even in 3 Safety Rods insertion situation, 309 rod shielding is less effective and sample power rises.
Turning to MADISON T12, first feature is the reduction in power deposition due to Normal Shutdown insertion. It is opposite to T10 characteristic and it is due to strong reduction in fission reactions about assembly 315 caused by relative Pilot Rod absorptions.

Device	Configuration	BoC	Δ	XSP	Δ	MoC	Δ	EoC	Δ
MADISON T12	Nominal	0,128	-	0,122	-	0,115	-	0,114	-
	4 PR	0,124	-4%	0,116	-5%	0,109	-6%	0,109	-4%
	3 SR	0,134	5%	0,125	3%	0,120	4%	0,118	3%
	4 SR + 4 PR	0,133	4%	0,124	1%	0,116	1%	0,115	1%
MADISON T10	Nominal	0,126	-	0,129	-	0,121	-	0,114	-
	4 PR	0,129	2%	0,135	5%	0,126	4%	0,117	2%
	3 SR	0,127	1%	0,132	3%	0,123	2%	0,115	1%
	4 SR + 4 PR	0,137	9%	0,144	12%	0,135	12%	0,124	8%
ADELINE T8	Nominal	0,057	-	0,066	-	0,066	-	0,061	-
	4 PR	0,060	6%	0,072	8%	0,072	8%	0,065	7%
	3 SR	0,059	4%	0,070	6%	0,071	7%	0,065	7%
	4 SR + 4 PR	0,067	18%	0,081	23%	0,081	22%	0,072	20%
ADELINE T5	Nominal	0,052	-	0,059	-	0,062	-	0,065	-
	4 PR	0,054	3%	0,061	4%	0,064	4%	0,066	2%
	3 SR	0,053	2%	0,060	3%	0,063	2%	0,066	2%
	4 SR + 4 PR	0,059	13%	0,067	13%	0,070	13%	0,073	13%
MOLFI[1]T0 (LEU)	Nominal	0,368	-	0,354	-	0,347	-	0,399	-
	4 PR	0,356	-3%	0,333	-6%	0,333	-4%	0,388	-3%
	3 SR	0,397	8%	0,377	6%	0,371	7%	0,431	8%
	4 SR + 4 PR	0,410	11%	0,375	6%	0,367	6%	0,435	9%
MOLFI[1]T1 (LEU)	Nominal	0,348	-	0,327	-	0,324	-	0,383	-
	4 PR	0,348	0%	0,320	-2%	0,322	-1%	0,385	1%
	3 SR	0,384	11%	0,354	8%	0,351	8%	0,422	10%
	4 SR + 4 PR	0,402	16%	0,363	11%	0,362	12%	0,439	15%
MOLFI[1]T2 (LEU)	Nominal	0,352	-	0,329	-	0,331	-	0,381	-
	4 PR	0,367	4%	0,344	4%	0,346	5%	0,396	4%
	3 SR	0,385	10%	0,359	9%	0,355	7%	0,414	9%
	4 SR + 4 PR	0,428	22%	0,390	18%	0,392	18%	0,450	18%
MOLFI[1]T3 (LEU)	Nominal	0,358	-	0,349	-	0,354	-	0,380	-
	4 PR	0,382	7%	0,376	8%	0,377	6%	0,397	5%
	3 SR	0,384	7%	0,371	6%	0,372	5%	0,402	6%
	4 SR + 4 PR	0,436	22%	0,417	19%	0,422	19%	0,448	18%
MOLFI T0 (HEU)	Nominal	0,623	-	0,600	-	0,591	-	0,680	-
	4 PR	0,608	-2%	0,574	-4%	0,574	-3%	0,665	-2%
	4 SR + 4 PR	0,703	13%	0,648	8%	0,640	8%	0,757	11%
MOLFI T1 (HEU)	Nominal	0,615		0,571	-	0,572	-	0,680	-
	4 PR	0,612	0%	0,569	-1%	0,568	-1%	0,675	-1%
	4 SR + 4 PR	0,723	18%	0,653	14%	0,651	14%	0,785	16%
MOLFI T2 (HEU)	Nominal	0,617		0,579	-	0,583	-	0,673	-
	4 PR	0,643	4%	0,606	5%	0,607	4%	0,695	3%
	4 SR + 4 PR	0,764	24%	0,702	21%	0,698	20%	0,809	20%
MOLFI T3 (HEU)	Nominal	0,623	-	0,606	-	0,616	-	0,663	-
	4 PR	0,665	7%	0,651	7%	0,659	7%	0,695	5%
	4 SR + 4 PR	0,763	23%	0,736	21%	0,734	19%	0,792	19%

Table 6.7: Device-core coupling coefficients for normalized core power (σ=1%)

This effect is quite constant during equilibrium cycle. 3 Safety Rods injection remains the most relevant power increase for T12. In fact, 001 element maintains peak close to center and Pilot Rod 315 is not completely inside allowing fission reactions in this element to occur for T12 samples power. By contrast, Safety Shutdown reduces both central elements fissions and 209 and 315 reactions. Device T12 flux shape is then affected by strong reduction. This feature has not turned out to be modified by burnup, except for BoC. In latter configuration 312, 104 and 308 Compensation Rods insertion cause the peak to stay in right part of the core. Thus after these withdrawn, fissions move towards left part, further from T12.
Basically, MADISON devices are differently affected by shutdown flux distortion. T10 gets higher power increase in all cases, conversely Normal Shutdown reduces power ratio in T12 and Safety Shutdown does not induce flux shape to augment power.
Concerning ADELINE, they have been found to present a similar behaviour for T5 and T8. Both devices are interested by a change in shape which induces 3 Safety Rods insertion to be the least effective, up to 7% increase for ADELINE T8 and up to 3% increase for T5. Then Normal Shutdown configuration makes power to rise up to 8% for T8 and 4% for T5. Safety Shutdown flux shape is the most effective in both cases concerning power increasing of about 20% for T8 and 13% for T5. Difference comes out regarding relative control rod positions. ADELINE T8 power is always more elevated then T5 samples case. T8 device is sufficiently far from both 206 Pilot Rod and 209 Safety Rod. Normal Shutdown does not lead 206 and 315 Pilot Rods to shield ADELINE T8 and then core neutrons can reach 312 and 208 fresh fuel assemblies. The peak shift towards left core advantaging T8 is more effective after XSP since Compensation Rods 312 and 104 are withdrawn, even 310 after MoC. 3 Safety Rods impact yields less power increase since 209 rod is close to fresh 208 assembly whose flux is reduced. Conversely, T5 pin flux is influenced by 206 and 205 rod effects. 3 Safety Rods insertion appears to be less effective then 4 Pilot Rods because in first case 206 rod acts on high burnup element leaving 205 and 309 fresher assemblies for fissions to occur. Safety Shutdown provokes both 205 and 206 injections shielding T5 and inducing its power to rise less then T8. T5 sample change in power deposition is almost the same during equilibrium cycle as some 308, 309 and 310 Compensation Rods are place in front of it and relative extraction compensates cycle flux shape change effects.
Finally, MOLFI devices are divided in two groups regarding their responses to control rod insertions. In fact, Normal Shutdown inserted rod 304, together with 305 Compensation Rod, shields T0 and T1 modifying neutron flux and power of about -3% for T0 and inducing no changes for T1. Conversely, less fresh fuel assemblies and free from control rods 306 and 307 host flux peak inducing power released within T2 and T3 to rise up to 4% and 7% respectively. It is worth to notice how percentage is increasing from T0 to T3 namely getting far from Pilot Rod 304. Test with 3 Safety Rods insertion causes a part of central core flux peak to shift upward. Keeping constant 305 Compensation Rod and 304 Pilot Rod position, peak move attains fresh fuel in 304, 305 and 306 yielding fission to rise hereabout. Then T1 and T2 power increase of some 11% and 10% respectively. By

contrast, Safey Rod insertions in 201 and 205 impacts close MOLFI T0 and T3 as far as less augmentation of about 8% and 7% is concerned.
Safety Shutdown matches both Normal Shutdown and Safety Rods contributions. Thus, Safety Rods in 001, 201 and 205 make the flux to shift upward but Pilot Rod in 304 avoid T0 and T1 to recevice this effect. T3 and T2 may increase power since fresh assemblies 305, 306 and 307 take advantage of that to rise occurring fission reactions. T3 and T2 power attain 22% gain, conversely T0 and T1 remain about 11% and 16% respectively.
As it has been computed, MOLFI devices exhibit previously described features about power deposition modification both concerning HEU frame and LEU conception.

Device	Normal Shutdown [kJ]				Safety Shutdown [kJ]			
	BoC	XSP	MoC	EoC	BoC	XSP	MoC	EoC
MADISON T10	2,48	9,19	8,48	2,75	7,23	9,45	8,04	6,57
MADISON T12	-11,73	-12,06	-11,14	-13,42	3,85	2,08	1,42	1,42
ADELINE T5	2,69	2,98	3,39	0,22	4,25	4,85	4,88	4,90
ADELINE T8	3,86	8,98	9,45	5,47	5,90	8,63	8,63	6,47
MOLFI[1] T0 (LEU)	-30,50	-37,86	-21,57	-28,83	30,89	18,97	18,28	28,32
MOLFI[1] T1 (LEU)	-5,18	-10,78	1,43	-1,47	37,03	26,79	27,86	38,98
MOLFI[1] T2 (LEU)	22,35	26,74	29,00	22,08	48,74	40,31	40,33	45,80
MOLFI[1] T3 (LEU)	37,76	45,27	41,90	25,79	50,22	42,56	44,95	45,56
MOLFI T0 (HEU)	-30,50	-53,86	-34,32	-36,44	49,52	32,86	32,77	50,10
MOLFI T1 (HEU)	-5,18	4,26	4,25	4,98	65,36	48,91	48,91	66,16
MOLFI T2 (HEU)	22,35	52,06	51,69	39,37	81,21	70,24	70,24	81,86
MOLFI T3 (HEU)	37,76	67,79	67,58	58,49	81,58	76,22	65,83	76,90

Table 6.8: Difference in energy deposition for 10 sec simulation between nominal deposition due to standard flux shape and values related to control rod insertion flux change

In order to obtain conservative calculations regarding safety margins about shutdowns, transients have been computed either utilising nominal coupling features or after-shutdown parameters. Comparisons are possible about total difference in deposited energy concerning first 10 seconds (see table 6.8). Flux shape distortion plots are available in Appendix A and is it worth to underline how important lack in symmetry is due to shielding devices present in right part of the reactor core. This is the reason why ADELINE device gamma energy deposition fraction is more significant than equivalent MADISON pins (see table 6.8). Moreover, device power transients concerning both nominal and after-insertion coupling flux shape are provided in Appendix B.

6.5 Delayed Neutron Source Analysis

Lumped kinetic models have been provided in the previous sections for both prompt and delayed core neutrons, but nuclear reactor operation induces delayed neutron pre-

[1]LEU configuration is not optimized, additional studies are under progress to increase the power in the LEU targets and to reach a similar value than the ones of the HEU frame

cursors concentration to reach an equilibrium value and to generate delayed neutrons steadily like a diffused source.
Results of the present section are aimed at investigating the inherent delayed neutron source effect on device power regarding nominal static irradiation. Intensity decreasing of these sources after shutdown related to nuclide decay process is worth to be investigated as well.
Provided the change in flux shape due to control rod insertion highlighted in previous section, source activity decrease implies this concurrent effect. As delayed production continues until about 4 min after complete control rod insertion (see tables 5.19-22), particular analysis in source emission is required in order to manage relative impact. Eventual departures from nominal spatial flux configuration and effective impact on devices power are interesting to be evaluated in present section.
Indeed, such a delayed neutron generation phenomenon induces the presence of an intrinsic source within the core. Therefore, reactor piloting and control procedures are performed by means of absorbing rods - hafnium in the JHR reactor case - having two main objectives:

- Absorption of neutrons actually present in the system and generated through istantaneous prompt multiplication - a variation of the core multiplication factor k_{eff} is achieved
- Management of an intrinsic and diffused delayed neutron source maintaining k_{eff} reduced and not allowing generated neutrons to multiplicate again through prompt and delayed productions

For this reason, during a shutdown process, prompt neutrons decrease in number since their multiplication becomes less and less effective. Conversely regarding delayed source, the emission intensity decreases exponentially as far as precursor family decay constants are concerned. They vary from some tenths of second to about a minute. Some example data for delayed neutron precursors constants are given in table 6.9.

Group	Half-life [sec]	Decay Constant λ_i [sec^{-1}]	Yield, Neutrons per Fission	Fraction [β_i]
1	55.72	0.0124	0.00052	0.000215
2	22.72	0.0305	0.00346	0.001424
3	6.22	0.111	0.00310	0.001274
4	2.30	0.301	0.00624	0.002568
5	0.610	1.14	0.00182	0.000748
6	0.230	3.01	0.00066	0.000273
Total			0.0158	0.00650

Table 6.9: Delayed neutron data for thermal fission in U235

It is worth to underline how main neutron population is interested by rapid decrease concerning prompt neutrons. Delayed neutron generation continues and prompt neutrons are still produced by delayed emissions coherently with actual system multiplication.

During flux transient, neutron population within the core may be thought of as a superposition of actual prompt and delayed-induced prompt neutrons. The first are concerned by a fast decrease.
By contrast, delayed sources and related neutrons behave with time constants which are long compared to control rod insertion and for kinetic analysis a quasistatic approach is suitable. Several applications and modelling in nuclear engineering require evaluation

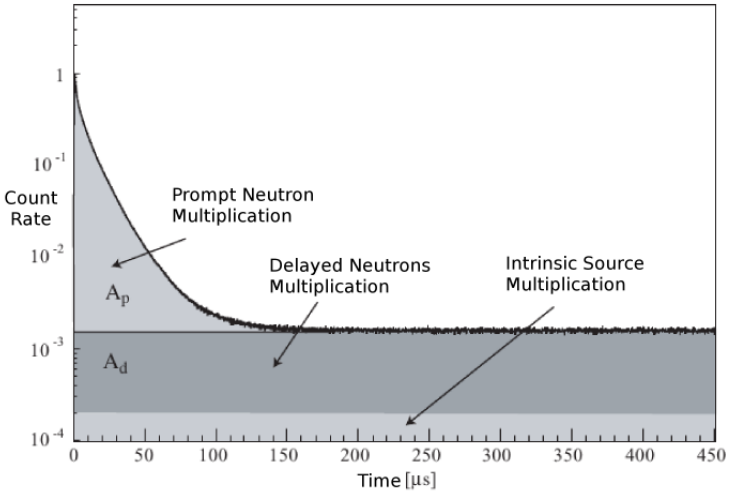

Figure 6.25: Prompt and delayed neutron transients

of prompt and delayed neutrons behavior considered as two different neutron species. This is aimed at better accounting for time response of the global system.
In addition, particular attention is paid to spatial and diffuse delayed neutron sources during and after shutdown in the present thesis. In fact, JHR reflector devices transients and residual power are influenced also by fission reactions caused by such a kind of delayed neutron flux.
Theoretically, as showed in chapter 2, it is quite straightforward to define a twofold transport approach concerning the current neutron flux φ as a superposition of two functions - namely prompt neutron flux φ_p and delayed netron flux φ_d. Such that: $\varphi = \varphi_p + \varphi_d$ everywhere in the domain. Therefore, transport equations for both species are as follows:

$$\begin{cases} \dfrac{1}{v}\dfrac{\partial \varphi_p}{\partial t} = -\underline{L}\varphi_p + \underline{M}_p\varphi_p + \underline{M}_p\varphi_d \\ \dfrac{1}{v}\dfrac{\partial \varphi_d}{\partial t} = -\underline{L}\varphi_d + \displaystyle\sum_{i=1}^{m} \frac{\chi_{d_i}}{4\pi}\lambda_i c_i \\ \dfrac{\partial c_i}{\partial t} = -\lambda_i c_i + \underline{M}_{d_i}\varphi_p + \underline{M}_{d_i}\varphi_d \end{cases} \tag{6.7}$$

Provided usual and coherent boundary conditions for both functions.
These models are mainly utilised in subcritical reactors aiming at defining fast transients regarding source and prompt neutrons. Those systems require k_{eff} on-line measurements during operation. In fact, a proper level of subcriticality has to be maintained even

during long burnup cycles and fertile material irradiation which possibly induce multiplication features of the system to increase.
Regarding the present analysis, a spatial delayed neutron source is modelled and a steady source problem is envisaged. Neutron precursors buildup is supposed to be negligible during shutdown and source term is assumed to decrease according to usual decay law. Pure static transport problem does not describe properly the system since precursors c_i are not at equilibrium but just decaying starting from nominal power concentration values. Finally, this source problem does not involve delayed emission which is all comprised in source term. Then, stationary form of eq. (6.7) yields:

$$\begin{cases} 0 = -\underline{L}\phi_p + \underline{M}_p\phi_p + \underline{M}_p\phi_d \\ 0 = -\underline{L}\phi_d + \sum_{i=1}^{m} \frac{\chi_{d_i}}{4\pi}\lambda_i c_i(t^*) \end{cases} \tag{6.8}$$

After impletementation in a transport computer tool, TRIPOLI code, induced neutron flux and power deposition within reflector test devices have been investigated and evaluated.
Delayed neutrons impact is effective mainly since prompt neutron production related to these particles is interesting for device power contribution. Then a source-term transport problem has been solved:

$$0 = \underline{L}\phi + \underline{M}_p\phi + \sum_{i=1}^{m} \frac{\chi_{d_i}}{4\pi}\lambda_i c_i(t^*) \tag{6.9}$$

In the latter, the studied flux is due to delayed source evaluated at different times: nominal and after rod insertion configurations take into account exponential decrease. Both Nominal and Safety Shutdown completed, delayed neutron source is expected to be the same since insertion duration is equivalent: 2,36 sec for BoC and EoC, 2,50 sec for XSP and 2,47 sec for MoC . Different is for 3 Safety Rods injection as this procedure is faster - namely 1,23 sec.
Delayed neutron emission has been simulated through a diffuse source according to stationary precursors concentration, starting from eq. (6.7):

$$0 = -\lambda_i c_i(\mathbf{r}, 0) + \iint \beta_i \nu\Sigma_f \phi \,\mathrm{d}E \,\mathrm{d}\hat{\mathbf{\Omega}} \qquad \Rightarrow c_i(\mathbf{r}, 0) = \frac{1}{\lambda_i} \iint \beta_i \nu\Sigma_f \phi \,\mathrm{d}E \,\mathrm{d}\hat{\mathbf{\Omega}} \tag{6.10}$$

Every single fuel plate k has been treated as containing six sources according to proper delayed spectra. Relative source intensity about activity is then referred to stationary neutron production as follows:

$$\lambda_i C_i^k(t) = \int_{V_k} \Big(\iint \beta_i \nu\Sigma_f \phi \,\mathrm{d}E \,\mathrm{d}\hat{\mathbf{\Omega}} \Big) \,\mathrm{d}\mathbf{r} \tag{6.11}$$

Device irradiation objective has been aimed at simulating not only delayed neutrons effect on devices but mainly prompt generations induced by previous delayed. In fact, this

	Group 1	Group 2	Group 3	Group 4	Group 5	Group 6	Total
BoC Nominal	7,17E+17	3,19E+18	3,09E+18	6,73E+18	1,48E+18	2,53E+18	1,77E+19
Shutdowns	6,95E+17	2,95E+18	2,32E+18	3,19E+18	1,44E+17	2,40E+15	9,30E+18
3 Safety Rods	7,06E+17	3,06E+18	2,66E+18	4,56E+18	4,40E+17	6,73E+16	1,15E+19
XSP Nominal	7,15E+17	3,18E+18	3,08E+18	6,72E+18	1,48E+18	2,53E+18	1,77E+19
Shutdowns	6,92E+17	2,93E+18	2,27E+18	3,04E+18	1,25E+17	1,58E+15	9,07E+18
3 Safety Rods	7,04E+17	3,05E+18	2,65E+18	4,55E+18	4,39E+17	6,71E+16	1,15E+19
MoC Nominal	7,09E+17	3,15E+18	3,06E+18	6,66E+18	1,47E+18	2,50E+18	1,75E+19
Shutdowns	6,86E+17	2,91E+18	2,26E+18	3,05E+18	1,28E+17	1,72E+15	9,03E+18
3 Safety Rods	6,98E+17	3,03E+18	2,63E+18	4,51E+18	4,35E+17	6,65E+16	1,14E+19
EoC Nominal	7,02E+17	3,12E+18	3,03E+18	6,59E+18	1,45E+18	2,48E+18	1,74E+19
Shutdowns	6,81E+17	2,89E+18	2,27E+18	3,12E+18	1,41E+17	2,35E+15	9,11E+18
3 Safety Rods	6,91E+17	3,00E+18	2,61E+18	4,47E+18	4,31E+17	6,59E+16	1,13E+19

Table 6.10: Delayed precursors activities after Shutdowns and 3 Safety Rod Insertions

is the main contribution since prompt spectrum is harder being 2 MeV energy on average compared to about 500 keV delayed (Rudstam et al., 2002). Thus, prompt neutrons have more chances to reach external samples out of the core.

Device	Global BoC-XSP	Delayed BoC-XSP	Global BoC-MoC	Delayed BoC-MoC	Global BoC-EoC	Delayed BoC-EoC
MADISON T12	-5%	-4%	-10%	-10%	-11%	-13%
MADISON T10	2%	3%	-4%	-6%	-10%	-13%
ADELINE T8	16%	18%	16%	16%	7%	5%
ADELINE T5	13%	12%	19%	18%	25%	22%
MOLFI T0 (LEU)	-4%	-9%	-6%	-11%	8%	-1%
MOLFI T1 (LEU)	-6%	-12%	-7%	-14%	10%	2%
MOLFI T2 (LEU)	-7%	-12%	-6%	-14%	8%	2%
MOLFI T3 (LEU)	-3%	-6%	-1%	-7%	6%	-3%

Table 6.11: Nominal and Delayed neutron flux change during equilibrium cycle

Delayed source simulated through protection calculation has been coupled to prompt neutron generation only. This reproduced operational core conditions even regarding induced prompt productions. At first, nominal power deposition in delayed neutron case is coherent with total previously computed. However, some differences are worth to be underlined, as it is possible to see in table 6.11. In fact, static Monte Carlo criticality calculations, showed in previous sections, have been carried out in view of statistical counting flux shape, regardless code imposed source used to initialize.
Conversely, particular irradiation evaluations are performed here: a delayed and less energetic spectrum is implemented. Total precursors activity is conserved and single fuel plate fraction then depends on relative fission density.
Foremost, attenuation in core crossing is the main feature regarding core burnup impact

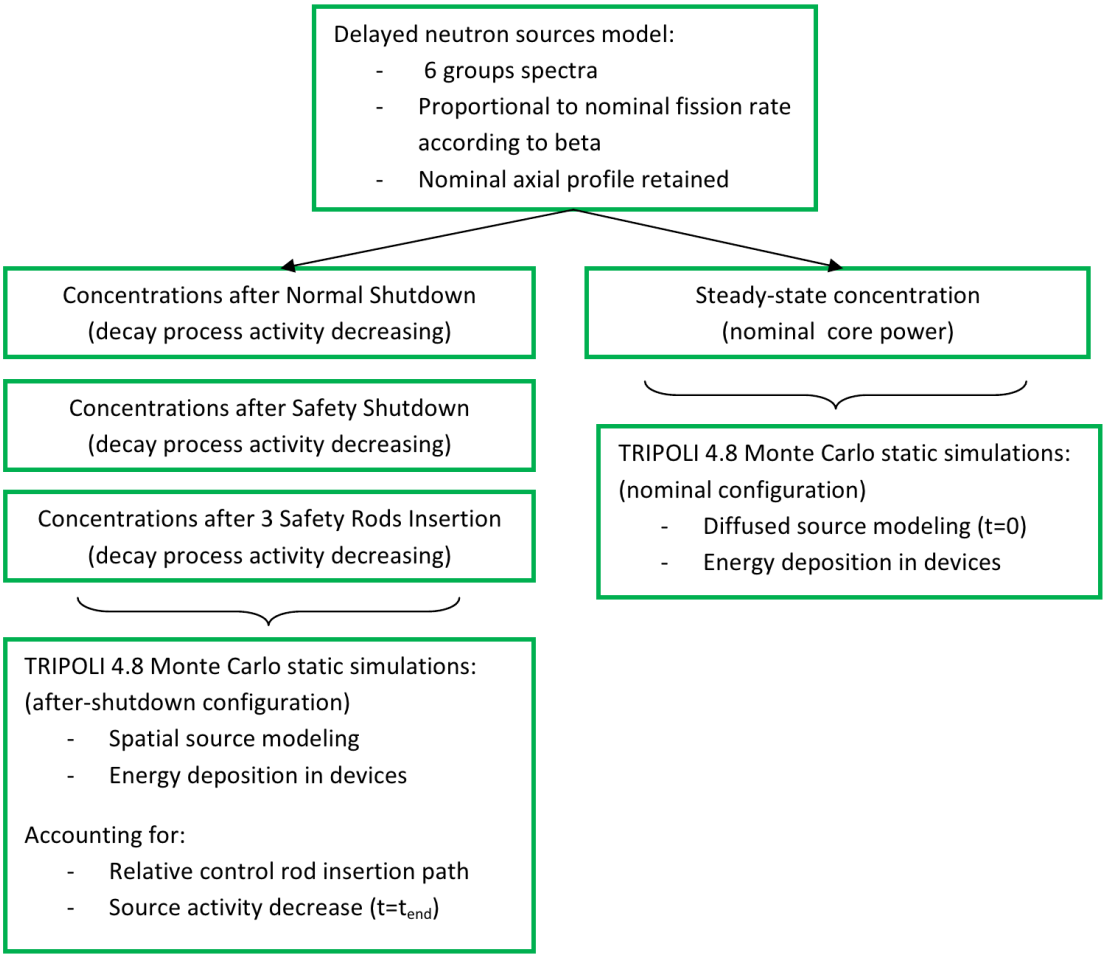

Figure 6.26: Delayed neutron simulation method flow chart

during equilibrium cycle on delayed neutrons. Different control rods charging impacts neutron transport throughout the core. In addition, fuel element burnup concerning fission product poisoning is the second effect which leads to some departures from global flux shape behaviour.
Reference nominal configuration at BoC shows a significant fission reaction density occurring in central high burnup assemblies namely 001, 101, 105 and 106. This is also main source location for delayed simulation scopes and then the bulk of generated neutrons have to cross all core from centre to reach devices or to escape poison absorption resonances to undergo fission and produce other prompts. In addition, inner zone presents most burned fuel elements in which poison concentration is the highest. Fresher fuel assemblies 212 and 201 are enough close to previous ones to take advantage of neutron generation but far from devices. Moreover, latter are shielded by Compensation Rods in 302 and 202 regarding MOLFI devices.
Hence, it is interesting to switch to depicted XSP fission map configuration in figure 6.12-

15 to see how in this case the peak spreads since mainly Compensation Rods 104, 308 and 312 are extracted. Peak-to-average ratio is reduced and total source activity is spread within the core. In fact, Compensation Rod 104 withdrawal, as well as 312, enable close fresh assembly 208 and related 313 and 314 to enhance fissions. Basically, source is moved to core periphery and consequently the fraction of nominal delayed neutrons power for MADISON T12 reduces only about -4%, compared to total amount change -5%. Moreover, T10 device which increases produced power as a whole 2%, is concerned by a relative increase by delayed neutrons which is slightly higher, 3%.
The same concerns ADELINE T5 device but Compensation Rod extraction in 312 makes T8 sample to increase fissions of about 18% with respect to global 16%, taking advantage of ignited delayed sources.
The opposite regards MOLFI devices. In fact, main Compensation Rod withdrawal at XSP concerns the opposite part of the core, fissions spread far from MOLFI locations. In addition, no control rod extraction are performed and core crossing and multiplication events occur too far. MOLFI nominal power at XSP reduces from -3% up to -7% and delayed contribution ranges from -6% to -12%. The latter is coherently referred to T1 and T2 mainly for Compensation Rod in 305 and for Pilot Rod in 304.
For what concerns MoC configuration, extraction of Compensation Rod in 102 brings core configuration back to similar BoC plan enabling neutronic important region of the core centre. Figures 6.12-15 point out a fission increase in central 001 and 101, 106 and 102 assemblies. Thus, T12 presents same nominal and delayed variation. T10 nominal reduction of about -4% concerns delayed of some -6% since fission source in assemblies 313 and 314 decrease concerning differed fraction. Even power enhance in ADELINE samples is the same in global and delayed cases. Finally, MOLFI reduction of some -6% is referred also to delayed neutrons up to -14%.
Last EoC core composition is the most interesting. Only Compensation Rod 208 remains in core. Therefore, main fission regions are closest to centre even considering relative fresh assemblies. Trade-off has turned out to be about freshest fuel elements in second assembly rounding. In fact, 201, 202 and 203 take advantage of both this position and proximity with freshest assemlies. Except for this peak, delayed sources are spread in core center and a drop in periphery is highlighted in figure 6.16. Then MADISON sample drop up to -13% reduction in delayed power and ADELINE nominal increases are reduced for delayed radiation referring to same core source distribution. MOLFI global augmentation is reduced or even negative for T3 and T0.
Needless to say that in all cases gross contribution is due to prompt power as it always is, but such spatial effects are worth concerning some minutes after shutdown, even regarding small power magnitudes.
Moreore, a second order phenomenon impacting nominal initial delayed neutron source intensity is β evolution of the system. For the sake of completeness, delayed emission stock capacity of the system is expressed through this parameter by which burnup effects possibly concern reduction in total delayed source. This has not been the case for JHR as far as small breeding features of this core are concerned.

BoC Nominal		Normal Shutdown			3 Safety Rods			Safety Shutdown		
	[kW]	[kW]	Δ Source	Δ Shape	[kW]	Δ Source	Δ Shape	[kW]	Δ Source	Δ Shape
MADISON T10	1,63	0,83	-49%	2%	1,04	-36%	1%	0,83	-49%	9%
MADISON T12	1,63	0,83	-49%	-4%	1,03	-37%	5%	0,82	-50%	4%
ADELINE T8	0,81	0,42	-48%	6%	0,52	-36%	4%	0,41	-49%	18%
ADELINE T5	0,53	0,28	-48%	3%	0,34	-36%	2%	0,27	-49%	13%
MOLFI T0 (LEU)	4,24	2,16	-49%	-3%	2,74	-35%	8%	2,16	-49%	11%
MOLFI T1 (LEU)	3,86	1,97	-49%	0%	2,49	-36%	11%	1,97	-49%	16%
MOLFI T2 (LEU)	3,86	1,97	-49%	4%	2,49	-36%	10%	1,97	-49%	22%
MOLFI T3 (LEU)	4,06	2,11	-48%	7%	2,62	-35%	7%	2,11	-48%	22%

Table 6.12: Delayed contributions to device power at BoC (σ=1%)

XSP Nominal		Normal Shutdown			3 Safety Rods			Safety Shutdown		
	[kW]	[kW]	Δ Source	Δ Shape	[kW]	Δ Source	Δ Shape	[kW]	Δ Source	Δ Shape
MADISON T12	1,57	0,78	-51%	5%	1,01	-36%	3%	0,78	-50%	12%
MADISON T10	1,68	0,84	-50%	-5%	1,08	-36%	3%	0,83	-50%	1%
ADELINE T8	0,95	0,48	-50%	8%	0,61	-36%	6%	0,48	-50%	23%
ADELINE T5	0,60	0,30	-50%	4%	0,38	-36%	3%	0,30	-50%	13%
MOLFI T0 (LEU)	3,88	1,92	-50%	-6%	2,49	-36%	6%	1,92	-50%	6%
MOLFI T1 (LEU)	3,40	1,70	-50%	-2%	2,19	-36%	8%	1,69	-50%	11%
MOLFI T2 (LEU)	3,41	1,71	-50%	4%	2,20	-36%	9%	1,70	-50%	18%
MOLFI T3 (LEU)	3,81	1,93	-49%	8%	2,45	-36%	6%	1,93	-49%	19%

Table 6.13: Delayed contributions to device power at XSP (σ=1%)

MoC Nominal		Normal Shutdown			3 Safety Rods			Safety Shutdown		
	[kW]	[kW]	Δ Source	Δ Shape	[kW]	Δ Source	Δ Shape	[kW]	Δ Source	Δ Shape
MADISON T12	1,46	0,73	-50%	4%	0,93	-36%	1%	0,73	-50%	12%
MADISON T10	1,53	0,77	-50%	-6%	0,98	-36%	3%	0,77	-49%	1%
ADELINE T8	0,93	0,48	-49%	8%	0,60	-35%	7%	0,48	-49%	22%
ADELINE T5	0,63	0,32	-50%	4%	0,40	-36%	2%	0,32	-50%	13%
MOLFI T0 (LEU)	3,78	1,87	-50%	-4%	2,42	-36%	8%	1,88	-50%	6%
MOLFI T1 (LEU)	3,33	1,65	-50%	-1%	2,14	-36%	10%	1,67	-50%	12%
MOLFI T2 (LEU)	3,34	1,66	-50%	5%	2,14	-36%	9%	1,67	-50%	18%
MOLFI T3 (LEU)	3,78	1,93	-49%	6%	2,42	-36%	6%	1,92	-49%	19%

Table 6.14: Delayed contributions to device power at MoC (σ=1%)

Once delayed contribution to nominal power computed, next step has been the determination of contol rods insertion impact. After shutdown, diffuse delayed source emits neutrons for time interval which is longer compared to insertion procedure. Such a source decreases depending upon exponential behaviour of precursors activity and twofold mech-

EoC Nominal		Normal Shutdown			3 Safety Rods			Safety Shutdown		
	[kW]	[kW]	Δ Source	Δ Shape	[kW]	Δ Source	Δ Shape	[kW]	Δ Source	Δ Shape
MADISON T12	1,41	0,72	-49%	2%	0,90	-36%	1%	0,71	-50%	8%
MADISON T10	1,41	0,73	-48%	-4%	0,91	-36%	3%	0,73	-49%	1%
ADELINE T8	0,85	0,44	-49%	7%	0,54	-36%	7%	0,44	-49%	20%
ADELINE T5	0,65	0,34	-48%	2%	0,41	-36%	2%	0,34	-48%	13%
MOLFI T0 (LEU)	4,19	2,15	-49%	-3%	2,71	-35%	8%	2,14	-49%	9%
MOLFI T1 (LEU)	3,94	2,01	-49%	1%	2,52	-36%	10%	2,00	-49%	15%
MOLFI T2 (LEU)	3,95	2,01	-49%	4%	2,52	-36%	9%	2,01	-49%	18%
MOLFI T3 (LEU)	3,95	2,04	-48%	5%	2,52	-36%	6%	2,04	-49%	18%

Table 6.15: Delayed contributions to device power at EoC (σ=1%)

anism acts on power release within devices. First variation regarding nominal features is due to activity exponential reduction. In addition, flux shape derived by control rod injection impacts on neutron transport.
In tables 6.12, 6.13, 6.14 and 6.15 variations Δ due to neutron precursors group decay "Source" and flux shape distortion "Shape" are pointed out.
Irradiations have been performed even with decreased source intesities, corresponding to shutdown duration in present analysis. Delayed power difference between nominal and after-shutdown has been compared to actual nominal modification concerning only flux shape. This has been carried out for usual Normal Shutdown, Safety Shutdown and 3 Safety Rods insertion.
Source reduction about -48% regards both Normal and Safety Shutdown corresponding to some 2,36 sec and some -35% about 1,23 sec concerns 3 Safety Rods insertion. In tables 6.12-15 relative variations referred to as Δ Source are showed concerning simulated source decreasing. By contrast, Δ Shape is just nominal previously evaluated impact on device power due to flux shape modification. It is easy to note how small departure from simple source impact occurs. Hence, no relevant source distortion is expected for control rods insertions. In fact, flux shape change is largely small compared to source decrease in time. More details about delayed neutron irradiation effects are provided in Appendix C.

6.6 Delayed Gamma Irradiation Analysis

Power release in fissile samples is mainly due to occurring fission reactions, anyway a contribution to total energy deposition is also induced by gamma radiation. Moreover, gamma radiation is much more relevant considering all device structures which need heating evaluation for cooling design optimization.
Gamma heating is a particular topic in JHR design since high reactor power density (460 kW/l) causes significant gamma productions and elevated temperature gradients that are worth to be controlled for experimental environment characterization.

Hence it is currently a key-issue in material testing reactor design and for this reason several studies have been carried out concerning temperature monitoring of non-fissile devices regarding nuclear data uncertainties (Blanchet, 2006). Nuclear gamma heating normally attains 10% of total power within the core, concerning gamma radiation as a whole (prompt + delayed) (Rimpault et al., 2012) which may be split as follows:

- 20% for gamma produced in radiative capture
- 40% for prompt gamma emitted by fission fragments
- 30% for delayed gamma emitted by fission products
- 10% for inelastic scattering reactions

Moreover, longer mean free path allows photons to diffuse out of the core and to reach surrounding structures and reflector. For this reason, a complete analysis of power deposition in test devices has to account for delayed gamma emissions as well.
Normally, static calculation schemes consider delayed contribution as 30% of total (prompt + delayed) (Blanchet et al., 2008). It is a standard approach for core complete description. By contrast, in the present thesis, a time-dependent analysis has been performed and some necessary enhancements have been applied (Camprini et al., 2012c).
Previously presented 30% accounts for both delayed and prompt gamma induced by delayed fission reactions. One may consider this percentage as the amount of energy released after a subsequent transient related to certain initial nominal situation. Since this study deals with transient analysis, simply applying such a correction factor would lead to an overestimation of delayed neutron-induced prompt gamma of about 20%.
Device-core coupling coefficients have been produced accounting for TRIPOLI calculations which consider prompt gamma. Thus, all prompt contributions are inside such a coefficient and only portion related to delayed gamma needs to be added.
Regarding model conceived and previously presented, twofold distinction has been operated between prompt and delayed effects. Prompt phenomena from core are related to neutronic transient. In addition, prompt and delayed neutrons induce fissions which generate prompt gamma. All this amount of energy in the device has been modeled as proportional to total core power.
Moreover, delayed gamma from core are expected to exhibit an independent transient which is linked to longer fission product decay time constants. Following presented model in eq. (6.6), power deposition is mainly due to following contributions:

$$P_{device}(t) = (P_n(t) + P_{\gamma_p}(t)) + P_{\gamma_d}(t) = CP_{core}(t) + P_{\gamma_d}(t) \tag{6.12}$$

In fact, first two terms are proportional to core power, the latter has been computed through a methodology explained in this section. Adding this last delayed gamma term, the model conceived in present thesis to describe power transients in reflector devices is properly completed. It takes into account all relevant energy deposition processes. Radiation due to β and α particles is largely negligible since they remain within fuel plate and do not reach external devices.
Isotope evolution calculations have been performed by means of PEPIN2 code which

computes delayed gamma power evolution for core. The code permitted also to evaluate overall delayed gamma spectrum as depicted in figure 6.27. Main delayed gamma emitters have turned out to be quite independent of burnup.

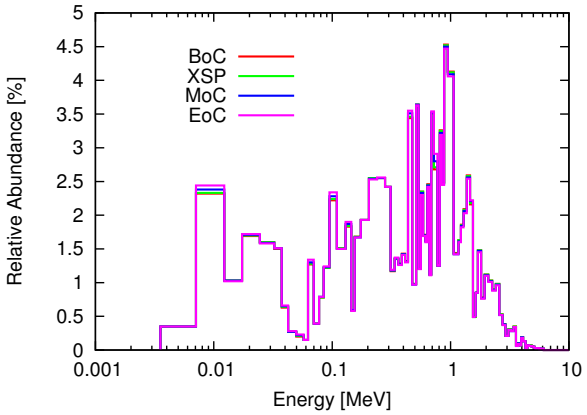

Figure 6.27: Delayed gamma spectra

^{89}Rb and ^{91}Rb contribute with some 5% of total gamma delayed release power, ^{93}Sr and ^{94}Sr to a 5% as well. The most important nuclide is ^{134}I with some 4% alone, ^{132}I and ^{135}I are relevant as well, even being a radiation protection issue with half lives of 2 hours and 6,57 hours respectively. In addition ^{140}La, ^{142}La and ^{144}La sum up to 8%, first nuclide having a half life of about 1 day.
Evolution calculation reported solutions of Bateman equations for initial conditions and 30 sec after the end of irradiation. Average spectrum considered for transient interval resulted to be quite similar to initial one since half lives of relevant nuclei are long compared to 10 sec shutdown period. Except for ^{91}Kr, ^{96}Y, ^{93}Rb and ^{90}Rb, initial concentrations do not vary to such an extent for which delayed emission spectrum may significantly change as reference in table 6.16. Core source location has been supposed to be proportional to nominal and static fission reaction density, as for delayed neutron emissions.
Nominal BoC conditions turned out how delayed gamma effect comprises 3% - at most - of initial device power. ADELINE T8 and T5 are the most concerned by this irradiation for 6,5 kW and 6,9 kW respectively - as for prompt gamma - since no Zr shielding is present around left part of reactor core. Difference is caused by absence of Compensation Rod in 311 and then a closer gamma source is placed. Provided lack of shielding, this is also due to important Zr tubes present around experimental ADELINE pins.
By contrast, MOLFI devices exhibit lower nominal power, gamma deposition is induced by large amount of water in sample tanks which attains some 3,5 kW, in addition Zr tubes absorb about 1,6 kW each.
Finally MADISON devices are less concerned by gamma irradiation since neither large amount of water nor Zr thick tubes are present. Basically, T10 and T12 are behind core Zr shielding and gamma effects are less important.

BoC		XSP		MoC		EoC			
Isotope	Power [%]	Isotope	Power [%]	Isotope	Power [%]	Isotope	Power [%]	Half-life	After 10 sec
Br 86	1,30	Br 86	1,30	Br 86	1,28	Br 86	1,27	55,1 s	88,18%
Br 87	1,38	Br 87	1,38	Br 87	1,36	Br 87	1,34	55,6 s	88,28%
Br 88	1,16	Br 88	1,15	Br 88	1,14	Br 88	1,13	16,34 s	65,44%
Kr 88	1,49	Kr 88	1,49	Kr 88	1,47	Kr 88	1,45	2,84 h	99,93%
Kr 89	1,71	Kr 89	1,70	Kr 89	1,69	Kr 89	1,67	3,15 m	96,40%
Kr 91	1,15	Kr 91	1,14	Kr 91	1,13	Kr 91	1,12	8,57 s	44,55%
Rb 89	2,21	Rb 89	2,20	Rb 89	2,18	Rb 89	2,15	15,15 m	99,24%
Rb 91	2,69	Rb 91	2,68	Rb 91	2,66	Rb 91	2,63	58,4 s	88,81%
Rb 92	1,63	Rb 92	1,62	Rb 92	1,61	Rb 92	1,59	4,5 s	21,44%
Rb 93	1,77	Rb 93	1,77	Rb 93	1,75	Rb 93	1,74	5,84 s	30,52%
Rb 90	1,82	Rb 90	1,82	Rb 90	1,80	Rb 90	1,77	2,6 m	95,65%
Sr 92	1,77	Sr 92	1,77	Sr 92	1,75	Sr 92	1,74	2,7 h	99,93%
Sr 93	3,01	Sr 93	3,00	Sr 93	2,98	Sr 93	2,96	7,42 m	98,46%
Sr 94	1,85	Sr 94	1,84	Sr 94	1,83	Sr 94	1,82	75,3 s	91,21%
Sr 95	1,23	Sr 95	1,23	Sr 95	1,22	Sr 95	1,21	23,9 s	74,83%
Y 98	1,01	Y 98	1,01	Y 98	1,01	Y 98	1,01	0,54 s	0,00%
Y 94	1,05	Y 94	1,05	Y 94	1,04	Y 94	1,03	18,7 m	99,38%
Y 96	1,20	Y 96	1,20	Y 96	1,20	Y 96	1,20	5,34 s	27,31%
Y 95	1,52	Y 95	1,52	Y 95	1,51	Y 95	1,50	10,3 m	98,88%
Mo 101	1,62	Mo 101	1,62	Mo 101	1,62	Mo 101	1,63	14,61 m	99,21%
Sb 133	1,13	Sb 133	1,12	Sb 133	1,12	Sb 133	1,11	2,5 m	95,49%
Te 134	1,27	Te 134	1,27	Te 134	1,26	Te 134	1,26	41,8 m	99,72%
Te 133	1,27	Te 133	1,27	Te 133	1,27	Te 133	1,27	55,4 m	99,79%
I 134	4,23	I 134	4,22	I 134	4,21	I 134	4,19	52,5 m	99,78%
I 135	2,19	I 135	2,19	I 135	2,19	I 135	2,18	6,57 h	99,97%
I 136	1,47	I 136	1,47	I 136	1,46	I 136	1,45	83,4 s	92,03%
I 132	2,14	I 132	2,14	I 132	2,14	I 132	2,14	2,29 h	99,92%
Xe 138	1,55	Xe 138	1,55	Xe 138	1,54	Xe 138	1,53	14,08 m	99,18%
Cs 140	2,16	Cs 140	2,16	Cs 140	2,15	Cs 140	2,14	63,7 s	89,69%
Cs 138	3,41	Cs 138	3,41	Cs 138	3,40	Cs 138	3,39	33,41 m	99,65%
Ba 141	1,10	Ba 141	1,10	Ba 141	1,10	Ba 141	1,09	18,27 m	99,37%
Ba 142	1,31	Ba 142	1,31	Ba 142	1,30	Ba 142	1,30	10,6 m	98,92%
La 140	2,76	La 140	2,83	La 140	2,98	La 140	3,08	1,67 d	100,00%
La 142	2,95	La 142	2,94	La 142	2,93	La 142	2,92	91,1 m	99,87%
La 144	2,71	La 144	2,70	La 144	2,69	La 144	2,67	40,8 s	84,38%
Total	64,22	Total	64,17	Total	63,97	Total	63,68		

Table 6.16: Main isotope contributons to delayed gamma emission

Burnup effect in source displacing has not particular impact, it is of about 1% which is similar to Monte Carlo statistical error. Anyway, ADELINE devices - as far as it has been highlighted - appear to be slightly more sensitive in source location changing and Compensation Rod 308 and 312 extraction at XSP provokes a delayed gamma deposition enhancement up to 4%. Compensation Rod withdrawal on fresh fuel element 309 at EoC achieves ADELINE T5 increase of some 3%. In the same way, MOLFI are interested by Rod extraction in 302 and 305 at EoC and fresh fuel elements 302-305 sources are ignited inducing 4% enhancement in delayed gamma irradiation for all T0, T1, T2 and T3 samples.

	BoC (t=0 s) [kW]	XSP (t=0 s) [kW]	BoC-XSP Δ	MoC (t=0 s) [kW]	XSP-MoC Δ	EoC (t=0 s) [kW]	EoC-MoC Δ
MADISON T12	3,14	3,19	1%	3,19	0%	3,18	0%
MADISON T10	3,27	3,31	1%	3,35	1%	3,35	0%
ADELINE T8	6,47	6,66	3%	6,78	2%	6,81	1%
ADELINE T5	5,87	6,08	4%	6,14	1%	6,34	3%
MOLFI T0 (LEU)	5,43	5,46	1%	5,47	0%	5,60	3%
MOLFI T1 (LEU)	5,46	5,52	1%	5,54	0%	5,74	4%
MOLFI T2 (LEU)	5,74	5,79	1%	5,78	0%	6,01	4%
MOLFI T3 (LEU)	5,49	5,49	0%	5,48	0%	5,60	2%
Total Source Activity	1,80E+19	1,80E+19		1,81E+19		1,82E+19	

Table 6.17: Delayed gamma power deposition in devices ($\sigma = 1\%$)

Finally it is worth to point out how gamma diffusion within core depends on control rod only concerning nominal fission source locations. For this reason burnup core management impacts on delayed energy deposition only for some 4% at most, on the contrary neutron flux shape change induces variations even of the order of 25%. According to PEPIN2 evolution calculations, delayed gamma power deposition within devices exhibits same time-dependent behaviour of these nuclide decreasing. Decay curves reported on computed values, first 10 sec transients have been plotted in pictures 6.28, 6.29, 6.30 and 6.31.

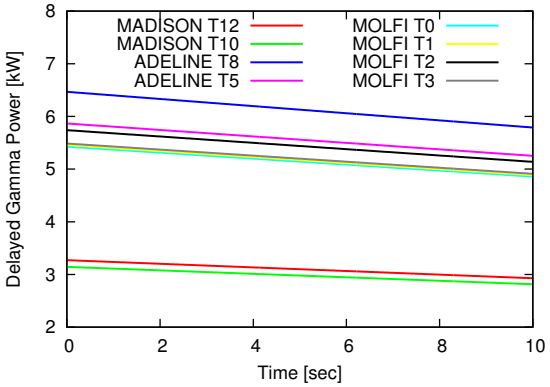

Figure 6.28: Delayed gamma at BoC

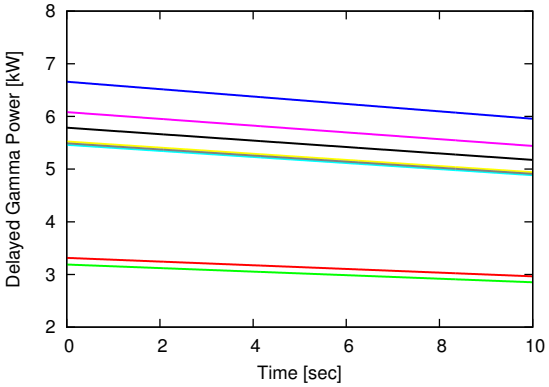

Figure 6.29: Delayed gamma at XSP

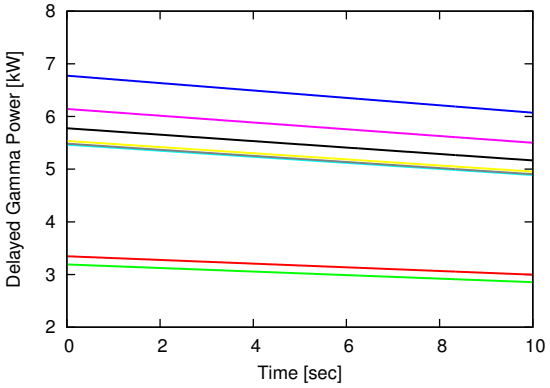

Figure 6.30: Delayed gamma at MoC

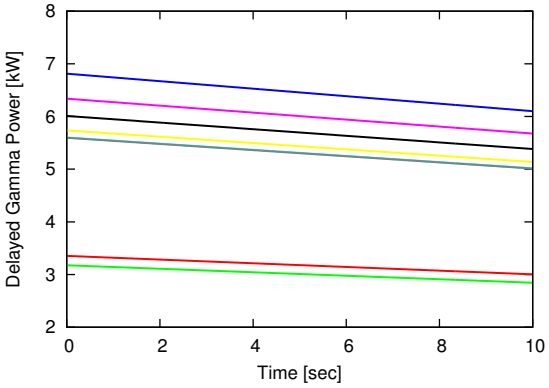

Figure 6.31: Delayed gamma at EoC

Chapter 7

Conclusions and Perspectives

The aim of the present thesis is the analysis of thermal power transients regarding experimental devices placed in the reflector of Jules Horowitz Material Testing Reactor (JHR). French Atomic Energy Commission (CEA) has launched the construction of this irradiation facility which is intended to be the most important research reactor in Europe for the next decades. High flux 100 MW power core has been designed in order to achieve elevated experimental capability and several irradiation test positions are envisaged in core and within the reflector. Challenging thermal power levels are then expected to be attained inside devices containing fissile samples.
Therefore, safety issues requested detailed evaluations and present state-of-the-art methodology has been enhanced in this work to obtain best-estimate results about devices power during shutdown transients. An innovative calculation approach has been conceived and flux shape change during control rod insertions has been taken into account through improved device-core coupling coefficients determination. In addition, nominal powers and time-dependent device transients have been properly evaluated accounting for all nuclear heating effects both concerning core neutron and prompt gamma irradiation. In addition, delayed gamma energy deposition has been computed for different core burnup levels during equilibrium cycle.
Results obtained in this study are aimed at design feedback and reactor management optimization by JHR project team. Moreover, Safety Report is intended to utilize present analysis for improved device characterization.

Shutdown Procedures Simulations

Since research objective is power transients description of experimental devices, a multiple kinetic model has been implemented. Aiming at splitting the whole reactor in many interacting neutronic domains, every device has been treated as single multiplying system irradiated by a strong external neutron source - provided by JHR core - during different shutdown procedures. Kinetics analysis has been performed by means of DULCINEE code considering neutronic features of the system regarding 25 days equilibrium U_3Si_2 27% U235 enriched fuel composition, for Beginning of Cycle, Xenon Saturation Point,

Middle of Cycle and End of Cycle. Thermal hydraulic model of core channels about every single plate has been conceived for complete time-dependent description through reactivity feedback coefficients.
Modifications in neutronic parameters have been evaluated regarding cycle duration, fuel enrichment and device impact on global reactivity. In addition, core thermal feedback has turned out to be of second order compared to antireactivity injected by control devices.
Burnup impact of shutdown neutronic kinetics has turned out mainly to depend upon control devices management by means of 3 rod groups: Compensation Rods for core depletion, Pilot Rods aimed at core control and Safety Rods for emergency procedures.
Normal Shutdown is performed through 4 Pilot Rods bank insertion. By contrast, Safety Shutdown implies both 4 Pilot and 4 Safety Rods clusters.
Kinetics calculations and core burnup evolution computations with PEPIN2 code allowed: detailed description of core power transients during Normal and Safety Shutdown procedures decay heat contribution due to core fission products beta-gamma radiations related to different burnup configuration in equilibrium cycle verification of shutdown characteristics on fuel and cladding temperature Thus, core power transients have been determined both regarding a best-estimate and a safety calculation approach to verify effectiveness in power and temperature decreasing.

Device Transient Analyses

JHR experimental capability is reached by means of several test locations in core and within the reflector. Hence twofold neutronic spectrum has been envisaged to cope with these important design features. Fast neutron irradiation is available in core aimed at delivering high flux up to 5 10^{14} n/cm^2/sec to cladding and vessel structural material samples. Conversely, a large beryllium reflector has been particularly conceived in order to take advantage of a thermal neutron spectrum for fuel properties study. Here, fissile targets are irradiated through flux of about 7 10^{13} n/cm^2/sec.
Within the framework of the present thesis, following reflector fuel-loaded devices are considered:

- MADISON device aimed at hosting up to 4 UO_2 pins 1% U235 enriched to simulate high burnup fuel nominal operating conditions or slow transients for PWR power reactors
- ADELINE device designed to accommodate a single UO_2 fuel pin 1% U235 enriched in order to reproduce abnormal operating conditions leading to clad failure
- MOLFI device utilized for HEU (93% in U235) and LEU (20% in U235) UAl targets irradiation aimed at radioisotope production for medical purposes .

High core power is significantly elevated with respect to European MTR fleet and then devices containing fissile samples for fuel irradiation tests are critical components con-

cerning safety topics about normal operations and scenarios ranging from incidental conditions up to severe accidents.
In fact, MADISON devices are expected to attain 130 kW, conversely ADELINE nominal power is of some 60 kW. In addition, MOLFI test samples reach 650 kW for what concerns HEU configuration and about 400 kW according to the present LEU frame (to be improved in order to attain higher values). Globally, they are responsible for a total power up to some 3 MW.
Transient descriptions needed a particular model and an innovative method have been conceived and implemented. Main improvements consist of accounting for change in flux shape and power distribution in reflector locations due to control rod insertions during shutdown. Provided a normalized core power, this effect concerning Pilot Rod insertion during Normal Shutdown has turned out to increase MADISON power up to 5% and ADELINE up to 8%. Control rod locations induce MOLFI power to rise up to 8%. Safety Shutdown flux distortion has highlighted more effective power distribution modification up to 12% increase in MADISON and 20% in ADELINE. In addition, MOLFI devices are concerned by power changes ranging from 15% up to 22%.
This impacting neutronic feature has been taken into account together with power transients by means of proper device-core coupling coefficients evaluated with energy deposition simulations through TRIPOLI 4.8 Monte Carlo code.
Moreover, enhanced calculation methodology proposed in the present thesis considered time-dependent core-induced effects as well as sample self-produced energy deposition. Neutron kinetics approach accounts for prompt and delayed core neutrons impact on device power through a proper multi-point revised model. Sample neutron power self-contributions have been calculated as some 3% for MADISON, 4% for ADELINE, up to 25% for MOLFI. Particular attention has been paid to self-delayed neutron generation aiming at time behavior distortion investigation with respect to core source transients. Single device reactivity and kinetics- considered as an independent system - has been worth to be evaluated since its response to source irradiation is strictly related to its neutron multiplication feature and delayed generation.
In addition, prompt core gamma dose on devices is modeled following neutron transient and computing relative coupling coefficients. This relevant fraction accounts for some 20 kW for ADELINE, 18 kW for MADISON. MOLFI LEU devices are concerned for 25 kW, 30 kW for HEU frame. Self-generated irradiation attains some 2% for MADISON and ADELINE, MOLFI fissile samples reach about 15%. Thus delayed gamma radiations dose to devices due to core fission products decay has been considered regarding different burnup conditions. Once gamma spectra evaluated, radiation transport problem has been solved and contribution to sample transients determined as far as emitters time-dependent behavior are concerned. Nominal power turned out to attain some 3 kW for MADISON, 5 kW for MOLFI and up to 6 for ADELINE.

Perspectives

Finally, present developed innovative calculation method achieved results determination about device transients during Normal and Safety Shutdown procedures accounting for all nuclear heating processes and related time features. Nominal and time-dependent power has been evaluated for MADISON ADELINE and MOLFI devices. Core transients impact on samples and consequent self-contribution effectiveness is computed. Complete prompt and delayed gamma source effects are investigate to improve state-of-the-art computation methodology. Provided relevant system parameters normalization, obtained results showed to be coherent with representative experimental data regarding power transient tests carried out in OSIRIS reactor.
This analysis regards U_3Si_2 equilibrium cycle fuel through 34 assemblies at 100 MW nominal power. Further estimations are foreseen concerning operational core configurations in which 37 fuel elements with 19,75% enriched fuel are charger and 70 MW thermal power is envisaged for reactor exploitation. Consequent rods worth and control devices management has to be updated. Shutdown procedures antireactivity insertions need relative verifications as well.
Therefore, device power transients require additional estimations about flux distortion concerning control rod insertions. Modified power and fuel loading induce variations in burnup and fission products buildup, impacting on local poisoning reactivity swing and delayed effects contribution as well. Present methodology is expected to be utilized also for core property updating related to JHR design team feedback in order to better manage devices standard operations, characterize safety features even in challenging conditions and thus enhance JHR experimental capability.

Appendix A

Reflector Energy Deposition

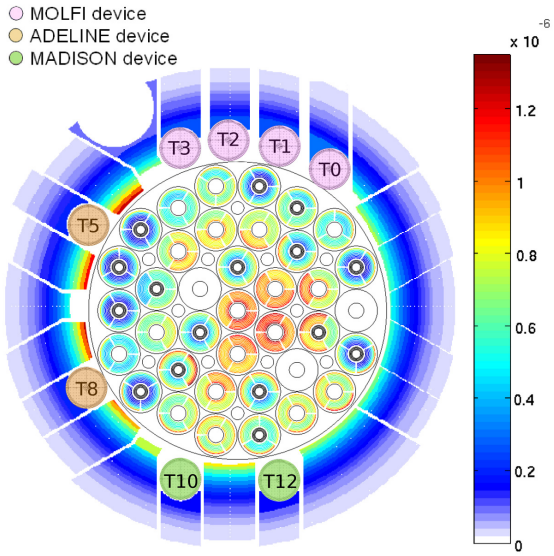

Figure A.1: Core fissions and reflector power shape at nominal BoC

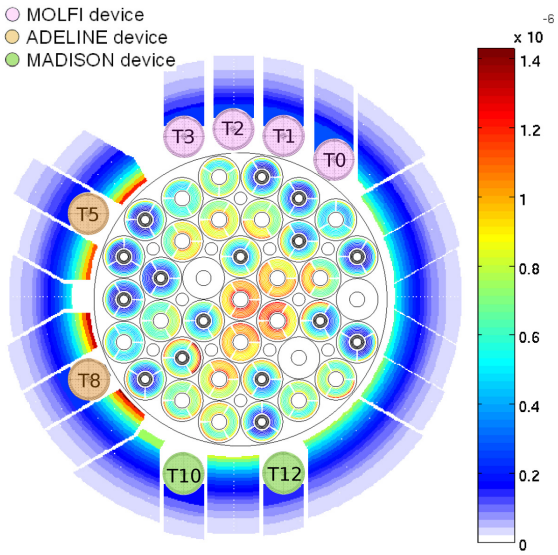

Figure A.2: Core fissions and reflector power shape for 4 PR at BoC

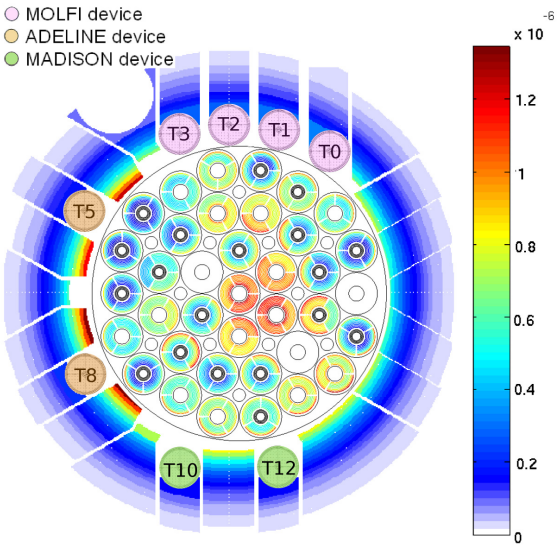

Figure A.3: Core fissions and reflector power shape for 3 SR at BoC

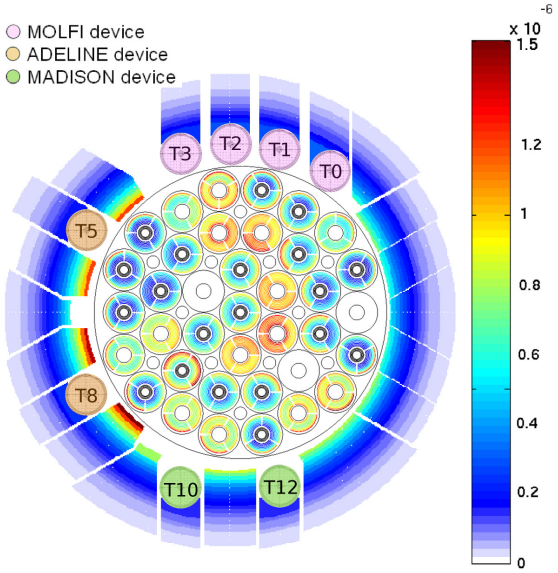

Figure A.4: Core fissions and reflector power shape for 4 SR + 4 PR at BoC

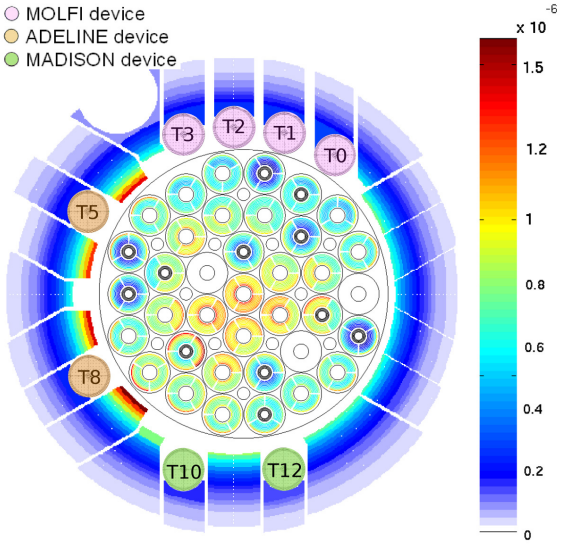

Figure A.5: Core fissions and reflector power shape at nominal XSP

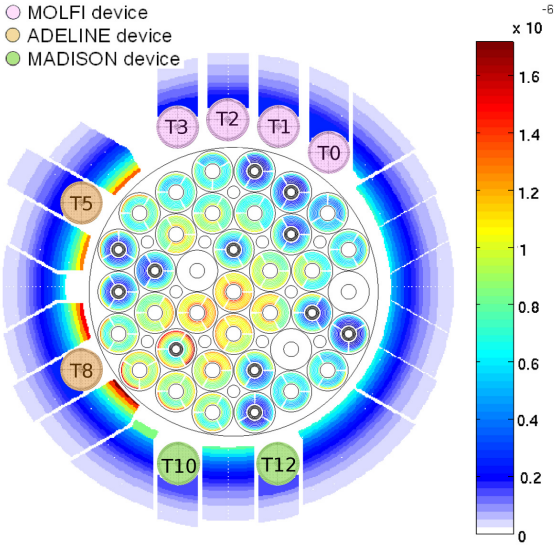

Figure A.6: Core fissions and reflector power shape for 4 PR at XSP

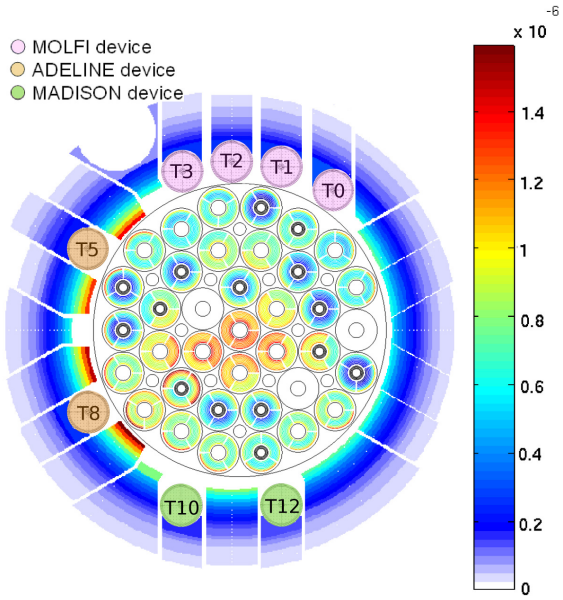

Figure A.7: Core fissions and reflector power shape for 3 SR at XSP

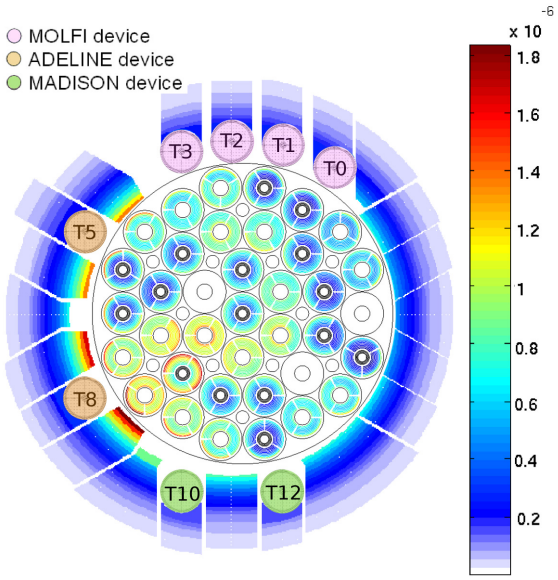

Figure A.8: Core fissions and reflector power shape for 4 SR + 4 PR at XSP

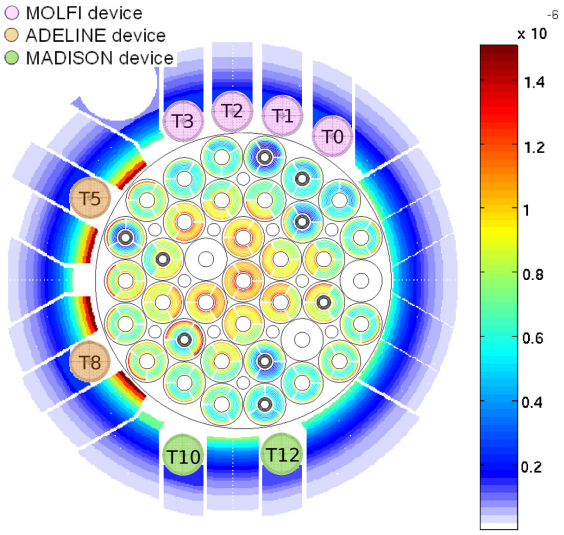

Figure A.9: Core fissions and reflector power shape at nominal MoC

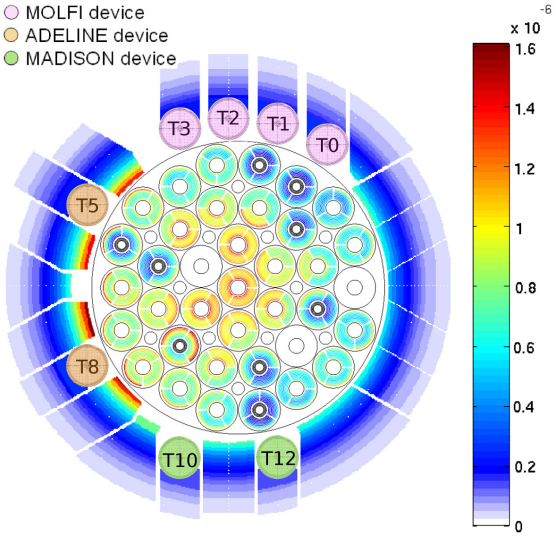

Figure A.10: Core fissions and reflector power shape for 4 PR at MoC

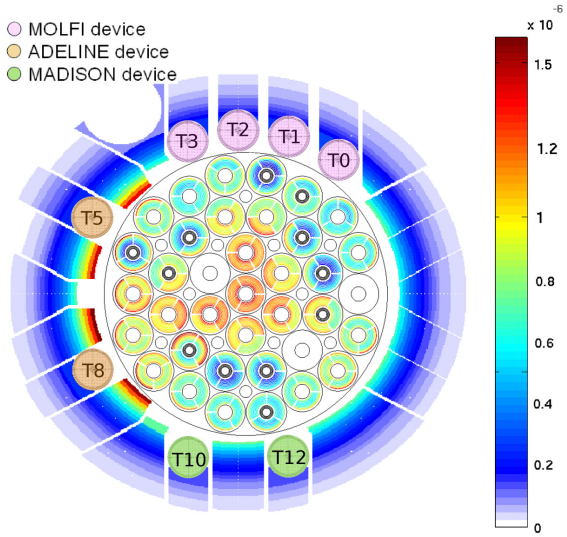

Figure A.11: Core fissions and reflector power shape for 3 SR at MoC

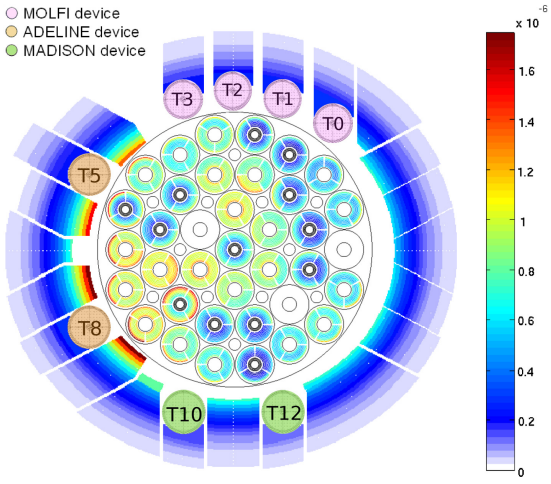

Figure A.12: Core fissions and reflector power shape for 4 SR + 4 PR at MoC

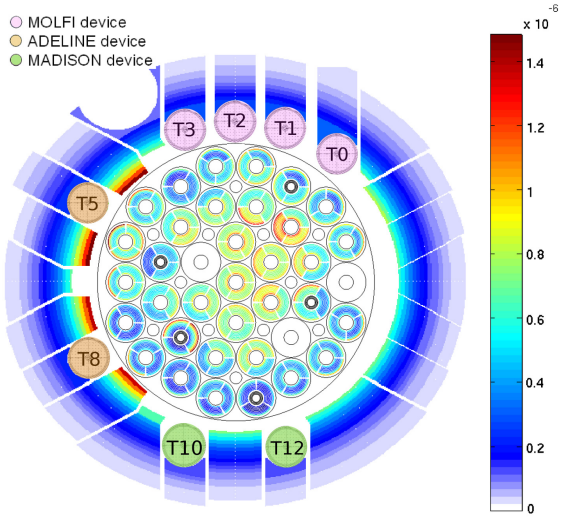

Figure A.13: Core fissions and reflector power shape at nominal EoC

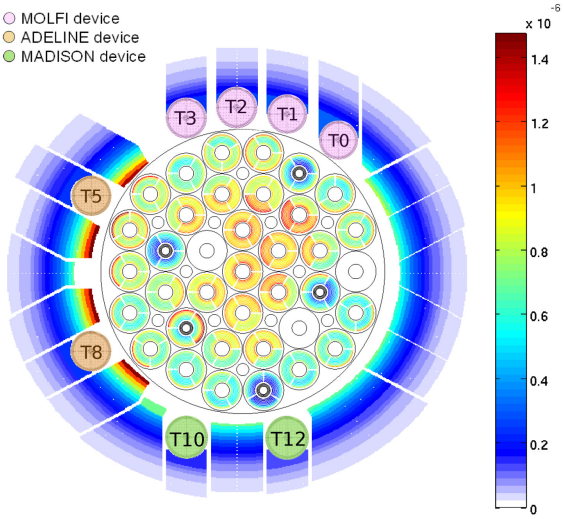

Figure A.14: Core fissions and reflector power shape for 4 PR at EoC

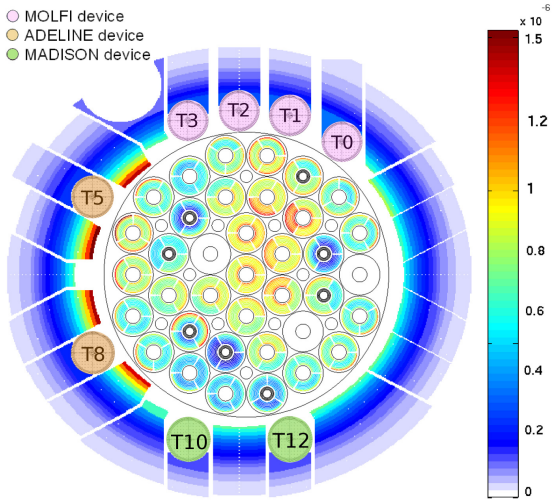

Figure A.15: Core fissions and reflector power shape for 3 SR at EoC

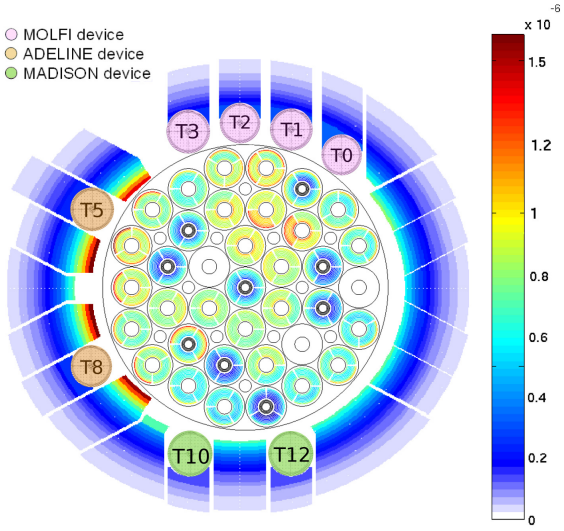

Figure A.16: Core fissions and reflector power shape for 4 SR + 4 PR at EoC

Appendix B

Device Power Transients

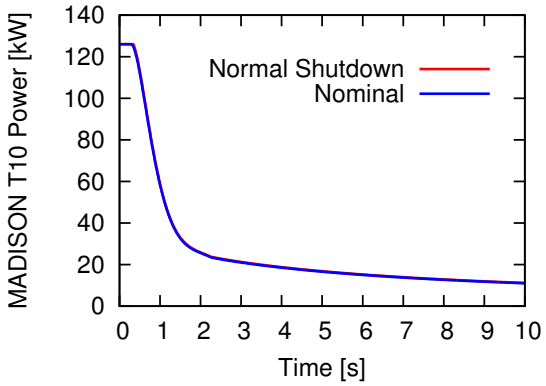

Figure B.1: Normal Shutdown at BoC, MADISON T10

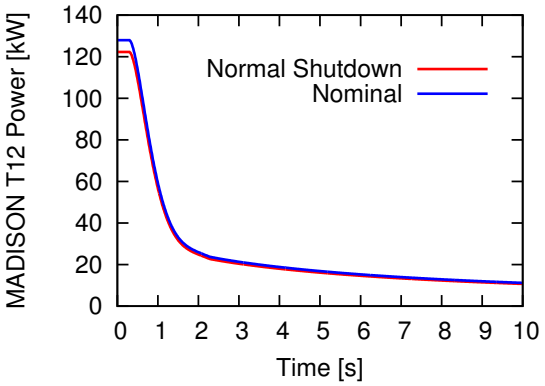

Figure B.2: Normal Shutdown at BoC, MADISON T12

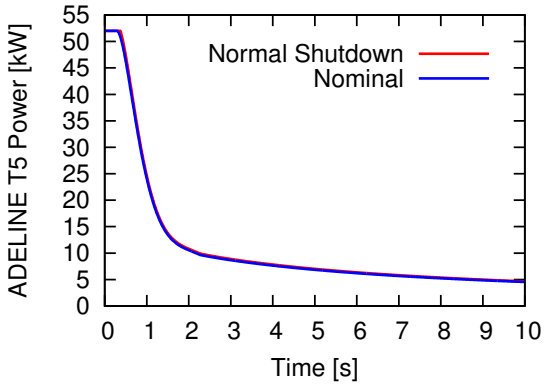

Figure B.3: Normal Shutdown at BoC, ADELINE T5

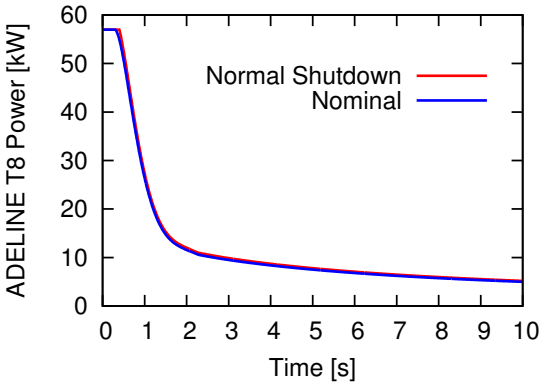

Figure B.4: Normal Shutdown at BoC, ADELINE T8

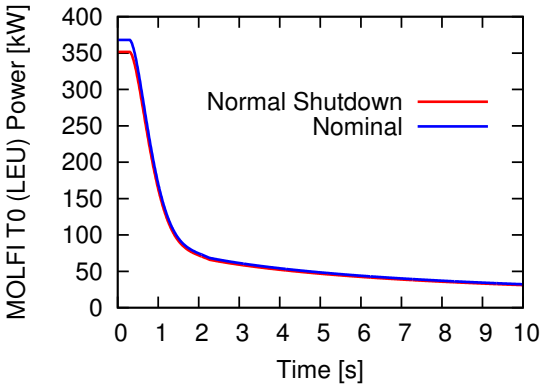

Figure B.5: Normal Shutdown at BoC, MOLFI T0 (LEU)

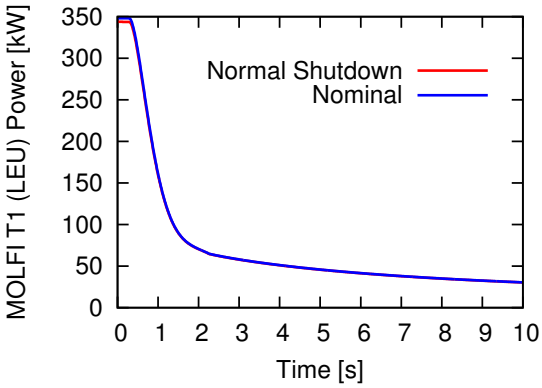

Figure B.6: Normal Shutdown at BoC, MOLFI T1 (LEU)

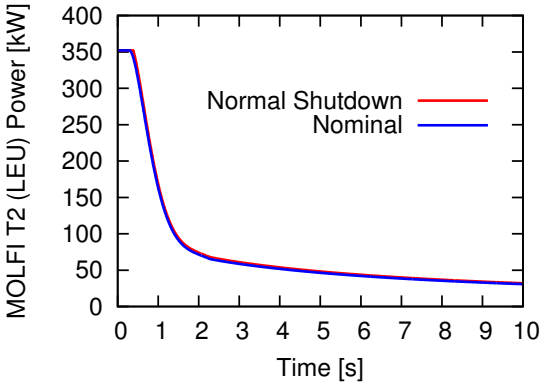

Figure B.7: Normal Shutdown at BoC, MOLFI T2 (LEU)

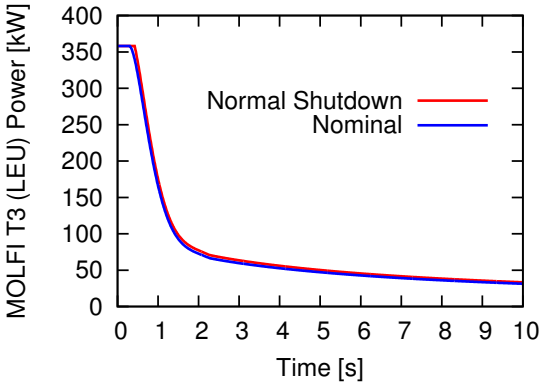

Figure B.8: Normal Shutdown at BoC, MOLFI T3 (LEU)

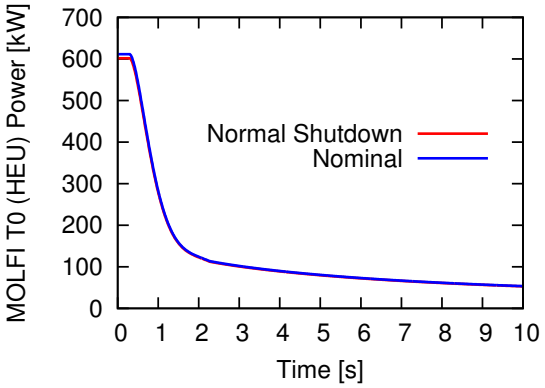

Figure B.9: Normal Shutdown at BoC, MOLFI T0 (HEU)

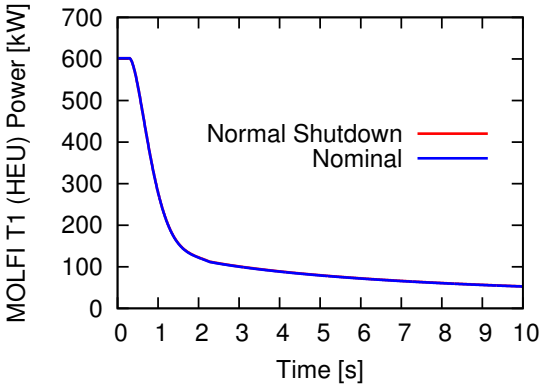

Figure B.10: Normal Shutdown at BoC, MOLFI T1 (HEU)

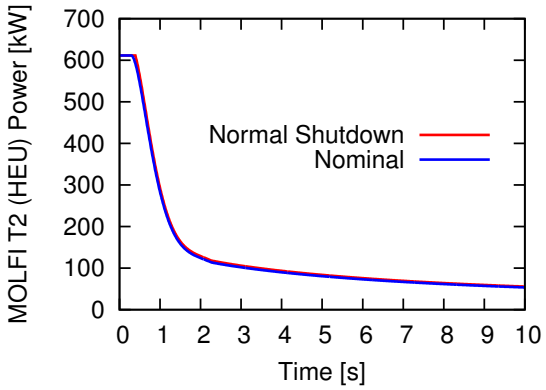

Figure B.11: Normal Shutdown at BoC, MOLFI T2 (HEU)

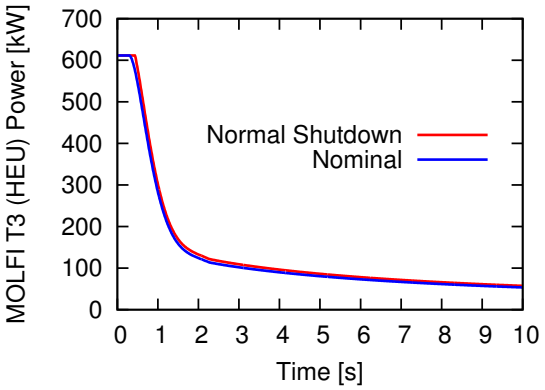

Figure B.12: Normal Shutdown at BoC, MOLFI T3 (HEU)

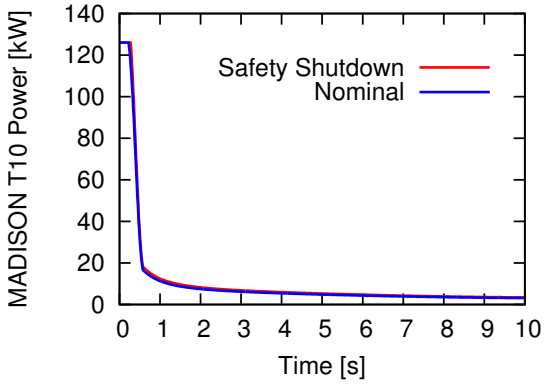

Figure B.13: Safety Shutdown at BoC, MADISON T10

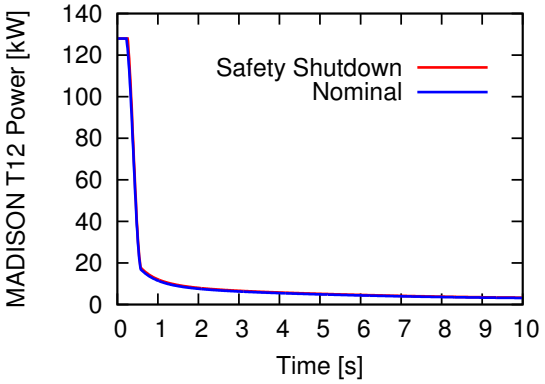

Figure B.14: Safety Shutdown at BoC, MADISON T12

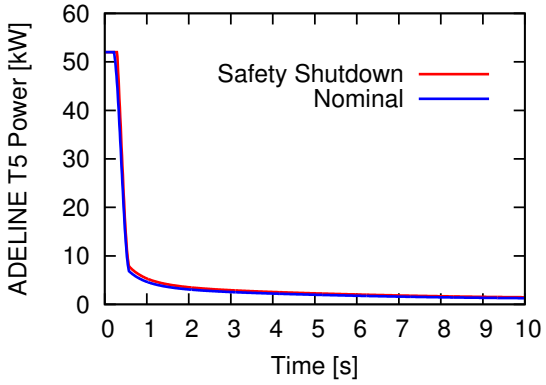

Figure B.15: Safety Shutdown at BoC, ADELINE T5

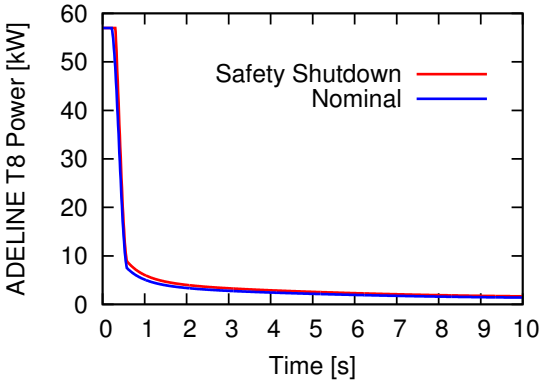

Figure B.16: Safety Shutdown at BoC, ADELINE T8

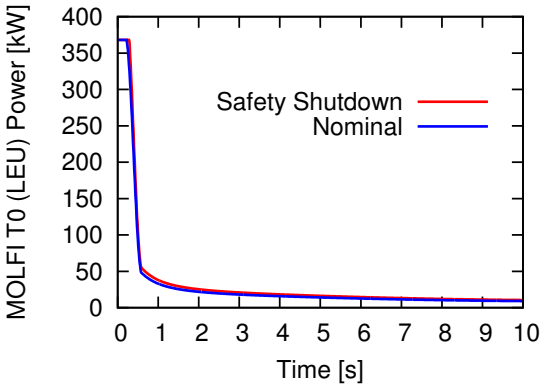

Figure B.17: Safety Shutdown at BoC, MOLFI T0 (LEU)

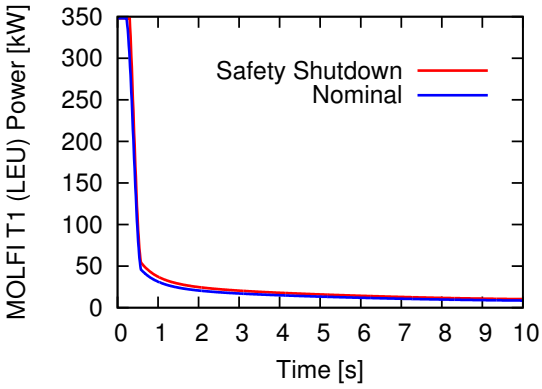

Figure B.18: Safety Shutdown at BoC, MOLFI T1 (LEU)

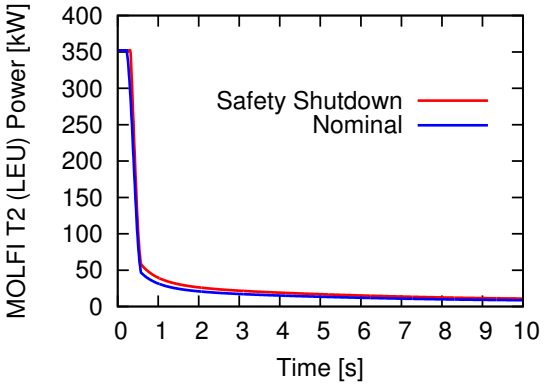

Figure B.19: Safety Shutdown at BoC, MOLFI T2 (LEU)

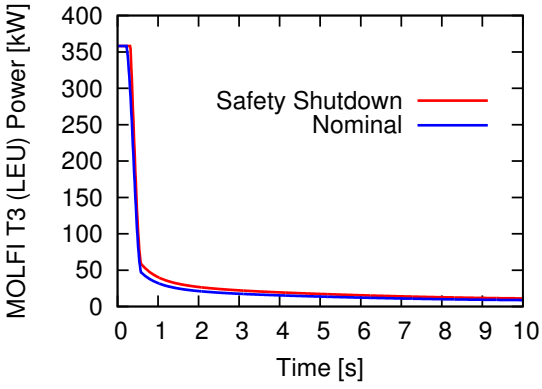

Figure B.20: Safety Shutdown at BoC, MOLFI T3 (LEU)

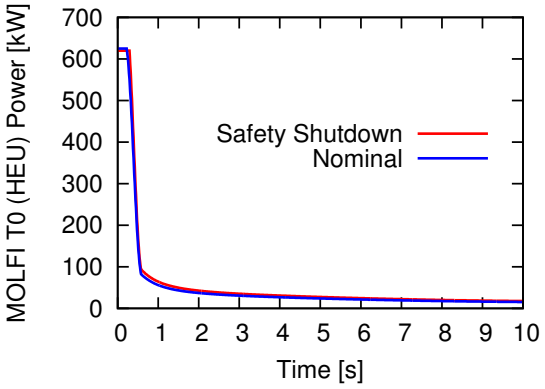

Figure B.21: Safety Shutdown at BoC, MOLFI T0 (HEU)

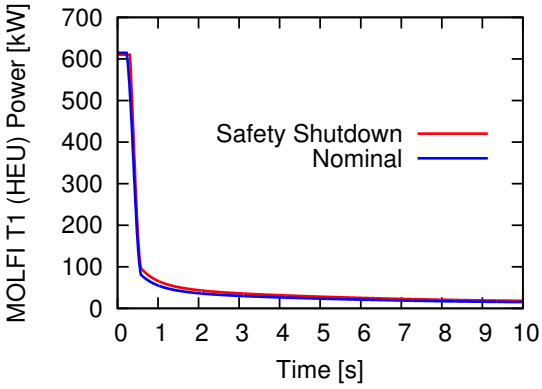

Figure B.22: Safety Shutdown at BoC, MOLFI T1 (HEU)

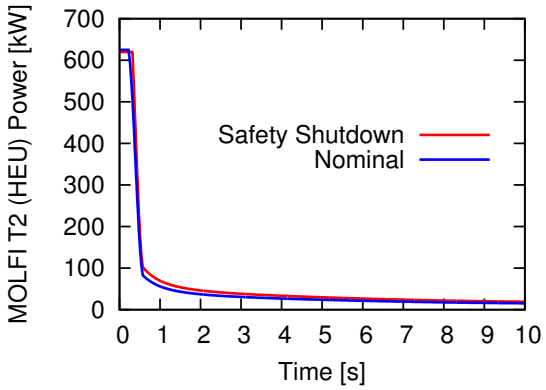

Figure B.23: Safety Shutdown at BoC, MOLFI T2 (HEU)

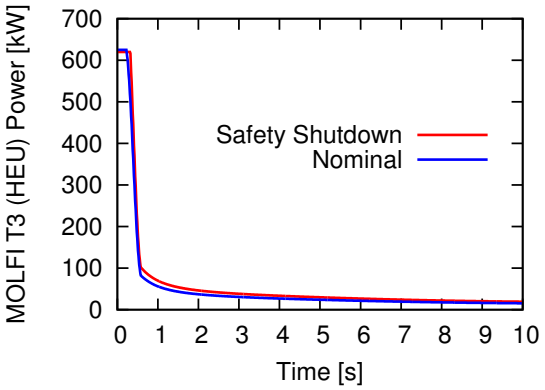

Figure B.24: Safety Shutdown at BoC, MOLFI T3 (HEU)

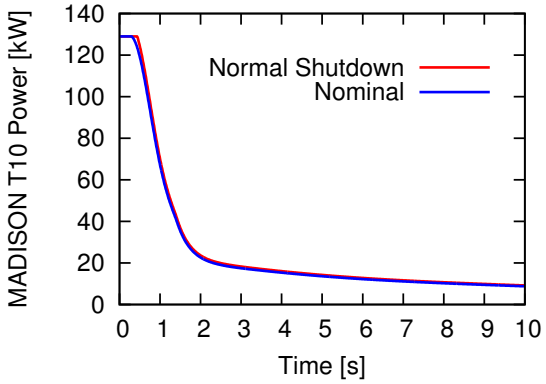

Figure B.25: Normal Shutdown at XSP, MADISON T10

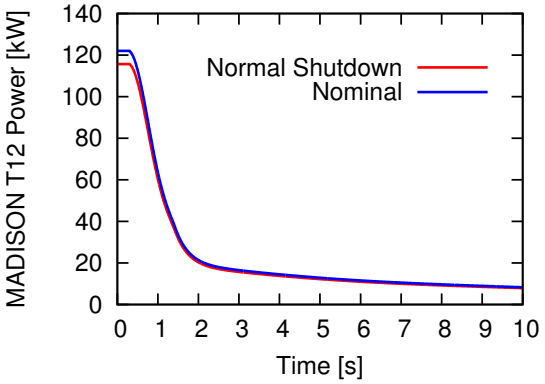

Figure B.26: Normal Shutdown at XSP, MADISON T12

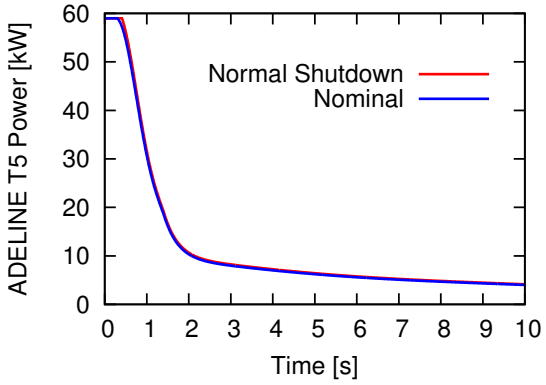

Figure B.27: Normal Shutdown at XSP, ADELINE T5

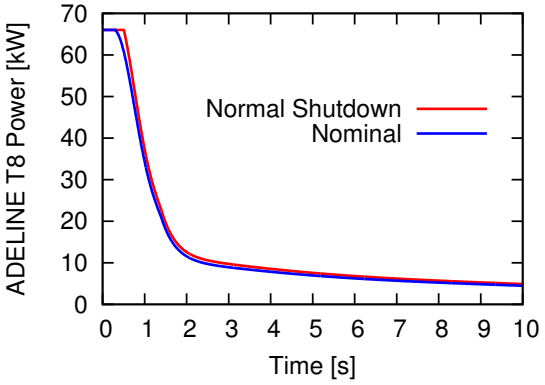

Figure B.28: Normal Shutdown at XSP, ADELINE T8

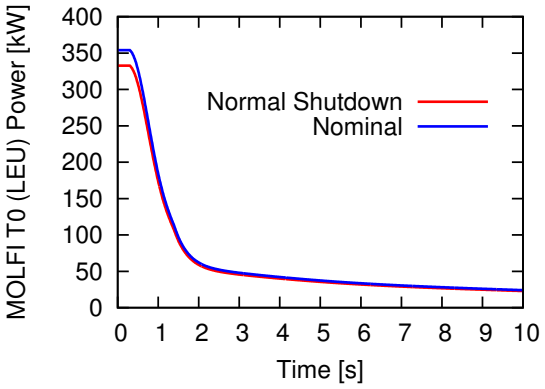

Figure B.29: Normal Shutdown at XSP, MOLFI T0 (LEU)

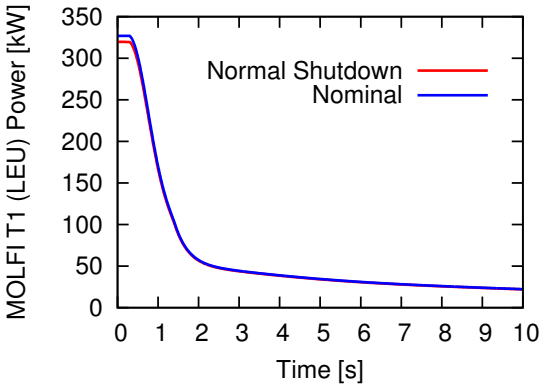

Figure B.30: Normal Shutdown at XSP, MOLFI T1 (LEU)

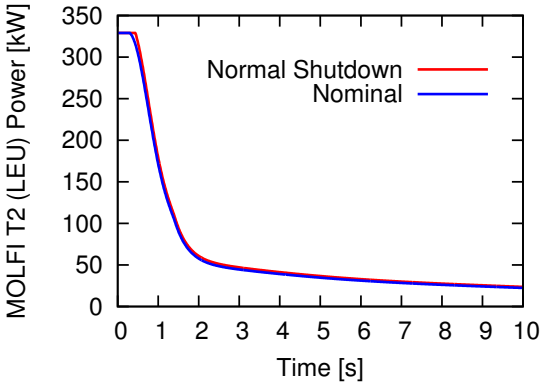

Figure B.31: Normal Shutdown at XSP, MOLFI T2 (LEU)

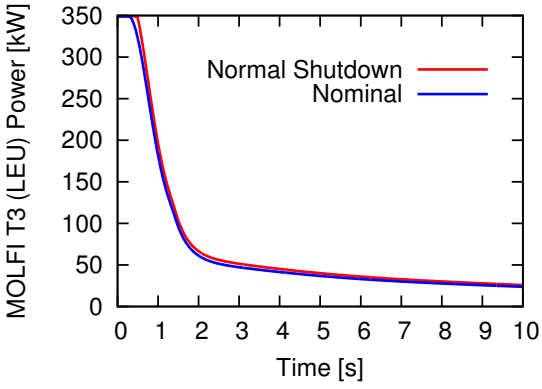

Figure B.32: Normal Shutdown at XSP, MOLFI T3 (LEU)

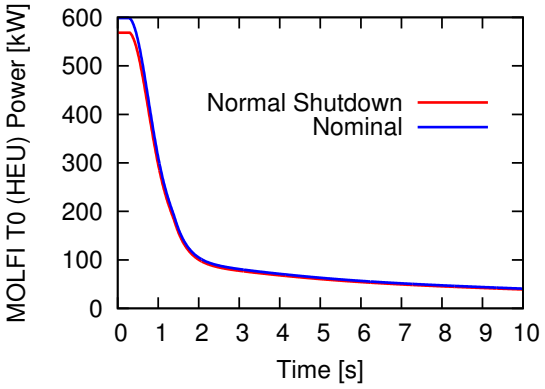

Figure B.33: Normal Shutdown at XSP, MOLFI T0 (HEU)

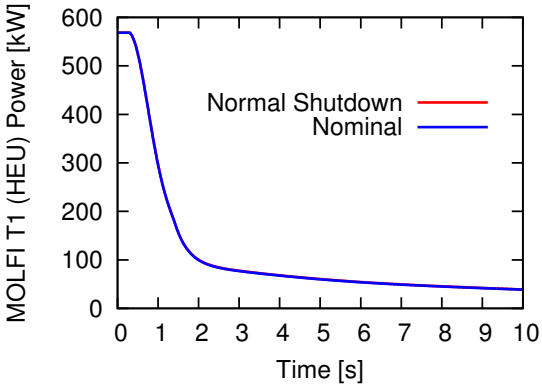

Figure B.34: Normal Shutdown at XSP, MOLFI T1 (HEU)

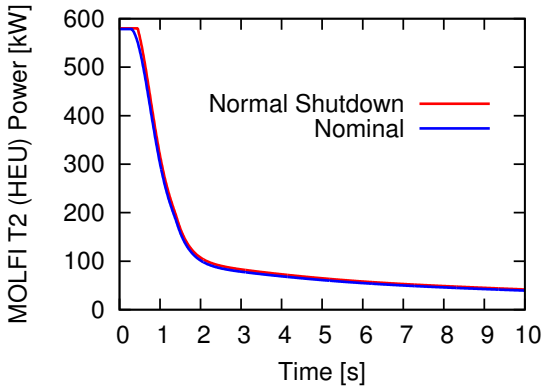

Figure B.35: Normal Shutdown at XSP, MOLFI T2 (HEU)

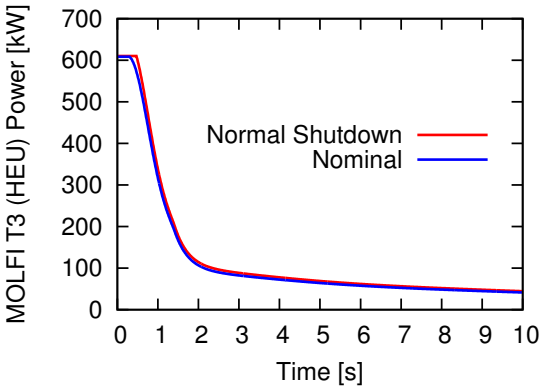

Figure B.36: Normal Shutdown at XSP, MOLFI T3 (HEU)

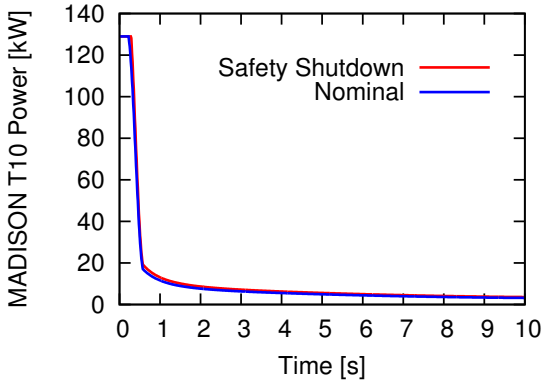

Figure B.37: Safety Shutdown at XSP, MADISON T10

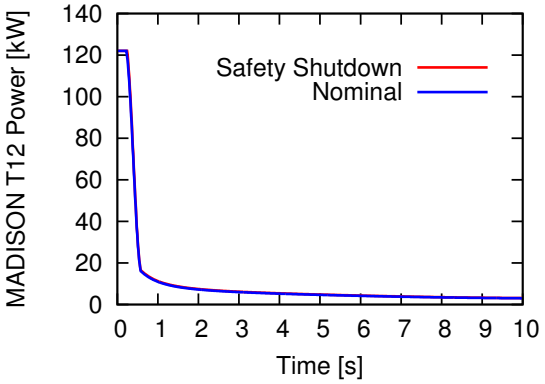

Figure B.38: Safety Shutdown at XSP, MADISON T12

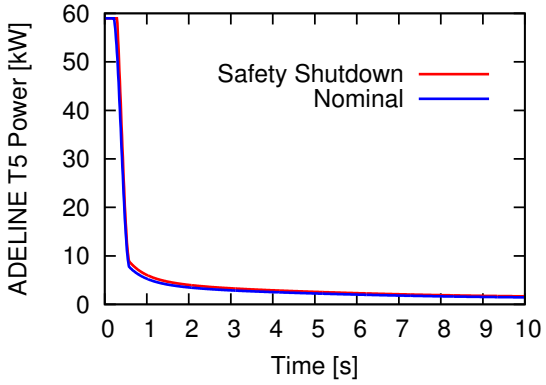

Figure B.39: Safety Shutdown at XSP, ADELINE T5

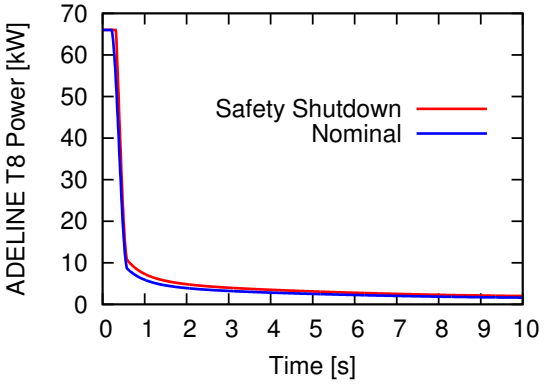

Figure B.40: Safety Shutdown at XSP, ADELINE T8

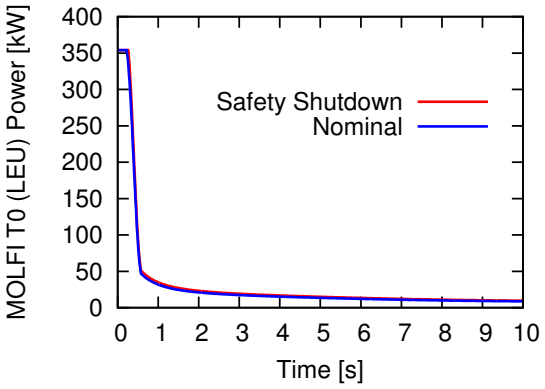

Figure B.41: Safety Shutdown at XSP, MOLFI T0 (LEU)

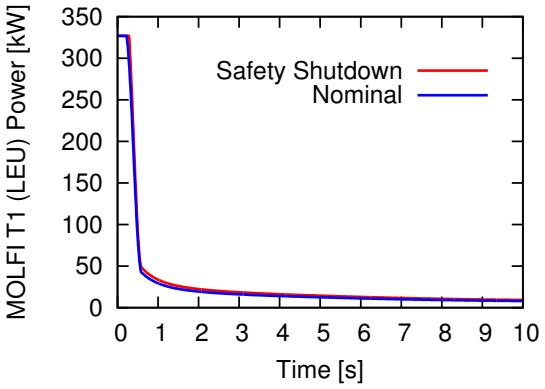

Figure B.42: Safety Shutdown at XSP, MOLFI T1 (LEU)

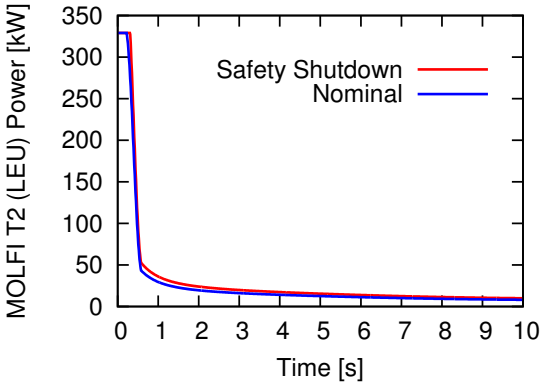

Figure B.43: Safety Shutdown at XSP, MOLFI T2 (LEU)

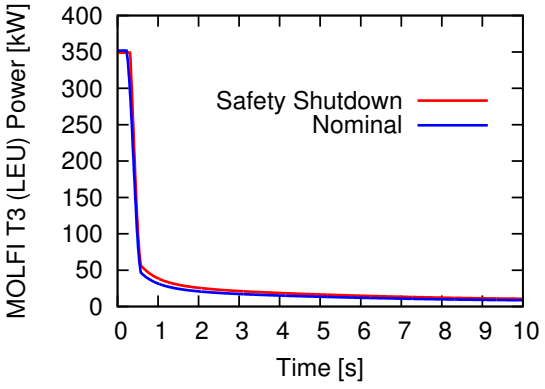

Figure B.44: Safety Shutdown at XSP, MOLFI T3 (LEU)

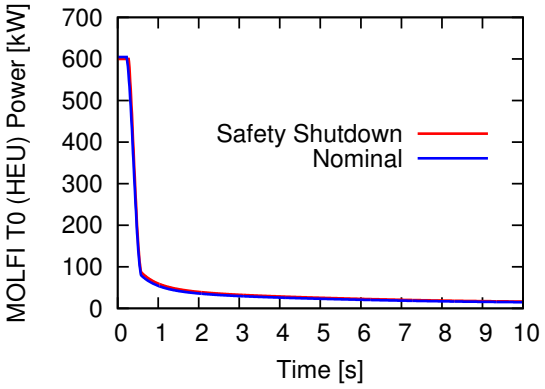

Figure B.45: Safety Shutdown at XSP, MOLFI T0 (HEU)

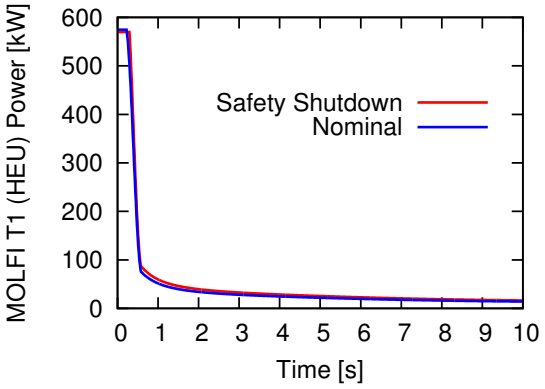

Figure B.46: Safety Shutdown at XSP, MOLFI T1 (HEU)

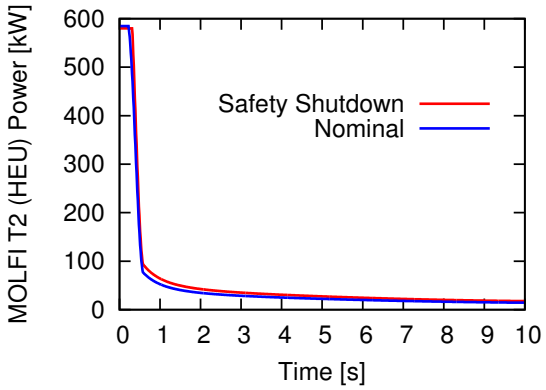

Figure B.47: Safety Shutdown at XSP, MOLFI T2 (HEU)

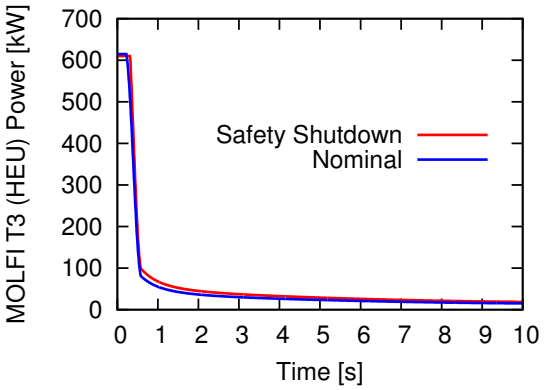

Figure B.48: Safety Shutdown at XSP, MOLFI T3 (HEU)

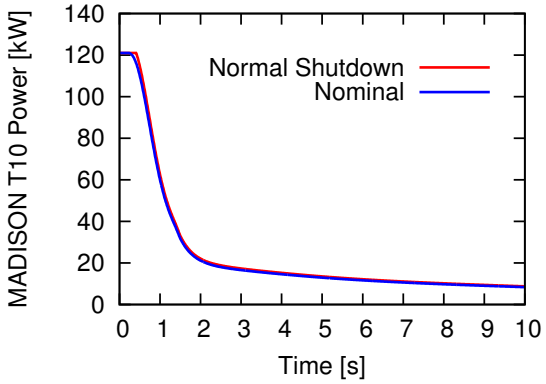

Figure B.49: Normal Shutdown at MoC, MADISON T10

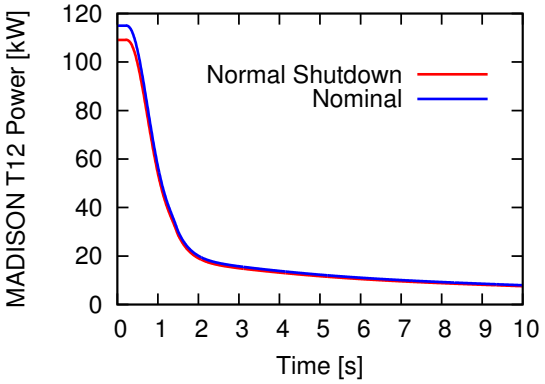

Figure B.50: Normal Shutdown at MoC, MADISON T12

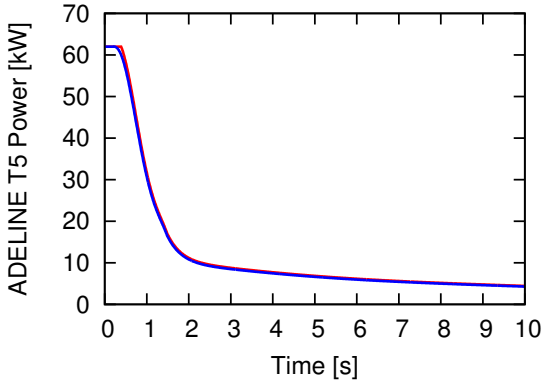

Figure B.51: Normal Shutdown at MoC, ADELINE T5

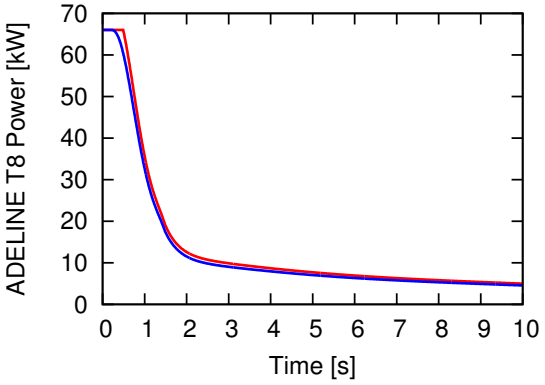

Figure B.52: Normal Shutdown at MoC, ADELINE T8

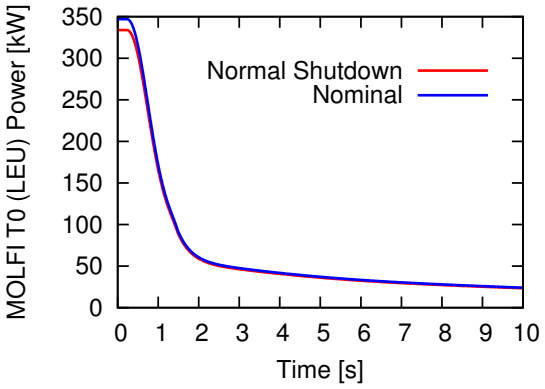

Figure B.53: Normal Shutdown at MoC, MOLFI T0 (LEU)

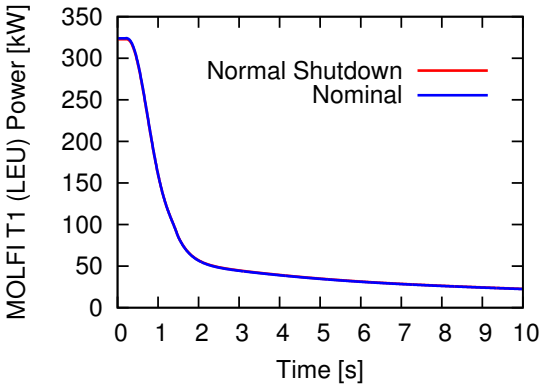

Figure B.54: Normal Shutdown at MoC, MOLFI T1 (LEU)

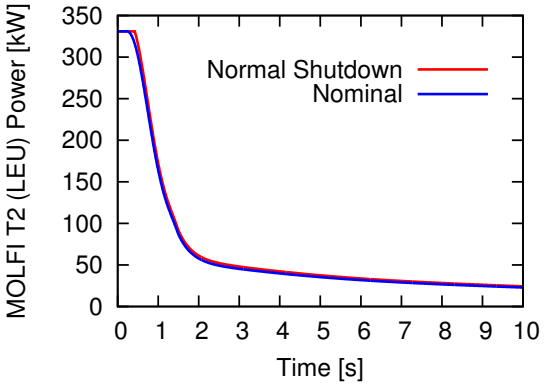

Figure B.55: Normal Shutdown at MoC, MOLFI T2 (LEU)

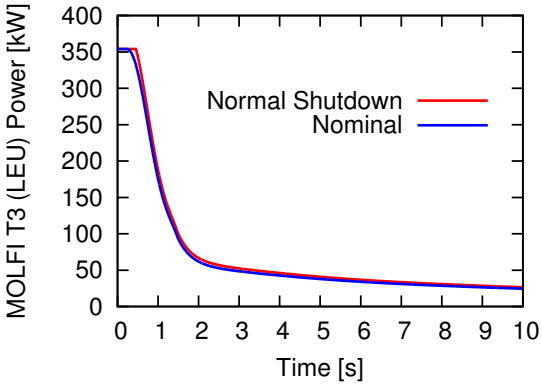

Figure B.56: Normal Shutdown at MoC, MOLFI T3 (LEU)

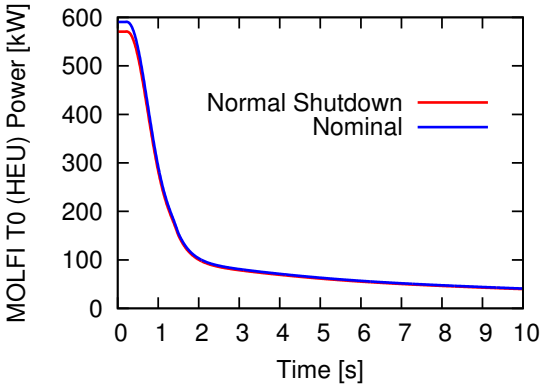

Figure B.57: Normal Shutdown at MoC, MOLFI T0 (HEU)

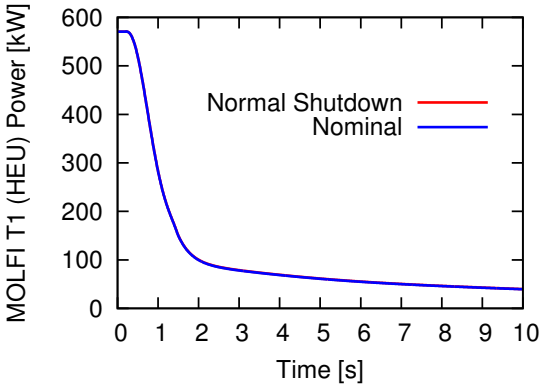

Figure B.58: Normal Shutdown at MoC, MOLFI T1 (HEU)

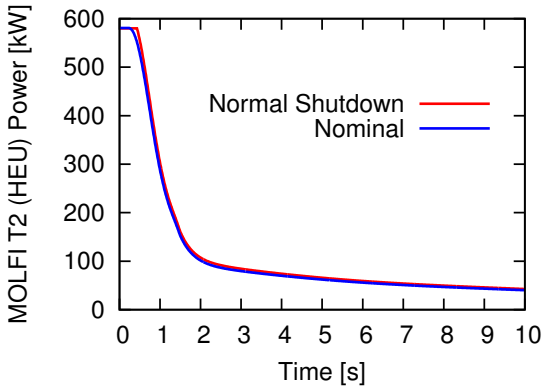

Figure B.59: Normal Shutdown at MoC, MOLFI T2 (HEU)

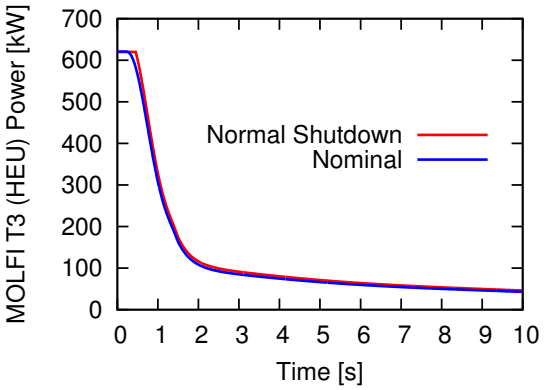

Figure B.60: Normal Shutdown at MoC, MOLFI T3 (HEU)

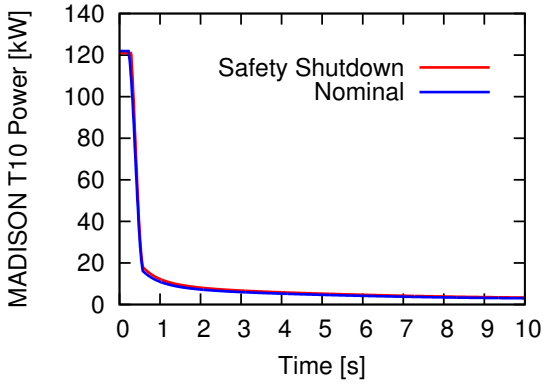

Figure B.61: Safety Shutdown at MoC, MADISON T10

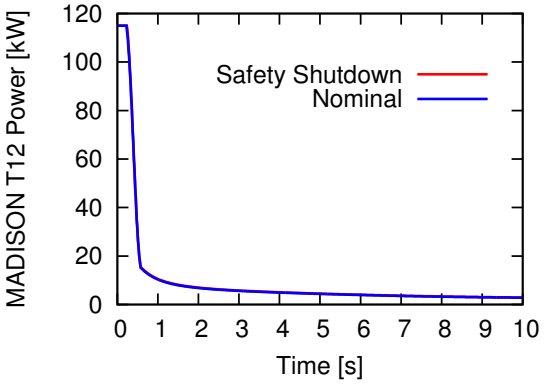

Figure B.62: Safety Shutdown at MoC, MADISON T12

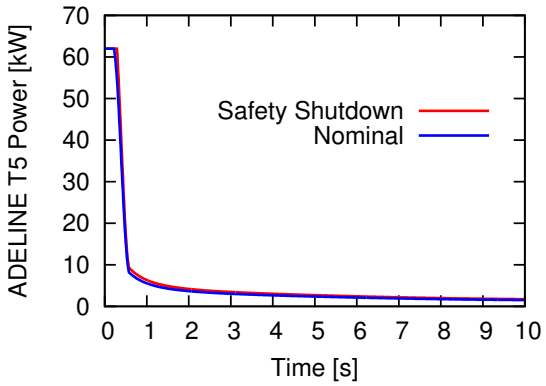

Figure B.63: Safety Shutdown at MoC, ADELINE T5

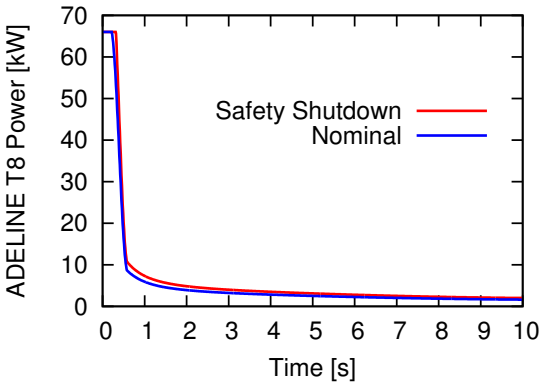

Figure B.64: Safety Shutdown at MoC, ADELINE T8

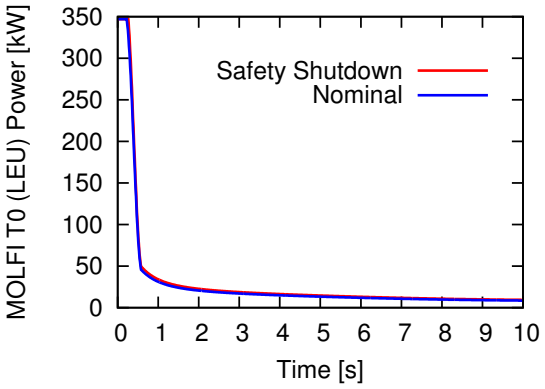

Figure B.65: Safety Shutdown at MoC, MOLFI T0 (LEU)

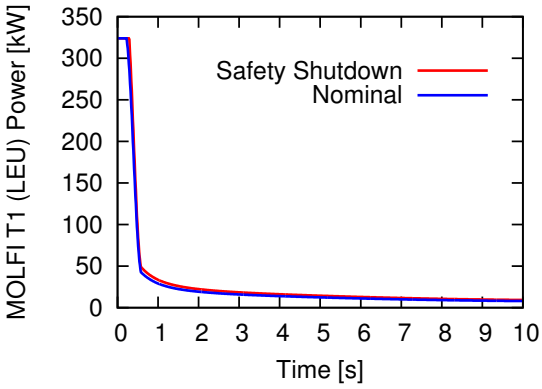

Figure B.66: Safety Shutdown at MoC, MOLFI T1 (LEU)

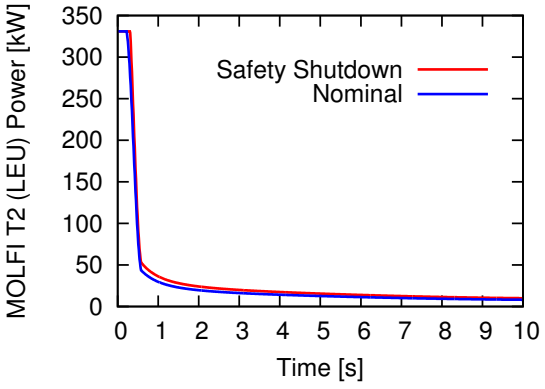

Figure B.67: Safety Shutdown at MoC, MOLFI T2 (LEU)

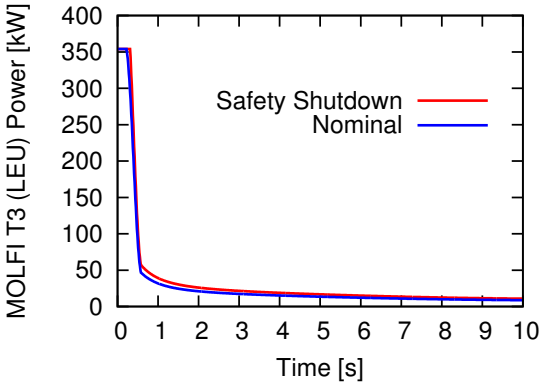

Figure B.68: Safety Shutdown at MoC, MOLFI T3 (LEU)

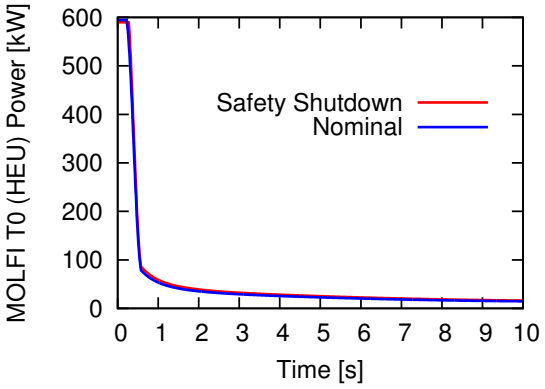

Figure B.69: Safety Shutdown at MoC, MOLFI T0 (HEU)

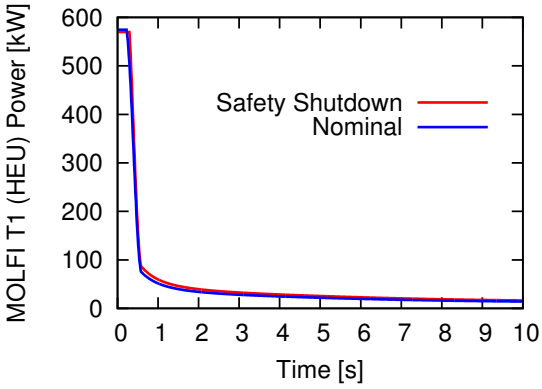

Figure B.70: Safety Shutdown at MoC, MOLFI T1 (HEU)

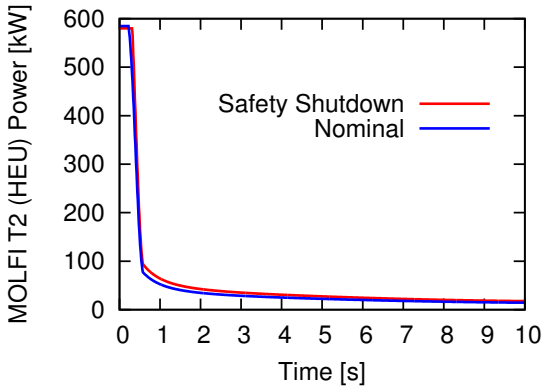

Figure B.71: Safety Shutdown at MoC, MOLFI T2 (HEU)

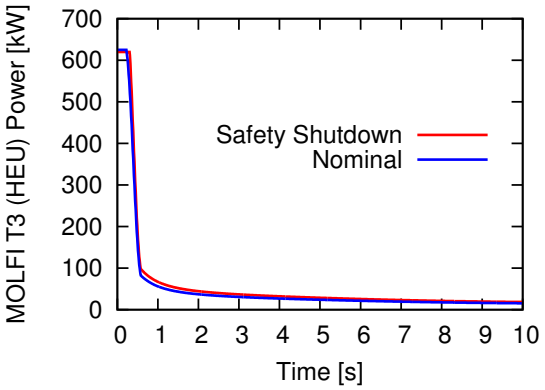

Figure B.72: Safety Shutdown at MoC, MOLFI T3 (HEU)

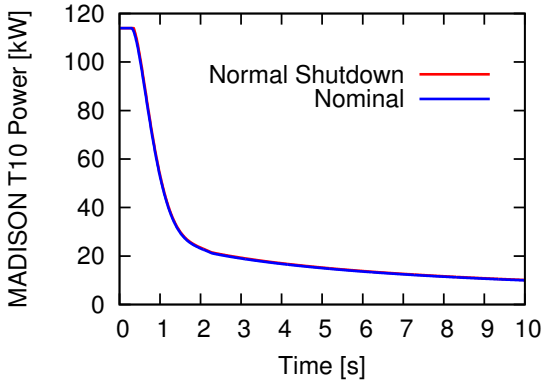

Figure B.73: Normal Shutdown at EoC, MADISON T10

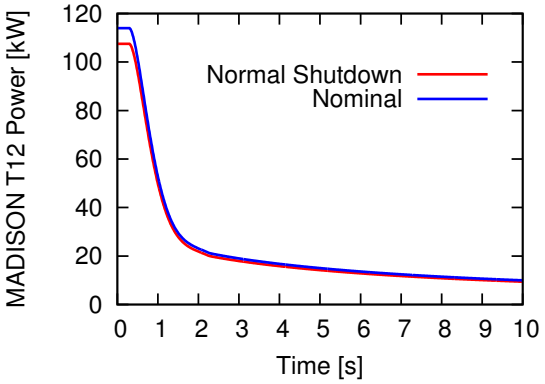

Figure B.74: Normal Shutdown at EoC, MADISON T12

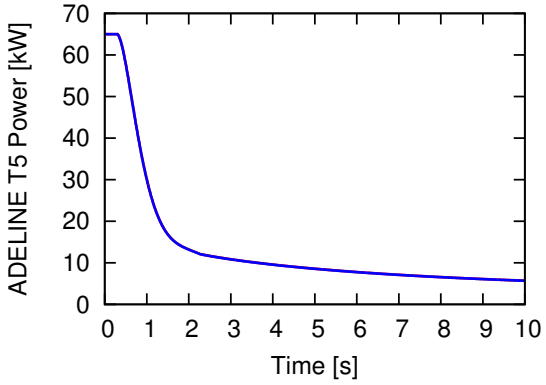

Figure B.75: Normal Shutdown at EoC, ADELINE T5

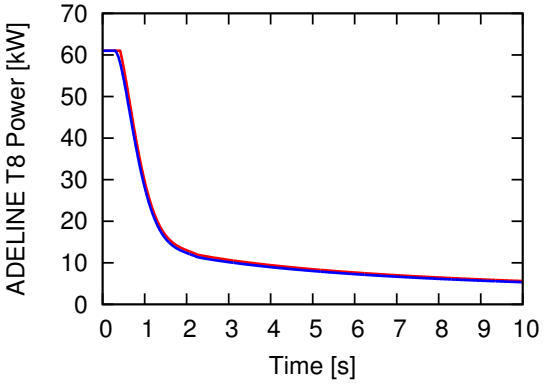

Figure B.76: Normal Shutdown at EoC, ADELINE T8

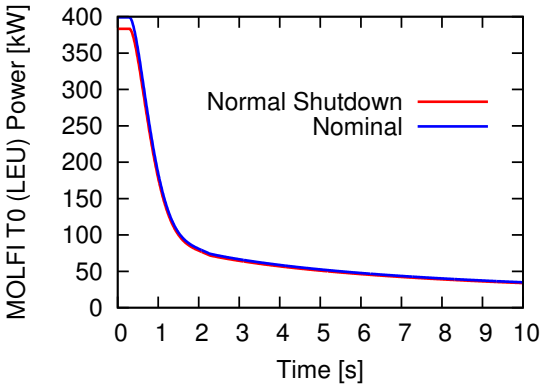

Figure B.77: Normal Shutdown at EoC, MOLFI T0 (LEU)

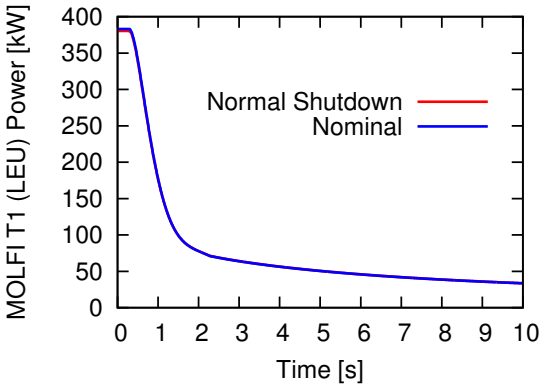

Figure B.78: Normal Shutdown at EoC, MOLFI T1 (LEU)

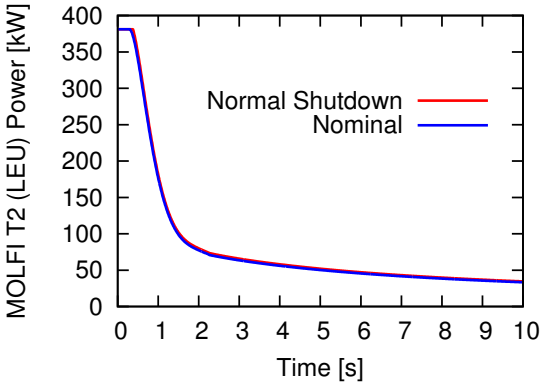

Figure B.79: Normal Shutdown at EoC, MOLFI T2 (LEU)

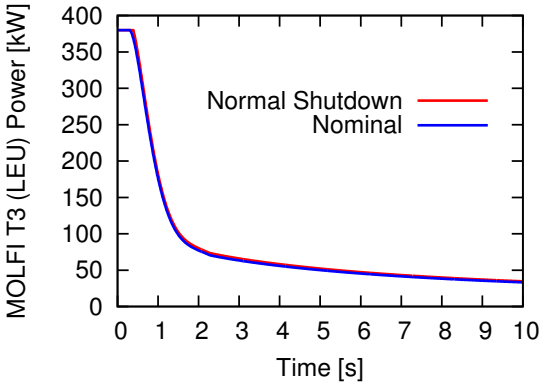

Figure B.80: Normal Shutdown at EoC, MOLFI T3 (LEU)

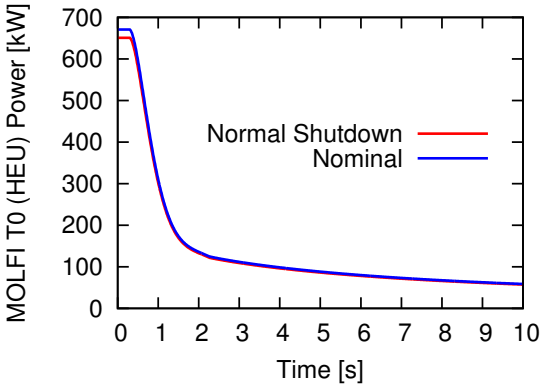

Figure B.81: Normal Shutdown at EoC, MOLFI T0 (HEU)

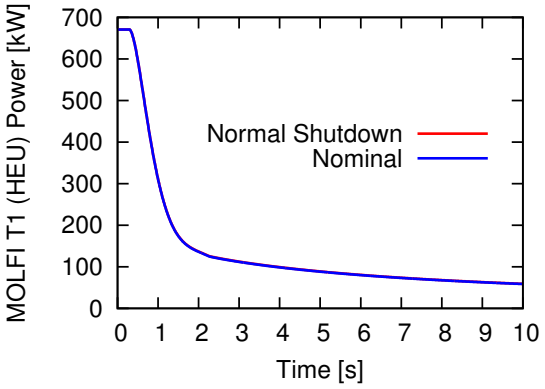

Figure B.82: Normal Shutdown at EoC, MOLFI T1 (HEU)

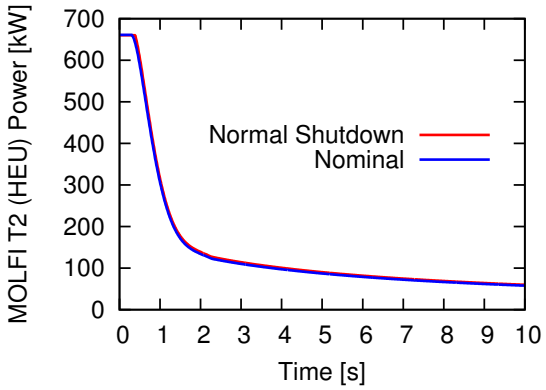

Figure B.83: Normal Shutdown at EoC, MOLFI T2 (HEU)

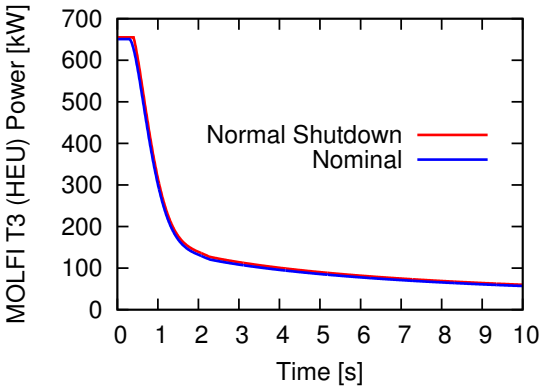

Figure B.84: Normal Shutdown at EoC, MOLFI T3 (HEU)

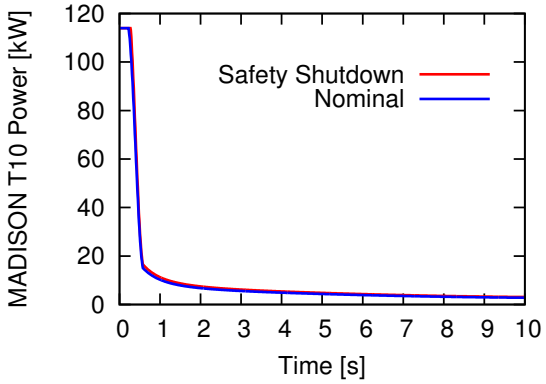

Figure B.85: Safety Shutdown at EoC, MADISON T10

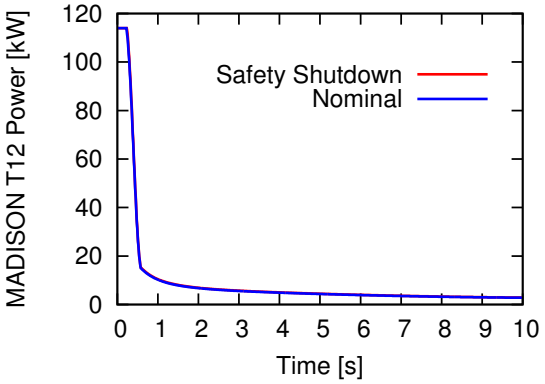

Figure B.86: Safety Shutdown at EoC, MADISON T12

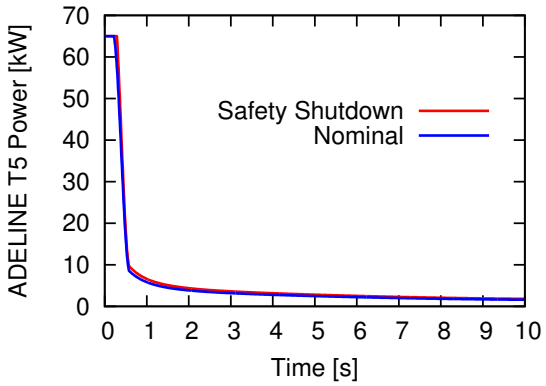

Figure B.87: Safety Shutdown at EoC, ADELINE T5

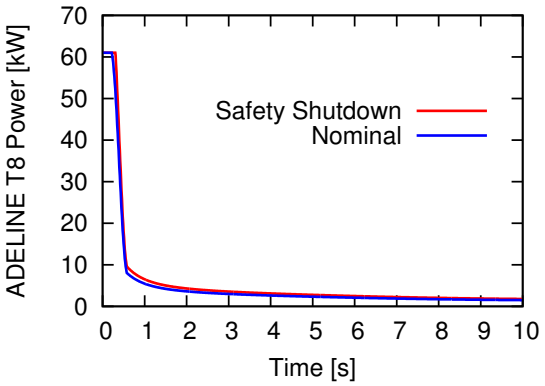

Figure B.88: Safety Shutdown at EoC, ADELINE T8

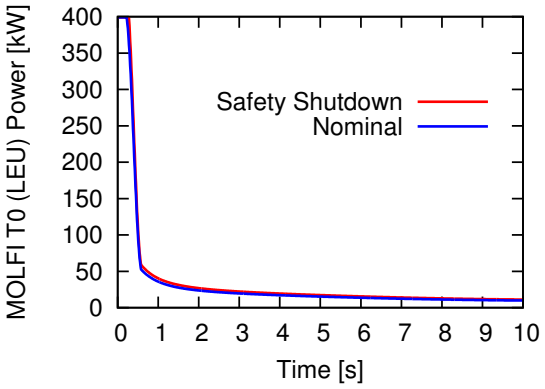

Figure B.89: Safety Shutdown at EoC, MOLFI T0 (LEU)

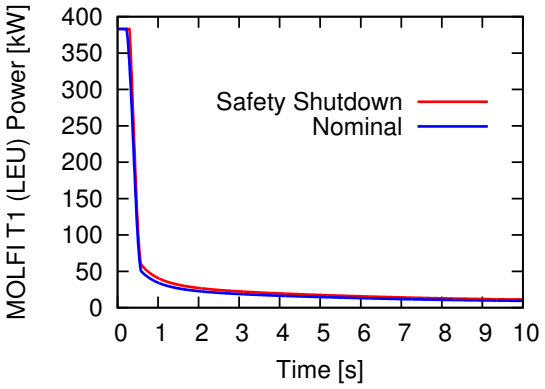

Figure B.90: Safety Shutdown at EoC, MOLFI T1 (LEU)

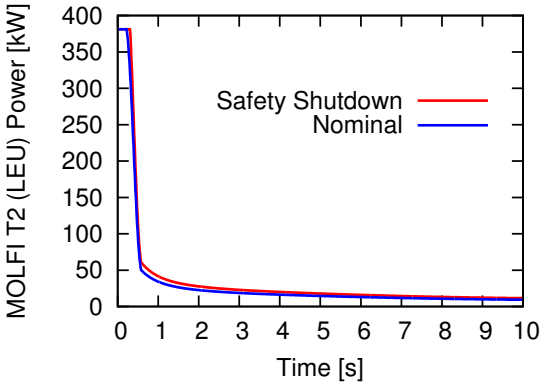

Figure B.91: Safety Shutdown at EoC, MOLFI T2 (LEU)

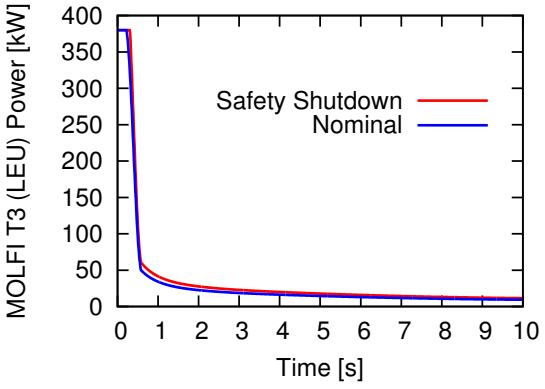

Figure B.92: Safety Shutdown at EoC, MOLFI T3 (LEU)

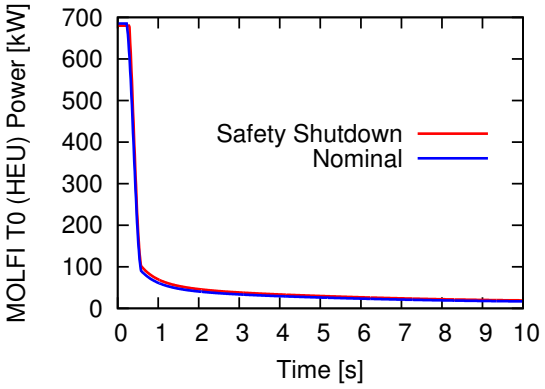

Figure B.93: Safety Shutdown at EoC, MOLFI T0 (HEU)

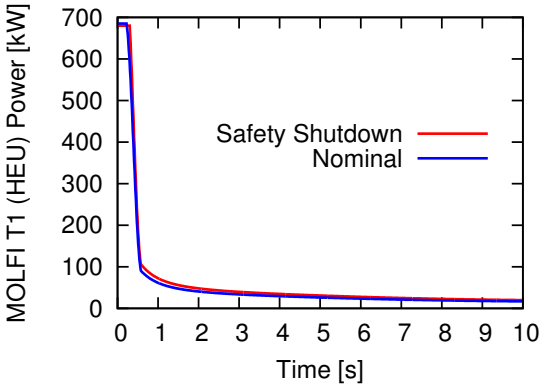

Figure B.94: Safety Shutdown at EoC, MOLFI T1 (HEU)

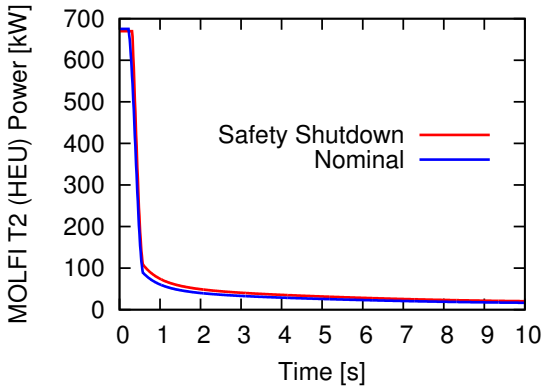

Figure B.95: Safety Shutdown at EoC, MOLFI T2 (HEU)

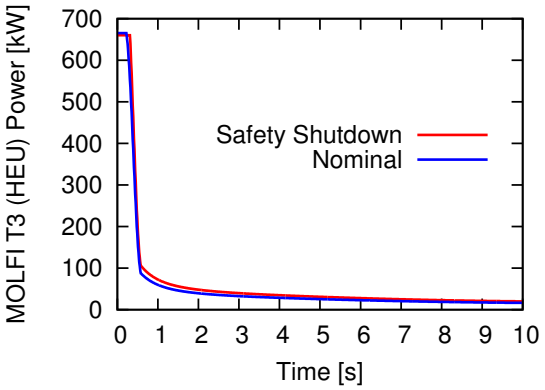

Figure B.96: Safety Shutdown at EoC, MOLFI T3 (HEU)

Appendix C

Delayed Gamma Energy Deposition

BoC	Nominal		Normal Shutdown		3 Safety Rods		Safety Shutdown	
	N [kW]	G [kW]	N [kW]	G [kW]	N [kW]	G [kW]	N [kW]	G [kW]
MADISON T10	1,35	0,28	0,69	0,14	0,86	0,18	0,68	0,14
MADISON T12	1,35	0,28	0,68	0,14	0,85	0,18	0,68	0,14
ADELINE T8	0,51	0,30	0,26	0,15	0,33	0,19	0,26	0,15
ADELINE T5	0,47	0,07	0,24	0,03	0,30	0,04	0,24	0,03
MOLFI T0 (LEU)	3,95	0,29	2,01	0,15	2,55	0,19	2,01	0,15
MOLFI T1 (LEU)	3,57	0,29	1,82	0,15	2,30	0,19	1,82	0,15
MOLFI T2 (LEU)	3,57	0,29	1,82	0,15	2,30	0,19	1,82	0,15
MOLFI T3 (LEU)	3,78	0,28	1,96	0,15	2,44	0,18	1,96	0,15

Table C.1: Delayed contributions to device power at BoC, neutron and gamma

XSP	Nominal		Normal Shutdown		3 Safety Rods		Safety Shutdown	
	N [kW]	G [kW]	N [kW]	G [kW]	N [kW]	G [kW]	N [kW]	G [kW]
MADISON T10	1,30	0,27	0,64	0,13	0,84	0,17	0,64	0,13
MADISON T12	1,39	0,29	0,69	0,15	0,89	0,19	0,69	0,14
ADELINE T8	0,61	0,34	0,31	0,17	0,39	0,22	0,31	0,17
ADELINE T5	0,53	0,07	0,27	0,04	0,34	0,05	0,26	0,04
MOLFI T0 (LEU)	3,62	0,26	1,79	0,13	2,32	0,17	1,79	0,13
MOLFI T1 (LEU)	3,14	0,26	1,57	0,13	2,03	0,17	1,56	0,13
MOLFI T2 (LEU)	3,14	0,26	1,57	0,13	2,03	0,17	1,56	0,13
MOLFI T3 (LEU)	3,54	0,26	1,80	0,13	2,28	0,17	1,80	0,13

Table C.2: Delayed contributions to device power at XSP, neutron and gamma

MoC	Nominal		Normal Shutdown		3 Safety Rods		Safety Shutdown	
	N [kW]	G [kW]	N [kW]	G [kW]	N [kW]	G [kW]	N [kW]	G [kW]
MADISON T10	1,21	0,25	0,60	0,12	0,77	0,16	0,60	0,12
MADISON T12	1,26	0,27	0,64	0,13	0,81	0,17	0,64	0,13
ADELINE T8	0,60	0,34	0,31	0,17	0,39	0,22	0,31	0,17
ADELINE T5	0,56	0,07	0,28	0,04	0,35	0,05	0,28	0,04
MOLFI T0 (LEU)	3,52	0,26	1,74	0,13	2,25	0,16	1,75	0,13
MOLFI T1 (LEU)	3,07	0,25	1,52	0,13	1,97	0,16	1,54	0,13
MOLFI T2 (LEU)	3,07	0,26	1,52	0,13	1,97	0,17	1,54	0,13
MOLFI T3 (LEU)	3,51	0,26	1,79	0,13	2,25	0,17	1,78	0,13

Table C.3: Delayed contributions to device power at MoC, neutron and gamma

EoC	Nominal		Normal Shutdown		3 Safety Rods		Safety Shutdown	
	N [kW]	G [kW]	N [kW]	G [kW]	N [kW]	G [kW]	N [kW]	G [kW]
MADISON T10	1,17	0,24	0,59	0,12	0,75	0,15	0,59	0,12
MADISON T12	1,17	0,25	0,60	0,13	0,75	0,16	0,60	0,13
ADELINE T8	0,55	0,30	0,28	0,16	0,35	0,19	0,28	0,16
ADELINE T5	0,58	0,08	0,30	0,04	0,37	0,05	0,30	0,04
MOLFI T0 (LEU)	3,91	0,28	2,00	0,15	2,53	0,18	2,00	0,14
MOLFI T1 (LEU)	3,66	0,29	1,86	0,15	2,34	0,18	1,86	0,15
MOLFI T2 (LEU)	3,66	0,29	1,86	0,15	2,34	0,19	1,86	0,15
MOLFI T3 (LEU)	3,68	0,27	1,90	0,14	2,34	0,18	1,89	0,14

Table C.4: Delayed contributions to device power at EoC, neutron and gamma

Nomenclature

BOC Beginning of cycle
BWR Boiling water reactor
CANDU Canadian deuterium uranium
CEA French Atomic Energy Commission
CR Compensation rod
CS Complex situation
CSA Controlled severe accident
EOC End of cycle
ESA Excluded severe accident
FOM Figure of merit
GFR Gas fast reactor
HEU Highly enriched uranium
IRSN Radioprotection and Safety French Institute
JHR Jules Horowitz Reactor
KERMA Kinetic energy released to matter
LEU low enriched uranium
LFR Lead fast reactor
LOCA Loss of coolant accident
LWR Light water reactor
MOC Middle of cycle
MOX Mixed oxide nuclear fuel
MSR Molten salt reactor
MTR Material testing reactor
NDE Non destructive examination
NS Normal shutdown
PR Pilot rod
PWR Pressurized water reactor
RLS Risk limitation situation
SCWR Supercritical water reactor
SFR Sodium fast reactor
SR Safety rod
SS Safety Shutdown
VHTR Very high temperature reactor

VVER Russian pressurized water reactor
WS Working situation
XSP Xenon saturation point

v: neutron velocity
$\mathbf{r}$: neutron position
$\hat{\mathbf{\Omega}}$: neutron velocity direction
E: neutron energy
$\varphi(\mathbf{r}, E, \hat{\mathbf{\Omega}}, t)$: neutron angular flux
Σ: total removal macroscopic cross section
$\Sigma_s(\mathbf{r}, E' \rightarrow E, \hat{\mathbf{\Omega}}' \rightarrow \hat{\mathbf{\Omega}}, t)$: macroscopic scattering cross section
χ_p: prompt neutron energy distribution
β: delayed neutron fraction
β_i: delayed neutron fraction referred to i-th precursors group
ν: neutron generated on average per fission reaction
$\Sigma_f(\mathbf{r}, E\hat{\mathbf{\Omega}}, t)$: macroscopic fission cross section
χ_{d_i}: delayed neutron energy distribution referred to i-th precursors group
λ_i: i-th precursors group decay constant
$c_i(\mathbf{r}, t)$: i-th group precursors concentration
$\hat{q}(\mathbf{r}, E, \hat{\mathbf{\Omega}}, t)$: neutron source
$\underline{G}$: streaming operator
$\underline{\Sigma}$: total removal operator
$\underline{\Sigma_s}$: scattering operator
$\underline{M_p}$: prompt generation operator
$\underline{M_{di}}$: i-th group delayed generation operator
$\underline{L}$: total leakage operator
$\underline{M}$: total generation operator
$\overline{\chi}$: average generated neutron spectrum
$\phi(\mathbf{r}, E, \hat{\mathbf{\Omega}})$: static neutron flux
$\phi_i(\mathbf{r}, E, \hat{\mathbf{\Omega}})$: generic eigensolution to neutron transport equation
$\phi_i^0(\mathbf{r}, E, \hat{\mathbf{\Omega}})$: generic eigensolution to neutron transport equation for vanishing eigenvalue
k: first eigenvalue to neutron transport equation
k_i: generic eigenvalue of neutron transport equation
$\underline{L}^\dagger$: adjoint total leakage operator
$\underline{M}^\dagger$: adjoint total generation operator
$\phi^\dagger(\mathbf{r}, E, \hat{\mathbf{\Omega}})$: adjoint static neutron flux
$\phi_i^\dagger(\mathbf{r}, E, \hat{\mathbf{\Omega}})$: generic eigensolution to adjoint neutron transport equation
$k_i^\dagger$: generic eigenvalue of adjoint neutron transport equation
Q: static neutron source
$Q^\dagger$: adjoint neutron source
$\phi_s(\mathbf{r}, E, \hat{\mathbf{\Omega}})$: static solution to source neutron transport equation
$\phi_s^\dagger(\mathbf{r}, E, \hat{\mathbf{\Omega}})$: static solution to adjoint source neutron transport equation

$\Sigma_d(\mathbf{r}, E, \hat{\mathbf{\Omega}})$: detector macroscopic cross section
$\psi(\mathbf{r}, E, \hat{\mathbf{\Omega}}, t)$: weight function for neutron kinetics formulation
$A(t)$: neutron flux amplitude
$\Phi(\mathbf{r}, E, \hat{\mathbf{\Omega}}, t)$: generic time-dependent neutron flux shape
$C_i(t)$: weighted delayed neutron precursors concentration for i-th group
$S(t)$: weighted neutron source
k_{eff}: first eigenvalue for neutron transport equation
$\rho(t)$: reactivity
β_{eff}: effective delayed neutron fraction
β_{eff_i}: i-th group delayed neutron fraction
$\ell(t)$: mean neutron generation time
ϕ_0: initial static neutron flux
$\phi_0^\dagger$: initial adjoint flux
$\delta\underline{L}$: leakage operator perturbation
$\delta\underline{M}$: generation operator perturbation
$\phi_p(\mathbf{r}, E, \hat{\mathbf{\Omega}}, t)$: prompt neutron flux generated in core
$\phi_{d_i}(\mathbf{r}, E, \hat{\mathbf{\Omega}}, t)$: i-th group delayed neutron flux generated in core
$\phi_d(\mathbf{r}, E, \hat{\mathbf{\Omega}}, t)$: one-group delayed neutron flux generated in core
$\varphi_p(\mathbf{r}, E, \hat{\mathbf{\Omega}}, t)$: prompt neutron flux generated in device
$\varphi_{d_i}(\mathbf{r}, E, \hat{\mathbf{\Omega}}, t)$: i-th group delayed neutron flux generated in device
$\varphi_d(\mathbf{r}, E, \hat{\mathbf{\Omega}}, t)$: one-group delayed neutron flux generated in device
$\underline{G}^{(in)}$: incoming streaming operator
$\underline{G}^{(out)}$: outcoming streaming operator
E_d: fission reaction deposited energy
$A_p(t)$: core prompt neutron flux amplitude
$A_d(t)$: core delayed neutron flux amplitude
$\Phi_p(\mathbf{r}, E, \hat{\mathbf{\Omega}}, t)$: core prompt neutron flux shape
$\Phi_d(\mathbf{r}, E, \hat{\mathbf{\Omega}}, t)$: core delayed neutron flux shape
$P_p(t)$: device power induced by core prompt neutron flux
$P_d(t)$: device power induced by core delayed neutron flux
$C_p(t)$: prompt neutron device-core power coupling coefficient
$C_d(t)$: delayed neutron device-core power coupling coefficient
$\ell_0(t)$: average prompt/delayed neutron lifetime
$P_{core}(t)$: total core power (neutron + prompt gamma)
$c(\mathbf{r}, t)$: one-group delayed neutron precursors concentration
λ: one-group neutron precursors decay constant
$C(t)$: integrated one-group delayed neutron precursors concentration
$\underline{M}_d$: one-group delayed neutron generation operator
$p_p(t)$: device power induced by self-generated prompt neutron flux
$p_d(t)$: device power induced by self-generated delayed neutron flux
$C^*(t)$: one-group delayed neutron precursors normalized to power formulation
ρ_{th}: fluid density for thermal hydraulic equations

v: fluid local velocity
g: gravity acceleration constant
p: pressure field
F: friction force
h: specific enthalpy
G: volumic heat generation term
ϕ_h: surface heat flux
$\mathcal{S}$: pellet cross-section
Q: volumic power generation in fuel
p_w: cladding external wet perimeter
$\Delta T_{channel}$:channel time calculation step
Δz: channel nodes step interval
$\overline{v}$: average fluid velocity
C_γ: fission energy fraction deposited outside pin via gamma radiation
q: mass rate per unit surface
s: specific volume
ρ_m^P: fluid density evaluated at time step P and node m
q_m^P: massa rate per unit surface evaluated at time step P and node m
P_m^P: pressure evaluated at time step P and node m
h_m^P: enthalpy evaluated at time step P and node m
ρ_l: liquid phase density
ρ_v: vapour phase density
α_m^P: void fraction evaluated at time step P and node m
X_r: steam quality of the coolant
c_{th}: specific heat capacity for solid media
$T(\mathbf{r}, t)$: temperature field in solid media
λ_{th}: thermal conductivity
h_c: convection coefficient for cladding-coolant
T_w: cladding wall average temperature
$\overline{T}$: coolant bulk temperature
R_{th}: thermal resistance
$g(z)$: axial power profile
$h(r)$: radial power profile
V_r: volume of generic domain region
$\overline{\phi}_r$: average neutron flux in a region
H_r: region height
NB_r: number of fuel pellet within a region
S_r: fuel pellet surface for region
ρ_0: initial reactivity
ρ_{ext}: external reactivity
ρ_{fb}: feedback reactivity
$D_v(z)$: void effect axial profile

$D_D(z)$: Doppler effect axial profile
$D_T(z)$: coolant temperature effect axial profile
$\overline{\mu}$: average value of a random variable
σ^2: variance of a random variable
S_n: sum of a group of n of random variales
T_{calc}: calculation time
$f(\xi)$: function of phase space
$\zeta(\xi)$: incoming collision density
$\kappa(\xi)$: outcoming collision density
$\mathcal{C}(\mathbf{v}' \rightarrow \mathbf{v}; \mathbf{r})$: velocity phase collision kernel
$\mathcal{L}(\mathbf{r}', \mathbf{v}' \rightarrow \mathbf{r}, \mathbf{v})$: global phase space collision kernel

Bibliography

B. D. Abramov. Modifications to the theory of coupled reactors. *Atomic Energy*, 90:348–356, 2001.

A. Alberman, G. Krysztoszek, M. Ciocanescu, k. Charlton, L. Sannen, B. Ponsard, D. Ceuterick, W. Petry, H. Gerstenberg, and V. Vrban. Scenario for sustainable Molybdenum-99 production in Europe. Technical report, European Research Reactor Position Paper for DGE Energy Draft 3, 2010.

C. Artioli. personal communication, 2011.

A. Barletta. *Introduzione Matematica alla Trasmissione del Calore*. Pitagora, 2006.

G. I. Bell and S. Glasstone. *Nuclear Reactor Theory*. Van Nostrand Reinhold Company, 1970.

G. Bignan, X. Bravo, and P. M. Lemoine. The Jules Horowitz Reactor, a new high performances European MTR (material testing reactor) with modern experimental capacities toward an international centre of excellence. *Proceedings of Meeting of the International Group on Research Reactors (RRFM 2012), Prague, Czech Republic, March 18-22, 2012*, 2012.

D. Blanchet. *Développements méthodologiques et qualification de schémas de calcul pour la modélisation des échauffements photoniques dans les dispositifs expérimentaux du futur réacteur d'irradiation technologique Jules Horowitz (RJH)*. PhD thesis, Université Blaise Pascal, 2006.

D. Blanchet, N. Huot, P. Sireta, H. Serviere, M. Boyard, M. Antony, V. Laval, and P. Henrard. Qualification of a gamma-ray heating calculation scheme for the future Jules Horowitz material testing reactor (RJH). *Annals of Nuclear Energy*, 35:731–745, 2008.

S. Bortot, A. Cammi, C. Artioli, P. Console Camprini, and R. Ghazy. A simplified model for a preliminary study of the dynamic behaviour of a small Gen IV LFR DEMO. *Proceedings of the 18th International Conference on Nuclear Engineering, ICONE18, May 17-21, 2010, Xi'an, China, 2010*, 2010.

F. Brown, B. Kiedrowski, and J. Bull. MCNP a general N-particle transport code, version 5, overview and theory. Technical Report LA-UR-03-1987, Los Alamos National Laboratory, 2003.

F. Brown, B. Kiedrowski, and J. Bull. MCNP5-1.60 release notes. Technical Report LA-UR-10-06235, Los Alamos National Laboratory, 2010.

P. Console Camprini, D. Mostacci, M. Sumini, C. Artioli, C. Gonnier, B. Pouchin, and S. Bourdon. Thermal hydraulic and neutronic core model for Jules Horowitz Reactor (JHR) kinetics analysis. Technical Report RdS/2011/39, ENEA Agenzia per le Nuove Tecnologie, l'Energia e lo Sviluppo Economico Sostenibile, 2011.

P. Console Camprini, C. Artioli, M. Sumini, F. Teodori, C. Gonnier, B. Pouchin, and S. Bourdon. Power transient analyses for reflector experimental devices during shutdowns in Jules Horowitz Reactor (JHR). Technical Report RdS/2012/1353, ENEA Agenzia per le Nuove Tecnologie, l'Energia e lo Sviluppo Economico Sostenibile, 2012a.

P. Console Camprini, M. Sumini, C. Artioli, C. Gonnier, B. Pouchin, and S. Bourdon. Power transient analyses of experimental in-reflector devices during safety shutdown in Jules Horowitz Reactor (JHR). *Proceedings of the International Conference on the PHYSics Of Reactors, PHYSOR, Knoxville TN, USA, 15-20 April 2012*, 2012b.

P. Console Camprini, M. Sumini, C. Artioli, C. Gonnier, B. Pouchin, and S. Bourdon. Thermal hydraulic and neutronic core model for power transient analyses of reflector experimental devices during shutdowns in Jules Horowitz Reactor (JHR). *Proceedings of Meeting of the International Group on Research Reactors (RRFM 2012), Prague, Czech Republic, March 18-22, 2012*, 2012c.

S. Carassou, G. Panichi, F. Julien, P. Yvon, M. Auclair, S. Tahtinen, P. Moilanen, S. Maire, and L. Roux. Experimental material irradiation in Jules Horowitz Reactor. *Proceedings of Meeting of the International Group on Research Reactors (IGORR Joint Meeting 2005), Gaithersburg MD, USA, September 12-16, 2005*, 2010.

J. P. Chauvin. Jules Horowitz Reactor collaborative project. Technical Report Grant Agreement n 206300, Deliverable NA3.D1, CEA, Commissariat á l'Énergie Atomique et aux Énergies Alternatives, 2009.

C. Colin, J. Pierre, C. Blandin, C. Gonnier, and D. Moulin. Experimental devices in Jules Horowitz Reactor dedicated to the material studies in support to the current and future nuclear power plants. *Proceedings of Meeting of the International Group on Research Reactors (RRFM 2012), Prague, Czech Republic, March 18-22, 2012*, 2012.

C. Doderlein, T. Bonaccorsi, C. DAletto, J. Di Salvo, O. Gueton, L. Lamoine, F. Moreau, G. Naudan, and P. Sireta. The 3D neutronics scheme for the development of the Jules Horowitz Reactor. *Proceedings of the International Conference on the PHYSics Of Reactors, PHYSOR, Interlaken Switzerland, (2008)*, 2008.

T. Dousson, P. Roux, C. Gonnier, L. Ferry, S. Gaillot, and D. Parrat. Experimental devices in Jules Horowitz Reactor dedicated to the fuel studies in support to the actual and

future nuclear power plant. *Proceedings of Meeting of the International Group on Research Reactors (RRFM 2012), Prague, Czech Republic, March 18-22, 2012*, 2012.

C. Edon. Études neutroniques parametriques. Technical Report (Internal) TA-524601 Ind. A, AREVA-TA, 2004.

C. Edon. RJH - Cœur - Paramètres neutroniques pour études de sûreté et de fonctionnement. Technical Report (Internal) TA-508278 Ind. G NP, AREVA-TA, 2008.

M. Eriksson, J. E. Cahalan, and W. S. Yang. On the performance of point kinetics for the analysis of accelerator driven systems. *Nuclear Science and Engineering*, 149:298–311, 2005.

J. Fache and H. Khadhraoui. Guide d'utilisation DULCINEE. Technical Report (Internal) DEN/CAD/DER/SRES NT 09 0007, Commissariat á l'Énergie Atomique et aux Énergies Alternatives, 2009.

M. A. Gaheen. Sensitivity of operational limits with respect to heat removal parameters in a high power MTR. *Annals of Nuclear Energy*, 43:150–156, 2012.

Y. Guélénec and Y. Le Roux. Étude de la transition de l'enrichissement du combustible du RJH de 19,75% á 27% et mise á l'équilibre. Master's thesis, INSTN, École des Applications Militaires de l'Énergie Atomique, France, 2010.

S. Guillot. RJH - RCR, STB du contrôle de la réactivité. Technical Report (Internal) TA-513153 Ind. C NP, AREVA-TA, 2007.

S. D. Hamieh and M. Saidinezhad. Analytical solution of the point reactor kinetics equations with temperature feedback. *Annals of Nuclear Energy*, 42:148–152, 2012.

M. J. Hancock. *The 1-D Heat Equation*. Fall, 2006.

A. F. Henry. *Nuclear Reactor Analysis*. The MIT Press, 1975.

D. Iracane. The Jules Horowitz reactor, a new material testing reactor in Europe. *Proceedings of the Meeting of the International Group on Research Reactors (IGORR Joint Meeting 2005), Gaithersburg MD, USA, September 12-16, 2005*, 2010.

D. Iracane, P. Chaix, and Ana Alamo. Jule Horowitz Reactor, a high performance material testing reactor. *C. R. Physiques*, 9:445–456, 2008.

K. Kobayashi. Rigorous derivation of multi-point reactor kinetics equations with explicit dependence on perturbation. *Journal of Nuclear Science and Technology*, 29:110–120, 1992.

J. Lamarsh and A. Baratta. *Introduction to Nuclear Engineering*. Prentice Hall, 2001.

J. C. Lee and V. V. Kulik. Space-time kinetics of subcritical systems. Technical report, Department of Nuclear Engineering and Radiological Sciences of University of Michigan, 2005.

J. Leppanen. Serpent a continuous-energy Monte Carlo reactor physics burnup calculation code. Technical report, VTT Technical Research Centre of Finland, 2012.

O. Litaize and B. Roesslinger. Introduction á la méthode de Monte Carlo et application au transport de particules. initiation aux codes de calcul TRIPOLI-4 et MCNP. Technical Report DESS MIIN - ULP Strasbourg, ULP Strasbourg, 2008.

V. Marelle, S. Maillard, S. Dubois, J-M Gatt, F. Huet, M. Pelletier, and J-D Piron. Lois matériaux combustible RJH-U_3Si_2. Technical Report (Internal) CEA/DEN/CAD/DEC/SESC/LSC NT 05/019 Ind. 2, Commissariat á l'Énergie Atomique et aux Énergies Alternatives, 2005.

D. Parrat, M. Tourasse, C. Gonnier, S. Gaillot, and P. Roux. Irradiation facilities and examination benches for implementing fuel programs in the future Jules Horowitz material testing reactor. *Proceedings of the Meeting of the International Group on Research Reactors (IGORR 2009), Bejing China, October 28-30, 2009*, 2009.

O. Petit, F. X. Hugot, N. Huot, Y. K. Lee, F. Malvagi, A. Mazzolo, and J.C. Trama. TRIPOLI-4 Version 8 User Guide. Technical Report (Internal) SERMA/LTSD/RT/11-5185/A, Commissariat á l'Énergie Atomique et aux Énergies Alternatives, 2011.

B. Pouchin. personal communication, 2011.

B. Pouchin and C. Huot-Marchand. Détermination de la puissance linéique des cibles MOLFI irradiées dans le réflecteur du RJH. Technical Report (Internal) CEA/DEN/CAD/DER/SRJH DO 20, Commissariat á l'Énergie Atomique et aux Énergies Alternatives, 2012.

G. Rimpault, D. Bernard, D. Blanchet, C. Vaglio-Gaudard, S. Ravaux, and A. Santamarina. Needs of accurate prompt and delayed γ-spectrum and multiplicity for nuclear reactor designs. *Physics Procedia*, 31:3–12, 2012.

G. Ritter, F. Rodiac, D. Beretz, C. Jammes, and O. Guéton. Neutron commissioning in the new CABRI water loop facility. *Proceedings of Meeting of the International Group on Research Reactors 13th Conference, (IGORR), Knoxville TN, USA, September 19-23, 2010*, 2010.

B. Roesslinger. TRIPOLI-4: Code de transport de particules par la méthode de Monte Carlo. principes théoriques. Technical Report (Internal) DM2S SERMA/LEPP/RT/05-3770/A, Commissariat á l'Énergie Atomique et aux Énergies Alternatives, 2005.

P. Roux. Demande d'evaluation du poids en réactivité du dispositif MADISON. Technical Report (Internal) CEA/DEN/CAD/DER/SRJH DO 315, Commissariat á l'Énergie Atomique et aux Énergies Alternatives, 2012.

P. Roux, C. Gonnier, D. Parrat, and C. Garnier. The MADISON experimental hosting system in the future Jules Horowitz Reactor. *Proceedings of Meeting of the International*

Group on Research Reactors (IGORR 2010), Knoxville TN, USA, September 19-23, 2010, 2010.

G. Rudstam, P. Finck, A. Filip, A. D'angeli, and R. D. McKnight. Delayed neutron data for the major actinides. Technical Report NEA/WPEC-6, Nuclear Energy Agency, Organisation for Economic Cooperation and Development, 2002.

P. Sireta. personal communication, 2011.

T. Trombetti. *Introduzione alla Cinetica Neutronica*. Cooperativa Libraria Universitaria, 1975.

A. Tsilanizara, T. D. Huynh, and L. Lunéville. Formulaire Darwin Version 2.1: Notice d'utilisation des modules PSAPHY, INTERPEP, PEPIN2, INVERSION. Technical Report (Internal) DM2S SERMA/LEPP/RT/Maj 02-2128 B, Commissariat á l'Énergie Atomique et aux Énergies Alternatives, 2002.

A. Tsilanizara, C. M Diop, and T. D. Huynh. Formulaire Darwin: Notice de Principe. Technical Report (Internal) DM2S SERMA/LEPP/RT/05-3772/A, Commissariat á l'Énergie Atomique et aux Énergies Alternatives, 2005.

P. Verbeek. Report on Molybdenum-99 production for nuclear medicine 2010-2020 state of the art. Technical report, Association of Imaging Producers and Equipment Suppliers, 2010.

Acknowledgements

Once the end of the work is reached, I want to thank all persons who allowed me to accomplish this very important and personal objective. Foremost I want to thank my supervisor Prof. Marco Sumini who gave me the opportunity to choose this research subject and supported me during all this activity. I want to express also my gratitude to Carlo Artioli my assistant supervisor who proposed me this collaboration and gave me a lot of important suggestions. He taught me how to search for right questions, in order to get the best answers and I hope our fruitful conversations will make me keeping and learning more and more his passion for research.
I want to thank Christian Gonnier for all discussions and precious teachings through which he kindly supported me as well as with comments regarding thesis writing; and I thank also Gilles Bignan who gave me the unique opportunity to spend more than two years in CEA Cadarache research center, joining the team working at Jules Horowitz Reactor which is the most important project in European nuclear research and technology which I am proud having been worked at.
I want to express my gratitude also to Jérôme Estrade executive for JHR group, and his assistant executive Jean-Luc Fabre, who hosted me between people of his team, allowing me to achieve this fascinating research experience.
I address special thanks to Patricia Siréta, Serge Bourdon, Clément Huot-Marchand, and Bernard Pouchin for all suggestions and explanations, precious discussions and patient answers, sometimes even until last bus time. My work would not have been possible without their support. My knowledge and my education is nothing but the fruitful everyday work with their irreplaceable human and scientific presence.
I want to thank also Christophe Blandin, Patrick Roux, Didier Tarabelli, Jocelyn Pierre, Dominique Drapeau, Manuel Bergman, Thierry Dousson and Pascal Manen for all kind answers that enriched my work and their pleasant friendship I will never forget.
A special thank is also for all foreign guests at JHR, the funniest research team in Europe and abroad: Lindee for chatting and discussions, Jagoda for her funny friendship, Thomas for his suggestions at physics coffee breaks, Saverio for his Italian presence in sharing my adventure, Ami for his very wise teachings (I hope to have crossed a part of that ocean...), Mikolaj for his kind friendship. Last, but never least, Raquel, the best and funniest friend, and colleague, I have ever met.
I thank also all Italian friends at Cadarache, Daniele, Francesco, Giorgio, Sofia, Claudia and a special French teacher Erika. A great thank is also for Benedetta and Elisabetta and

for some moments we spent together which are nice memory of this French adventure.
I want to thank also all the SRJH team, Marie-Nöelle Paoli, Valérie Catherine-Dumont, Lionel Ferry, Christian Colin, Frédéric Minot, Jean-Yves Malo, Muriel Antony, Damien Manon, Philippe Alexandre, François Bourrelly, Muriel Couvert, Gérard Dichtel, Pascal Gosset, Philippe Guimbal, Pierre Jaecki, Nicolas Lhullier, Jérôme Martial, Dominique Pepe, Alexandre Perrin and the young Alexandre Lacunza, Paulin Ferro, Marc Pescheux and Alexia Napol wishing them all the best.
I thank you all ... et je vous remercie pour votre amitié, tous petits moments ensemble et même pour m'avoir appris cette langue magnifique qui est le français, qui restera un des meilleurs souvenirs de cette expérience extraordinaire pour toute ma vie, merci.
Un grazie che non si descrive anche ai miei genitori Tiziano e Giordana, e a mia sorella Giorgia. Le distanze non esistono, per quel che si porta sempre con sè.